Titre: Title:	The use of Ag^{+}-β-alumina and Ca^{2+}-conducting aluminate solid electrolytes in thermodynamic measurements involving SO_2 (g)
Auteur: Author:	Jianzhong Wu
Date:	1992
Type:	Mémoire ou thèse / Dissertation or Thesis
Référence: Citation:	Wu, J. (1992). The use of Ag^{+}-β-alumina and Ca^{2+}-conducting aluminate solid electrolytes in thermodynamic measurements involving SO_2 (g) [Thèse de doctorat, Polytechnique Montréal]. PolyPublie. https://publications.polymtl.ca/57988/

URL de PolyPublie: PolyPublie URL:	https://publications.polymtl.ca/57988/
Directeurs de recherche: Advisors:	
Programme: Program:	Non spécifié

UNIVERSITÉ DE MONTRÉAL

The Use of Ag^+-β-alumina and Ca^{2+}-conducting Aluminate Solid Electrolytes in Thermodynamic Measurements Involving SO_2 (g)

Par

Jianzhong WU

DÉPARTEMENT DE GÉNIE MÉTALLURGIQUE

ÉCOLE POLYTECHNIQUE

THÈSE PRÉSENTÉE EN VUE DE L'OBTENTION

DU GRADE DE PHILOSOPHIAE DOCTOR (Ph.D.)

April 1992

ISBN 0-315-74998-9

UNIVERSITÉ DE MONTRÉAL

ÉCOLE POLYTECHNIQUE

Cette thèse intitulée:

The Use of Ag^{+}-ß-alumina and Ca^{2+}-conducting Aluminate Solid Electrolytes in Thermodynamic Measurements Involving $SO_2(g)$

présenté par: Jianzhong Wu

en vue de l'obtention du grade de: Philosophiae Doctor (Ph.D.)

a été dûment accepté par le jury d'examen constitué de:

M. PELTON, Arthur D., Ph.D., président

M. BALE, Christopher W., Ph.D.,membre et directeur de recherche

M. AJERSCH, Frank, Ph.D., membre

M. THOMPSON, William T., Ph.D., membre

ABSTRACT

It is well known that a non-stoichiometric phase in the Na_2O-Al_2O_3 binary system, generally referred to as ß-alumina, is a good sodium ion conductor. Through ion-exchange, Na^+ in ß-alumina can be replaced by other ions to obtain a variety of solid electrolytes. The ß-alumina family of ionic ceramics can provide a reliable means of obtaining thermodynamic data from electrochemical measurements.

In the present investigation, Ag^+-ß-alumina tubes have been prepared by ion-exchange of ß-alumina tubes in a molten $AgNO_3$ bath. In addition, attempts have been made to fabricate Ca^{2+}-conducting aluminate tubes. Both types of tubes have been used in galvanic cell measurements involving SO_x (x = 2,3) gas species.

In the development of an SO_x gas sensor based on emf measurements, many different electrolytes have been considered and tested. Among the electrolytes employed, ß-alumina is a promising candidate for in situ monitoring at high temperatures. Although a linear relation between emf and the logarithm of SO_2 concentration has been reported, there are still some points in question.

First, the establishment of equilibrium between SO_2 and

SO_3 in the gas phase may not always be favored in the experimental conditions. For example, a high flow rate of gas and a low temperature has a definite effect on the SO_2/SO_3 ratio. As a result, an emf dependence on the gas flow rate is often observed. In this case, the emf value recorded is not an equilibrium one but one at a steady state, which may invalidate any calculations of thermodynamic properties from the emf value.

Second, a layer of sulfate is formed on the surface of the ß-alumina when exposed to sulfur oxides at high temperatures. This is confirmed by electron microscopy. In an electromotive force measurement, the electrical current is suppressed by the high impedance of the potentiometer. When the ceramic material is predominantly ionic conducting, significant transport of the conducting element through the material can not be expected, irrespective of the presence of a chemical potential gradient of the element. It can not be taken for granted that the sulfate formed during emf measurement has the same physico-chemical properties as the bulk sulfate.

Third, since ß-alumina may be attacked by sulfur oxides to produce sulfate, a knowledge of the phase relations between ß-alumina and sulfate is essential. Furthermore, the

temperature and SO_2 concentration ranges within which the formation of sulfate will not lead to the failure of the solid electrolyte are more or less pertinent. This information may be retrieved from a well-established phase diagram. An effort has been made in this study to assess all the thermodynamic data available from known phase diagrams, from emf measurements, and from data compilations within the M-Al-O-S (M = Na,Ag,Ca) systems. A series of phase diagrams has been calculated with the aid of a computer.

The galvanic cell under study can be represented by the following expression:

$$\text{Ref. / ß-}Al_2O_3\text{ / (}SO_2\text{+Air), }MSO_4\text{, Pt} \qquad ...(I)$$

In the case of Ag^+-ß-alumina, pure silver is the reference electrode, and the overall cell reaction can be proposed as:

$$2\ Ag(s) + SO_3(g) + 1/2\ O_2(g) = Ag_2SO_4(s,l) \qquad ...(1)$$

(The formation of $CaSO_4$ will be the overall cell reaction in the case of a Ca^{2+}-conducting aluminate.) Since the activities of silver and silver sulfate are unity, $a_{Ag} = a_{Ag_2SO_4} = 1$, the Nernst equation for cell reaction (1) can be written as:

$$-2FE = \Delta G^{\circ} - RT\ln(P_{SO_3} \cdot P_{O_2}^{1/2}) \qquad \ldots(2)$$

This is the theoretical basis upon which the SO_x gas sensor operates by means of emf measurements.

At relatively high temperatures, the emf has been found to be a linear function of temperature at fixed initial P_{SO_2} levels (10,108,980,8600 ppm) in air, and to be reproducible with respect to different experimental runs. By a linear regression procedure, the following standard Gibbs energy changes for cell reaction (1) have been deduced:

$$\Delta G^{\circ}(J) = -290\ 460 + 202.99\ T \qquad (624 < T < 703\ K)$$

$$\Delta G^{\circ}(J) = -271\ 160(\pm 2236) + 175.54(\pm 1.68)T \qquad (703 < T < 926\ K)$$

$$\Delta G^{\circ}(J) = -252\ 060 + 154.91\ T \qquad (926 < T < 1146\ K)$$

The emf dependence on the flow rate of the gas mixture (SO_2 + air) has been observed throughout the measurements, especially at low flow rates. In general, the higher the SO_2 concentration and the lower the temperature, the stronger the dependence. This, coupled with the decline of the emf as the flow rate increases, implies that SO_3 rather than SO_2 is the electro-active species and can be monitored exactly by emf measurements.

By comparing the emf measurements at the same initial SO_2 concentration, same flow rate and temperature range but with or without Ag_2SO_4 powder being present in the working electrode compartment, the conclusion has been reached that in the absence of Ag_2SO_4 powder, at most a sulfate layer of a few atoms thickness can be formed on the surface of ß-alumina. The physico-chemical properties of the layer are different from those of the bulk sulfate.

According to the calculated potential-composition phase diagrams, in oxidizing atmospheres and at SO_2 concentrations from 1 ppm to 1 %, sulfates may thermodynamically coexist with α- rather than ß-alumina at a relatively low temperature range; the exception is Ag^+-ß-alumina, which shows a limited stable range of Ag_2SO_4 coexisting with ß-alumina. This does not rule out the validity of using ß-alumina as a solid electrolyte in the presence of SO_x, but the critical point beyond which aluminium sulfate is more stable than α-alumina may indicate the point of electrolyte failure.

The use of Ag^+-ß-alumina to monitor SO_3 contents in air is recommended with the following optimal operation conditions:

(1) a standard (calibration) curve is established

for emf against logarithm SO_3 concentration at low temperatures, without a catalyst, and at high flow rates;

(2) subsequent emf value measurements correspond to a definite concentration of SO_3 on the standard curve.

In the case of monitoring SO_2 contents, precautions must be taken to establish equilibrium in the gas phase. From the SO_3 concentration determined above, the corresponding SO_2 concentration can be calculated.

On a qualitative basis, the Ca^{2+}-conducting aluminate ceramic tube used in this study may have potential applications in monitoring SO_2 contents. Further experimental work is required to establish the quantitative relationships between emf and SO_2 concentrations for this material.

RÉSUMÉ

Il est bien connu qu'une phase céramique du système binaire Na_2O-Al_2O_3, généralement connue sous le nom d'alumine bêta, est un bon conducteur des ions sodium. Par échange ionique, les ions Na^+ de l'alumine bêta peuvent être remplacés par d'autres ions, pour obtenir une variété d'autres électrolytes solides. La famille des céramiques de type alumine bêta permettent d'obtenir des données thermodynamiques au moyen de mesures électrochimiques.

Dans cette étude, des tubes d'alumine bêta à l'argent ont été préparés par échange ionique dans un bain de nitrate d'argent. De plus, on a tenté de fabriquer des tubes d'aluminate conduisant par Ca^{2+}. Ces deux types de tubes ont été utilisés dans des mesures de piles galvaniques en présence de mélanges gazeux SO_x ($x = 2,3$).

Afin de développer des détecteurs de SO_x par l'entremise de mesures de potentiels, plusieurs électrolytes ont été testés. Parmi ceux-ci, l'alumine bêta s'est avéré prometteur pour la mesure in situ dans des environnements corrosifs à haute température. Même si on fait part de relations linéaires entre la tension et le logarithme de la concentration en SO_2, certains points restent tout de même à clarifier.

Premièrement, l'atteinte d'un état d'équilibre entre le SO_2 et le SO_3 de la phase gazeuse n'est pas toujours favorisé par les conditions expérimentales. Par exemple, on sait qu'un fort débit (de gaz) et une basse température ont un effet marqué sur le rapport SO_2/SO_3. Dans de tels cas il n'y a pas équilibre mais régime permanent, ce qui invalide toute propriété thermodynamique dérivée des mesures de f.e.m..

Deuxièmement, une couche de sulfate se forme à la surface de l'alumine bêta lorsque celle-ci est exposée à des oxydes de soufre à haute température. Ceci a été confirmé par microscopie électronique. Lors d'une mesure de force électromotrice, le courant électrique est bloqué par la haute impédance du potentiomètre. Lorsque le matériau céramique est conducteur à prédominance ionique, on ne s'attend donc pas à une diffusion importante de l'espèce conductrice même s'il y a un gradient de potentiel chimique de l'élément dans l'épaisseur de la céramique. On ne peut prendre pour acquis que le sulfate formé en surface, lors de la mesure de f.e.m., a les mêmes propriétés que le sulfate formé en volume.

Troisièmement, puisque l'alumine bêta peut être attaquée par les oxydes de soufre pour produire des sulfates, la connaissance des équilibres entre ces sulfates et l'alumine bêta est primordiale. De plus, la température ainsi que la

gamme de concentrations en SO_2 qui amèneront la formation de sulfate sans dégradation de l'électrolyte solide ont une importance plus ou moins grande.

Ces informations peuvent être déduites à partir d'un diagramme de phase. Un effort particulier a été fourni dans cette étude pour rassembler et analyser les données thermodynamiques de toutes provenances; diagrammes d'équilibre connus; mesures effectuées à l'aide de piles galvaniques; compilations de données thermodynamiques des systèmes M-Al-O-S (M = Na, Ag, et Ca). Ensuite, une série de diagrammes ont été calculés au moyen de logiciels du système F*A*I*T disponible à l'École polytechnique de Montréal.

La pile galvanique à l'étude peut être représentée de la façon suivante:

$$\text{Réf. / ß-alumina / } (SO_2+\text{Air}),\ MSO_4,\ \text{Pt} \qquad ...(I)$$

Pour ce qui est de l'alumine bêta à l'argent, l'argent pur sert d'électrode de référence et la réaction globale de la pile peut être décrite par la réaction:

$$2\ Ag(s) + SO_3(g) + 1/2O_2(g) = Ag_2SO_4(s,l) \qquad ...(1)$$

Pour l'aluminate conduisant par Ca^{2+}, la réaction est la même mais elle donne lieu à la formation d'un sulfate de calcium. Puisque les activités de l'argent et du sulfate sont unitaires ($a_{Ag} = a_{Ag_2SO_4} = 1$), l'équation de Nernst pour la réaction (1) de la pile peut s'écrire:

$$-2FE = \Delta G° - RT\ln(P_{SO_3} \cdot P_{O_2}^{1/2}) \qquad ...(2)$$

Cette équation constitue le fondement théorique à partir duquel il est possible de déterminer la teneur en SO_x d'un mélange gazeux en mesurant des f.e.m..

À des températures relativement élevées, on a pu observer que la f.e.m. est une fonction linéaire de la température lorsque la teneur initiale en SO_2 dans l'air est constante. Ces résultats sont reproductibles pour tous les essais effectués avec des teneurs en SO_2 de 10, 108, 980 et 8600 ppm. Au moyen de techniques de régressions linéaires, on a pu déterminer les enthalpies libres standards de formation de la réaction de pile (1) qui ont les valeurs suivantes:

$$\Delta G°(J) = -290\ 460 + 202.99\ T \qquad (624 < T < 703)$$

$$\Delta G°(J) = -271\ 160(\pm 2236) + 175.54(\pm 1.68)\ T \qquad (703 < T < 926)$$

$$\Delta G°(J) = -252\ 060 + 154.91\ T \qquad (926 < T < 1146)$$

La dépendance de la tension mesurée en fonction du débit du mélange (SO_2 + air) a été observée d'essai en essai, plus particulièrement à faible débit. De façon générale on a pu constater que la dépendance est d'autant plus forte que la teneur en SO_2 est élevée et que la température est faible. Ce comportement, ainsi que la chute de potentiel résultant d'une augmentation de débit, impliquent que c'est le SO_3 plutôt que le SO_2 qui est l'espèce électro-active et que la mesure de tension permet de suivre la teneur en SO_3 du mélange.

En comparant les mesures de f.e.m. sous des conditions expérimentales identiques (même teneur en SO_2, même gamme de température et de débit) mais avec ou sans Ag_2SO_4 dans le compartiment de l'électrode de travail, on parvient à la conclusion, qu'en l'absence de Ag_2SO_4, qu'il se forme une couche mince de sulfate (tout au plus quelques épaisseurs atomiques) à la surface de l'alumine bêta. Les propriétés physico-chimiques de cette couche sont différentes d'un sulfate formé en volume.

Les diagrammes de phase potentiel vs composition calculés nous ont révélé que les sulfates peuvent coexister avec l'alumine alpha, et non avec l'alumine bêta, dans des atmosphères oxydantes contenant des concentrations en SO_2 allant de 1 ppm a 1% lorsque la température est basse;

l'exception à cette règle est l'alumine bêta à l'argent qui peut coexister avec le sulfate d'argent dans une gamme limitée de température. Cette constatation n'élimine pas pour autant l'alumine bêta comme détecteur de SO_x. Cependant la température au-dessus de laquelle le sulfate d'aluminium est plus stable que l'alumine alpha peut constituer le point de défaillance de la sonde.

L'alumine bêta à l'argent peut servir à mesurer la teneur en SO_3 dans l'air si l'on procède à l'étalonnage de la tension en fonction de teneurs en SO_3 connues à basse température, sans catalyseur et à fort débit. Ces courbes d'étalonnage permettront de déterminer la teneur en SO_3 d'un mélange inconnu à partir de la mesure de tension.

Pour arriver à mesurer la teneur en SO_2 il est essentiel d'atteindre l'équilibre thermodynamique dans le mélange. De la concentration en SO_3 déterminée ci-haut il est possible de déterminer la teneur en SO_2 par simple calcul.

D'un point de vue qualitatif, il semble que les tubes d'aluminate de calcium puissent servir à la détection de SO_2. Il reste toutefois à établir quantitativement la relation entre la teneur en SO_2 et la f.e.m., chose qui n'a pas été faite dans cette étude.

ACKNOWLEDGEMENTS

To complete a Ph.D. thesis requires not only the persistent effort of the author but also the guidance, the assistance, and the co-operation involving many people in many different ways. I wish, if possible, that I could express my thanks to everyone who helped me in reaching this goal.

First and most importantly, I want to thank my director, C.W. Bale. His experienced introduction and supervision activated my interest in this research field and his continuous encouragement made me feel confident in the work I undertook.

I want to express my gratitude to Dr. A.D. Pelton, who enriched my knowledge in thermodynamics and phase diagram calculation and provided me many valuable discussion in my study, to Dr. W.T. Thompson at Royal Military College for his constructive criticism and discussion in my thesis writing.

Thanks are due to Dr. J. Kirchnerova and Dr. A. Dubreuil, who shared with me their experimental knowledge in e.m.f. measurement, and instructed me in preparing the solid electrolyte tube used in my experiment.

I wish to thank the professors, F. Ajersch and M. Rigaud, at the department, who brought me quite a few fundamental knowledge, which is indispensable in carrying out my study, through their effective instructions of courses.

I wish to thank Dr. J. Melançon and P. Talley at CRCT for their constant, prompt, and patient instruction for me to be familiar with FACT system and to make a full use of computer.

I also wish to mention all the names of my colleagues at Ecole Polytechnique who contributed to my research. They are D. Bouchard, C. Armand, I. De Sousa, R. Lacroix, S. Larose, Y. Dessureault, A. Romero-Serrano, P. Wu, and L. Li.

I wish to thank the technicians in the department, especially L. Gosselin and A. Desilets, who were always ready to provide assistance with the many daily problems. Thanks are also due to J. Desrochers and J. Claudinon for the X-ray and other electron microscopic analysis.

I want to thank the secretaries in the department for their prompt and friendly assistance in administrative matters, especially J. Gaulin, who contributed herself in taking care of the needs of our research group.

The financial support of this study from NSERCC (Natural Sciences and Engineering Research Council of Canada) is greatly appreciated.

Finally I want to add a word of thanks to my wife, L. Na, and my family for their support.

TABLE OF CONTENTS

LIST OF FIGURES

LIST OF TABLES

LIST OF APPENDICES

CHAPTER I INTRODUCTION

From a classical thermodynamic point of view, the information about the equilibria in a system can be provided by the determination of the thermodynamic properties of the system. For example, the equilibrium constant of a reaction is related to the standard Gibbs energy change of the reaction. Usually if a gas phase and one or several condensed phases are involved in the reaction, it is the equilibrium constant of the reaction which is determined experimentally by controlling and analyzing the composition of the gas phase and used afterwards for calculating the thermodynamic properties of the reaction. On the other hand, the thermodynamic properties obtained from electromotive force (EMF) measurements of a Galvanic cell with a solid electrolyte may be used to describe the overall cell reaction under equilibrium more precisely because of the higher measurement accuracy characteristic of the electrochemical method.

Independent of any specific knowledge of the mechanism of ionic conduction in a solid electrolyte which exhibits exclusive ionic conduction, a simple consideration of energy conversion provides the relationship between the reversible cell potential E and the Gibbs energy change ΔG for the virtual chemical reaction of the cell:

$$\Delta G = - n F E \qquad ...(1.1)$$

where n is the equivalents of charge passed through the external circuit, and F is Faraday constant. The application of Gibbs-Helmholtz relations to the temperature dependence of the cell voltage provides values of ΔH and ΔS for the reaction.

Unlike liquid electrolytes, which are used at relatively low temperature and have exclusively ionic conductivities, there is always the possibility of the electronic conductivity in a solid electrolyte due mainly to the defect transport mechanism in the crystal. Therefore all solid electrolytes are, to some extent, mixed conductors. The total electrical charge is transported by both ionic species and electrons and/or holes:

$$\sigma_T = \Sigma \sigma_i = \Sigma q_i \cdot c_i \cdot B_i \qquad ...(1.2)$$

where σ_T is the total conductivity, σ_i is the partial conductivity of i species, and c_i, B_i, and q_i are the concentration, the mobility, and the electrical charge of species i respectively. Unless the concentration of ionic charge carriers is many orders of magnitude greater than that of electronic charge carriers (which is the case in doped

oxide electrolytes, CSZ and YDT, under certain conditions), according to equation (1.2), it is important always to consider the relative mobilities of electrons, positive holes, and ions in solid electrolytes because of the fact that in ionic solids the ionic mobilities seldom exceed 10^{-7} m^2/Vs which may be an operational lower limit for electron and hole mobilities. Since the presence of significant electronic conductivity will allow a continual transport of material from one electrode to the other even under open circuit conditions, attention must be paid to not making conclusions simply from steady emf values without the knowledge of electronic conductivity on the specific solid electrolyte used.

In general, a galvanic cell is composed of a solid electrolyte, in which a cation conducts exclusively, and two electrodes which fix the chemical potential of the conducting component at both sides of the electrolyte. The cell can be represented as follows:

$$\mathbf{Pt},\mu'_M \ \mathbf{/\ Solid\ Electrolyte\ /}\ \mu''_M\mathbf{,\ Pt} \qquad \ldots\mathbf{(I)}$$

where μ'_M and μ''_M are the chemical potentials of the metal component in the electrodes. At constant temperature and pressure, the theoretical (or thermodynamic) emf expression for the above galvanic cell may be derived[1]:

$$E = -\frac{1}{Z_M \cdot F} \int_{\mu'_M}^{\mu''_M} t_{ion} d\mu_M \qquad \ldots(1.3)$$

where Z_M is the valence of the cation; t_{ion} is the ionic transport number which is defined as:

$$t_{ion} = \frac{\sigma_{ion}}{\sigma_{ion} + \sigma_e} \qquad \ldots(1.4)$$

If $t_{ion} = 1$, the Nernst equation follows from equation (1.3)

$$E = -\frac{1}{Z_M \cdot F} \cdot (\mu''_M - \mu'_M) = -\frac{RT}{Z_M F} \cdot \ln \frac{a''_M}{a'_M} \qquad \ldots(1.5)$$

This relationship is the basis on which chemical sensors operate by means of emf measurements. A general review is given in Chapter II for the electrochemical methods involving solid electrolytes.

A phase diagram has been defined[2] as a geometrical representation of the loci of thermodynamic parameters when equilibrium between different phases under a specified set of conditions is established. Therefore, the conditions under which phases can stably coexist may be available from a well

determined phase diagram.

In a galvanic cell involving a solid electrolyte, the equilibrium is usually characteristic of a multi-phase reaction in a multi-component system. Due to the lack of relevant phase diagrams for the systems in the present investigation, the knowledge of certain phase equilibria are not complete. With the aid of computer, the construction of the phase diagram has been made easier, and an effort has been made to calculate a series of phase diagrams for M-Al-O-S (M = Na, Ag, and Ca) system. The details of the phase diagram calculation are presented in Chapter III.

In the development of the SO_x gas sensor based on emf measurements, many kinds of electrolytes, such as molten sulfate mixtures, solid sulfates, solid solution of sulfates, and ß-alumina, have been considered and tested[58,68,74-88]. Usually the initial gas mixture contained only one type of sulfur oxide, either SO_2 or SO_3, and the equilibrium between SO_2 and SO_3 in the gas phase was assumed so that a theoretical calculation of emf was made possible. The emf dependence on the flow rate of the gas mixture was often not reported. In fact, the establishment of the equilibrium in the gas phase is in question, especially under unfavorable experimental conditions. Therefore, an investigation of the dependence of

emf on the flow rate of the gas mixture in a variety of temperatures and concentrations of SO_2 would be helpful to resolve the dispute, which constitutes a part of the experimental work in the present study.

β-alumina is considered a good candidate as a solid electrolyte for an SO_x gas sensor. While being exposed to SO_x under oxidizing conditions, β-alumina may react with sulfur oxide to form a sulfate. Under the experimental conditions of the emf measurement, the current is suppressed by the high impedance of the potentiometer. Consequently, massive formation of the sulfate on the surface of β-alumina can not be expected. How the emf may be influenced by the state of sulfate is another experimental aspect in this study. The experimental details of using Ag^+-β-alumina and Ca^{2+}-conducting aluminate to monitor SO_x are described in Chapter IV.

Three types of working electrodes, where the activity of the conducting element is determined from the measured emf, have been studied. The results of the experiments, including the emf dependence on the temperature, on the flow rate of the gas mixture, and on the concentration of SO_2, are reported in Chapter V.

From the emf measured with Ag^+-ß-alumina being the solid electrolyte, the standard Gibbs energy change for the cell reaction has been deduced as a function of temperature and a cathode reaction mechanism has been proposed to explain the experimental observations. The formation of a layer of sulfate due to the reaction between SO_x and the ß-alumina solid electrolyte, the state of the reaction layer, and other aspects pertaining to the SO_x gas sensor are discussed. These constitute Chapter VI.

CHAPTER II LITERATURE SURVEY
-- ELECTROCHEMISTRY IN GAS SENSORS

The potential application of solid electrolytes in modern science and technology has activated an interest in the electrochemistry of solid electrolytes. As a result, the number of publications in this field has been increasing annually. There are numerous reviews on the theory[3-10] and experimental techniques[11,12] of solid electrochemistry, on solid electrolytes and applications[13-20]. This chapter is directed towards the application of solid electrolytes as gas sensors, particularly with respect to the SO_x sensor.

2.1 Basic Requirement for a Gas Sensor

A gas sensor has been defined[21] as a device by which the concentration of certain gaseous components can be measured. Usually an electrical property, such as voltage or current, of the system containing the gaseous species is monitored. The general requirements for a gas sensor are as follows:

* high accuracy,
* wide range of measurement,
* good reproducibility and constancy of the indicated value,

* low sensitivity to external disturbances,
* high selectivity for the component being monitored,
* rapid response, particularly when the sensor is used as a control function.

2.2 Oxygen Sensor with Oxide Solid Electrolyte

In principle, many types of solid electrolytes may be used to monitor the content of oxygen in a system by means of emf measurement as long as equilibrium is attained at the reference and working electrodes. Solid oxide electrolytes provide a direct means for oxygen to be monitored and, together with their high temperature stability, are preferred both in the laboratory and in the industrial applications. For example, calcia stabilized zirconia (CSZ) and yttria doped thoria (YDT) solid oxide electrolytes, which have high oxygen ionic conductivities under certain conditions, have been popular for the past 30 years.

Oxygen Ion Conductors, CSZ and YDT

From a crystal structure point of view, only those oxides which have the fluorite crystal structure, a face-centred-cubic arrangement of cations with the anions occupying all the tetrahedral sites, are potentially useful oxygen ion

conducting electrolytes. As shown in Figure 2.1, each metal cation in the crystal is surrounded by eight oxygen anions, and each oxygen anion is tetrahedrally coordinated with four metal cations. The large number of octahedral interstitial voids makes this structure a rather "open" one, thus rapid ion diffusion might be expected.

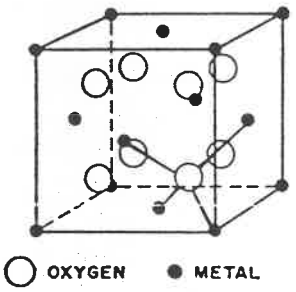

Figure 2.1 The fluorite crystal structure

At room temperature pure ZrO_2 has a monoclinic crystal structure which changes to a tetragonal form above 1200 °C, and finally to a cubic one above 2300 °C. The high-temperature cubic fluorite phase in zirconia can be stabilized by addition of some of the aliovalent oxides. In contrast to ZrO_2, pure thoria has the cubic CaF_2-type structure up to its melting point, and therefore does not need any stabilization. However, it is the solid solution such as $ThO_2(YO_{1.5})$ and $ZrO_2(CaO)$ which exhibits high ionic conductivity. The phase diagrams of these two binary systems[113,114] are shown in Figure 2.2.

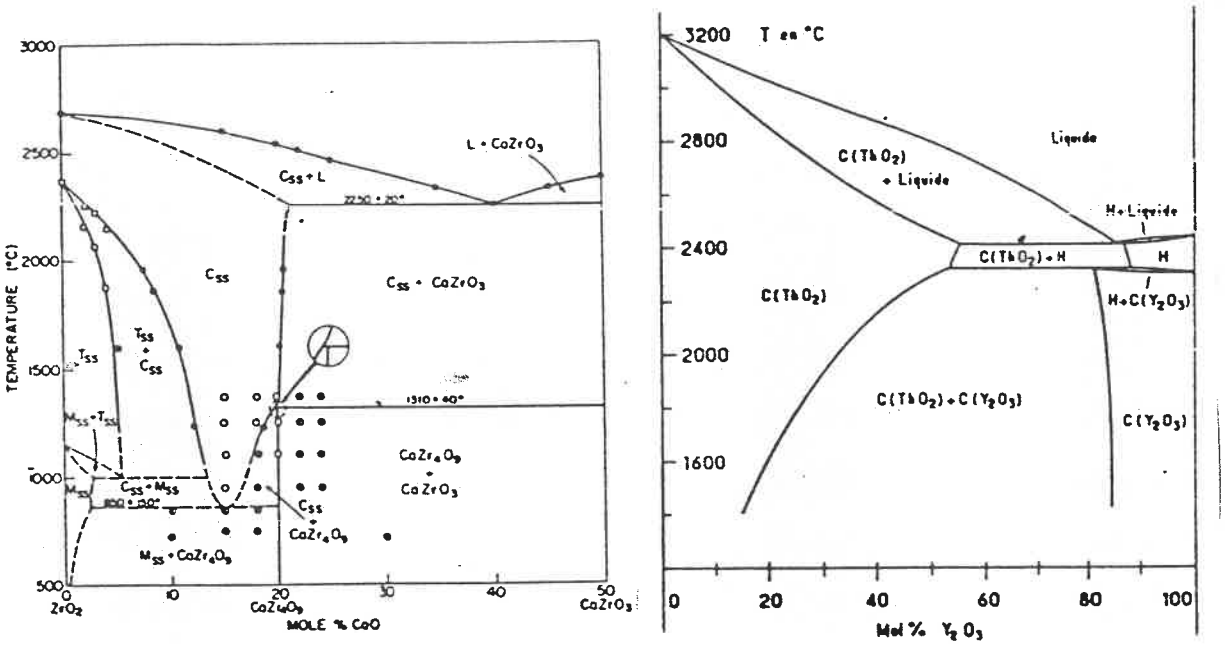

Figure 2.2 ZrO_2-CaO and ThO_2-Y_2O_3 phase diagrams[113,114]

The ionic conductivity in this kind of electrolyte is due to oxygen-ion migration by a defect transport mechanism. The determination of the oxygen self-diffusion coefficient in polycrystalline samples of ZrO_2 (CaO) by means of radioactive-tracer measurement has shown that the oxygen ion migrated about 10^{10} times faster than the cations[22,23]. In addition, density[24] and x-ray intensity[25] measurements on CSZ have confirmed that the predominant defects present in the solid solution are anion vacancies. Higher concentrations of oxygen-ion vacancies are created in both CSZ and YDT solid electrolyte, leading to their higher ionic conductivities.

The most commonly used CSZ contains 15 mol% CaO, whereas the YDT contains 7 to 15 mol% $YO_{1.5}$.

Electronic Conductivity and Electrolytic Domain

As pointed out in Chapter I, the electronic conductivity cannot be ignored. The relative magnitude of the electronic conductivity in a solid electrolyte should always be given consideration in order to obtain meaningful information from measurements (especially thermodynamic measurements) involving a solid electrolyte.

For a solid oxide electrolyte, there are two possible equilibrium reactions in which the oxygen at the electrodes, the oxygen ionic vacancies in the electrolyte and the electrons or holes are involved:

$$1/2\ O_2 + V_O^{\cdot\cdot} + 2\ e' = O_O \qquad ...(2.1)$$

$$1/2\ O_2 + V_O^{\cdot\cdot} = O_O + 2\ h^{\cdot} \qquad ...(2.2)$$

where $V_O^{\cdot\cdot}$ denotes the oxygen ionic vacancy, O_O the oxygen in an anionic lattice site, e' and $h^{\cdot}$ the electron and hole respectively. Application of the mass action law to these equilibria with the assumption of idea behavior of all the

species involved results in the following expressions:

$$K_1 = \frac{[O_O]}{P_{O_2}^{1/2}[V_O^{\cdot\cdot}]n^2} \qquad \ldots(2.3)$$

$$K_2 = \frac{[O_O]p^2}{P_{O_2}^{1/2}[V_O^{\cdot\cdot}]} \qquad \ldots(2.4)$$

where n and p are the concentrations of electrons and holes respectively. Since $[O_O]$ = const. and $[V_O^{\cdot\cdot}]$ is independent of P_{O_2}, it follows that:

$$n \propto P_{O_2}^{-1/4} \qquad \ldots(2.5)$$

$$p \propto P_{O_2}^{1/4} \qquad \ldots(2.6)$$

With the assumption of independence of mobility on concentration of electron or hole, the dependence of electronic conductivity on the partial pressure of oxygen results from the combination of equation (2.5) or (2.6) with equation (1.2). Furthermore, the ionic transport number, t_{ion} in equation (1.3), as a function of P_{O_2} can be obtained by substituting the dependence of electronic conductivity on P_{O_2} into equation (1.4), leading to the theoretical evaluation of

emf from equation (1.3) for oxide solid electrolytes[26]:

$$E = \frac{RT}{F}\left(\ln\frac{P_{\oplus}^{1/4} + P''^{1/4}_{O2}}{P_{\oplus}^{1/4} + P'^{1/4}_{O2}} + \ln\frac{P_{\ominus}^{1/4} + P'^{1/4}_{O2}}{P_{\ominus}^{1/4} + P''^{1/4}_{O2}}\right) \qquad \ldots(2.7)$$

where the parameters $P_{\oplus}$ and $P_{\ominus}$ are the oxygen pressures at which the ionic transport number t_{ion} is equal to the hole and electron transport number respectively, and P'_{O_2} and P''_{O_2} denote the oxygen pressures at the anode and cathode of the galvanic cell respectively. Several limiting situations in equation (2.7) are of practical value:

$$a)\ If\ P_{\ominus} < P'_{O_2} < P_{\oplus} < P''_{O_2},\quad E_a = \frac{RT}{4F}\ln\frac{P_{\oplus}}{P'_{O_2}} \qquad \ldots(2.8)$$

$$b)\ If\ P_{\ominus} < P'_{O_2} < P''_{O_2} < P_{\oplus},\quad E_b = \frac{RT}{4F}\ln\frac{P''_{O_2}}{P'_{O_2}} \qquad \ldots(2.9)$$

$$c)\ If\ P'_{O_2} < P_{\ominus} < P_{\oplus} < P''_{O_2},\quad E_c = \frac{RT}{4F}\ln\frac{P_{\oplus}}{P_{\ominus}} \qquad \ldots(2.10)$$

$$d)\ If\ P'_{O_2} < P_{\ominus} < P''_{O_2} < P_{\oplus},\quad E_d = \frac{RT}{4F}\ln\frac{P''_{O_2}}{P_{\ominus}} \qquad \ldots(2.11)$$

$$e)\ If\ P_{\ominus} < P'_{O_2} \approx P_{\oplus} < P''_{O_2} \quad \vee \quad P'_{O_2} < P_{\ominus} \approx P''_{O_2} < P_{\oplus},$$

$$E_e = \frac{RT}{F}\ln 2 \qquad \ldots(2.12)$$

A schematic illustration of equations (8) through (12) is shown in Figure 2.3.

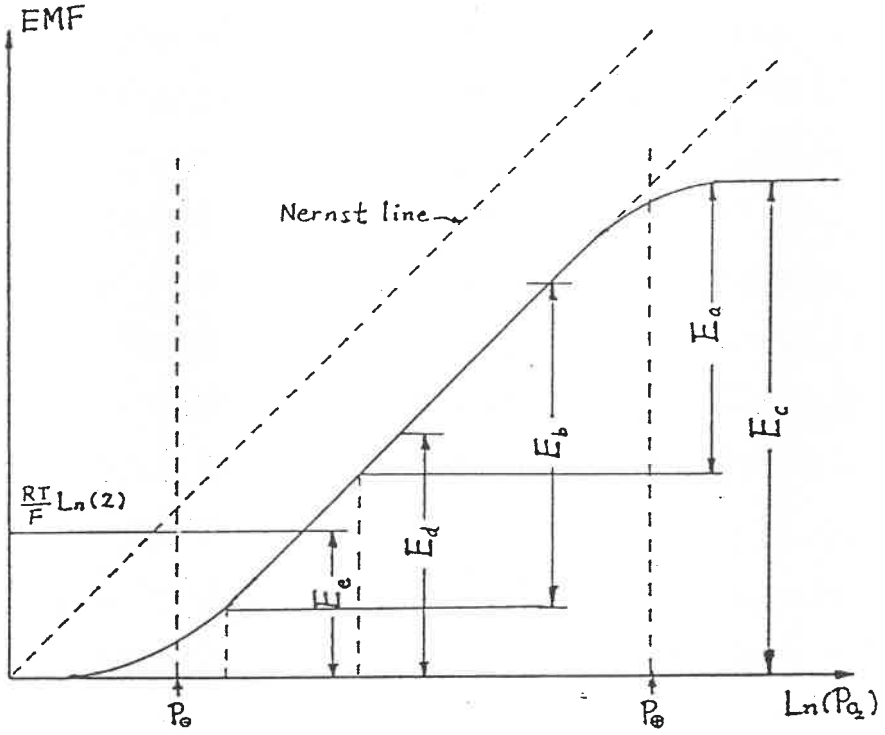

Figure 2.3 Schematic drawing of equation (8) to (12).

Following the experimental determination of $P_\oplus$ and $P_\ominus$[27-34], the extended work on this subject[35,36] has reached the definition of the electrolytic domain, in which the ionic transport number $t_{ion} \geq 0.99$, as a function of P_{O_2} and temperature. The electrolytic domain for CSZ and YDT has been tentatively delineated by considering all the data available, although there was a disagreement on the $P_\ominus$ value for YDT[29-32]. As shown in Figure 2.4, the oxygen partial pressure

range, over which a thermodynamic measurement can be conducted for a galvanic cell using either CSZ or YDT, will become smaller as the temperature goes higher. At a certain temperature, CSZ covers a higher P_{O_2} limit, whereas YDT favors the lower P_{O_2} measurement.

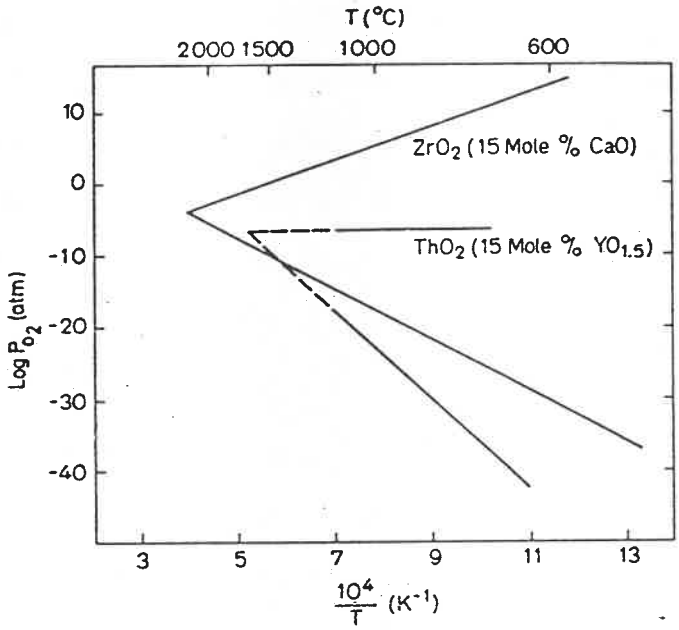

Figure 2.4 Electrolytic domain for CSZ and YDT[15]

A "double cell" involving a combination of CSZ and YDT solid electrolytes has been developed[29] for emf measurements at elevated temperatures, in order to broaden the measurable range of P_{O_2} by making use of both the desired properties of CSZ at relatively high oxygen pressures and that of YDT at very low oxygen pressures. The cell assembly is schematically shown in Figure 2.5. A metal-metal oxide which acts as a

oxygen buffer has been placed between the two solid electrolyte tubes thereby maintaining the oxygen partial pressure in the electrolytic domain of both CSZ and YDT. In this manner, the cell can perform thermodynamic measurements over a considerably wider range of oxygen pressures than using either solid electrolyte alone.

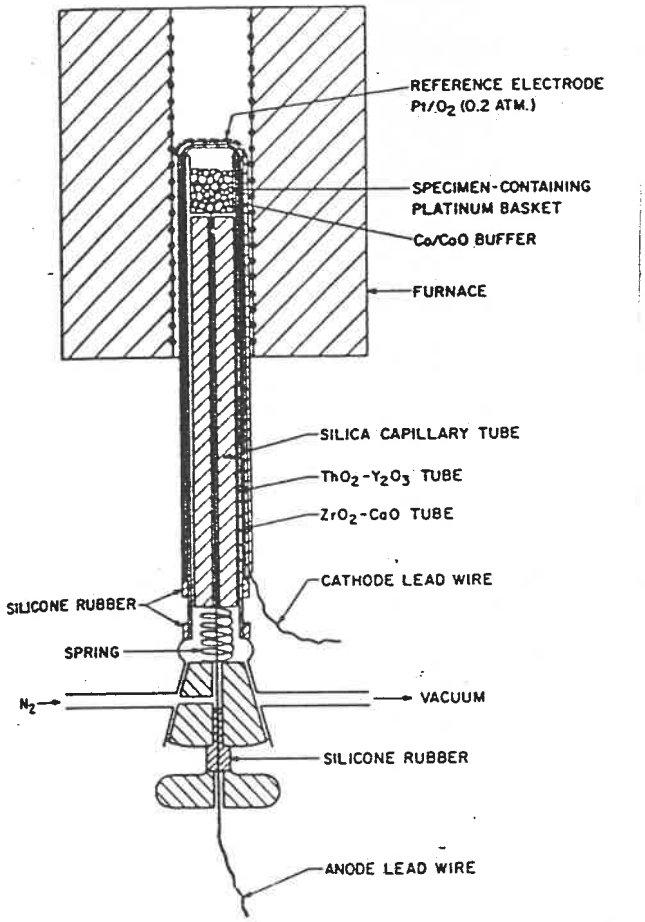

Figure 2.5 A schematic view of a "double cell"[29].

There has been discussion[37] concerning the advantages of the bielectrolyte cell arrangement on a theoretical basis where the oxygen pressure in between the two solid electrolytes was not fixed and might be calculated from the knowledge of the oxygen pressures in the two terminal electrodes and the electrical conductivity parameters for both electrolytes. The analysis[38] based on the theoretical calculation of the steady-state chemical potential profile in a solid electrolyte under open circuit or ion-blocking condition has, in contrast to the above, stressed the importance of keeping P_{O_2} at the interface of two solid electrolytes always lying within the electrolytic domain for both of them. It is clear that voltages less than the thermodynamic value must be expected for the bielectrolyte cell when one or both electrolytes exhibit considerable electronic conductivity.

Methods of Determining Electronic Conductivity Parameters

The values of $P_{\oplus}$ and $P_{\ominus}$ (equation (2.7)) for a specific solid electrolyte play an important role in both the theoretical evaluation of emf and the determination of the electrolytic domain. Several kinds of experimental methods have been developed, including dc polarization measurement[28,39-42], emf measurement on cells with known

oxygen activities[34,43,44], and coulometric titration procedures[29,44,45].

The dc polarization technique, proposed by Hebb[46] and Wagner[47], is based on the steady-state current-voltage measurement on a cell between a reversible and a non-reversible electrode. Although the dc polarization studies were also carried out in a cell between two irreversible electrodes[39-42], its validity was questioned by Joshi[48]. According to Hebb and Wagner, either the ionic or electronic current in a mixed conductor can be suppressed by a properly chosen electrode. To measure the electronic conductivity in an oxide electrolyte, such a non-reversible electrode is chosen that no oxygen ion can be provided from the electrode, and is made negative relative to the reversible electrode. A voltage less than the decomposition voltage of the solid electrolyte is then imposed on the cell. In the steady-state condition, all the current is carried by the electronic charge carrier, i.e. by electrons and/or holes.

Under the assumptions of independent migration of all species, local equilibrium throughout the specimen, independence of the mobilities, $B_{\oplus}$ and $B_{\ominus}$, on concentrations and concentration gradients of ionic and electronic defects, zero ionic current at steady state, and negligible specimen

decomposition, an expression of steady-state current, I_∞, as a function of voltage, E, and temperature has been deduced[28]:

$$I_\infty = \frac{RT}{FL}(\sigma_\oplus^\circ[1 - e^{-u}] + \sigma_\ominus^\circ[e^u - 1]) \qquad ...(2.13)$$

where $\sigma_\oplus^\circ$ and $\sigma_\ominus^\circ$ are respectively the partial positive hole and partial excess electron conductivities, for the oxide electrolyte at the μ_{O_2} of the reversible electrode. L is the distance between the two electrodes. The dimensionless quantity u is given by

$$u = E \cdot F/R \cdot T \qquad ...(2.14)$$

From measurements of I_∞ and E at different P_{O_2} values at the reversible electrode, the dependencies of $\sigma_\oplus^\circ$ and $\sigma_\ominus^\circ$ on the partial pressure of oxygen have been obtained and can be used for the determination of the parameters, $P_\oplus$ and $P_\ominus$ for both CSZ and YDT, in equation (2.7) if the ionic conductivities have been measured separately. This method is characteristic of the simultaneous determination of both parameters.

The emf comparison method has been used in several different ways. Using two different solid electrolytes, CSZ and YDT, to study the same system, Steele and Alcock[43] have

obtained the $P_{\ominus}$ value at 1000°C for CSZ by comparing the emf measurements made with CSZ and YDT which were believed to be totally ionic conductors under the experimental conditions. Alternatively, Baker et al[34] have measured the emf of the cell:

$$Pt,H_2,H_2O(P'_{O_2})/CSZ/(P''_{O_2})H_2,H_2O,Pt \qquad ...(II)$$

at various P_{H_2O}/P_{H_2} ratios, then plotted emf vs. P'_{O_2} to deduce the $P_{\ominus}$ values at different temperatures by noting the kink on the curves. Clearly the $P_{\ominus}$ (or $P_{\oplus}$) value determined in this way would stand in error if the measured emf deviated from the equilibrium value to a large extent by virtue of the material transport through the solid electrolyte. This was observed by Etsell and Flengas[44] in their measurement of emf for a cell similar to (II) with the exception that the P''_{O_2} was fixed at one atm. A strong dependence of emf on the flow rate of H_2O/H_2 mixtures was found and the higher emf at a higher flow rates was attributed to the formation of water by the reaction between hydrogen and oxygen which continuously migrated from the cathode to the anode due to the onset of electronic conductivity at a very low oxygen partial pressure. In fact the increase of the electronic conductivity as P_{O_2} decreases will not only lower the emf by a factor, t_{ion}, but also bring about the electrode polarization. The oxygen

build-up at the anode due to the internal current, if it could not be removed quickly by the formation of water, would definitely result in a lower emf, which should always be avoided in a thermodynamic study.

Compared with the other methods, the coulometric titration technique is rapid and should be accurate if special attention is paid to the conditions required in its application. There are similarities between dc polarization and coulometric titration techniques. In both cases the oxygen is removed from the low partial pressure electrode. The oxygen ion migration will stop completely in the final steady-state when the electronic conductivity becomes predominant.

In the dc polarization technique, the current-time curve is recorded under constant voltage, and the current plateau indicates the steady-state. In the coulometric titration technique, the forced removal of oxygen from the low P_{O_2} side by electrolysis eventually makes $P'_{O_2} << P_{\Theta}$ and the equation (2.11) becomes valid if the reference electrode is kept unpolarized. Then by the interruption of the current withdraw and immediate emf measurement at different temperatures, P_{Θ} can be calculated if an emf plateau is reached. After the interruption, an unsteady emf, followed by a steady one, has

been observed[29] for a cell of double electrolyte in which the oxygen was removed from a gas phase. Alternatively a liquid metal, from which the oxygen was withdrawn, was used[44,45] in consideration of the experimental difficulties of keeping the system gas tight.

Equilibrium at Triple Points

The first two steps for a thermodynamic study by emf measurement constitute choosing a solid electrolyte and being aware of its electrolytic domain. The next step is to prepare electrodes which must quickly attain equilibrium with the solid electrolyte. Usually, the electrochemical reactions taking place at the electrodes of a galvanic cell with a solid electrolyte are characterised by multi-phase reactions. If a gaseous species is involved in an electrochemical reaction, as in the case of a gas sensor, the presence of triple points where the electrode, the gas species, and the solid electrolyte are in physical contact has been considered indispensable to facilitate the establishment of equilibrium[9].

The triple point has also been defined as an electrode microsystem[49] in a study of oxygen electrochemical semipermeability in solid oxide electrolytes. Such a

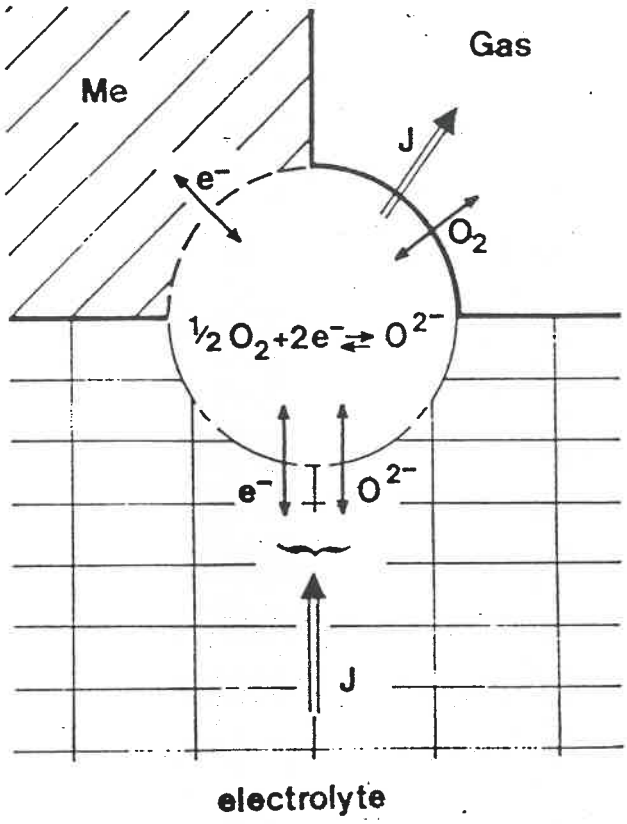

Me: inert metal;
J: local oxygen semipermeability flux.

Figure 2.6 Oxygen electrode microsystem[49].

microsystem is shown in Figure 2.6. EMF measurements with a point electrode[49,50], as shown in Figure 2.7, have demonstrated that it was the concentration of the electro-active species at the triple points which determines the electrical potential of the electrodes.

By considering the presence of the second phase which may be formed on the surface of a solid electrolyte by the penetration of the gas species, Heyne et al[51] have identified two key parameters which determine the response speed of solid electrolyte Galvanic cells for gas sensing.

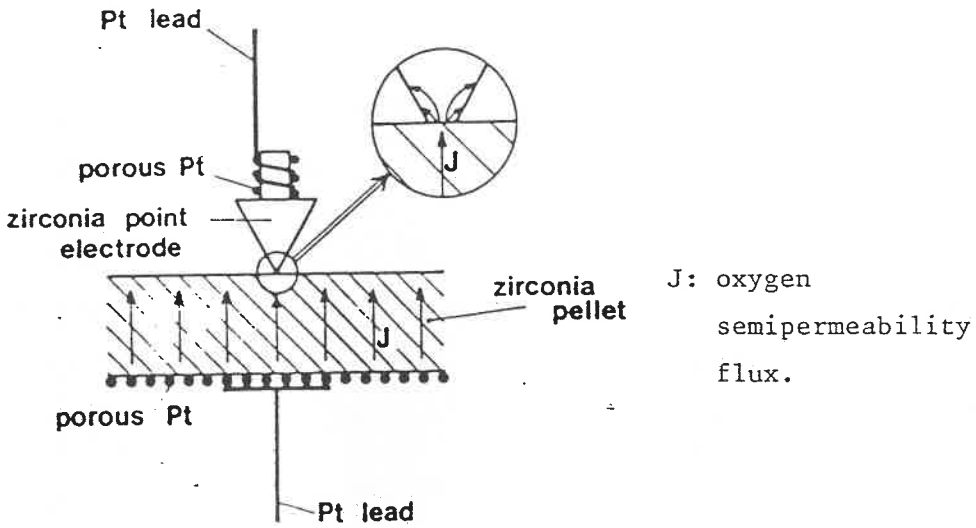

Figure 2.7 Oxygen gauge with ZrO_2 point electrode[49].

The first is the amount of active material involved in the composition change on the surface of the solid electrolyte. The second is the density of material flux with which the required amount can be supplied. Therefore, the analysis of the surface micro-structure of solid electrolyte should be emphasized.

A porous platinum layer is applied to the solid electrolyte surface in nearly all gaseous oxygen sensors because it provides many triple points, making the electrodes less polarizable and emf measurement more reliable. Thus by controlling the type, thickness, and way of application of the metal electrode, the quality of the electrode and the performance of the cell can be improved to a large extent[52,53].

In addition to the number of triple points and the ease of access for the electroactive species to get in and/or away from these points, which can be effectively enhanced by a proper electrode preparation, the catalytic activity of a particular electrode also plays a important role in the achievement of the optimizing conditions for an equilibrium measurement.

Pre-reactions in the Electrodes

In the application of the oxygen sensor to a non-equilibrium system, such as the mixture of air and a fuel in a combustion engine, the emf response has been found[54-57] to depend on the catalytic activity of the electrode material as well as on its physical characteristics, such as porosity and size, the flow rate of the non-equilibrium gas mixture, and the temperature range in which the emf measurement was made. This could be attributed to the pre-reactions which are taking place in the electrodes. Reducing gas species, such as CO or CH_4, tend to react with oxygen at high temperatures, but at reaction rates which depend very much upon the use of catalysts. This makes the measurements non-reproducible and unreliable. Similar problems in cell behavior were observed in developing gas sensors for SO_x[58,59] and AsH_3[60].

Two different possible mechanisms[21,61] have been proposed to describe this kind of phenomena. One is referred to as an electrochemical mechanism, in which the components react with each other in consecutive anodic and cathodic reactions with a zero net current at the phase boundary. This results in a mixed potential at the electrode[62,63]. The other is referred to as a non-electrochemical mechanism, in which a purely chemical transfer reaction proceeds in the adsorbed state. Many catalytic processes involving gaseous species[64] belong to this category. The reactants are adsorbed and dissociate at the electrode surface, where a transfer of atomic species occurs. In stationary reaction conditions, the velocities of yielding and receiving the transmitted particles are equal, and a definite activity of the species determining the potential is attained at the surface and is different from the equilibrium activity[59].

2.3 Other Gas Sensors

In addition to the oxygen sensor, sensors of gaseous species such as CO_2, NO_x, SO_x, etc., have also stimulated much interest[65-89]. These gaseous species are discharged into the atmosphere from metallurgical industrial gas stack or automobile exhausts and constitute a primary source of pollutants in the air.

CO_2 Sensor

The partial pressure of carbon dioxide, in the range 9 ppm to 1.2 % in air, has been successfully measured[65] by the following electrochemical concentration cell:

$$Au \;/\; CO_2, O_2 \;/\; K_2CO_3\,(s) \;/\; O_2', CO_2' \;/\; Au \quad ...(III)$$

The measured emf was found to obey the Nernst equation within ±1.5 mV in the temperature range 575 to 1025 K for all of the CO_2 concentration levels except the lowest one. No emf dependence on flow rate was observed from 100 to 400 ml/min.. The same cell assembly was used to measure the decomposition pressure of $CaCO_3$ from which the standard Gibbs energy change for the decomposition reaction was deduced. The fairly good agreement of ΔG° with published data served as an indication of the valid use of K_2CO_3 as a CO_2 sensor.

NO_x Sensor

An oxide chalcogenide glass with the composition $Se_{60}Ge_{28}Sb_{12}Fe_n$ (n = 1.3 - 2), after being activated by an oxidative heat treatment, has been used[66,67] as an electrode material sensitive to NO_2. Linear proportionality between emf

and $\log(P_{NO_2})$ was found down to 1 ppm NO_2. The exclusive response of emf to NO_2 in the presence of other gas species such as O_2, NO, N_2, CO, SO_2, and CH_4 has been attributed to the preferred chemisorption process of NO_2 on the electrode. Since no simple redox couple was found to be responsible for the emf, a mixed potential mechanism has been considered[21] but could not be reconciled with the mechanism of a reversible chemisorption suggested by the authors[67]:

$$NO_2(g) + G_{(\text{electrode surface})} = NO_2G(s) = NO_2^- + G^+ \quad ...(2.15)$$

A solution of fused salts[68] has been used as the electrolyte in the following cell assembly:

$$Ag/\ Ag^+ \text{ in } (Na,K)NO_3\ //\ (Na,K)NO_3\ /\ NO_2,\ O_2,\ Pt \quad ...(IV)$$

The overall cell reaction is the formation of silver nitrate in the nitrate solution electrolyte from pure Ag, NO_2, and O_2. The partial pressures of NO_2 and O_2 were controlled by N_2, NO_2, and O_2 mixtures. Over the temperature range of 250° to 325 °C, the P_{NO_2} range of 0.363 to 0.754 atm., and the P_{O_2} range of 0.11 to 0.454 atm., the emf for cell (IV) was found to follow the Nernst equation although the dependence of the Nernst plot slope on the flow rate of gas mixture above 60 ml/min. was detectable.

The substitution of gold for platinum had no effect on the results, indicating a non-catalytic electrode reaction at the cathode. From a known activity coefficient of $AgNO_3$ in the electrolyte, and from the Nernst equation, the standard Gibbs energy change for the overall cell reaction was obtained. The value agrees with previous measurements, indicating that this cell unit might be used as a NO_2 gas sensor. The fused salt was replaced by solid $Ba(NO_3)_2$ with 1% AgCl addition in a similar work[58] for the purpose of developing a NO_2 sensor and a linear relation between emf and $\log(P_{NO_2})$ was observed.

More recently, a sensor for gas species which is not the charge carrier in the solid electrolyte has been proposed[69-72]. The activities of the mobile component in the electrolyte and the gas component under measurement are correlated by an auxiliary gas sensitive layer. The auxiliary layer may be porous or should show high chemical diffusion coefficients in the case of dense materials. In the NO_2 sensor studied[70] (Figure 2.8), Ag^+-ß-alumina and Na^+-ß-alumina have been chosen as the solid electrolytes whereas $AgNO_3$ and $NaNO_3$ as the gas sensitive materials in the following cell design:

Pt/M/M-ß or ß"-alumina/MNO_3/Pt, NO_2(g),O_2(g) ...(V)

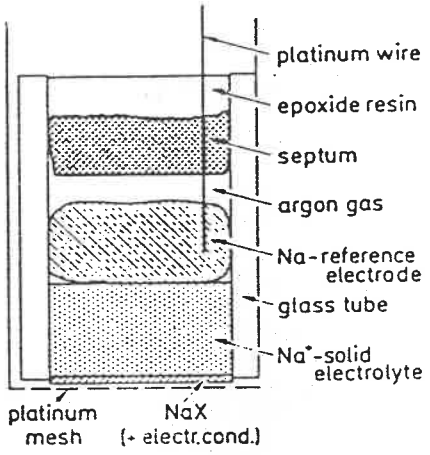

Figure 2.8 A schematic representation of cell (V)[70].

The overall cell reaction is the formation of the nitrate:

$$M(s,l) + NO_2(g) + O_2(g) = MNO_3(s,l) \quad ...(2.16)$$

where M = Ag or Na. Under the conditions of fixed P_{O_2} and unit activities of metal and metal nitrate, the emf of the cell will respond to the concentration of NO_2 in a definite way. Values of emf corresponding to concentration of NO_2 as low as 0.1 ppm, which is beyond the detection limit of the infrared spectroscopic measurement, were measured and agreed with the theoretical values from the Nernst equation.

In a second series of measurements, large amounts of NO (0.01 atm.) were added to the gas mixture. The emf corresponding to the NO_2 formed by the oxidation of NO was approached, indicating that the most oxidized state of the gas

species was detected by this cell design.

It is worth pointing out that this form of cell assembly can be applied to many gas species, including those mentioned above as air pollutants (CO_2, SO_2 etc.). From a thermodynamic point of view, the gas sensitive layer present on the surface of the solid electrolyte is an indispensable part of the electrode in which the activity of the conducting element is fixed, making the cell unit behave reversibly. Furthermore, the state of the sensitive layer and its reactivity with the solid electrolyte are two important factors which are considered to have a direct effect on the operative qualities of the gas sensors, for example, the response time, the reproducibility and reliability of the measurement, and so on.

AsH_3 Sensor

Arsine, AsH_3, appears as an undesirable toxic impurity in hydrometallurgical processing of certain Cu, Ni, Au and Ag ores. In order to develop a highly sensitive and selective as well as inexpensive sensor for arsine, several cationic conducting ceramics such as Na^+-β-Al_2O_3, Ag^+-β-Al_2O_3, $NaCaAsO_4$, and $AgZr_2(AsO_4)_3$ [73] have been tested with a successful emf response to the content of AsH_3 in air. Among the solid electrolytes tested, the Ag^+-β-alumina was found to

be particularly attractive due to its simple cell design. Two types of sensor assemblies were tested and are shown in Figure 2.9. The cell unit is represented[60] as follows:

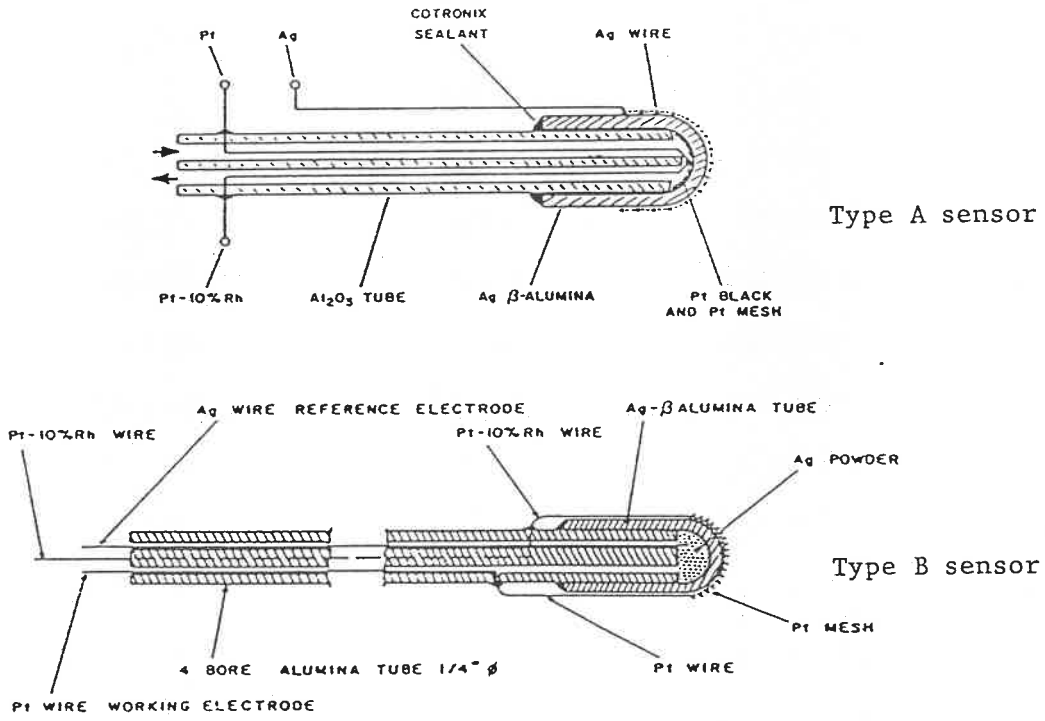

Figure 2.9 A schematic depiction of cell (VI)[60].

$$\mathbf{Ag(s) \;/\; Ag^{+}\text{-}\beta\text{-alumina} \;/\; AsH_3(g),\; O_2(g),\; Pt \;\ldots (VI)}$$

Compared with cell (V), there are two special features in cell (VI) which are different although similar.

The first is the oxidation of arsine in the gas phase to form the arsenic oxide which is electro-active species in the

electrode reaction before the gas mixture gets to the surface of electrolyte. Therefore the dependence of emf on the flow rate of gas mixture was observed and it was necessary for a catalyst to be present along the gas passage so that the pre-reaction can be promoted to reach the equilibrium.

The second is the formation of silver ortho-arsenate on the surface of the solid electrolyte during the initial period of an experiment run, which made the electrode eventually reversible. In fact, it is the formation of Ag_3AsO_4 which provides the gas sensitive layer mentioned previously. The consequence of this feature is the uncertainty of the physical and chemical properties for the sensitive layer because its formation, which requires a massive transport of conducting component from one side to the other, is not favored under the conditions of emf measurement.

2.4 Electrolytes Used in Developing SO_x Sensor

A fairly large number of investigations[58,59,68,74-89] have been conducted in order to develop an SO_x (SO_2 or SO_3) sensor because of the severe environmental problems caused by sulfur dioxide emissions, for example, "acid rain", which is mainly attributed to the SO_x absorbed by water.

Mixture of Molten Sulfates

A molten salt mixture composed of Ag, Li, Na, and K sulfates has been used[68] as an electrolyte in the following galvanic cell:

$$Ag/Ag^{+}(1M) \text{ in } (Li,Na,K)_2SO_4//(Li,Na,K)_2SO_4/SO_3,\ O_2,Pt \quad \text{(VII)}$$

The emf was found to be independent of the gas flow rate (up to 180 ml/min.) at the cathode. A linear relation between emf and $\log(P_{SO_3}\ P_{O_2}^{1/2})$ was observed at 550°C, from which the standard Gibbs energy change for the overall cell reaction:

$$Ag(s) + SO_3(g) + 1/2\ O_2(g) = AgSO_4\ _{\text{(in molten salt)}} \quad \ldots(2.17)$$

was deduced to be -111.3 ± 4.2 kJ/mole. In this study the gas mixture was prepared by passing a mixture of N_2 and O_2 over liquid SO_3 in a boiling flask. Any decomposition of SO_3 to SO_2 was ignored, probably due to the unfavorable kinetic conditions in the experiment.

In a more recent study[74], a similar mixture of the same sulfates was used as the electrolyte and a gas mixture of SO_2 and O_2 was passed over both the reference and working electrode, at a relatively low concentration of SO_2. A

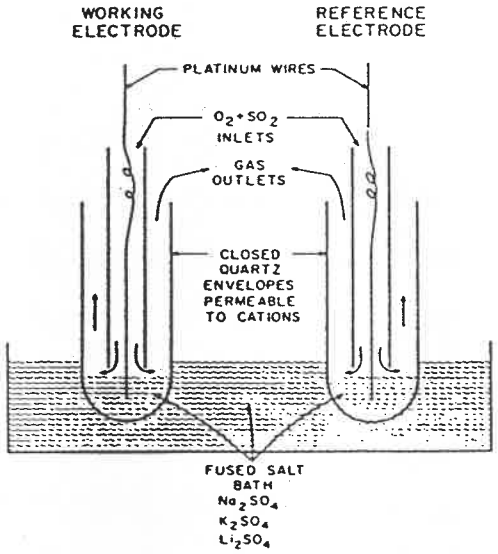

Figure 2.10 The cell using a molten sulfates mixture[74].

schematic view of the cell is shown in Figure 2.10. Since the basic response of the cell was found to be to SO_3, the oxidation of SO_2 was assumed and the dependence of emf on the flow rate of gas mixture was ascribed to the unequilibrated conversion of SO_2 at a higher flow rate. If the two gas electrodes matched each other (having same P_{O_2} at equilibrium), the cell unit would function as a SO_2 detector in the low concentration range. A Nernstian slope for SO_2 concentration lower than 1% was observed.

Pure Solid Sulfate

Unlike a liquid electrolyte, the solid electrolyte can be fabricated in the form of a tube or pellet. The tube (or pellet) simplifies the cell design and the gas sensor can be

readily used to monitor the content of a gaseous species. This feature is particularly attractive for applications in process control where high temperatures are involved, such as in metallurgical processing.

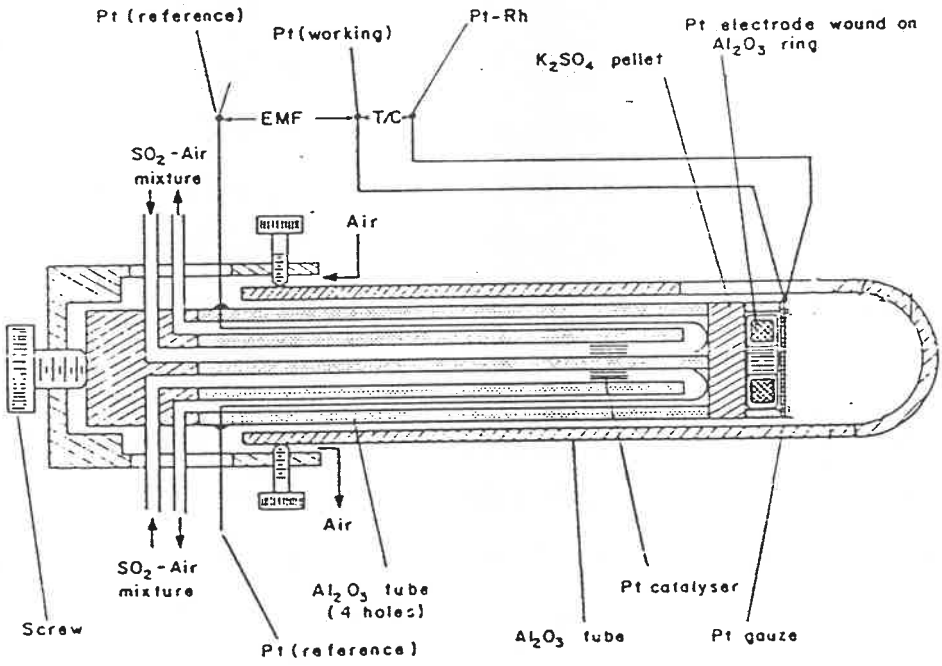

Figure 2.11 The cell using pure K_2SO_4 (s) electrolyte[58].

Solid potassium sulfate has been employed[58] as the electrolyte in a cell with the application of both a gas reference electrode and an Ag/Ag_2SO_4 reference electrode. A cell unit is depicted in Figure 2.11. Although there is no report on the study of the ionic transport number for this electrolyte, it is believed to be equal to unity because the emf measured agreed within ±1mV with that calculated

theoretically above 650 °C. Below 650 °C, the deviation from linear relation of emf vs. temperature plot at one SO_2 ratio was found to occur in the case of gas reference electrode. A straight line of emf vs. $\log(P_{SO_2})$ plot was observed at 820°C in the case of $Ag/AgSO_4$ reference electrode. Since several different gases of sulfur-containing species, such as H_2S, CH_3SH, and COS, produced the same emf signal as SO_2 at the same concentration level in air, it was concluded that these gases were converted rapidly into SO_2 under the experimental conditions. It was also concluded that under certain given conditions, equilibrium among SO_2, O_2, and SO_3 was reached quickly, at least in the area closest to the electrode.

Further work on different types of reference electrodes[75,76] has revealed that the gas-circulation electrode is more stable and reliable than the $Ag/AgSO_4$ electrode although it presents certain practical drawbacks. The prospect of the reference electrode based on the thermal decomposition of solid sulfate-oxide mixtures as well as the application of non-catalytic metal electrode to monitor exclusively SO_3 in the presence of SO_2 was also proposed.

In another experiment, a study on sodium sulfate[77] was carried out by first measuring the ionic transport number of its high temperature form, Na_2SO_4-I, (which has a modified α-

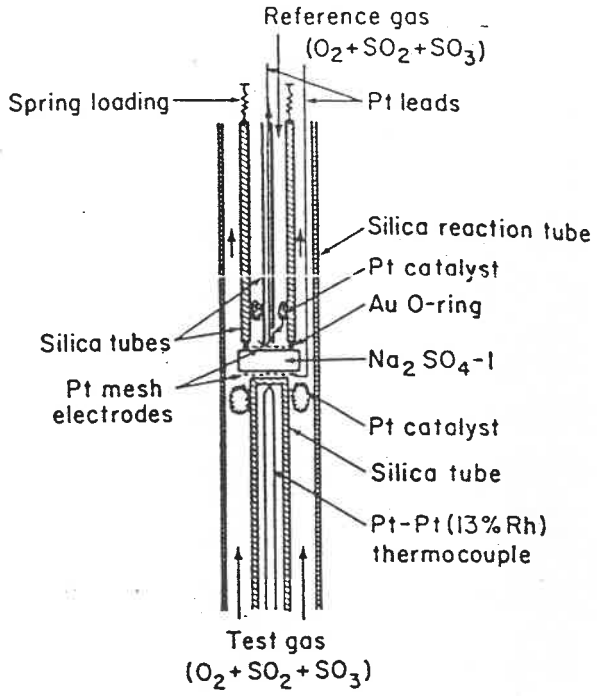

Figure 2.12 The cell using pure Na_2SO_4-I(s) electrolyte[77].

Ca_2SiO_4 structure) at 700 K, then monitoring the concentration of SO_3 in an identical cell design, as shown in Figure 2.12. The ionic transport number was found to be unity and the behavior of the emf as a function of $\log(P_{SO_3} \cdot P_{O_2}^{1/2})$ led to the same conclusions as above. Pure lithium sulfate has also been considered[78] as a candidate for monitoring SO_x but without success due to its hydroscopic nature, although it has comparatively high ionic conductivity.

Solid Solution of Sulfates

From a practical point of view, the solid reference electrode such as $Ag/AgSO_4$ simplifies the cell unit design and

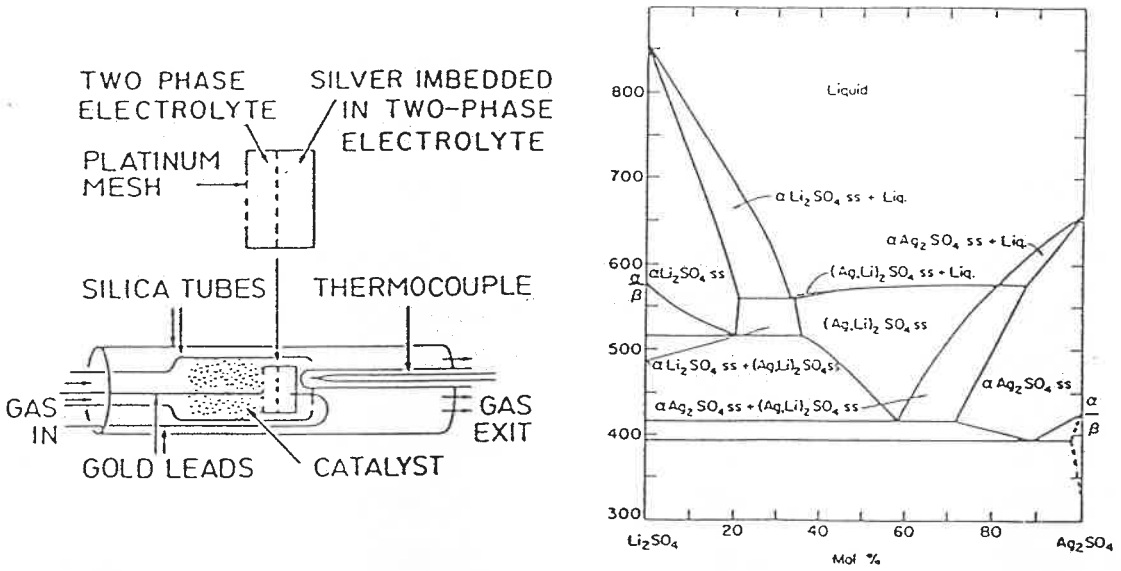

Figure 2.13 The cell using a two-phase electrolyte[79].

makes the emf measurement more convenient. Unfortunately, the convenience is often accompanied by a lose of stability of emf created by the interaction between the electrode and the electrolyte. A mixture of two solid solutions in the Li_2SO_4-Ag_2SO_4 binary system has led to a better performance[79,80] for both the reference electrode and the solid electrolyte for the SO_x sensor. A schematic view of the two phase electrolyte sensor, together with the phase diagram of Li_2SO_4-Ag_2SO_4 binary system, is shown in Figure 2.13. The two phase mixture functioned as a buffer for the sulfate which was involved in the overall cell reaction. The activities of the sulfates were kept constant during a long term experiment. The only shortcoming of the two phase mixture solid electrolyte lies in the limited temperature range of 510° to 560°C where the two phases can stably coexist.

Sodium sulfate doped with $NaVO_3$ and $Ln_2(SO_4)_3$ (Ln = Pr, Y) has also been found[81] to have good properties as a solid electrolyte. It shows no phase transformation and maintains a Na_2SO_4-I-like phase. As a potential SO_x gas sensor material, it was tested at 400°C and relatively high SO_2 concentration levels. The concentration of SO_2 in the reference electrode had an effect upon the measured emf. Below about 5% SO_2, a deviation of measured emf from that calculated occurred. Further measurements at different temperatures and lower SO_2 concentration levels are needed to fully characterise this behavior.

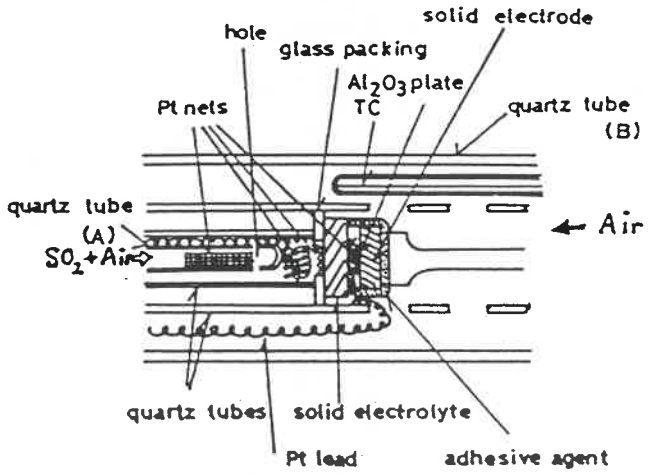

Figure 2.14 The cell using a mixture of solid sulfates[81].

In order to overcome the phase transformation problem for alkali-metal sulfate solid electrolytes, a mixture from the Na_2SO_4-$Y_2(SO_4)_3$-SiO_2 ternary system was prepared[82] and used as an electrolyte. The cell assembly is shown in Figure 2.14.

Various metal sulfate-oxide mixtures were employed as the reference electrode: $MgO/MgSO_4$, $Mn_2O_3/MnSO_4$, $NiO/NiSO_4$. The $NiO/NiSO_4$ mixture showed the best agreement between the measured and theoretical emf.

An effort was made[83,84] to increase the ionic conductivity at relatively low temperatures by adding Li_2SO_4 to the mixture. The emf measurement using the mixture of the quaternary system as the solid electrolyte to monitor SO_2 has shown that the best agreement with the calculation was achieved for the solid reference electrode at the higher temperature range studied. The disagreement of emf with the calculation at the lower temperature range was attributed to the uncertainty of the thermodynamic data for the sulfates involved in the overall cell reaction.

β(β")-alumina

β-alumina, by virtue of its high chemical stability and ionic conductivity, has been considered recently[85-88] as an electrolyte for monitoring the content of SO_x in a gas phase. The following cell design was first studied[85]:

Pt,Ref. / Na^+-β"-alumina / $SO_2+SO_3+O_2$,Pt ...(VIII)

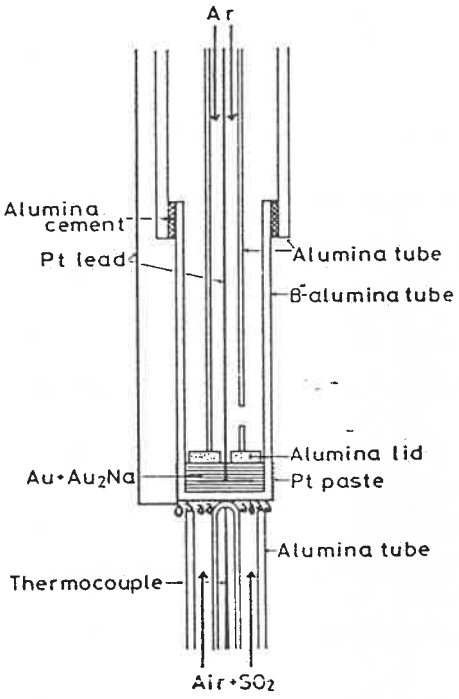

Figure 2.15 Schematic representation of cell (VIII)[85].

where Ref. is the reference electrode which fixes the chemical potential of sodium. A solid reference electrode is preferred. A mixture of Au + Au_2Na(s) has been employed successfully as the reference electrode to sensor SO_2 in the range of 0.9 - 9000 ppm in the temperature range from 821 K to 1108 K. Figure 2.15 is the schematic representation of the cell studied. The determination of sodium activity in the mixture was carried out by another independent Galvanic cell measurement in order to compare the theoretical emf and the experimental value measured in cell (VIII). The mixture of β and β" alumina powder is a possible alternative reference electrode in the higher temperature range.

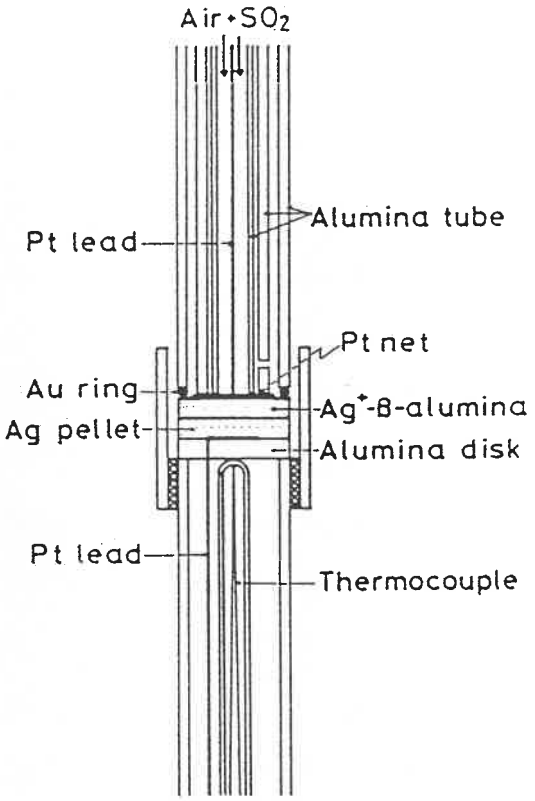

Figure 2.16 Cell unit using Ag^+-ß-alumina electrolyte[86].

Replacing Na^+-ß-alumina in cell (VIII) by Ag^+-ß-alumina[86] is an attractive alternative because of the potential application of pure silver as the reference electrode. The cell assembly is shown in Figure 2.16. A linear relation between emf and $\log(P_{SO_2})_{in}$ was observed for the concentration of SO_2 in the range from 10 ppm to 1% over the temperature range from 713 K to 1113 K. Under the assumption of silver sulfate formation being the overall cell reaction, the measured emf was compared with, and found to be higher than that calculated theoretically in all the concentration

and temperature ranges studied. A response time of 3 minutes, which is superior to the Na^+-ß-alumina, was reported.

The essential requirement for thermodynamic measurements is the formation of a layer of sulfate on the surface of the ß-alumina in the working electrode compartment. This layer was identified[86,87] by means of an electron probe X-ray microanalyzer (EPMA). After being exposed to the gas mixture of SO_x + O_2 for more than 3 hours, the surface of the ß-alumina samples was analyzed for Na, S, and Al. The scanning electron microscope (SEM) photographs of the samples showed that there was an abrupt increase of the concentrations of sodium and sulfur on the surface, which, together with X-ray emission spectra of the surface and a weight increase of the sample, was attributed to the formation of the sulfate. Accordingly, the higher emf measured than that calculated in the case of Ag^+-ß-alumina was explained[86] by a proposed formation of sulfate solution in the Ag_2SO_4-$Al_2(SO_4)_3$ binary system instead of pure silver sulfate. This explanation is still open to discussion, taking into account the uncertain chemical and physical properties of the sulfate formed on the surface of the ß-alumina.

Other Solid Electrolytes

NASICON, which is known to be a fast sodium ion conductor with the stoichiometric formula $Na_3Zr_2Si_2PO_{12}$, has been used[89] as a solid electrolyte with gas mixtures of $SO_2 + O_2$ flowing over both electrodes. As in the case of ß-alumina, sodium sulfate was formed on the surface of NASICON, leading to the same cell reaction as with Na_2SO_4. Nevertheless, NASICON was found to be superior, when used for measuring SO_2 pressure difference over several orders of magnitude, because of its high density obtained in the sintering process. In addition, good selectivity to SO_2 was reported. The presence of CO_2 and/or NO_2 in the gas mixture had no influence on the emf measured. At 1049 K, the emf response to a P_{SO_2} change was within 3 minutes, a relatively fast responding time. The Nernst equation was obeyed only above 929 K, limiting its application to a relatively high temperature range.

The possibility of using ZrO_2(8% Y_2O_3) solid electrolyte to monitor SO_x has been proposed[59] according to the measurement of steady-state oxygen activity on Pt electrode in the presence of SO_2. Depending on the temperature and gas phase composition, a cell with platinum electrodes could monitor SO_2 or SO_2/SO_3.

2.5 β-Alumina Solid Electrolyte

There are several reviews on β(β")-alumina solid electrolytes. Among them, the articles by Kummer[90], Kennedy[91], and Collongues et al[92] should be cited.

Crystal Structure

The composition of sodium β-alumina corresponds to $Na_2O \cdot 11Al_2O_3$ but varies up to $Na_2O \cdot 9Al_2O_3$ due to the presence of 15% - 30% excess Na_2O relative to the ideal formula. The crystal structure of hexagonal β-alumina, with a axis 5.594 Å and c axis 22.53 Å, consists of four cubic close-packed layers of oxygens with $3Al^{3+}$ ions occupying some of the resulting octahedral and tetrahedral positions between each pair of oxygen layers, giving a typical spinel-like composition of Al_3O_4. These spinel-like blocks are separated by so-called mirror planes containing a loose packing of Na and O ions, the spacing between these mirror planes being 11.2 Å. The nearest Na-O distance, 2.87 Å, is much larger than the sum of their ionic radii, 2.35 Å. This fact, together with the large number of the available but unoccupied sites for Na^+ ions, is responsible for the large Na^+ ion diffusion and ionic conductivity in the plane perpendicular to the c axis.

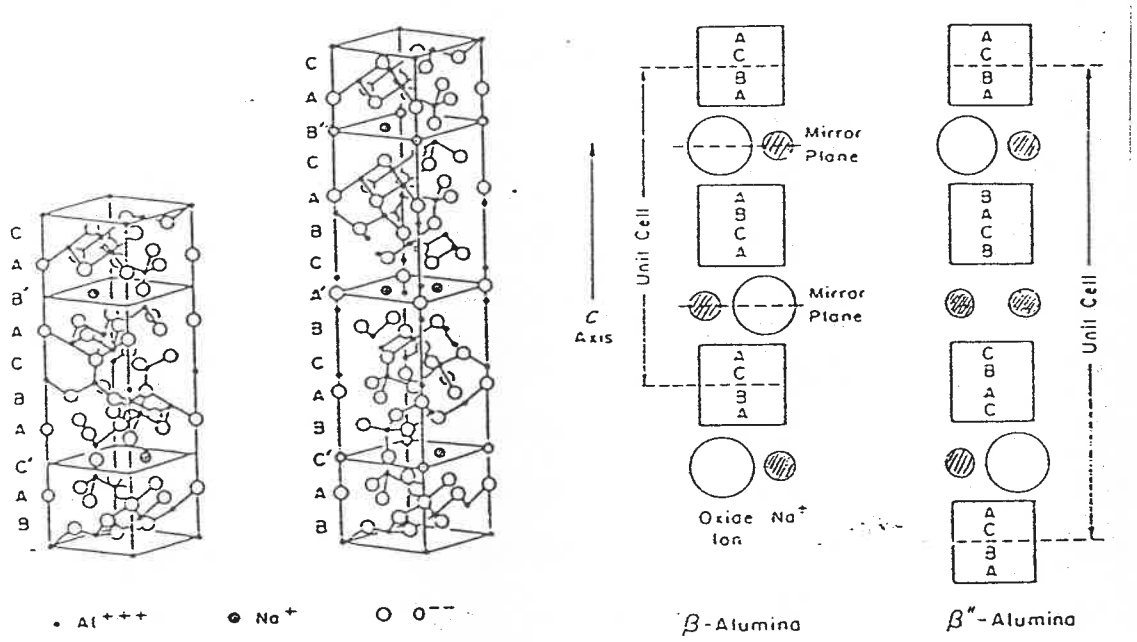

Figure 2.17 Distribution of Na^+ ions in ß and ß" alumina[91]

The ratio of Na_2O to Al_2O_3 is 1:5 - 1:7 for the related ß"-alumina which is stable below 1500°C but needs to be stabilized with MgO or Li_2O in order to be sintered at higher temperature. Compared with ß-alumina, the structure of ß" is more complicated. There are three spinel blocks per unit cell so that the c axis is enlarged to 33.51 Å. The conduction plane is sandwiched between two mirror planes. Due to the larger concentration of charge carriers (Na^+) and the greater space available for its motion, the ionic conductivity of ß" is larger than that of ß-alumina. A schematic representation of ß and ß" alumina crystal structure is shown in Figure 2.17.

Ion-exchange

From a practical point of view, a useful property of beta alumina is the fact that the cation in the conduction plane can be easily replaced by another cation through an ion-exchange process, making a variety of cation conducting solid electrolytes available. The feasibility and the extent of the ion-exchange depends upon both the relative magnitude of the ionic radii and the composition of exchanging medium. Usually, a molten salt is chosen as the medium. Complete substitution of Ag^+, Tl^+, K^+, Rb^+, and NH_4^+ for Na^+, Li^+ and In^+ for Ag^+ has been reported[93]. Partial substitution and slow exchanging rate of some divalent ions for Na^+ in β-alumina has also been observed and ascribed either to an unfavourable equilibrium or to a low diffusion rate, or to a combination of both. β"-alumina has been reported[94] to be superior to β for divalent ion exchange, probably due to the fact that more sodium ions are present on the conduction plane so that the accommodation of the divalent ions is made easier without breaking the electrical neutrality.

Ionic Conductivity

The relative ionic conductivity, or more precisely the ionic transport number, of a solid electrolyte is important in

thermodynamic measurements. In principle, the dependence of the electronic conductivity on the chemical potential of the conducting element in the solid electrolyte of a multicomponent system should be evaluated. This can be performed with the aid of dc polarization techniques and an electrolytic domain can be identified, as for example in the case of CSZ or YDT oxide solid electrolytes, as a function of temperature and chemical potential of conduction component. Unfortunately, it is not as easy to control the chemical potential of the metal cation conducting element. Therefore, the ionic conductivity of a single crystal of Na^+-β-alumina has been measured[95] by means of a standard ac bridge at -150° to 820°C under an inert atmosphere whereas the electronic transport number at 25°C was determined[96] to be well below 0.005 by an emf comparison method where the emf measurement based on an amalgam concentration cell was carried out.

The only work where the polarization method[46,47] has been used is the study on the transport properties of silver beta alumina[97]. By imposing a voltage which was below the decomposition voltage of Ag^+-β-alumina on the sample between a silver cathode and a platinum anode, a current plateau was recorded, from which the electron conductivity was found to be several orders less than the total conductivity determined by

ac impedance bridge method. The current-voltage characteristic curves were found to be similar to that obtained for AgBr[98] and AgCl[99], but depended on the oxygen partial pressure at the platinum anode side.

The ionic conductivity of a Ca^{2+}-β"-alumina single crystal obtained by ion-exchanging process was measured[100] by means of an ac impedance bridge. An Arrhenius behavior between 250° and 450°C with an activation energy of 0.57 eV for bulk Ca^{2+} ion conduction was reported. Measurements using a polycrystalline Ca^{2+}-β"-alumina tube fabricated by slip casting[101] were also performed and as expected, a relatively lower ionic conductivity than that of a single crystal was reported. Very often, the electronic conductivity of a solid electrolyte is not measured, but the thermodynamic measurements[102] with which the previously published data agreed has been considered as an indication of valid application of the electrolyte at least under those particular experiment conditions.

2.6 Electrodes and Electrode Process

From an experimental point of view, an electrode can be defined as a location in a chain of electric conductors where the conductivity changes in nature from an electronic to an

ionic conductivity. In thermodynamic measurements, an electrode must be a good electronic conductor. It must equally be a source or sink of the ionic conducting element in the solid electrolyte so that the measurement can be unambiguously related to the cell reaction.

Reference Electrode

There are several requirements for a reference electrode[6,16]. First of all, it should be able to fix the activity of either the conducting component or its counterpart in a solid electrolyte of a binary or quasi-binary system over the temperature range studied. For a gas electrode or any other kind of non-electronic conducting electrode, the second requirement is the employment of an electronic conductor, usually a noble metal, which is chemically inert to the solid electrolyte. For a coexistence electrode where two or more phases are physically mixed, absence of phase transformations as well as chemical inactiveness are required. Moreover, for an indirect electrode[16] where thermodynamic data are determined for reactions involving an element for which a solid electrolyte is not available, chemical and phase equilibria within the electrode are required.

Reversible Electrode and Reversible Process

An electrode which can provide or accept both electrons and ions is called a reversible electrode. For a cation conductor electrolyte, the corresponding metal is a candidate of the reversible electrode whereas in the case of an anion conductor, it is necessary to have an inert electronic conductor if the chemical potential of the conduction element is fixed by a non-electronic conducting system. A variety of reversible electrodes have been classified and discussed elsewhere[16]. There is also an experimental definition of the reversible electrode in which an electrode-electrolyte combination at equilibrium is not displaced from equilibrium by the passage of a small current in either direction through the cell. In addition, the latter definition is frequently used to check the reversibility of the cell reaction, but attention must be paid to the difference between the reversible electrode and the reversible process.

The Gibbs energy change of a cell reaction is related to the reversible emf of the cell. Experimentally it is necessary to pass a small current through the cell so that electrical measurements can be performed. As a result of this current flow, though it is restrained to a low level by the high internal impedance of the measuring instrument, there is

a consumption of the reactants and a release of the products of the cell reaction at the anode and the cathode respectively, which disturbs the equilibria built up at the electrodes. Steady emfs are not disturbed as long as all the elementary reaction steps of the cell reaction and other transport process, if any, can keep up with the current flow, leaving the activities of all the electroactive species unchanged. The ability for an electrode to keep its equilibrium state may be classified as its unpolarizability.

Thermodynamically, any process which occurs at an appreciable rate is proceeding irreversibly[103,104], and therefore strictly speaking any electrode reaction which proceeds at a finite rate is thermodynamically irreversible. Accordingly, the application of a reversible electrode in thermodynamic measurements does not guarantee that a reversible emf will be measured. The use of less polarizable electrodes tends to minimize experimental errors.

The polarizability of an electrode depends upon many factors, such as the physical state and the geometrical shape of the electrode, the temperature and pressure of the system, and even the electrochemical reaction taking place at the interface between electrode and electrolyte. Generally, an electrode reaction consists of several elementary steps[141],

one of which is the slowest and called the rate determining step (r.d.s.) because it governs the rate of the overall reaction. In fact, the study of electrode processes will eventually reveal the r.d.s. of the cell reaction, and lead to a means whereby the electrodes are made less polarizable.

Diffusion of Electro-active Species

The electro-active species are those which are directly involved in the electrochemical reactions occurring at the interface between the electrode and the electrolyte. It is the concentration of the electro-active species that determines the electrode properties such as the electrode potential, the double layer capacity and so on. The deviation of the emf from the reversible value, resulting from the variation of electro-active species concentrations, occurs if there are some difficulty in the diffusion processes for these species to get into and away from the electrode micro-system.

The electro-active species may be a gas species diffusing through a boundary layer in gas phase or through a condensed phase. In the former case, any factor that can reduce the thickness of the boundary layer will speed up the diffusion process, whereas in the latter case, an increase of the porosity of the condensed phase will be beneficial. Thus, the

use of a porous platinum layer as inert electrode has become a common practice, particularly in thermodynamic measurements involving gaseous species.

If ions are involved in the diffusion process, for example in the scaling process of a metal oxidation, the application of an electrical field will have an influence on the rate of the oxidation as demonstrated[105,106] in the studies of silicon oxidation where the oxygen ion was found to be the only species diffusing through the oxide film. AgI is an ionic conductor through which Ag^+ diffuses. By solving diffusion equations of the scaling process[16] of AgI on Ag, the average electronic transport number for AgI has been estimated and the possibility of using this method for identifying new solid electrolytes has been proposed.

Studies of direct current-voltage characteristics have been carried out[52,107,108] to investigate the electrode reaction of oxygen on platinum with CSZ solid electrolyte. The cathode process was found to be responsible for the non-ohmic overpotential recorded. From the observation of a limiting current at a relatively low applied voltage, a diffusion controlling step was readily identified[52]. Based on Fick's first law, the diffusion overpotential was expressed as[108]:

$$\eta = \frac{RT}{nF}\ln\frac{i_l}{i_l - i} \qquad \ldots(2.18)$$

where i_l is the limiting current density and n is the number of electrons associated with the slow diffusing species that are involved in the electrode reaction. From the slope of a plot of equation (2.18), using the experimental data with a porous platinum electrode[108], it was found that four electrons were involved in the diffusion process, indicating the r.d.s. is oxygen molecule diffusion through the platinum electrode pores.

The current-voltage characteristics method was also employed[109] to study the diffusion of oxygen in liquid silver. The diffusion overpotential was observed when the silver electrode was made a cathode, and was attributed to the depletion of oxygen at the metal-electrolyte interface due to the relatively low diffusion coefficient of oxygen in the liquid. The limiting current was found to be directly proportional to the concentration of dissolved oxygen, which could provide an alternative to the electromotive force method for the determination of the oxygen content in liquid metals and alloys.

Adsorption/Desorption Processes

There is an apparent relationship between the adsorption of a gas species on a solid surface and the catalytic effect of the solid on the reaction involving the gas. Because of its spontaneous feature, any adsorption process results in lowering the energy of the system. On the other hand, a catalyst present in a system will not change the energy of the system, but make a reaction occur more easily by lowering the activation energy for one of the elementary steps, usually the r.d.s., of the reaction. Thus, if one of the reaction steps involves adsorption, as proposed for many electrode reactions involving gas species[53-55,59,64,107], the use of a catalyst will lead to the activation of the adsorption process since it is the catalyst itself that usually provides the adsorption sites.

In the measurement of oxygen concentrations under non-equilibrium conditions with a solid electrolyte[54,55], it is the catalytic effect of the electrode that should be avoided. Therefore, a poisoned electrode[54] has been found to be suitable for non-equilibrium oxygen measurements without losing the good properties of the electrode (for example adsorption and/or dissociation of oxygen) for oxygen monitoring. A layer of an oxide on the platinum electrode

exposed to the non-equilibrium gas mixture has been found[55] to change the catalytic efficiency of the electrode drastically, which might result from the intimate contact between the oxide and platinum layer, thereby greatly reducing the surface area and associated catalytic effect of the platinum layer. Polarization studies on a variety of electrode materials[53] have demonstrated the importance of the catalytic nature of the electrode material and its surface.

Compared to the process of the adsorption, the desorption process usually proceeds with difficulty because it is required to overcome a higher energy barrier[142], making it a rate determining step. The SO_3 adsorbed on the platinum has been found[59] to reduce the catalytic activity of platinum for the oxidation of SO_2 because of the difficulty with which the liquid like adsorption layer of SO_3 could be removed. A method to remove electrochemically oxygen in order to enhance the decomposition of NO on platinum metal has been proposed[110,111] since the preferential chemisorption of O_2 over NO as well as the possible formation of an inhibiting platinum oxide surface must have caused the reduced catalytic activity.

Electro-chemical Reaction

If the electrochemical reaction step, in which the charge transfer is involved, is the rate determining step of an electrode reaction, the Butler-Volmer equation is readily deduced[112] with two parameters, i_0, the exchange current and α (or $\beta = 1 - \alpha$), the cathodic (or anodic) transfer coefficient, being determined. Usually the parameters can be obtained from a Tafel plot of the experimentally determined current-overpotential data. The overpotential caused by the slow electrochemical reaction step is called transition or charge-transfer overpotential. The anodic and cathodic processes of oxygen in the presence of CO/CO_2 mixture have been found[101] to be controlled by the electrochemical reaction:

$$O_{ad} + 2e = O^{2-} \qquad \ldots(2.19)$$

From the Tafel plots at 850 - 1100 °C, $\alpha = \beta = 0.5$ and the exchange current densities ranging between 0.1 and 1.6 mA/cm^2 were found. It was also reported that the current density increased as either temperature or the CO concentration increased.

Formation of Solid Layers

In some of the above gas sensors, the over-all cell reaction produces a solid layer[60,85,86,89] on the surface of the solid electrolyte during the experimental run. It was reasonably believed that the formation of the solid could not be the rate determining step, although no studies have been carried out on this subject, due to two facts, (1) the large negative standard Gibbs energy change for the overall reaction and (2) the small activity of the solid due to unfavorable experimental condition for its massive production. Both factors result in larger negative Gibbs free energy change for the solid to be formed. The latter fact was also observed in the electrolytic deposition of silver on platinum cathode[104] where silver ion was found to deposit more easily onto an incompletely covered platinum cathode. The explanation was that amounts of silver (and presumably other metals) too small to cover the surface of a platinum cathode had an apparent thermodynamic activity which was variable and much smaller than the activity of silver in the bulk standard state.

CHAPTER III THERMOCHEMICAL CONSIDERATIONS

3.1 Phase Diagram Calculations - PREDOM and POTCOMP

In order to measure thermodynamic data, a necessary requirement in electromotive force measurements is that the system under investigation be at equilibrium. Usually, a steady experimental emf is considered as an indication of equilibrium if the emf returns to its steady value after a small disturbance by letting a small current flow through the cell unit in either direction. In practice, this is not always as easy to attain as stated theoretically, because the magnitude of the current which is permitted to flow through the cell without inducing irreversible processes depends very much upon the electrodes. The two electrodes of the cell always react independently. A current small enough for one electrode may cause an irreversible change for another electrode. Thus it is preferable to obtain an indication of equilibrium by other means.

In addition to the local chemical equilibria at both electrodes in a Galvanic cell, which may be completely described by the relation $\Sigma\nu_i\mu_i = 0$ where ν_i and μ_i represent the stoichiometric coefficient and electrochemical potential of species i in an electrode reaction, the equilibria among

the relevant phases must also be considered.

An effective means of representing and studying phase equilibria is through the equilibrium phase diagram. In two dimensional space, phase diagrams have been classified[2] as three types according to their topological units of construction. Briefly, the "type-1" phase diagram is a potential-potential diagram. For example, the predominance area diagrams in pyrometallurgy and E-pH diagrams in hydrometallurgy belong to this class. The "type-2" phase diagram is a potential-composition diagram. The classical temperature-composition diagram for a binary system is the most common example in this category. The "type-3" diagram is a composition-composition diagram which is rarely calculated in the metallurgical field.

Generally speaking, before experimental measurements are carried out, thermodynamic calculations on the relevant phase equilibria involved in a Galvanic cell can provide useful information on the individual electrode equilibrium under the various experimental conditions such as temperature, partial pressure and activity of the reactants and the products. According to the information obtained, the experiment can be designed more fruitfully.

The predominance area diagram for a system of gas sensor by emf measurement can provide useful information in the selection of electrode materials and in the determination of gas composition range within which the cell unit functions properly. An example is the case of the alkali-metal sulfate solid electrolyte[79,80].

As discussed in Chapter II, the cell reaction, compared with that in the cell using metal sulfate as a solid electrolyte, is the same while using ß-Al_2O_3 as a solid electrolyte in SO_x sensor, but the phase relations might be different in consideration of the possible reactions between electrode and the solid electrolyte. Thus it is necessary to study both "type-1" and "type-2" phase diagrams for M_1-M_2-O-S systems (M_1 = Na, Ag, and Ca, M_2 = Al). The calculation and presentation of these phase diagrams is made easier by means of two programs, PREDOM and POTCOMP, from the FACT database[167] (FACT - Facility for the Analysis of Chemical Thermodynamics).

3.2 Predominance Area Diagram Calculation with PREDOM

Two types of predominance area diagrams can be calculated by the PREDOM program. They are one-metal based and two-metal based systems. Only those compounds containing the base metal

are included in the calculation of one-metal predominance area diagram, whereas those compounds bearing either base metal can be included in the two-metal diagram. In addition, a range of the base metal atomic ratio may be specified for the calculation of two-metal type[168].

3.2.1 Na-Al-O-S System

Sodium ß-alumina, $Na_2O \cdot 11Al_2O_3$, belongs to the Al-Na-O ternary system. The composition, the crystal structure and the related physical properties of ß-alumina were discussed previously. Several studies have been reported on the equilibrium phase diagram for the Na_2O-Al_2O_3 binary system[116-123], but the Na-Al-O-S predominance area diagram calculation has not been published.

Na^+-ß-alumina is a sodium ion conducting material. With the sodium activities defined at both electrodes, the general Galvanic cell can be represented as follows:

Reference electrode / ß-alumina / Working electrode

μ'_{Na} μ''_{Na}

The reference electrode subsystem is usually a ternary system, whereas the working electrode subsystem is a quaternary system. For example, in Itoh's study[85] (cell VII in Chapter

II), the reference electrode is the Al-Na-O system, and the working electrode is the Na-Al-O-S system.

Reference electrode subsystem

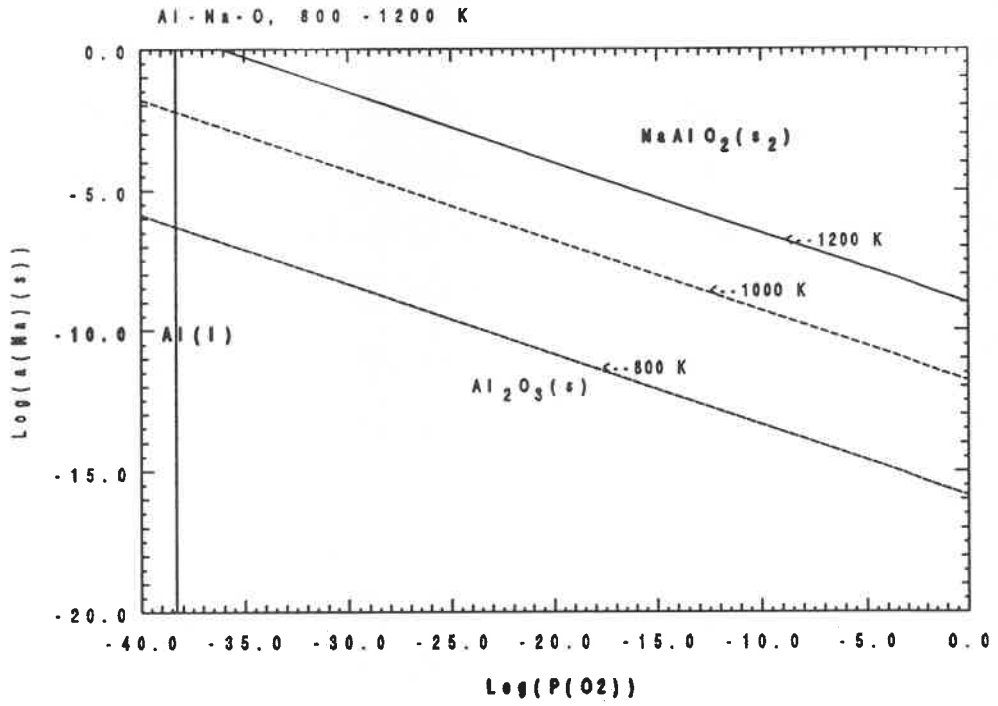

Figure 3.1 Predominance diagram for the Al-Na-O system

The calculated one-metal predominance area diagram for the Al-Na-O ternary system, superimposed at 800, 1000, and 1200 K, is shown in Figure 3.1. The thermodynamic data are taken from the FACT database. In Itoh's study[85], the sodium activity at the reference electrode was defined by a mixture of Au(s) and Au_3Na(s). The range of defined sodium activity

varied from 10^{-4} to 10^{-6}. Argon gas was employed to minimise the oxygen chemical potential in the reference electrode compartment. The exact partial pressure of oxygen in Ar was not reported. According to Figure 3.1, at 800 K, $NaAlO_2(s)$ is the predominant phase in the sodium activity range 10^{-4} to 10^{-6}, even at oxygen partial pressures as low as 10^{-40} atm. Increasing temperature promotes the stability of $Al_2O_3(s)$ at the expense of $NaAlO_2(s)$. Figure 3.2 shows the same system as Figure 3.1 with $a_{Na(s)}$ replaced by $a_{Na_2O(s)}$. No information concerning ß or ß" phases is provided in the two Figures due to the lack of thermochemical data for these two phases.

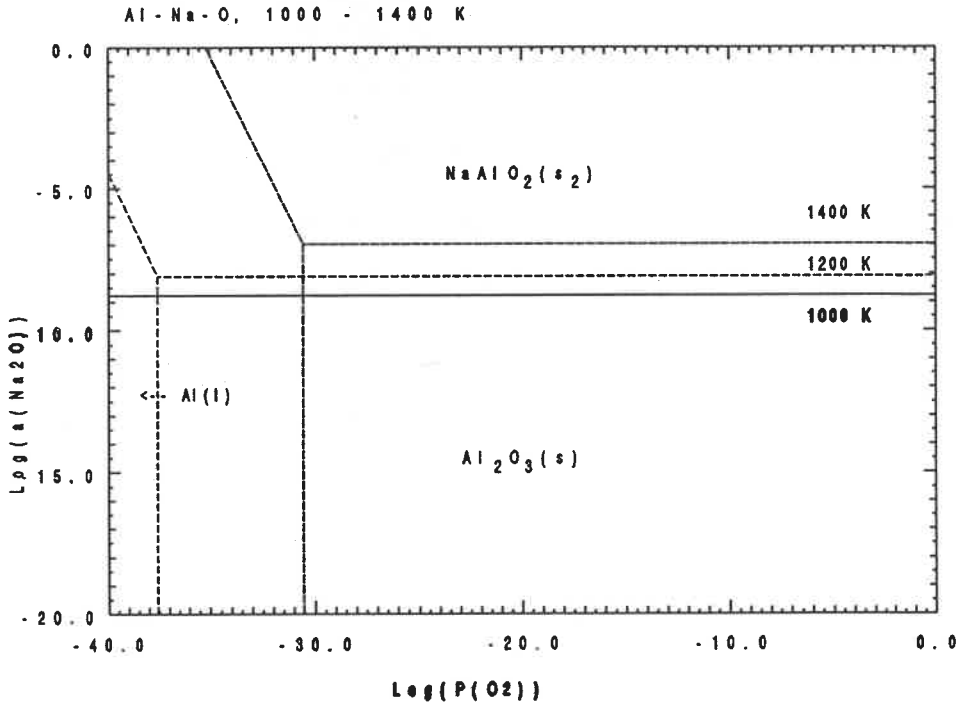

Figure 3.2 Predominance diagram for the Al-Na-O system

Working electrode subsystem

The two-metal predominance area diagrams for the Na-Al-O-S quaternary system, calculated at 800, 1000, and 1200 K, are shown in Figures 3.3 and 3.4 (also see Figures 1 - 4 in Appendix A). The ß and ß" phases are not included in the calculation due to the lack of basic thermochemical data for these phases.

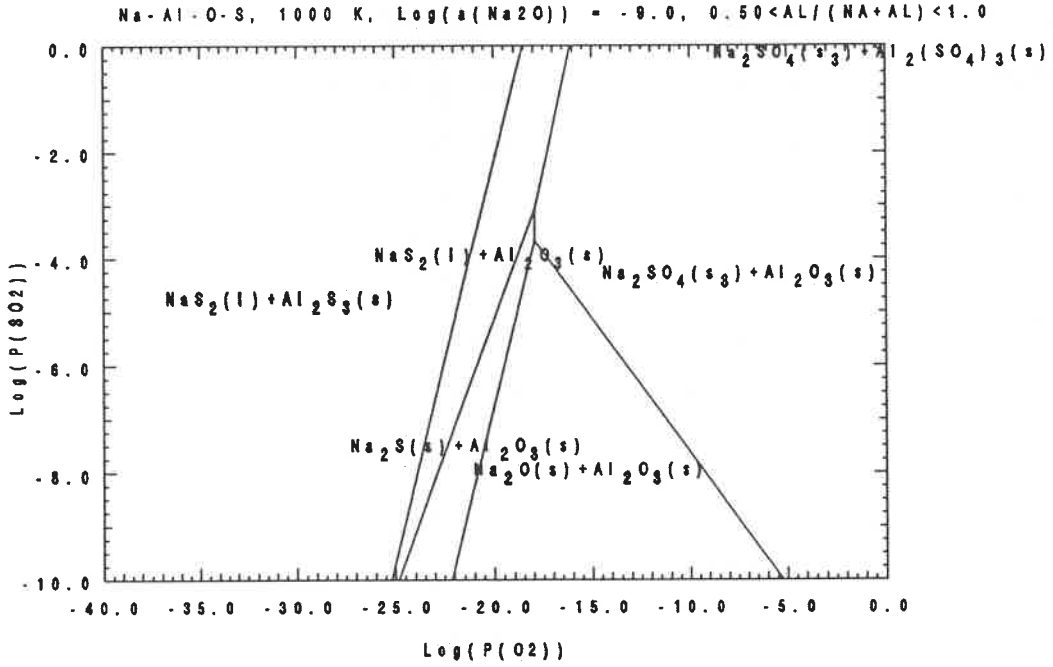

Figure 3.3 Predominance diagram for the Na-Al-O-S system

As mentioned earlier, ß and ß" are non-stoichiometric phases in the Na_2O-Al_2O_3 binary system with the empirical formula $Na_2O \cdot xAl_2O_3$. The activity of $Na_2O(s)$ in ß or ß" phase is as low as 10^{-9} at 1000 K[88]. In the calculation, the activity of $Na_2O(s)$ is defined as 10^{-9} and 10^{-12}. The metal atom ratio (indicated on the upper right of the Figures) is chosen to be on the aluminum rich side in consideration of the composition range of ß and ß" phases.

The Figures indicate that at a relatively low temperatures (Figures 1 and 2 in Appendix A), the system will change from an $Al_2(SO_4)_3 + Na_2SO_4$ area to an $Al_2O_3 + Na_2SO_4$ area as P_{SO_2} decreases. With increasing temperatures, the stable area for the mixture of sulfates becomes smaller, whereas that for the oxides, $Na_2O + Al_2O_3$, becomes larger. If the mixture of oxides is considered as the ß or ß" phase, the direct qualitative conclusion from these diagrams is that the stability of ß or ß" phase relative to sulfates increases as the temperature goes up. At a given temperature, a relatively large domain for the mixture of oxides as the activity of sodium oxide decreases may indicate a higher stability of ß phase than ß" phase (compare Figure 3.3 with 3.4) since there is less Na_2O content in the ß phase.

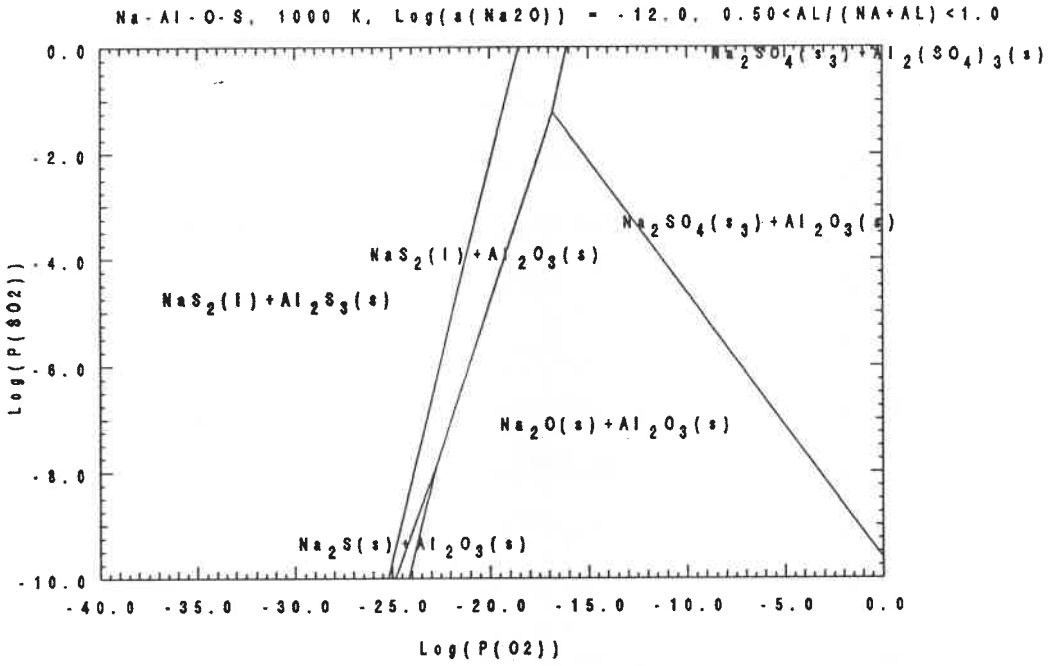

Figure 3.4 Predominance diagram for the Na-Al-O-S system

3.2.2 Ag-Al-O-S System

The predominance area diagram in the Ag-Al-O-S quaternary system has not been reported, but one is available for the Ag-S-O ternary system[79,80]. The Ag-S-O system is fairly unusual in that metallic silver can coexist with its sulfate, Ag_2SO_4. This makes silver metal an idea reversible reference electrode in a galvanic cell when Ag_2SO_4 is the solid electrolyte. In a reported study[86] using Ag^+-ß-alumina as solid electrolyte, pure silver was used as the reference electrode and a gas mixture of air and SO_2 was employed at the working electrode. The reference electrode was the Ag-Al-O

ternary system and the working electrode was the Ag-Al-O-S quaternary system.

Reference electrode subsystem

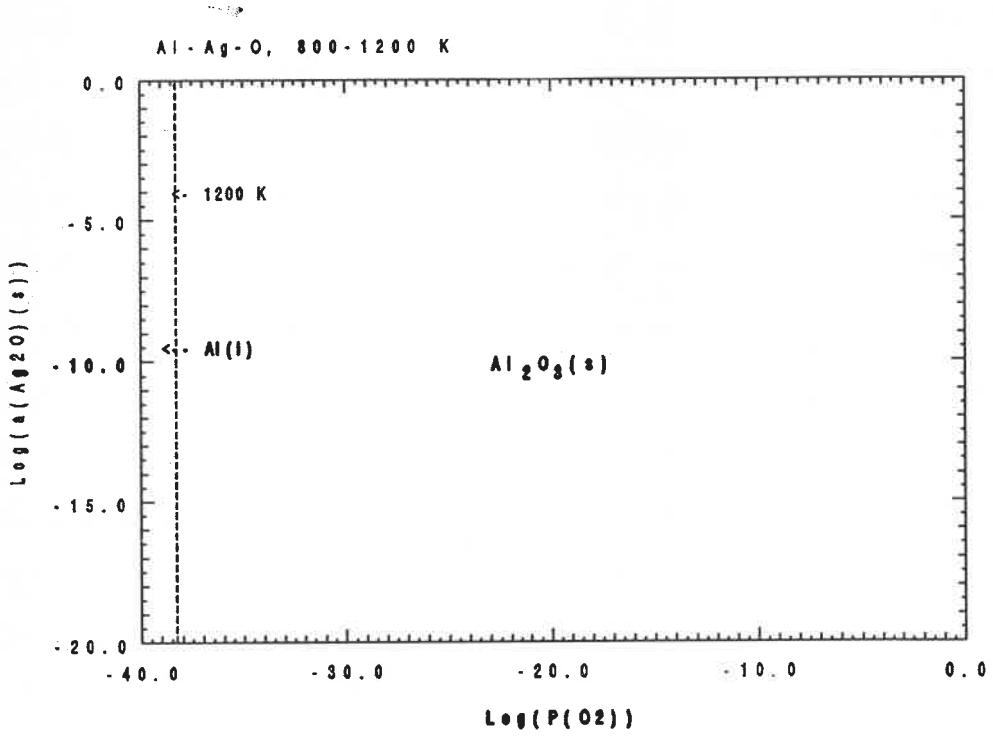

Figure 3.5 Predominance diagram for the Al-Ag-O system

With the assistance of the program PREDOM, the one-metal predominance area diagram for Al-Ag-O system was calculated at 800 K and 1200 K. (Figure 3.5) The beta alumina phase is excluded from the calculation due to the lack of thermochemical data for that phase. The only phase that appears is solid alumina over nearly whole range of the

calculation. This does not mean that silver metal can not stably coexist with alumina. This is the drawback of this kind of predominance diagram which includes only the phases containing the base element, Al, in the calculation.

Working electrode system

The two-metal predominance area diagrams for Ag-Al-O-S system have been calculated at 600 K, 800 K and 1000 K (Figures 5 to 10 in Appendix A). As with the Na-Al-O-S system, the ß phase is excluded from the calculation due to the lack of thermochemical data for that phase. An alternative approach was tried by assigning a small value to the activity of $Ag_2O(s)$. As a result, the domain containing $Ag_2O(s)$ increases as the activity of $Ag_2O(s)$ is lowered from 10^{-7} to 10^{-10}. Similar conclusions can be made if the mixture of oxides is considered as the ß phase. In contrast to the Na-Al-O-S system, silver sulfate is less stable than aluminum sulfate.

3.2.3 Ca-Al-O-S System

The one-metal predominance area diagram for Al-Ca-O ternary system at 1000, 1200, and 1400 K has been calculated (Figure 3.6). Several calcium aluminates appear in the

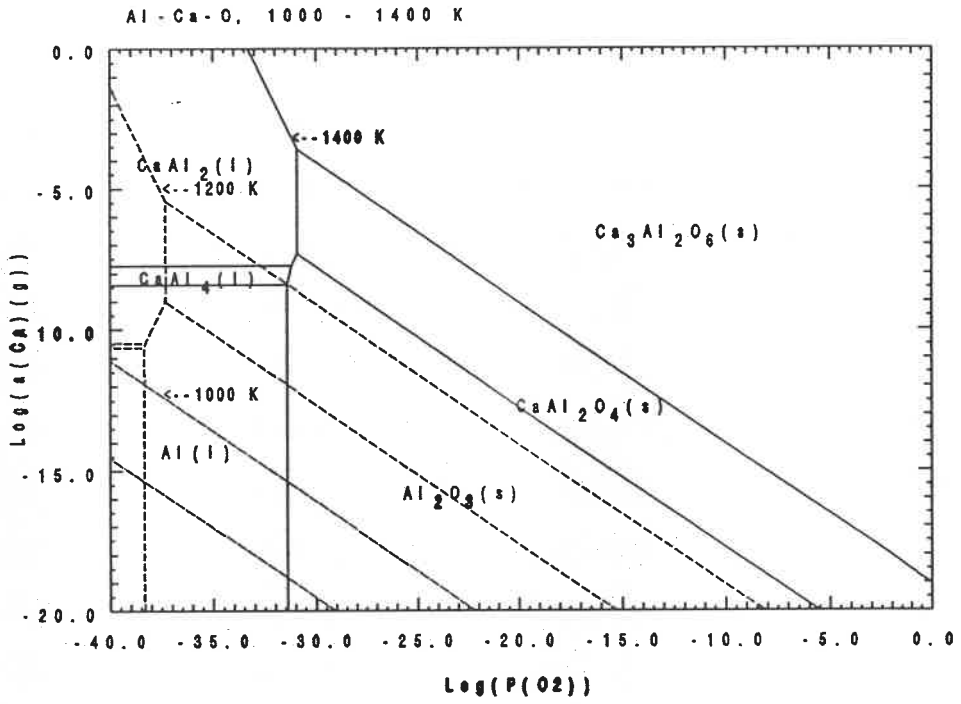

Figure 3.6 Predominance diagram for Al-Ca-O system

diagram. At 800, 1000, and 1200 K, the two-metal predominance area diagrams for the Ca-Al-O-S quaternary system have been calculated and shown in Figures 11 to 16 in Appendix A.

There are some similarities, compared with the Na-Al-O-S and Ag-Al-O-S systems. The domain of oxide mixtures becomes larger as the temperature increases and as the activity of CaO decreases. Calcium sulfate is more stable than aluminum sulfate. In this type of predominance diagram calculation, the atom ratio range of the two metal elements must be assigned, which is shown at the upper right of the diagram. Depending on the range of the atom ratio, different compounds

involving two metals or two metal oxides may appear in the diagram.

3.3 Potential-Composition Diagram Calculation with POTCOMP

No quantitative information concerning the phase relations between the solid electrolyte, ß alumina, and the electrodes is provided in the above predominance diagrams because the ß phase was excluded from the calculation due to the lack of thermochemical data in the FACT database. Even if the thermochemical data are available, as in the case of the Ca-Al-O-S system, there is still the composition range limit which reduces the phases being present in the diagram. These drawbacks are resolved in "type-2" phase diagram calculations. Unlike the calculation of predominance area diagram (PREDOM), the "type-2" phase diagram calculation by means of POTCOMP[167] needs only the expressions of Gibbs energy for the phases under consideration, which are often available, and even obtainable from known phase diagrams.

3.3.1 Na-Al-O-S System

Phases

The phases included in the calculation of the Na-Al-S-O

system are:

1. sodium oxide $Na_2O(s)$;
2. aluminum oxide $Al_2O_3(s)$;
3. ß-alumina with the stoichiometric composition $Na_2O \cdot 8Al_2O_3(s)$;
4. ß"-alumina with the stoichiometric composition $Na_2O \cdot 6Al_2O_3(s)$;
5. solid solution of $Al_2(SO_4)_3$ in Na_2SO_4;
6. aluminum sulfate $Al_2(SO_4)_3(s)$;
7. complex salt $Na_3Al(SO_4)_3(s)$;
8. liquid solution of sulfates, Na_2SO_4-$Al_2(SO_4)_3$;
9. mixed oxide $NaAlO_2(s)$;
10. sodium sulfide $Na_2S(s)$;

Thermodynamic data

The reference state for $\Delta G°$ can be chosen arbitrarily because only changes of the Gibbs energy are involved in the calculation. The standard Gibbs energy changes for the following two reactions have been set to zero:

$$\mathbf{Na(l) + 1/4\ O_2(g) = 1/2\ Na_2O(s)} \qquad \mathbf{...(3.1)}$$

$$\mathbf{Al(s) + 3/4\ O_2(g) = 1/2\ Al_2O_3(s)} \qquad \mathbf{...(3.2)}$$

Several studies have been reported[124-127] on the formation of ß and ß" alumina from the oxides. The results are not very consistent. The most recent emf measurements[88] lead to the following expressions of $\Delta G°$:

$$Na_2O(s) + 11Al_2O_3(s) = Na_2O\cdot 11Al_2O_3(s) \quad ...(3.3)$$

$$\Delta G°_3(J) = -232400 - 7.698\cdot T \quad (874 - 1055\ K)$$

$$Na_2O(s) + 6Al_2O_3(s) = Na_2O\cdot 6Al_2O_3(s) \quad ...(3.4)$$

$$\Delta G°_4(J) = -217800 + 16.292\cdot T \quad (823 - 1073\ K)$$

As mentioned previously, the real Na_2O content in the ß phase is varied and higher than that in the empirical formula $Na_2O\cdot 11Al_2O_3$. The formula $Na_2O\cdot 8Al_2O_3$ is used instead to represent ß phase, assuming the standard Gibbs energy is identical with $\Delta G°_3$.

The standard Gibbs energy changes for the formation of sulfates by the following reactions:

$$Na_2O(s) + SO_2(g) + 1/2\ O_2(g) = Na_2SO_4(s,l) \quad ...(3.5)$$

$$Al_2O_3(s) + 3\ SO_2(g) + 3/2\ O_2(g) = Al_2(SO_4)_3(s) \quad ...(3.6)$$

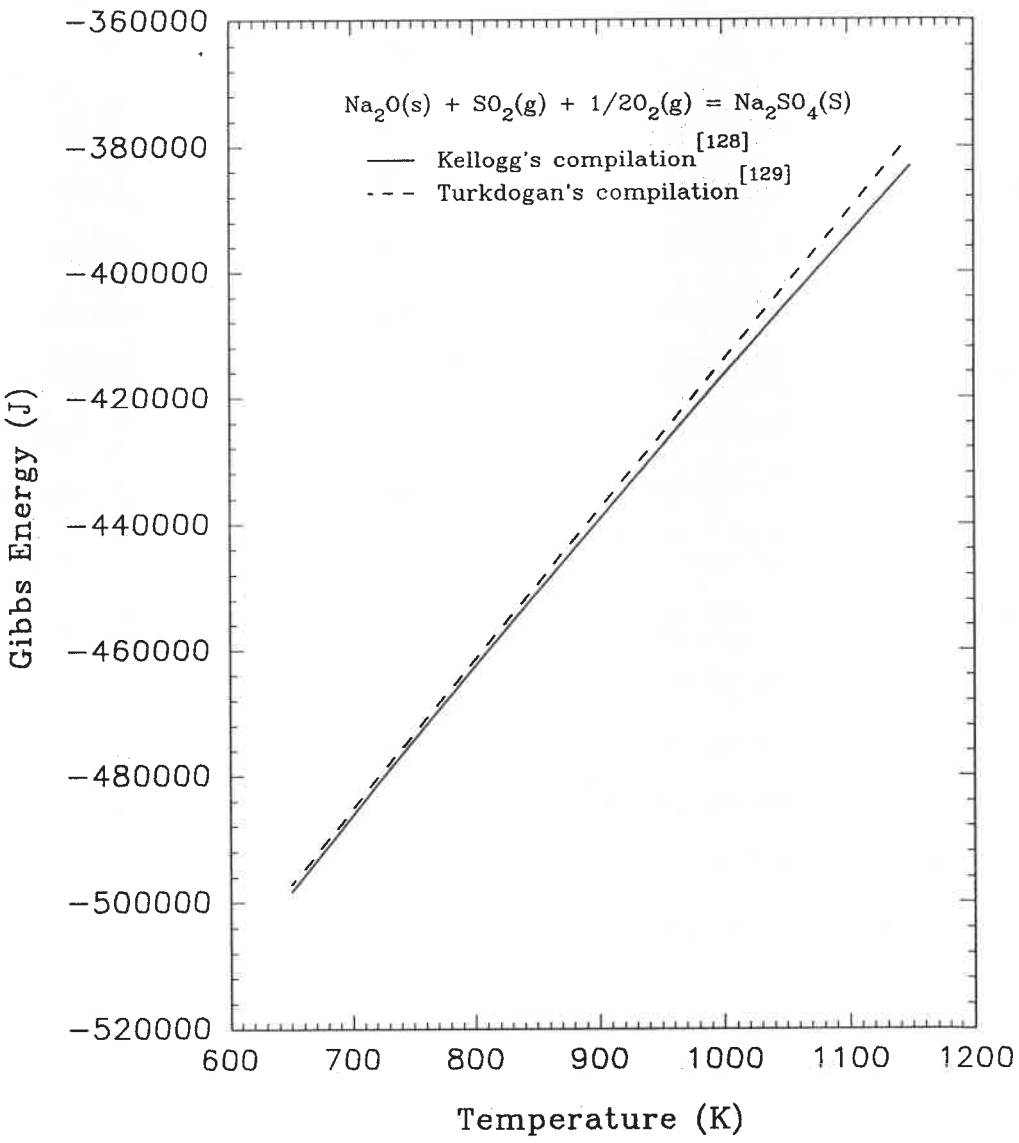

Figure 3.7 Comparison of Standard Gibbs energy for Na_2SO_4 from different sources

have been compiled by Kellogg[128]

$$\Delta G^\circ_5(J) = -679820 + 519.94 \cdot T - 37.18\ T \cdot \ln T \quad (700 - 1157\ K)$$

$$\Delta G^\circ_6(J) = -874750 + 1190.8 \cdot T - 50.42\ T \cdot \ln T \quad (700 - 1100\ K)$$

The alternative expression for ΔG°_5 is found in the compilation by Turkdogan[129], but there is little difference, as shown in Figure 3.7, between the two expressions. The standard Gibbs energy change for the following reactions are taken from Turkdogan's[129] compilation:

$$Na_2O(s) + Al_2O_3(s) = Na_2O \cdot Al_2O_3(s) \qquad ...(3.7)$$

$$\Delta G^\circ_7(J) = -184720 - 2.929 \cdot T \quad (773 - 1405\ K)$$

$$Na_2O(s) + SO_2(g) = Na_2S(s) + 3/2\ O_2(g) \qquad ...(3.8)$$

$$\Delta G^\circ_8(J) = 343920 - 70.08 \cdot T \quad (371 - 1251\ K)$$

Optimization of the published phase diagram

The Na_2SO_4-$Al_2(SO_4)_3$ binary phase diagram has been determined experimentally by Fedorov[130] using the "cooling curve" method, and by Kochubei[131] using DTA. There are

contradictory conclusions about the existence of a complex salt. Fedorov proposed the exclusive existence of $Na_3Al(SO_4)_3$ by assuming the instability of $NaAl(SO_4)_2$ during the annealing process in his experiment, whereas $NaAl(SO_4)_2$ was found to be the only compound in Kochubei's measurement. Consequently, there is disagreement concerning the eutectic temperature. Since the experimental data are not available in reference [131], the experimental data of Fedorov were treated by means of FITBIN[167] (a program in the FACT system) to obtain the excess Gibbs energy expression for the liquid solution of the sulfates:

$$G^E(J) = -13525X_1X_2 - 36945X_1X_2^2 + 194313X_1X_2^3$$

where X_1 and X_2 are mole fractions of $Na(SO_4)_{0.5}$ and $Al(SO_4)_{1.5}$ respectively. The standard Gibbs energy change for the following reaction was also obtained:

$$3/2\ Na_2SO_4(l) + 1/2\ Al_2(SO_4)_3(l) = Na_3Al(SO_4)_3(s) \quad ...(3.9)$$

$$\Delta G°_9(J) = -66360 + 42.643 \cdot T$$

There is limited solid solubility of $Al_2(SO_4)_3$ in Na_2SO_4 according to Fedorov's measurement. The excess Gibbs energy of the solution can be obtained by the calculation of

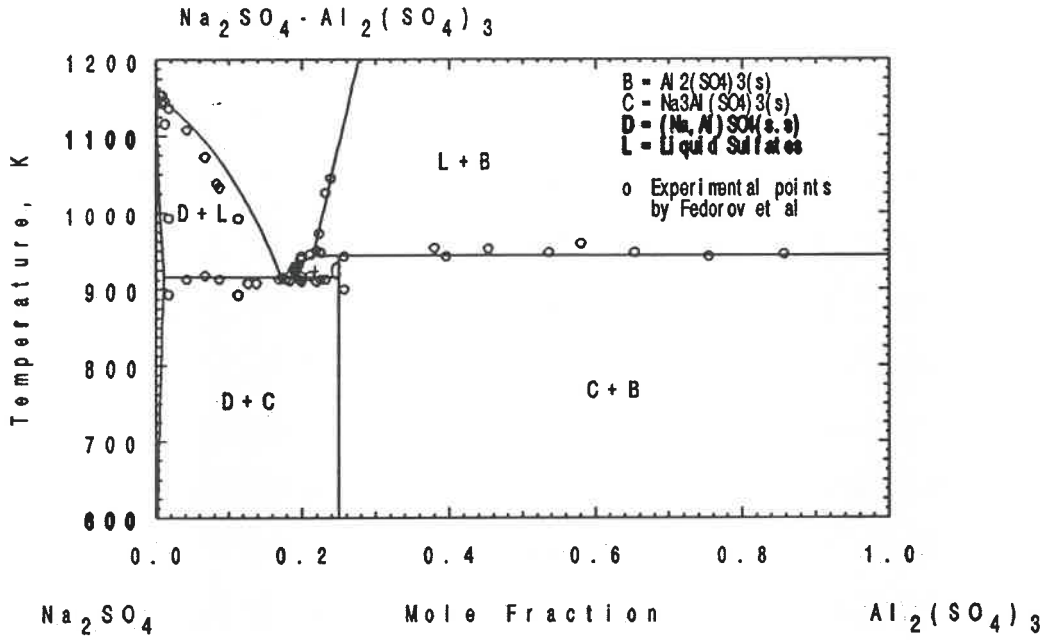

Figure 3.8 Optimized Na_2SO_4-$Al_2(SO_4)_3$ phase diagram

$\gamma^{\circ}_{Al_2(SO_4)_3}$, assuming that Henry's law is obeyed in the dilute solution. At 913 K, the solution with $X_2 = 0.0214$ is equilibrated with solid $Na_3Al(SO_4)_3$, the complex salt, where the activity of $Al_2(SO_4)_3$ is assumed to be unity. Accordingly,

$$\dot{\gamma}_{Al_2(SO_4)_3} = \frac{a_{Al_2(SO_4)_3}}{X_2} = \frac{1}{0.0214}$$

$$G^{E}_{Al_2(SO_4)_3} = RT \cdot Ln\dot{\gamma}_{Al_2(SO_4)_3} = 29200\,(J) \qquad \ldots(3.10)$$

The calculated phase diagram is compared with the experimental points of Fedorov in Figure 3.8.

In order to combine the data together on the same basis,

the Gibbs energy change for fusion of the sulfates must be known. Unfortunately neither the enthalpy of fusion nor the temperature of fusion for aluminum sulfate is known, although those of sodium sulfate are available. Therefore an estimated $\Delta G°$ expression was used in the calculation for the fusion of $Al_2(SO_4)_3$ according to Kubaschewski[132]:

$$Al_2(SO_4)_3(s) = Al_2(SO_4)_3(l) \qquad ...(3.11)$$

$$\Delta G°_{11}(J) = 74680 - 50.21 \cdot T$$

whereas that of Na_2SO_4 was calculated from the C_p data.

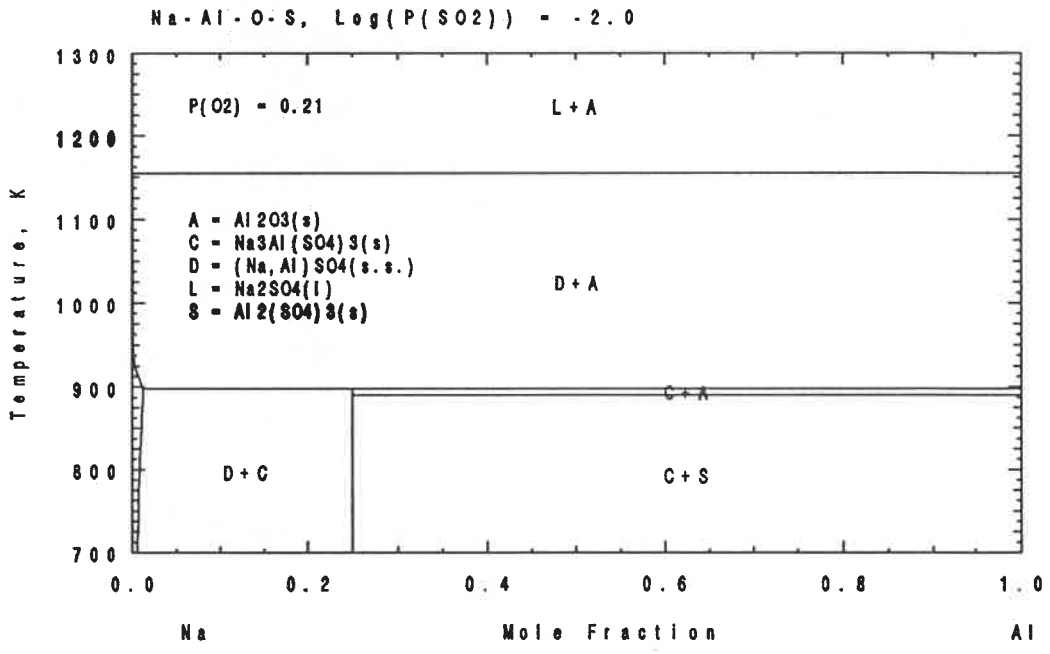

Figure 3.9 POTCOMP diagram for the Na-Al-O-S system

$$Na_2SO_4(s) = Na_2SO_4(l) \qquad ...(3.12)$$

$$\Delta G^\circ_{12}(J) = -597.89 + 352.17 \cdot T + 0.02965 \cdot T^2 - 54.72\ T \cdot \ln T$$

Results and discussion

The calculated potential-composition diagrams are shown in Figures 3.9 through 3.12 (also see Figures 17 - 29 in Appendix A). The following points are concluded:

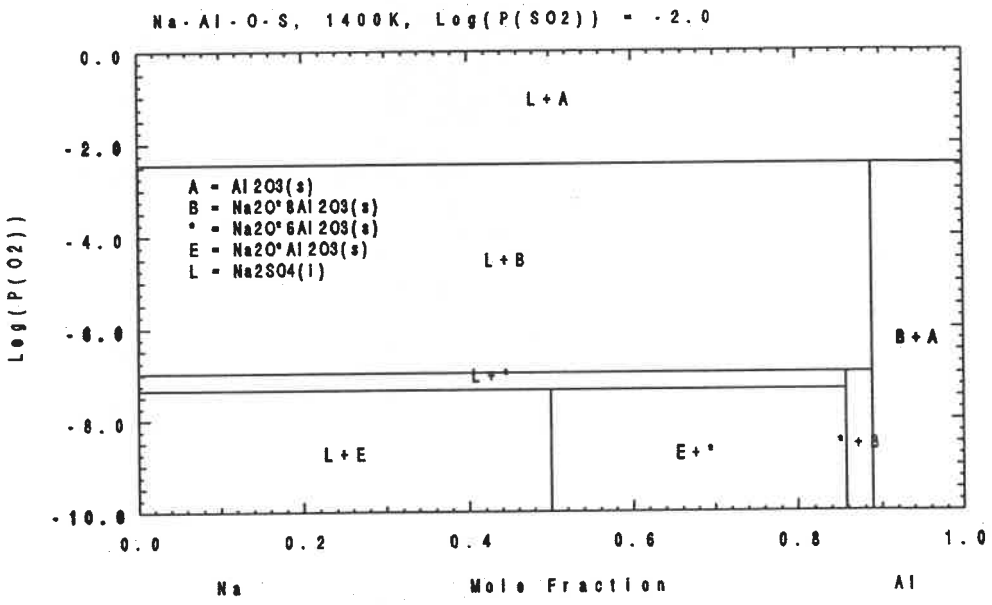

Figure 3.10 POTCOMP diagram for the Na-Al-O-S system

(a). At $Log(P_{SO_2}) = -2$ and $P_{O_2} = 0.21$ atm. (Figure 3.9), ß and ß"-alumina can not coexist with sodium sulfate, even at temperatures as high as 1400 K (Figure 3.10). Rather, it is α-alumina which is stable

with sodium sulfate.

(b). At Log(P_{SO_2}) = -6 and P_{O_2} = 0.21 atm. (Figure 3.11 and 3.12), ß and ß"-alumina can coexist with sodium sulfate in the temperature range 1157 to 1340 K above which $NaAlO_2$ is the more stable phase to equilibrate with Na_2SO_4. Below 1157 K, Na_2SO_4 coexists with α-Al_2O_3.

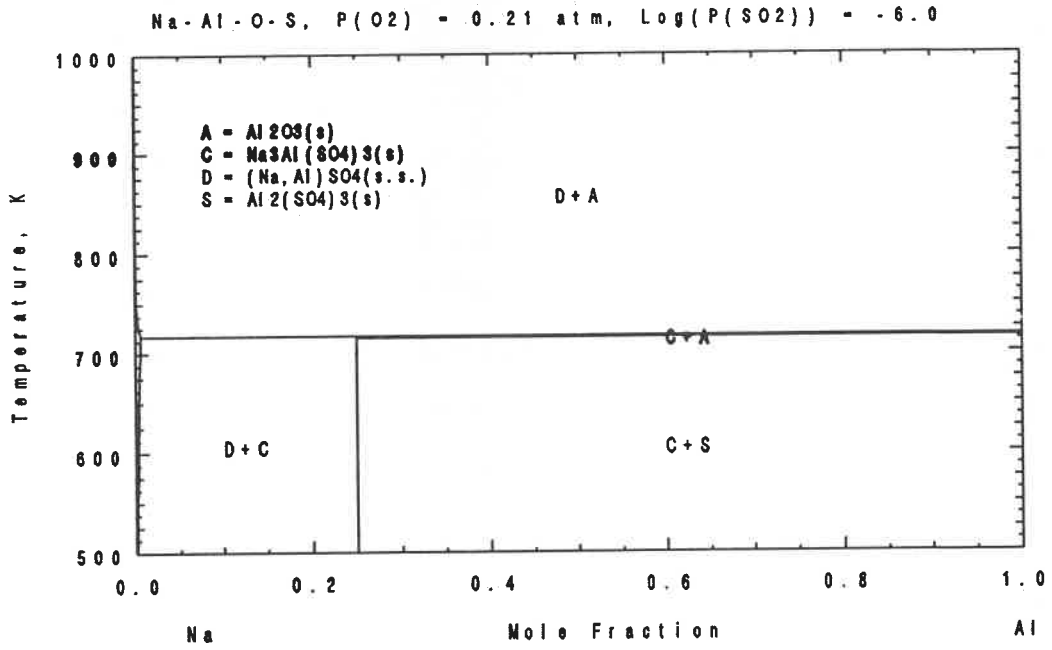

Figure 3.11 POTCOMP diagram for the Na-Al-O-S system

These points may not favor the emf measurements carried out by Itoh et al[85], at least at the higher P_{SO_2} and lower temperature range since, as predicted by the diagrams, the ß and ß" phases will be consumed by the cell reaction to produce

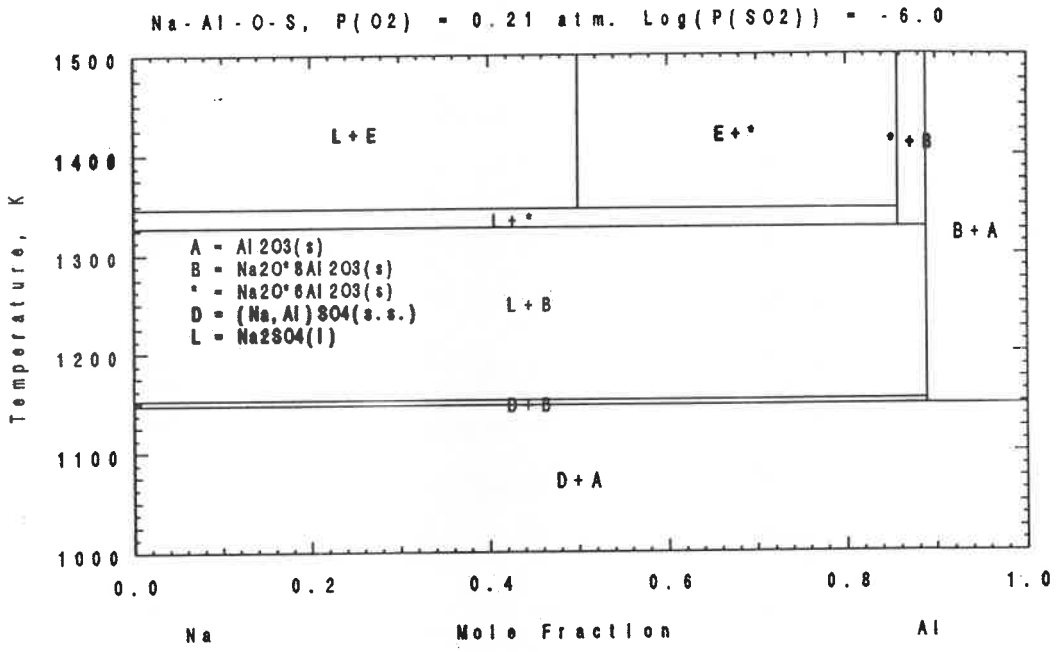

Figure 3.12 POTCOMP diagram for the Na-Al-O-S system

a mixture of Na_2SO_4 and α-Al_2O_3.

Although the uncertainties of the thermodynamic data have some effect on the phase diagram calculation results, the tendencies shown in the Figures should still hold, i.e. when the temperature and the partial pressures of SO_2 and O_2 are changed, the relative stabilities among the different phases remain the same.

Furthermore, it is possible that at the interface between the solid electrolyte and the sulfate which are supposed to coexist in the cell, the overall cell reaction will result in the disappearance of the ß phase and the appearance of α-

alumina. The attack on the ß phase by the cell reaction becomes suppressed, partly due to the measurement condition with a potentiometer, and partly to the kinetic factor in a heterogeneous reaction.

3.3.2 Ag-Al-O-S System

Phases

The phases considered in the phase diagram calculation for Ag-Al-O-S system are as follows:

1. silver oxide, $Ag_2O(s)$;
2. alumina, $Al_2O_3(s)$;
3. silver sulfate, $Ag_2SO_4(s)$;
4. aluminum sulfate, $Al_2(SO_4)_3(s)$;
5. silver beta alumina, $Ag_2O \cdot 8Al_2O_3(s)$;
6. silver sulfide, $Ag_2S(s)$;
7. mixed oxide $AgAlO_2(s)$;
8. liquid silver sulfate, $Ag_2SO_4(l)$;

Thermodynamic data

Basic thermochemical data for Ag_2O are found in Barin's[133] compilation but limited to the temperature range 300 to 500 K. To carry out the phase diagram calculation, the

following expression of ΔG° from Turkdogan[129] is used and extrapolated outside the temperature range limit:

$$2Ag(s) + 1/2O_2(g) = Ag_2O(s) \qquad ...(3.13)$$

$$\Delta G^\circ_{13}(J) = -30540 + 66.107 \cdot T \quad (T < 298\ K)$$

Unlike the Na-Al-O-S system, the pure metals are assigned zero standard Gibbs energy so that most standard Gibbs energy expressions from the literature can be used directly. The standard Gibbs energy change for the formation of α-alumina is found in reference [132],

$$2Al(s,l) + 3/2\ O_2(g) = Al_2O_3(s) \qquad ...(3.14)$$

$$\Delta G^\circ_{14}(J) = -1677000 + 366.68 \cdot T - 7.23 \cdot T\ln T \quad (298 - 933\ K)$$

$$\Delta G^\circ_{14}(J) = -1697700 + 385.85 \cdot T - 6.81 \cdot T\ln T \quad (933 - 1800\ K)$$

The expressions of the standard Gibbs energy change for the following reactions

$$Ag(s)+1/4O_2(g)+n/2Al_2O_3(s) = 1/2Ag_2O \cdot nAl_2O_3(s) \qquad ...(3.15)$$

$$Ag(s)+1/4O_2(g)+1/(2n-2)Ag_2O \cdot nAl_2O_3 = n/(n-1)AgAlO_2 \qquad ...(3.16)$$

have been developed[134] from emf measurements in the following cells:

$$Pt/Ag/Ag^{+}\text{-}\beta\text{-alumina}/Ag_2O\cdot nAl_2O_3, Al_2O_3/Pt$$

$$Pt/Ag/Ag^{+}\text{-}\beta\text{-alumina}/AgAlO_2, Ag_2O\cdot nAl_2O_3/Pt$$

$$\Delta G^{\circ}_{15}(J) = 1853.5 - 36.275\cdot T \quad (673 - 1173\ K)$$

$$\Delta G^{\circ}_{16}(J) = -38060 + 33.388\cdot T \quad (673 - 1173\ K)$$

The standard Gibbs energy change for the formation of silver sulfate by the reaction:

$$2Ag(s) + SO_2(g) + O_2(g) = Ag_2SO_4(s,l) \qquad ...(3.17)$$

is given in the compilation of Kellogg[128]

$$\Delta G^{\circ}_{17}(J) = -404340 + 679.65\cdot T - 55.39\cdot T\ln T \quad (930 - 1234\ K)$$

An alternative way to derive a ΔG° expression for silver sulfate employs the data from Barin's compilation[133]. The results are as follows:

$$\Delta G^{\circ}_{17}(J) = -398400 + 299.41\cdot T \quad (600 - 703\ K)$$

$$\Delta G^\circ_{17}(J) = -382900 + 276.61 \cdot T \quad (703 - 933\ K)$$

$$\Delta G^\circ_{17}(J) = -364990 + 257.41 \cdot T \quad (933 - 1200\ K)$$

There is little difference for ΔG°_{17} from the two sources. The expression from Barin's compilation is used in the calculation because it covers a lower temperature range. The standard Gibbs energy change for the formation of aluminium sulfate by the reaction:

$$2Al(s,l) + 3SO_2(g) + 3O_2(g) = Al_2(SO_4)_3(s) \quad ...(3.18)$$

is obtained by Hess' law:

$$\Delta G^\circ_{18}(J) = -2551740 + 1545 \cdot T - 57.65 \cdot T\ln T \quad (298 - 933\ K)$$

$$\Delta G^\circ_{18}(J) = -2572450 + 1576 \cdot T - 57.23 \cdot T\ln T \quad (933 - 1800\ K)$$

Finally, the standard Gibbs energy change for the formation of silver sulfide by the reaction:

$$2Ag(s) + 1/2S_2(g) = Ag_2S(s) \quad ...(3.19)$$

can be found both in reference [129] and in reference [132]. The values of enthalpy and entropy from [129] is as much as

twice that from [132]. It was also determined by emf measurements[140] with the fused chloride electrolyte saturated by Ag_2S, which agrees fairly well with that from reference [132]. Thus, the expression is taken from [132]:

$$\Delta G^\circ_{19}(J) = -87820 + 35.56 \cdot T \quad (452 - 1115\ K)$$

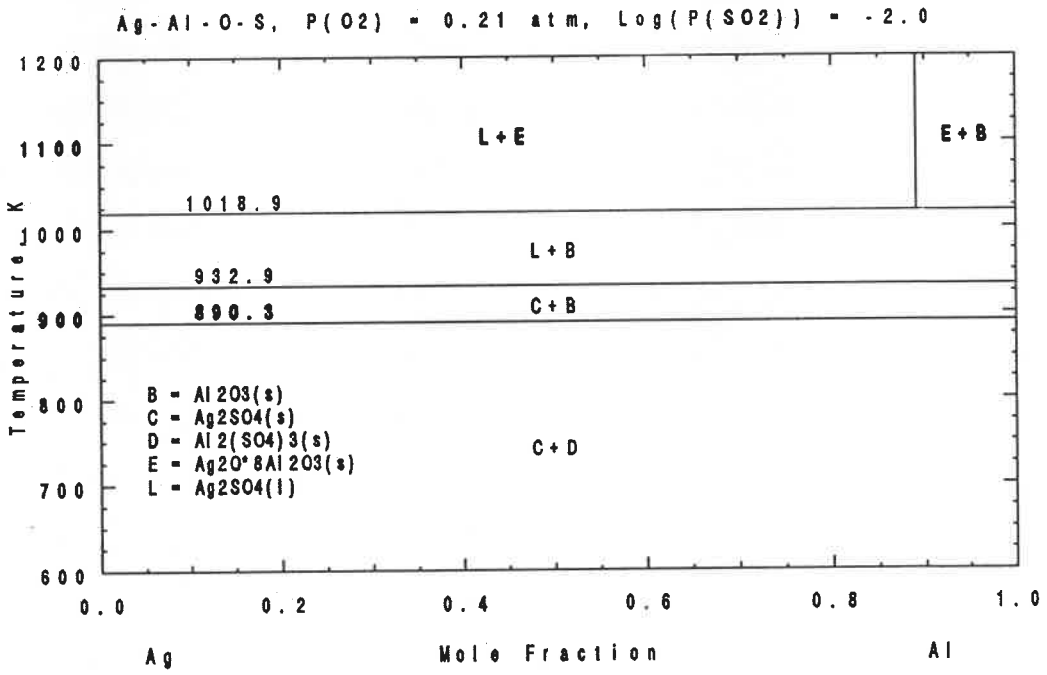

Figure 3.13 POTCOMP diagram for the Ag-Al-O-S system

Results and Discussion

Typical potential-composition diagrams are shown in Figures 3.13 and 3.14 (also see Figures 30 - 40 in Appendix A). The range of temperature and the concentration of SO_2 is

pre-selected to match the experimental conditions in reference [86]. According to these Figures, the conclusions are:

(a). At $Log(P_{SO_2})$ = -2 and P_{O_2} = 0.21 atm. (Figure 3.13), ß-alumina can equilibrate with Ag_2SO_4 above 1018 K. Between 890 and 1018 K, it is α-alumina which can stably coexist with silver sulfate. Below 890 K is the stable region for the sulfates mixture.

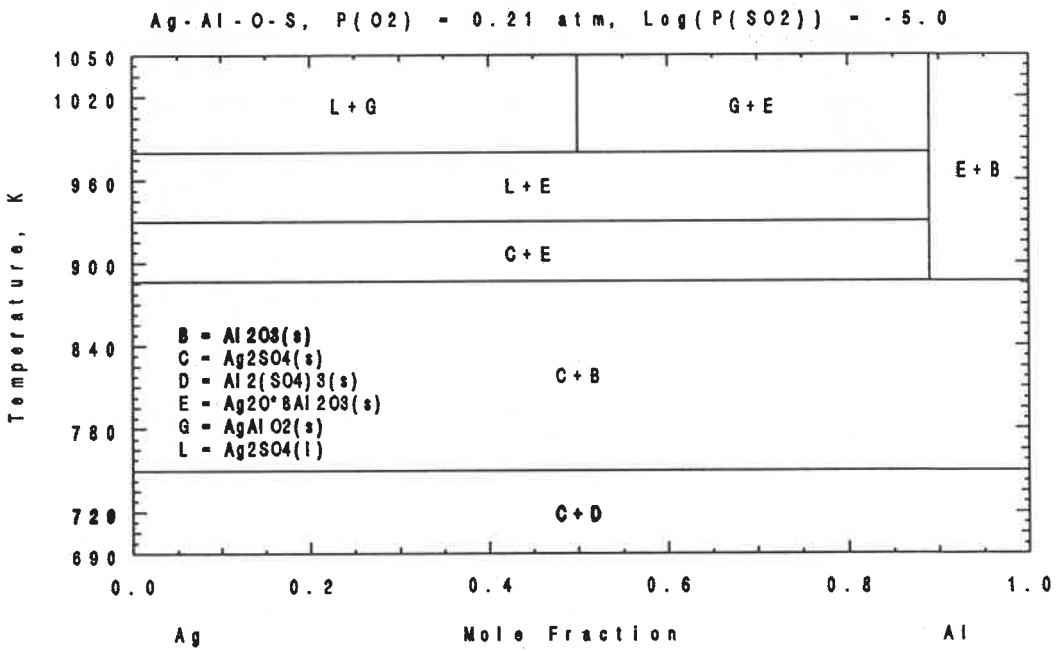

Figure 3.14 POTCOMP diagram for the Ag-Al-O-S system

(b). At P_{SO_2} = 10ppm and P_{O_2} = 0.21 atm., ß-alumina can coexist with Ag_2SO_4 between 886 and 980 K, above which $AgAlO_2$ is the more stable phase. It is α-alumina which equilibrates with silver sulfate

between 886 and 750 K, below which the sulfates mixture predominates.

In contrast to the Na-Al-O-S system, there is a temperature range within which silver sulfate, Ag_2SO_4, can coexist with Ag^+-ß-alumina at P_{O_2} = 0.21 atm. It is also apparent that below a certain temperature which depends on the concentration (partial pressure) of SO_2, the system will be comprised of only sulfates. That may correspond to a critical point beyond which the failure of the solid electrolyte caused by the formation of aluminum sulfate will occur, leading to a drastic change of emf with temperature.

3.3.3 Ca-Al-O-S System

Phases

The following phases were chosen in the calculation of the potential-composition phase diagram for the Ca-Al-O-S system:

1. calcia, CaO(s);
2. alumina, Al_2O_3(s);
3. calcium sulfate, $CaSO_4$(s);
4. aluminum sulfate, $Al_2(SO_4)_3$(s);
5. calcium sulfide, CaS(s);

6. mixed oxide, $CaO \cdot 6Al_2O_3(s)$;
7. mixed oxide, $CaO \cdot 2Al_2O_3(s)$;
8. mixed oxide, $CaO \cdot Al_2O_3(s)$;
9. mixed oxide, $3CaO \cdot Al_2O_3(s)$;

Thermodynamic data

The standard Gibbs energy changes for the following reactions have been set to zero:

$$Ca(l) + 1/2O_2(g) = CaO(s) \quad ...(3.20)$$

$$Al(l) + 3/4O_2(g) = 1/2Al_2O_3(s) \quad ...(3.21)$$

There are two sources for the standard Gibbs energy of formation for $CaSO_4$:

$$CaO(s) + SO_2(g) + 1/2O_2(g) = CaSO_4(s) \quad ...(3.22)$$

Kellogg's compilation[128]

$$\Delta G^\circ_{22}(J) = -572500 + 864.96 \cdot T - 75.60\ T \cdot \ln T \quad (1100 - 1638\ K)$$

and Turkdongan's compilation[129]

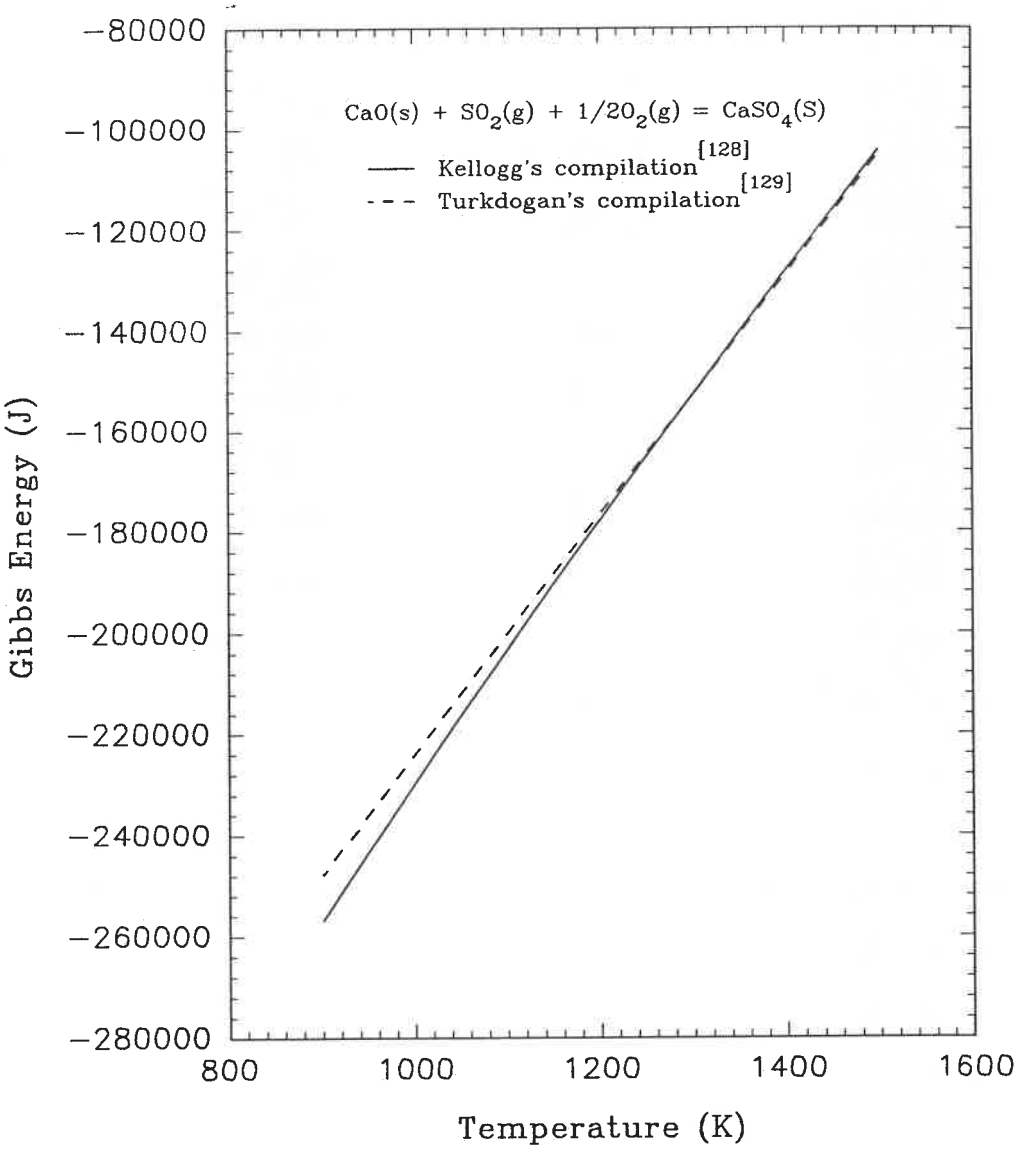

Figure 3.15 Comparison of Standard Gibbs energy for $CaSO_4$ from different sources

$$\Delta G^\circ_{22}(J) = -461790 + 237.73 \cdot T \quad (1223 - 1468\ K)$$

The data are compared in Figure 3.15. The standard Gibbs energy for aluminum sulfate is the same as that given in the Na-Al-O-S system. For calcium sulfide, there are two data sources giving nearly identical standard Gibbs energy expressions for the reaction

$$Ca(l) + 1/2S_2(g) = CaS(s) \qquad ...(3.23)$$

by Turkdogan[129],

$$\Delta G^\circ_{23}(J) = -548100 + 103.85 \cdot T \quad (1112 - 1757\ K)$$

by Kubaschewski[132],

$$\Delta G^\circ_{23}(J) = -551370 + 104.35 \cdot T \quad (1124 - 1760\ K)$$

The standard Gibbs energies for several mixed oxides in the $CaO-Al_2O_3$ binary system have been found in literatures[132,135-139]. Comparison is made among the data from these publications and shown in Figures 3.16 through 3.19. Accordingly, the expressions by Kumar and Kay[137] from emf measurement are taken, although there is a calculational error for ΔG°_{27} in the original article. The correct expressions for

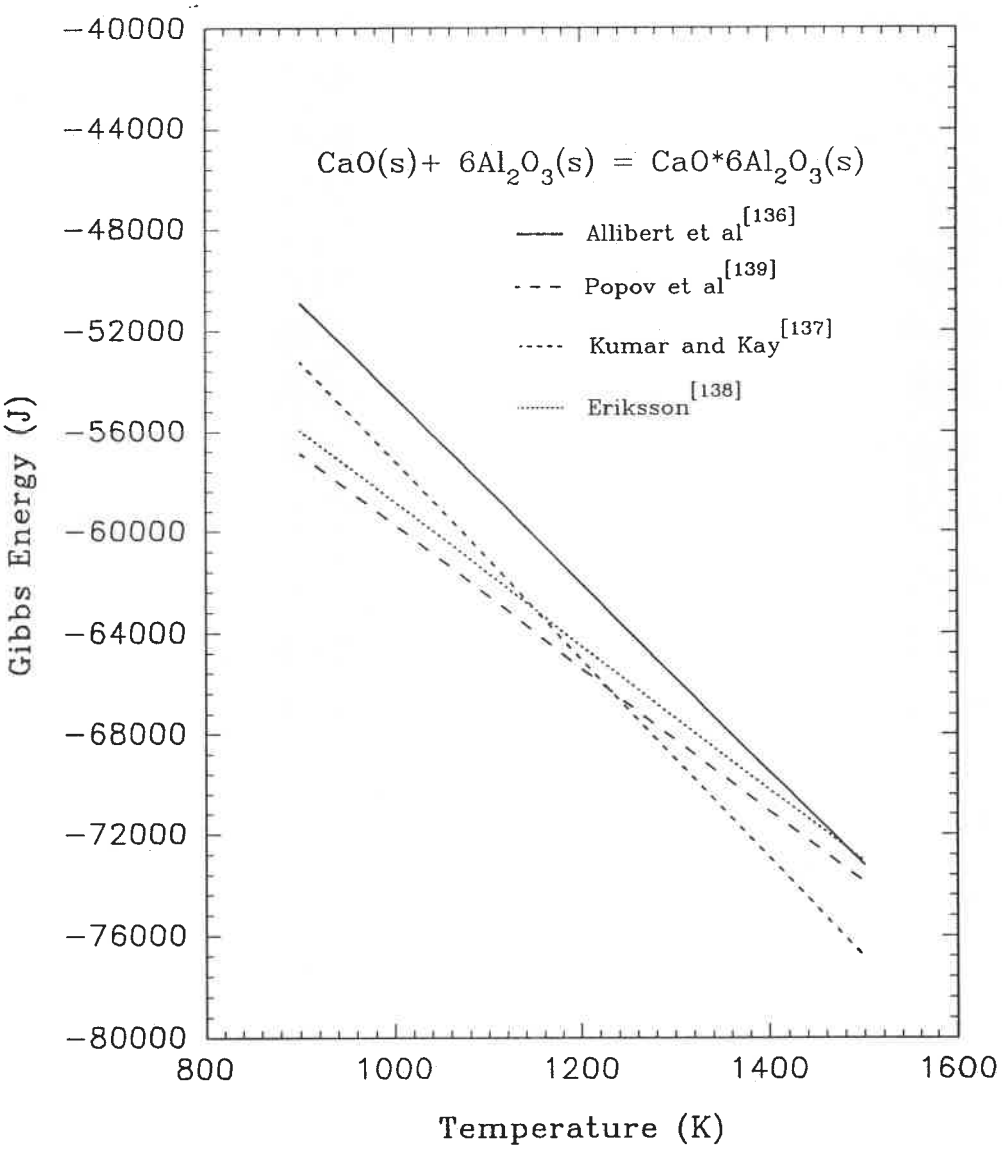

Figure 3.16 Comparison of Standard Gibbs energy of formation for $CaO6Al_2O_3$ from different sources

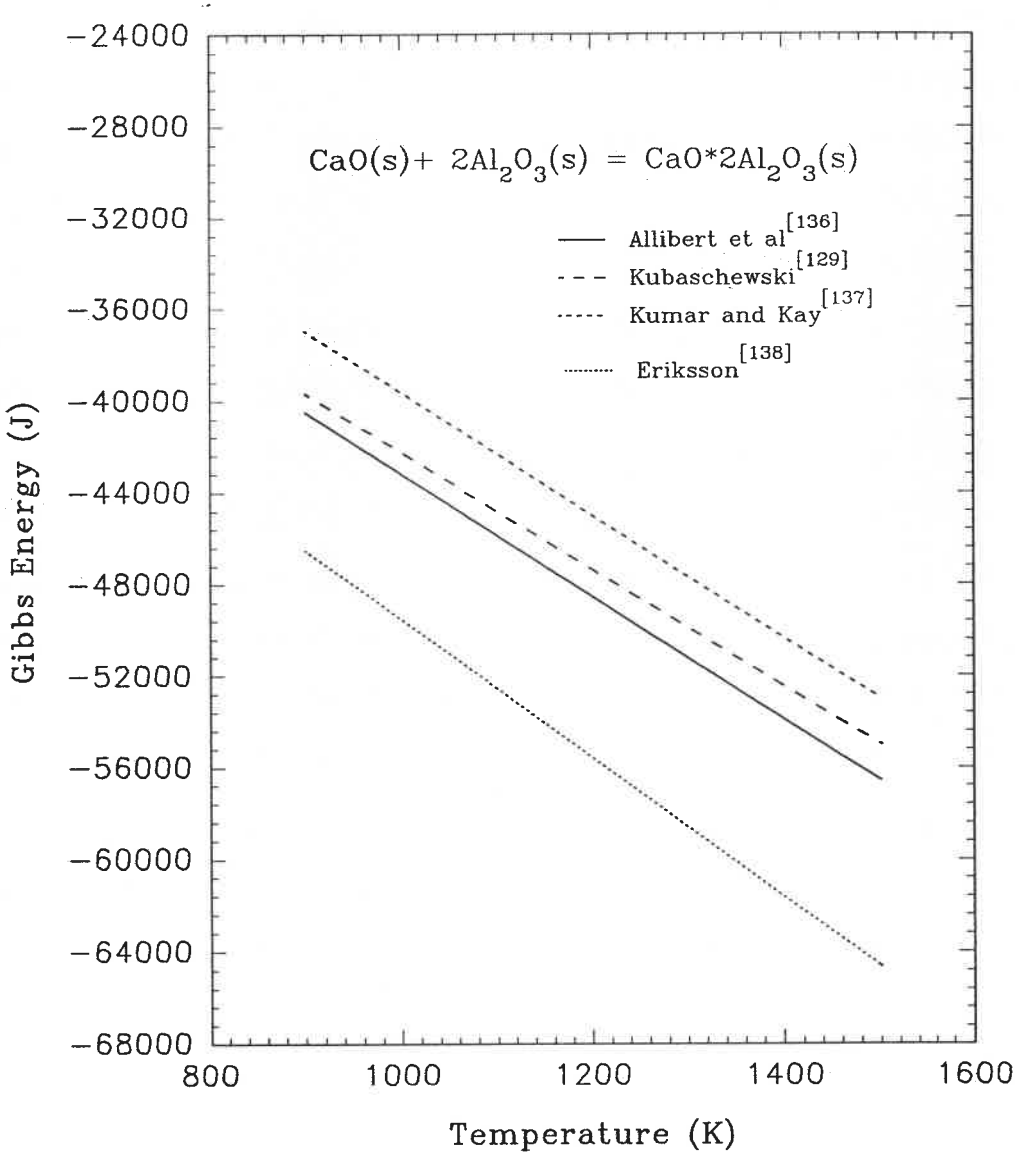

Figure 3.17 Comparison of standard Gibbs energy of formation for $CaO.2Al_2O_3$ from different sources

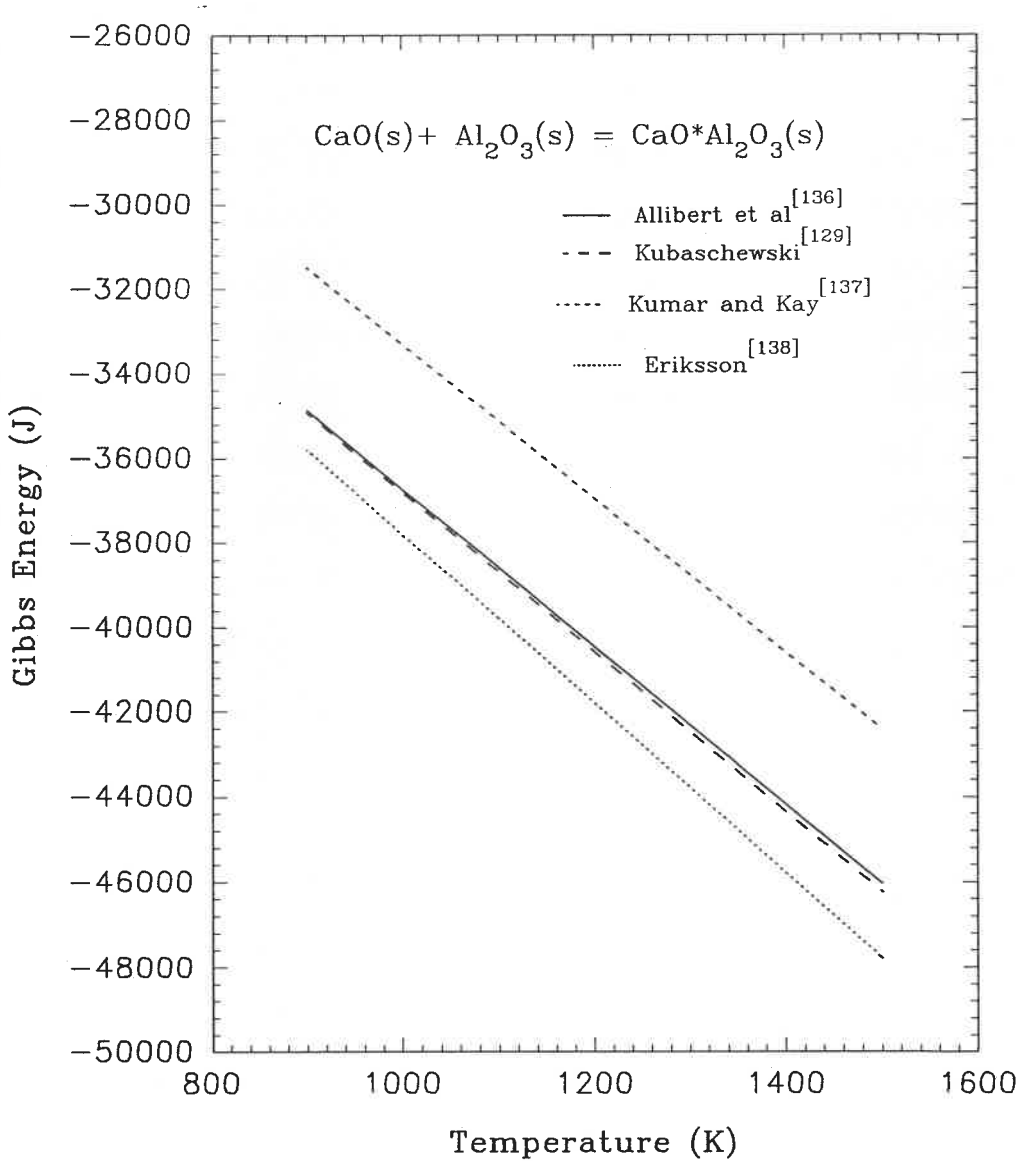

Figure 3.18 Comparison of standard Gibbs energy of formation for $CaO.Al_2O_3$ from different sources

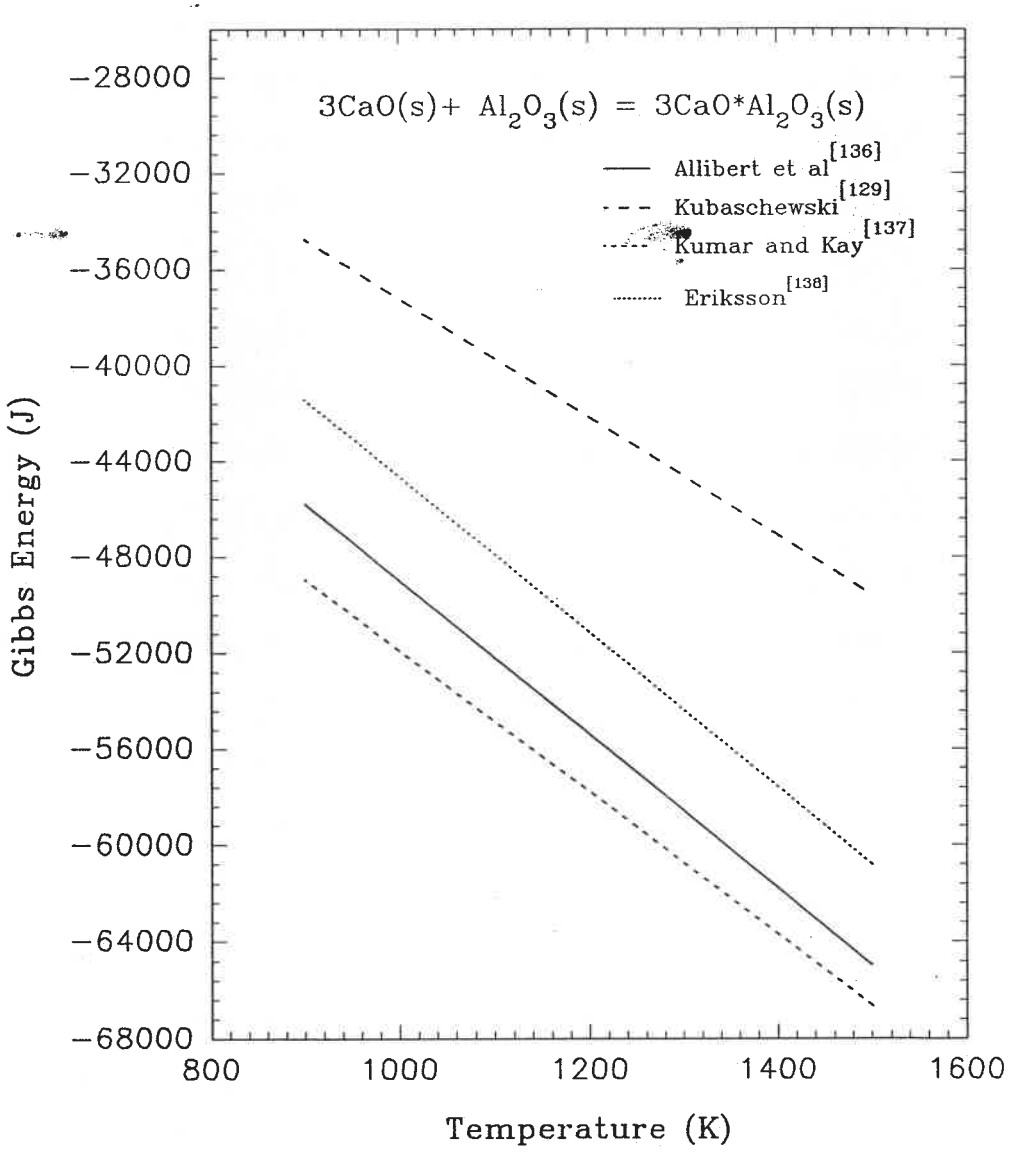

Figure 3.19 Comparison of standard Gibbs energy of formation for $3CaO.Al_2O_3$ from different sources

the standard Gibbs energies are as follows:

$$CaO(s) + 6Al_2O_3(s) = CaO\cdot 6Al_2O_3(s) \quad ...(3.24)$$

$$\Delta G^\circ_{24}(J) = -17870 - 39.33\cdot T \quad (1100 - 1500\ K)$$

$$CaO(s) + 2Al_2O_3(s) = CaO\cdot 2Al_2O_3(s) \quad ...(3.25)$$

$$\Delta G^\circ_{25}(J) = -12916 - 26.74\cdot T \quad (1000 - 1500\ K)$$

$$CaO(s) + Al_2O_3(s) = CaO\cdot Al_2O_3(s) \quad ...(3.26)$$

$$\Delta G^\circ_{26}(J) = -15113 - 18.20\cdot T \quad (1050 - 1500\ K)$$

$$3CaO(s) + Al_2O_3(s) = 3CaO\cdot Al_2O_3(s) \quad ...(2.27)$$

$$\Delta G^\circ_{27}(J) = -22407 - 29.50\cdot T \quad (1020 - 1320\ K)$$

Results and discussion

The calculated diagrams are shown in Figures 3.20 and 3.21 (also see Figures 41 - 59 in Appendix A). Compared with the Na-Al-O-S system, there are two points to mention:

(a). In a manner analogous to the system containing

sodium, at P_{O_2} = 0.21 atm. and $Log(P_{SO_2})$ = -2.0 (Figure 3.20), the compound $CaO \cdot 6Al_2O_3$ does not appear until above 1379 K. Between 875 and 1379 K, it is the α-alumina which equilibrates with $CaSO_4$. Below 875 K, two sulfates coexist.

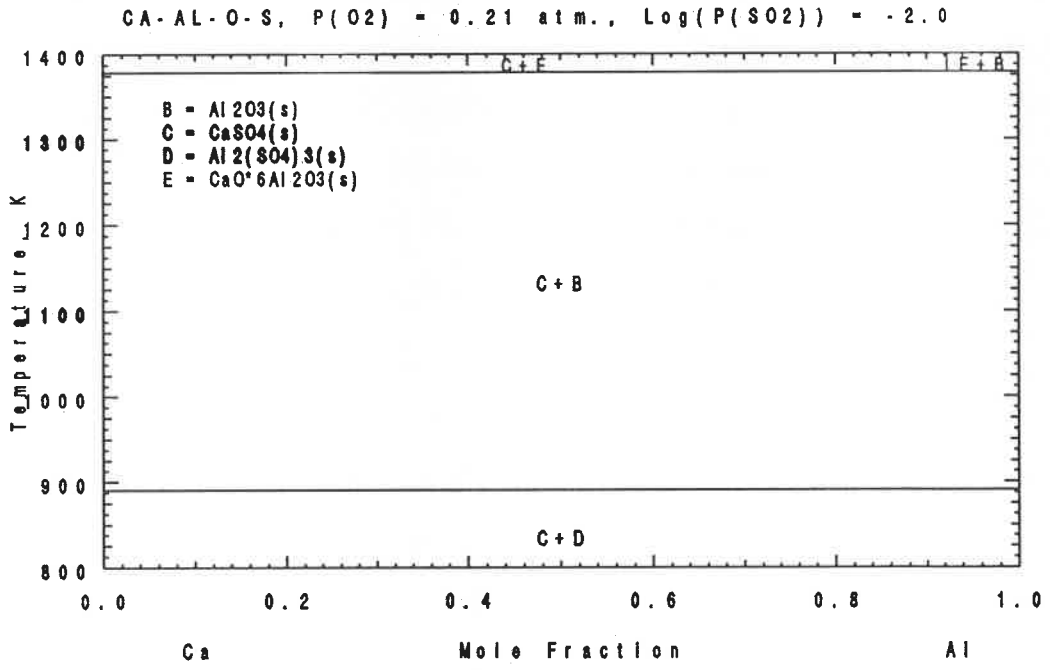

Figure 3.20 POTCOMP diagram for the Ca-Al-O-S system

(b). At P_{O_2} = 0.21 atm. and $Log(P_{SO_2})$ = -5.0 (Figure 3.21), there are several temperature ranges in which two phases can coexist. Between 1176 and 1255 K, it is the $CaSO_4$ + CA_6 two phase region, from 1255 to 1270 K, the $CaSO_4$ + CA_2 region, 1270 to 1325 K, the $CaSO_4$ + CA region, and from 1325 to 1350 K,

the $CaSO_4$ + C_3A region.

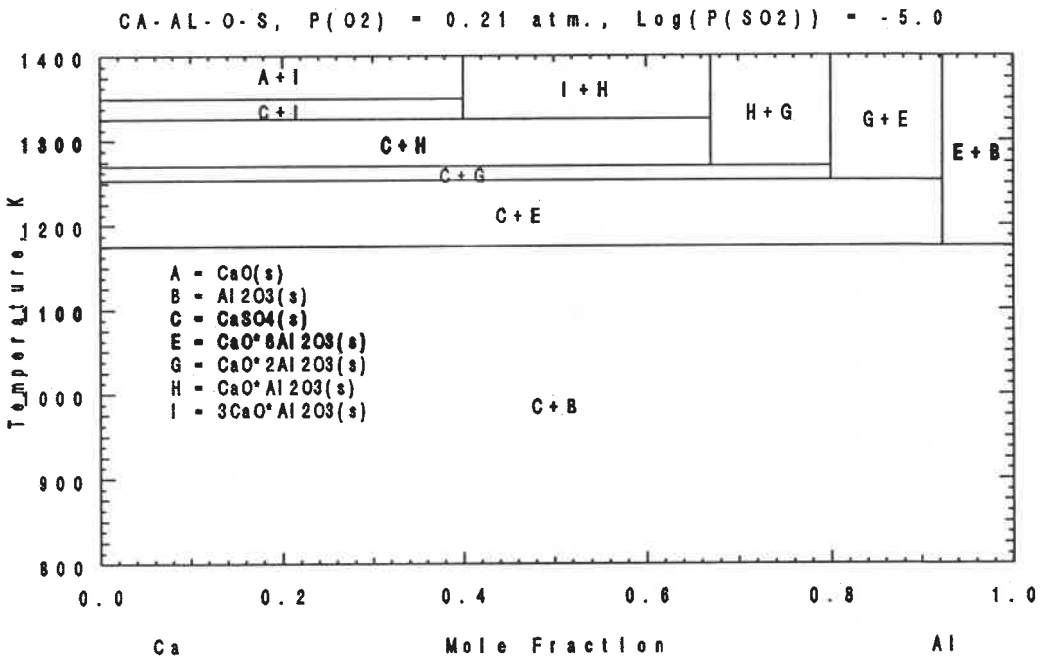

Figure 3.21 POTCOMP diagram for the Ca-Al-O-S system

3.4 Summary

Thermodynamic equilibrium information for a multi-component system is provided by the calculated phase diagrams. In all M-Al-O-S (M = Na, Ag, Ca) quaternary systems, the stability of ß and ß" with respect to sulphates is limited to high temperatures and low values of P_{SO_2} and P_{O_2}. At a given P_{O_2} and P_{SO_2}, Ag^+-ß-alumina may coexist with silver sulfate in a lower and wider temperature range than that for Na^+-ß-alumina or calcium aluminate. Therefore, to select a solid

electrolyte in a thermodynamic measurement involving SO_x gas, Ag^+-ß-alumina may be considered superior to Na^+-ß-alumina or calcium aluminate materials. In the stable coexisting range of Ag^+-ß-alumina with Ag_2SO_4, the cell using Ag^+-ß-alumina solid electrolyte will function reversibly. As the temperature decreases, the possibility of aluminum sulfate formation at the expense of the ß phase is pronounced and thus diminishes the reliability of the emf measurements.

CHAPTER IV EXPERIMENTAL INVESTIGATIONS

The experimental objective of this work was to develop an SO_x gas sensor with an alumina ceramic material being the candidate for the solid electrolyte. As discussed in the previous chapters, ß-aluminas have been employed[85,86] in galvanic cells to monitor SO_2 contents in oxidising atmospheres. In this study, Ag^+-ß-alumina was considered the primary candidate for the solid electrolyte. In addition, experiments were carried out on a Ca^{2+}-conducting aluminate material.

4.1 SO_x Monitoring by Ag^+-ß-alumina

Ag^+-ß-alumina Preparation

Tubes of the solid electrolyte Na^+-ß-alumina were prepared by the slip-casting method of PolyCeram[166]. The flat bottomed tubes were 3.5 - 4.0 cm long, 6 mm ID, with 1 mm wall thickness. Ag^+-ß-alumina tubes were produced by an ion-exchange procedure described elsewhere[93]. Briefly, the properly sintered Na^+-ß-alumina tubes were immersed into an alumina crucible containing pure silver nitrate (99.5%, Johnson Matthey) at 260 °C. The tubes were kept in the molten

Table 4.1 Ion-exchange Experiment Result

Batch No.	Weight Increase (%) 1	2	3	4	Thickness of wall (mm)	Exchange time (days)
1	18.15	18.20	19.00	19.43	1.0	5 + 1
2	18.76	18.69	18.31	B	1.5	5
3	19.39	18.45	19.22	18.79	1.0	5
4	18.80	18.39	18.54	B	1.0	5
5	19.33	19.27	19.12	B	1.0	2
6	*19.19	19.25	19.26	19.58	1.0	3
7	*18.62	19.20	19.00	19.25	1.0	2

B: tube was broken during ion-exchange;
*: thickest wall in that batch.

salt for 2 - 3 days with stirring intermittently in the bath, and then they were taken out of the crucible to check the weight increase. Another cycle of ion-exchange was carried out with fresh $AgNO_3$ in order to make sure that complete ion-exchange was reached and no further weight increase of the tubes was observed.

The results of the ion-exchange experiment are shown in Table 4.1. There were seven batches of tubes with four tubes in each batch. As seen from the Table, the weight increase varied between 18.15% and 19.58%. There was no further significant weight increase after two days of ion-exchange. The least weight increase for a given batch was always observed for the tube with greatest wall thickness, which is

understandable from a diffusion process point of view.

The chemical and physical properties of the Na^+-ß-alumina powder which was used in the slip casting have been reported elsewhere[143]. From the chemical composition of the powder, a value for x of 7.72 in the formula, $Na_2O \cdot xAl_2O_3$ of the beta phase can be deduced. The weight increase in the ion-exchange experiment can also be used to check the composition of the powder. Using the formula $Na_2O \cdot xAl_2O_3$ for the beta phase, the general expression for x in the case of complete substitution is as follows:

$$x = \frac{1}{M_{Al_2O_3}} \left(\frac{200}{WI} (M_i - M_{Na}) - M_{Na_2O} \right) \qquad \ldots(4.1)$$

where M_i and WI are the molecular weight of substitutive ion and the weight increase in percent respectively. Substituting the molecular weights, M_i = 107.9, M_{Na} = 22.99, M_{Na_2O} = 61.98, $M_{Al_2O_3}$ = 101.96 and the maximum weight increase from Table 4.1 into equation 4.1, a value of 7.89 for x is obtained, which is close to the value of 7.72 for the original beta alumina powder.

Cell Assembly

The cell unit for the emf measurement can be expressed as

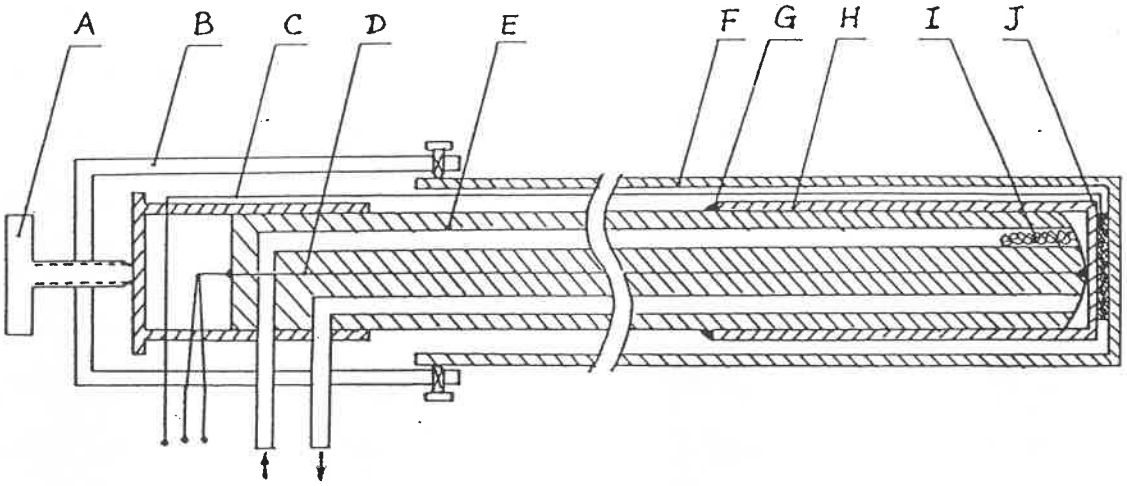

A. Set screw; B. Aluminium guide; C. Silver wire;
D. Pt-10%Rh,Pt thermocouple; E. 4 bores alumina tube;
F. Alumina support tube; G. Cement; H. Ag-Beta-alumina;
I. Platinum wire; J. Silver plate.

Figure 4.1 Schematic view of a cell unit

follows:

$$Ag/Ag^{+}\text{-}\beta\text{-alumina}/(SO_2 + Air), Ag_2SO_4, Pt \qquad \ldots(IX)$$

where pure silver on the left side is the reference electrode at which the activity of silver is fixed at unity. On the right side, the activity of silver is fixed by the reaction between the gas phase and the solid electrolyte. A schematic depiction of a cell unit is given in Figure 4.1. Pure silver wire (C) is connected to the outside bottom of the solid electrolyte tube by a load imposed by the set screw (A). A

four bore alumina tube (E) (50 cm long) serves as both a thermocouple sheath and a passage for the gas mixture. The tube (E) is put inside the solid electrolyte tube (H). Zirconia cement (G) is used to seal the solid electrolyte tube to the alumina tube. A Pt-10%Rh/Pt thermocouple (D) made from the wires (Johnson Matthey, 110 Industry St. Toronto, Ont. M6M 4M1) is located directly on the platinum mesh which provides the passage for the electronic current. Various gas mixtures of SO_2 + Air (SO_2 concentrations = 10ppm, 108ppm, 980ppm, 1019ppm and 8600ppm) provided by Canadian Liquid Air LTD (ALPHAGAZ, division of LIQUID AIR in Montreal) were directed into the electrolyte tube.

Working Electrode

The working electrode is the cathode of the cell (IX). Due to the complexity of the electrode system, for example, the possible non-equilibrium gas mixture and the unequilibrated electrode reaction, precautions must be taken to promote equilibrium. Three different configurations of the electrode were employed (Figure 4.2).

For type 1 (Figure 4.2), the inner surfaces of the tubes were platinized from a few drops of chloroplatinic acid solution. After baking at 600 °C, a porous layer (F) of

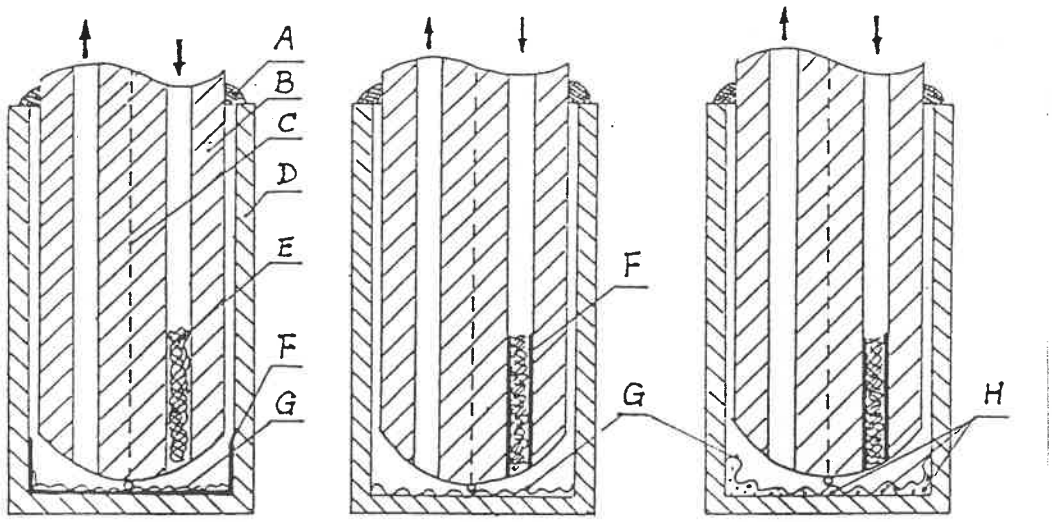

A. Cement; B. 4 bores alumina tube; C. Thermocouple;
D. Ag-Beta-Al2O3; E. Platinum wire; F. Porous Pt layer;
G. Platinum mesh; H. Ag_2SO_4 powder.

Figure 4.2 Three types of working electrode

platinum was formed on the surface of the solid electrolyte. The metallic layer functioned both as an electronic conductor and as a catalyst for the oxidation of SO_2. In addition, a platinum mesh (G) was used to maintain a good electric contact between the electrode and the lead wire. As indicated in Chapter II, a catalyst is indispensable for the pre-reactions which take place in the gas phase. Consequently, a roll of fine platinum wire (E) was inserted into the bore of the gas inlet and acted as the catalyst.

Unlike type 1, the surface of the solid electrolyte was

not platinized for type 2 and type 3 (Figure 4.2) electrode preparations. Instead, the end portion of the gas mixture inlet was platinized (F) in order to catalyze the equilibrium of the pre-reactions in the gas phase before the gas mixture reached the triple point area. Since the formation of silver sulfate on the surface of the solid electrolyte is expected to take place by the attack of the gas mixture on the electrolyte, type 2 and 3 electrode constructions are considered to be superior to type 1 in that more reaction sites will be available without the porous platinum layer on the surface of the electrolyte. For type 3, some solid silver sulfate powder (H) was also added between the solid electrolyte and the platinum mesh in order to compare the different electrode preparations.

Measurement Equipment

A schematic presentation of the measuring system is shown in Figure 4.3. The temperature was maintained at ±2 °C by a Lindberg Hevi-Duty temperature controller. A digital PH/mV meter, Model 701A, was used to measure the emf, and signals were recorded on a SOLTEC-1242 250mm 2 pen strip chart recorder.

The flow rate of the gas mixture was measured by two

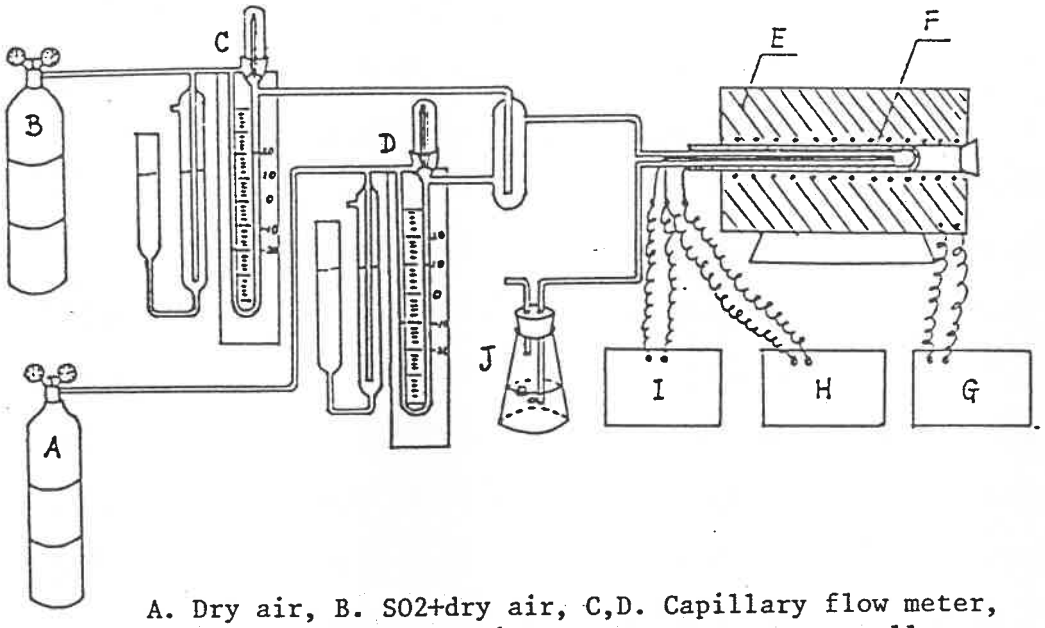

A. Dry air, B. SO2+dry air, C,D. Capillary flow meter,
E. Furnace, F. Cell unit, G. Temperature controllor,
H. Potential meter, I. Voltmeter, J. KOH solution.

Figure 4.3 Schematic view of experimental assembly

types of flow meters, depending on the flow rate range. A capillary flow meter was employed for flow rates less than 60 ml/min., whereas a floating ball flow meter was used for higher flow rates. Both flow meters were calibrated by the soap-bubble method before each experimental run.

Cell Reaction

The dominant reactants of a cell reaction are those for which changes in concentration directly result in noticeable

changes in the electrode properties. SO_2 may be excluded from the possible dominant reactants because in the primary measurement it has been found that the emf of the cell was not sensitive to changes in concentration of SO_2. This is in agreement with previous studies[58,74], i.e. it took a long time to get a reasonable emf change corresponding to a concentration change of SO_2, so the overall cell reaction can be proposed as follows:

$$2Ag(s) + SO_3(g) + 1/2O_2(g) = Ag_2SO_4(s) \qquad ...(4.2)$$

For the pure silver reference electrode, the activity of silver is unity and the Nernst equation for the cell reaction can be written as

$$E = -\frac{\Delta G^{\circ}}{2F} - \frac{RT}{2F}\ln\frac{a_{Ag_2SO_4}}{P_{SO_3}\cdot P_{O_2}^{1/2}} \qquad ...(4.3)$$

where ΔG° is the standard Gibbs energy change for the cell reaction (4.2). If the activity of silver sulfate is equal to unity, P_{O_2} is defined, and ΔG° is available, the partial pressure of SO_3 can be determined from the emf measurement.

Furthermore, the emf of the cell can be related to the initial partial pressure of SO_2 by the method first adopted in Gauthier's study[58]. Assuming that the equilibrium in the gas

phase

$$SO_2(g) + 1/2O_2(g) = SO_3(g) \qquad \ldots(4.4)$$

has been established and considering that

$$(P_{SO_2})_{initial} = (P_{SO_2} + P_{SO_3})_{equilibrium} \qquad \ldots(4.5)$$

the equilibrium constant of reaction (4.4) is

$$K = \frac{P_{SO_3}}{P_{SO_2} \cdot P_{O_2}^{1/2}} \qquad \ldots(4.6)$$

Combining equations (4.5) and (4.6) results in

$$P_{SO_3} = \frac{(P_{SO_2})_I \cdot K \cdot P_{O_2}^{1/2}}{1 + K \cdot P_{O_2}^{1/2}} \qquad \ldots(4.7)$$

Substituting equation (4.7) into equation (4.3) leads to

$$E = -\frac{\Delta G^\circ}{2F} - \frac{RT}{2F} \ln \frac{a_{Ag_2SO_4} \cdot (1 + K \cdot P_{O_2}^{1/2})}{(P_{SO_2})_I \cdot K \cdot P_{O_2}} \qquad \ldots(4.8)$$

In the present study, $(P_{O_2})_{initial} = 0.21$ atm, $(P_{SO_2})_{initial}$ is in the range of 10ppm to 8600ppm, and P_{O_2} can be considered unchanged during the measurement. Assuming unit activity of silver sulfate, equation (4.8) simplifies to

$$E = A + \frac{RT}{2F}\ln(P_{SO_2})_i \qquad \ldots(4.9)$$

where A depends only upon temperature and P_{O_2}. According to equation (4.9), at constant T and P_{O_2}, E is a linear function of $\ln(P_{SO_2})_i$, whereas at constant $(P_{SO_2})_i$ and P_{O_2}, E is a linear function of temperature (if ΔG° is a linear function of T).

EMF Measurement

For all three working electrode preparations, the emf was measured in the same manner. First the temperature of the cell unit was raised gradually to the higher part of the temperature range while keeping dry air flowing over the working electrode compartment. When the temperature became constant, an SO_2 + Air gas mixture at a fixed flow rate was introduced into the working electrode compartment (Figure 2). This resulted in a gradual increase in the emf. Depending upon the temperature and initial concentration of SO_2, the emf became stable after several hours. When the emf values remained constant to ±1 mV for more than 20 minutes, it was considered to be in equilibrium and the value was noted. Then the temperature was raised (or lowered) several decades of degrees for a new measurement. For increases in temperature, regardless of the SO_2 concentration, the emf value declined, implying that dE/dT was negative. Depending on the SO_2 level,

the highest temperature was limited to the point where a non-zero emf could be measured, this corresponded to an equal activity of silver on both sides of the electrolyte. The lowest temperature was determined when the emf started to deviate from the linear behavior indicated by equation (4.9). After several cycles of temperature, the concentration of SO_2 was changed and the temperature cycle was repeated, starting at the high temperature.

Two electrode leads were made of different metals, Ag and Pt. The thermopotential generated by the Ag/Pt thermocouple is well-known[68] and can be expressed by a simple linear function of temperature:

$$E(mV,Ag+) = -8.098 + 0.01914 \cdot T \quad (580 - 1130\ K)$$

Accordingly, the experimental emfs were corrected for this thermoelectric effect.

4.2 SO_2 Monitoring with $0.9CaO*0.72MgO*5.5Al_2O_3$

Preparation of Ca^{2+}-Conducting Ceramics

Experiments were carried out in order to prepare Ca^{2+}-conducting ceramic tubes by the slip-casting method. The composition of the tubes was designed to correspond to $0.9CaO \cdot 0.72MgO \cdot 5.5Al_2O_3$ by making the slip from oxides and/or

salts stoichiometrically. After being sintered at about 1600 °C, the crystal structure of the tubes was checked by X-ray diffraction. Although the tubes were well sintered, none was identified to have the ß or ß" structure. From the results of X-ray diffraction for the powder of a sintered tube, the phase of magnetoplumbite[144] was identified. Both ß-alumina and magnetoplumbite phase have a hexagonal structure with $c/a \approx 4$. Compared with the ß phase, less conductivity is expected for the magnetoplumbite phases.

Preparation of the Electrodes

The following cell design was employed using tubes of Ca^{2+} conducting ceramic electrolyte:

Pt,Air,CaO/0.9CaO·0.72MgO·5.5Al_2O_3/$CaSO_4$,(SO_2, Air),Pt ...(X)

The reference electrode was composed of pure CaO powder and dry air. This electrode covered the exterior of the tube. The activity of calcium was fixed by the equilibrium between air and solid calcia powder. Platinum mesh was put on both sides of the ceramic electrolyte tube in order to assure good electrical contact in the triple point area. The working electrode compartment was closed by sealing the joint between the electrolyte tube and the alumina tube of the gas mixture

passage with zirconia cement. A small amount of calcium sulfate powder, obtained by mixing $CaCO_3$ and $(NH_4)_2SO_4$ powder and then calcinating at 800 °C for 12 hours, was put inside the working electrode compartment. This promoted equilibrium and made the electrode reversible.

Cell Reaction

If calcium is the only cation migrating through the ceramic tube, the overall reaction in cell (X) could be proposed as follows.

At the anode which is the reference electrode on the left, the calcia decomposes by the reaction:

$$CaO - 2e = 1/2O_2 + Ca^{2+} \qquad ...(4.10)$$

whereas at the cathode of cell (X), the formation of calcium sulfate proceeds as follows:

$$Ca^{2+} + SO_2 + O_2 + 2e = CaSO_4 \qquad ...(4.11)$$

The overall cell reaction is given by the sum of the two electrode reactions:

$$CaO(s) + SO_2(g) + 1/2O_2(g) = CaSO_4(s) \quad ...(4.12)$$

If reaction (4.4) in the gas phase is taken into account, the alternative overall cell reaction will be

$$CaO(s) + SO_3(g) = CaSO_4(s) \quad ...(4.13)$$

From the dependence of emf on the flow rate of gas at the working electrode compartment, SO_3 has been experimentally ruled out as an electro-active species. Thus reaction (4.12) was considered to be the predominant overall cell reaction. Application of the Nernst equation to the cell reaction leads to:

$$E = -\frac{\Delta G^{\circ}}{2F} + \frac{RT}{2F}\ln(P_{SO_2} \cdot P_{O_2}^{1/2}) \quad ...(4.14)$$

where ΔG°, F, and R are the standard Gibbs energy change for reaction (4.12), the Faraday constant, and the gas constant respectively.

Apparently the conversion ratio of SO_2 to SO_3 at fixed P_{O_2} is a function of temperature, and it plays an important role in the theoretical calculation of emf by equation (4.14). If the conversion ratio is defined as follows:

$$C.R.(\%) = \frac{100 \cdot P_{SO_3}}{(P_{SO_2})_{initial}} \qquad ...(4.15)$$

then, from equation (4.7):

$$C.R.(\%) = \frac{100 \cdot K \cdot P_{O_2}^{1/2}}{1 + K \cdot P_{O_2}^{1/2}} \qquad ...(4.16)$$

According to equation (4.16), the conversion ratio at equilibrium depends upon both temperature and the partial pressure of oxygen. A schematic plot of C.R.(%) versus temperature at three P_{O_2} levels is shown in Figure 4.4, from which a C.R. of less than 10 % is expected above 1200 K. Consequently, P_{SO_2} in equation (4.14) can be replaced by $(P_{SO_2})_{initial}$ without introducing much error (maximum error would be less than 2.3%). At temperatures below 1200 K, an expression identical to equation (4.9) may be deduced:

$$E = -\frac{\Delta G^o}{2F} + \frac{RT}{2F} \ln \frac{(P_{SO_2})_i \cdot P_{O_2}^{1/2}}{1 + K \cdot P_{O_2}^{1/2}} \qquad ...(4.17)$$

EMF Measurement

Calcia powder was used as the reference electrode and it was situated outside the electrolyte tube. Since calcia tends

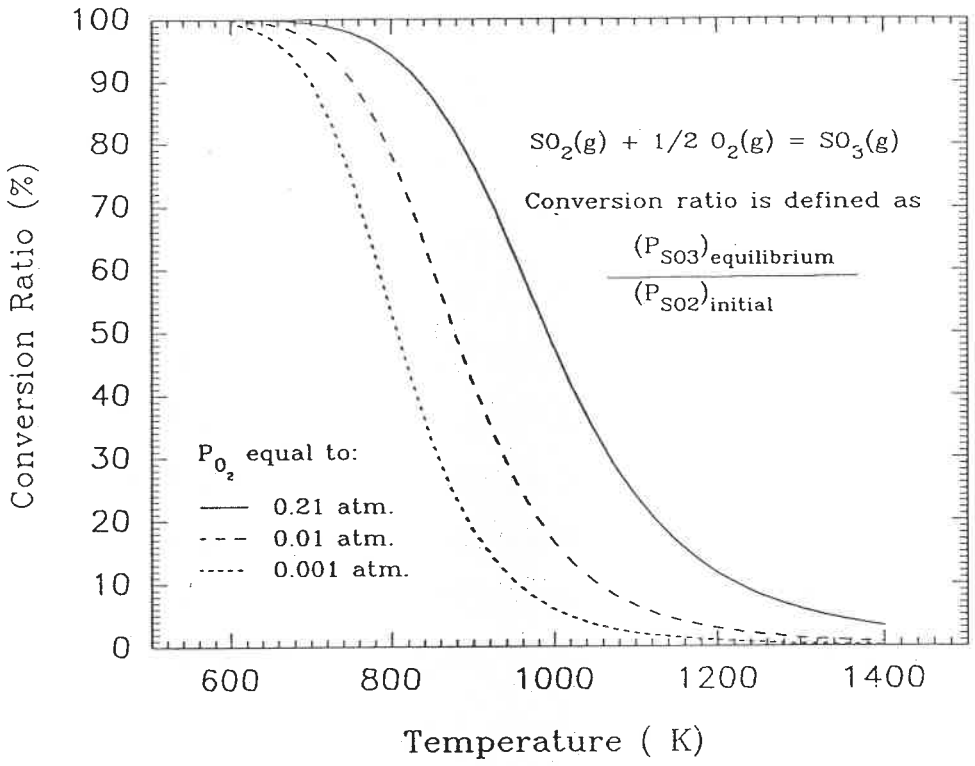

Figure 4.4 Conversion ratio of SO_2 to SO_3

to react with traces of water in the air to form hydroxide below 800 K, measurements were carried out by first raising the temperature of the cell unit above 800 K and then waiting for a steady value of emf.

Four different experimental runs were carried out, of which one was found to give an unexpected emf response to the temperature change. It was attributed to a leak at the cement joint, arising from the fact that an acid liquid (pH = 2-3) was condensed in the cold zone of the supporting alumina tube during the measurement.

The flow rate of gas in both electrode compartments was varied separately in order to examine the dependence of emf on the flow rate of the gas mixture. The flow rate of air over the reference electrode in the range 0 - 100 ml/min. produced only a few millivolts difference in emf. Unlike the case of Ag^+-ß-alumina, high flow rates of gas over the working electrode resulted in higher emf values, implying that SO_2 was the predominant electro-active species.

Compared with the emf measurement using Ag^+-ß-alumina, the emf value was not stable at certain temperatures and gas flow rates. An emf value within ± 3 mV over 20 min. was taken as a steady one. At the beginning of the experimental run, a relatively high emf value was observed, approaching the theoretical value from equation (4.17). The emf value then kept declining to a much lower value. The emf never regained its high level during subsequent cycles of temperature.

CHAPTER V RESULTS AND DATA TREATMENT

5.1 EMF Values Measured with Ag^+-ß-alumina

Following the experimental procedure presented in the proceeding Chapter, the dependence of emf on the temperature, on the flow rate of the gas mixture, and on the initial partial pressure of SO_2 was investigated for all the three types of working electrode construction. Generally speaking, the dependencies were different for the three types of working electrodes, although there were similar behaviors. From the dependence of emf on the temperature, the standard Gibbs energy change for the cell reaction can be deduced providing that the equilibria at the electrodes are sustained.

EMF Dependence on Flow Rate of Gas Mixture

It was found that the measured emf was dependent on the flow rate of the gas mixture in the working electrode compartment, and that the extent of the dependency was influenced by factors such as the temperature, the concentration of SO_2 in the gas mixture, and the range of the flow rate. When the flow rate was low, at high concentrations of SO_2, an acid liquid (pH = 2 - 3) appeared on the wall of the plastic tube which was connected to the outlet of the gas

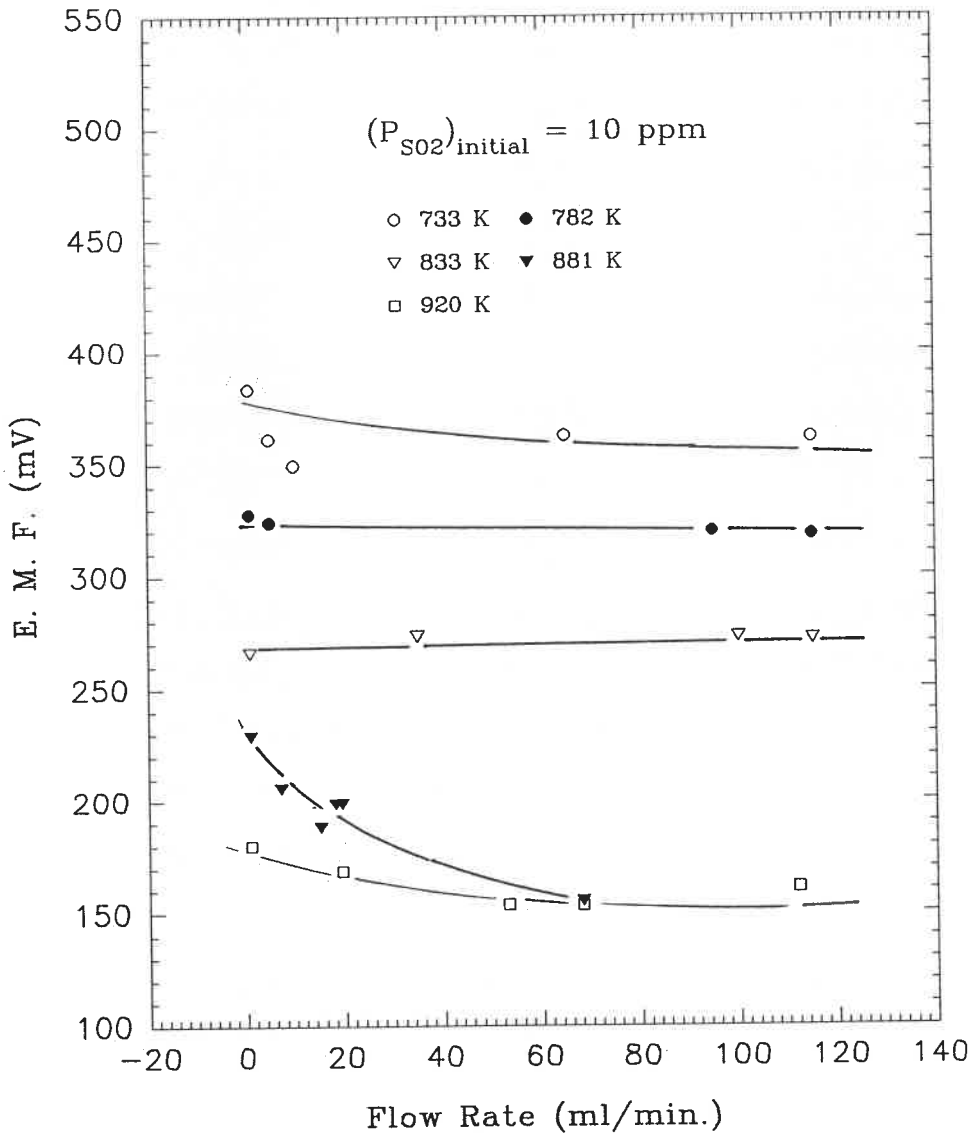

Figure 5.1 EMF Dependence on Flow Rate for Type 1 Electrode Preparation

mixture. The more concentrated the gas mixture in SO_2 and the lower the flow rate, the more liquid formed on cooling. As a result, it was difficult to control precisely the flow rate, especially at the low range.

For the type 1 working electrode construction, at the lowest SO_2 concentration level of 10 ppm (Figure 5.1), the dependence of emf on the flow rate was not strong, especially at relatively high temperatures. The dependence of emf on the flow rate became stronger as the concentration of SO_2 was increased, as illustrated by Figure 5.2 (see also Figures 1 and 2 in Appendix B). A plateau on the emf versus flow rate plot was observed at higher flow rates. Nevertheless, at higher temperatures this dependence was mitigated.

The type of electrode construction did not have a strong effect on this dependence, at least with respect to the behavior of emf for various flow rates. The dependence for the type 2 electrode is shown in Figures 3 to 6, and that for the type 3 in Figures 7 to 10 in Appendix B. Less strong dependence of emf on flow rate was observed at higher SO_2 concentration levels for these two latter electrode constructions (Figures 2, 6, and 10 in Appendix B).

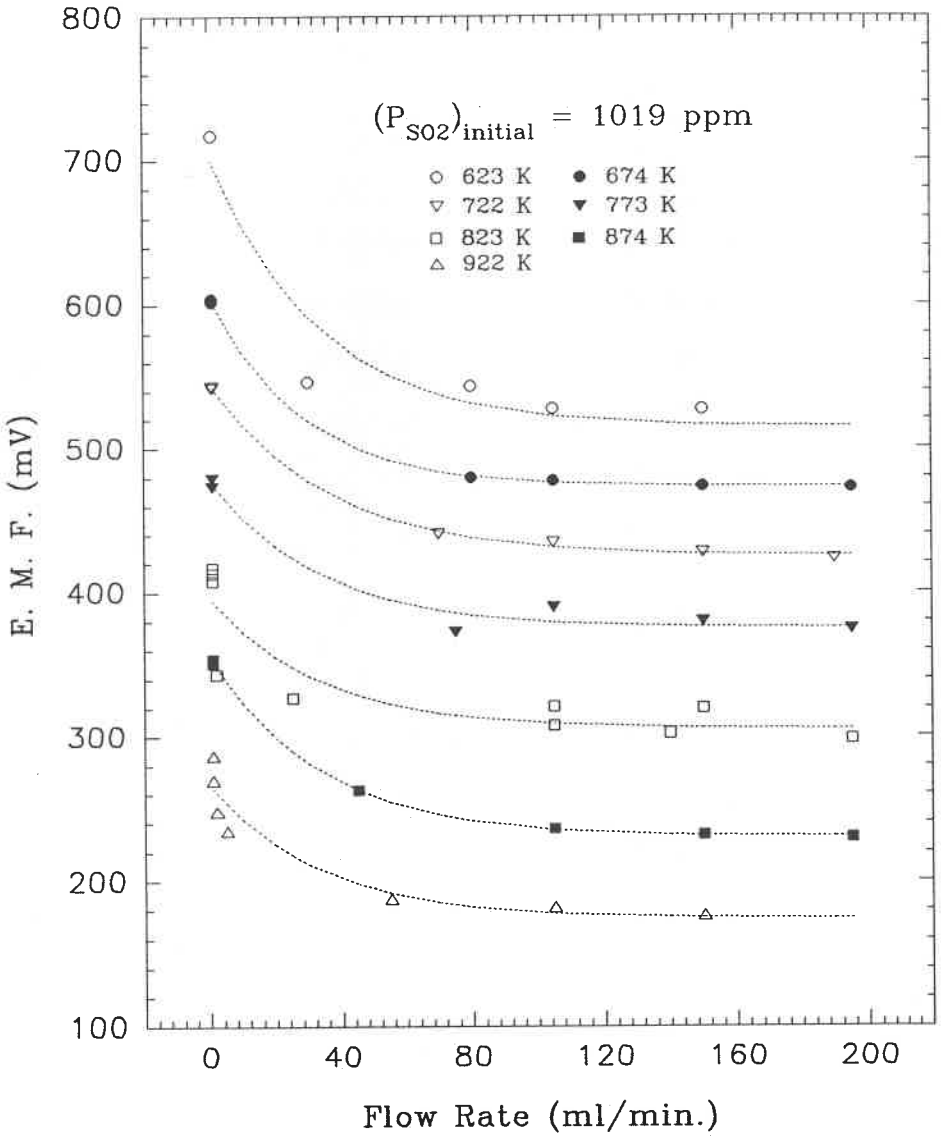

Figure 5.2 EMF Dependence on Flow Rate for Type 1 Electrode Preparation

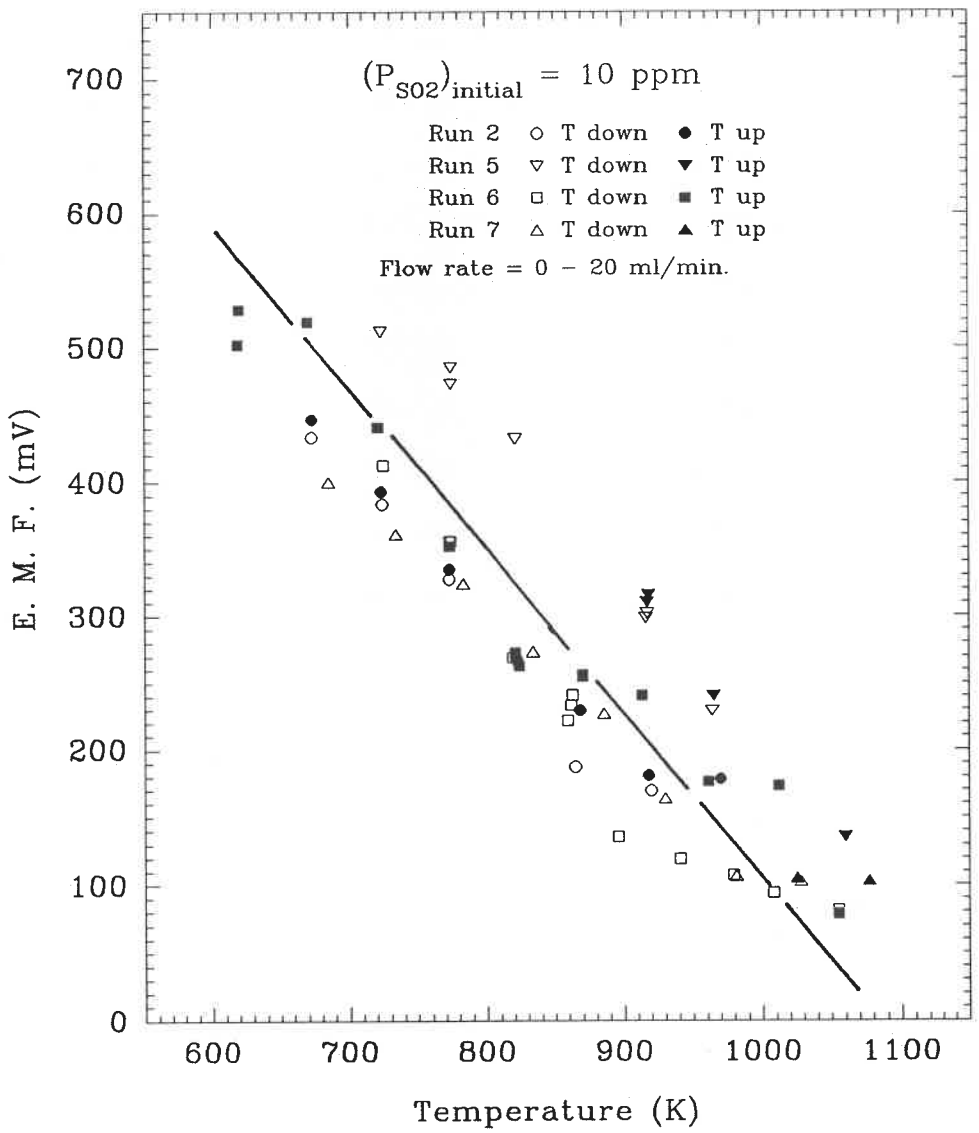

Figure 5.3 EMF Dependence on Temperature for Type 1 Electrode Preparation

EMF Dependence on Temperature

The measured emf at relatively low temperatures was always lowered by an increase in flow rate. This implies a lower conversion fraction of SO_2 at higher flow rates, as predicted by equation (4.3). The results shown in Figures 5.3 to Figure 5.13 were taken at such flow rates that a further decrease of the flow rate either resulted in a decrease of emf or no effect at all. For a given concentration of SO_2, the behavior of the emf as a function of temperature was found to depend upon the working electrode preparation.

For a given gas flow rate, the measured emfs for type 1 electrodes were not reproducible between different experimental runs, as shown in Figure 5.3 (also see Figures 11, 12 in Appendix B). This is probably due to the fact that the porosity of the platinum layer on the surface of the solid electrolyte is the least reproducible among many relevant factors involved in electrode performance[4]. In addition, there was a tendency of the steady emf at a certain temperature to decrease with time.

The measured emf as a function of temperature with the type 2 working electrode construction was found to depend on the duration of the run. As shown in Figures 5.4 and 5.5,

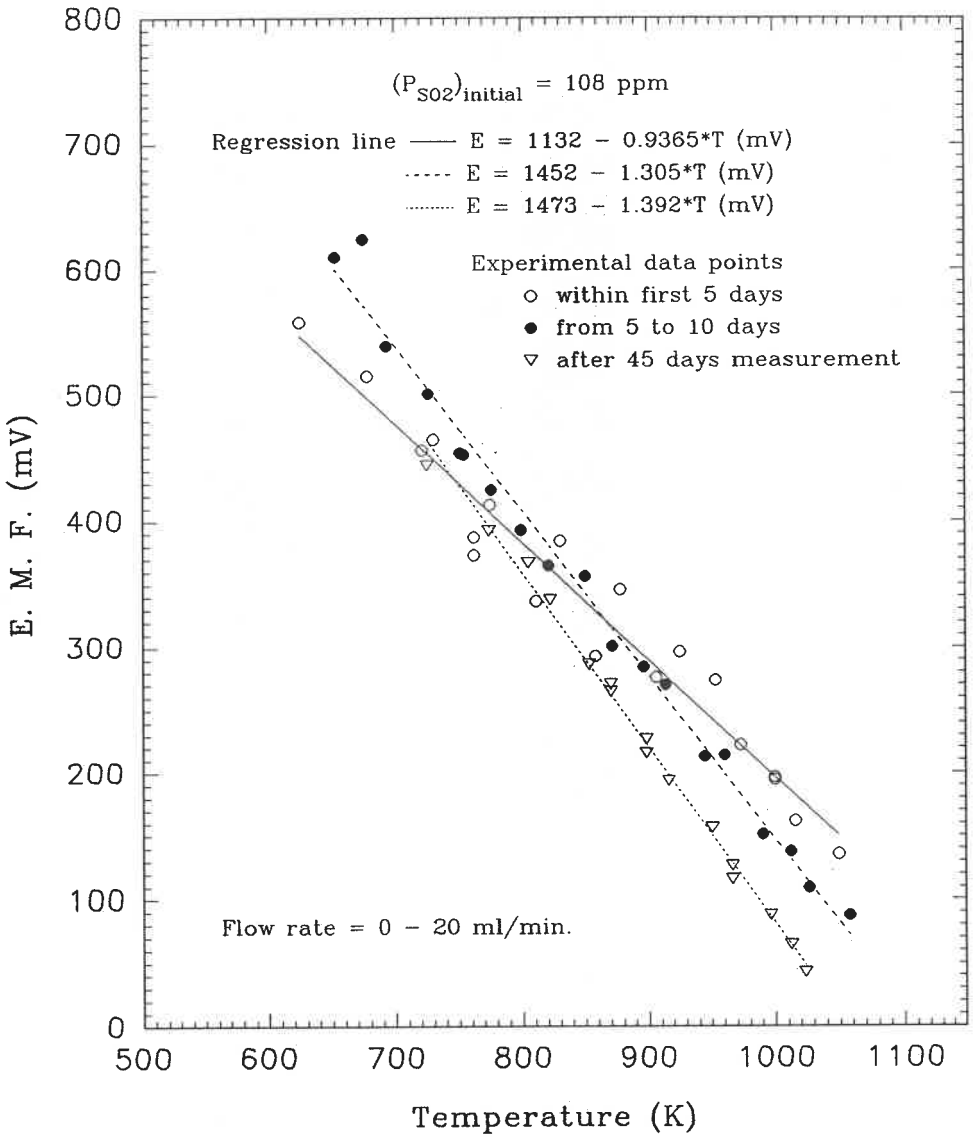

Figure 5.4 EMF Dependence on Temperature for Type 2 Electrode Preparation.

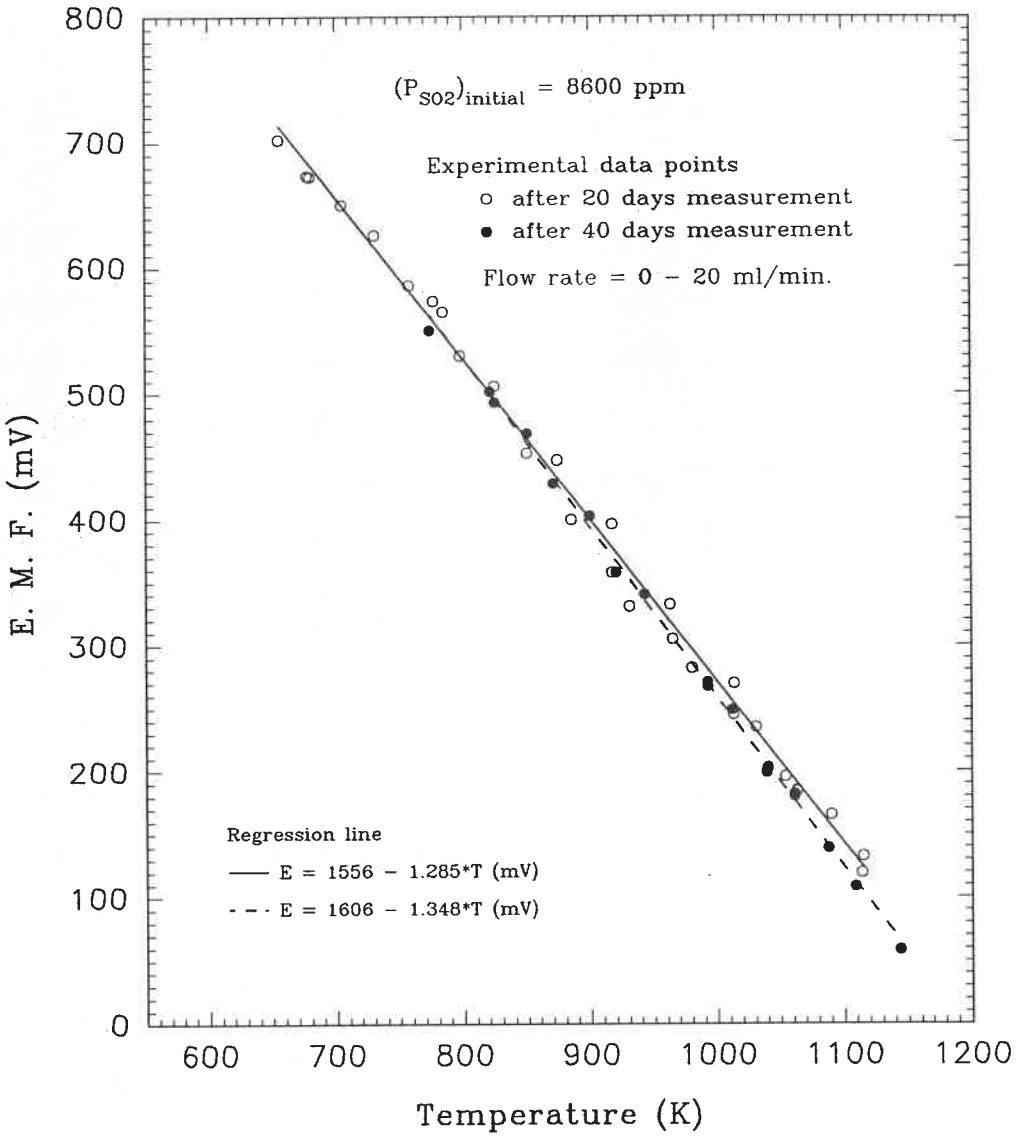

Figure 5.5 EMF Dependence on Temperature for Type 2 Electrode Preparation

both parameters in the linear regression equation vary with time.

At P_{SO_2} = 108 ppm (Figure 5.4), the experimental points within the first five days measurement are best fitted by the equation:

$$E = 1132 - 0.9365 \cdot T \text{ (mV)}$$

those from five to ten days by the equation:

$$E = 1452 - 1.305 \cdot T \text{ (mV)}$$

and those after 45 days by the equation:

$$E = 1473 - 1.392 \cdot T \text{ (mV)}$$

At P_{SO_2} = 8600 ppm (Figure 5.5), the dependence is not as noticeable as that at the lower SO_2 concentration.

Thermodynamically, the gradual change of slope of the emf vs. temperature plot, dE/dT, indicates that the entropy change for the cell reaction is a function of time. The slope change from -0.9365 to -1.392 mV/K after 45 days continuous measurement indicates that the entropy change was much higher after a long period of time. In fact, after about 15 days, the rate of slope change decreased by nearly a factor of 5. That is why little slope change can be observed in Figure 5.5, in which the data after 20 days measurement and that beyond 40 days are compared.

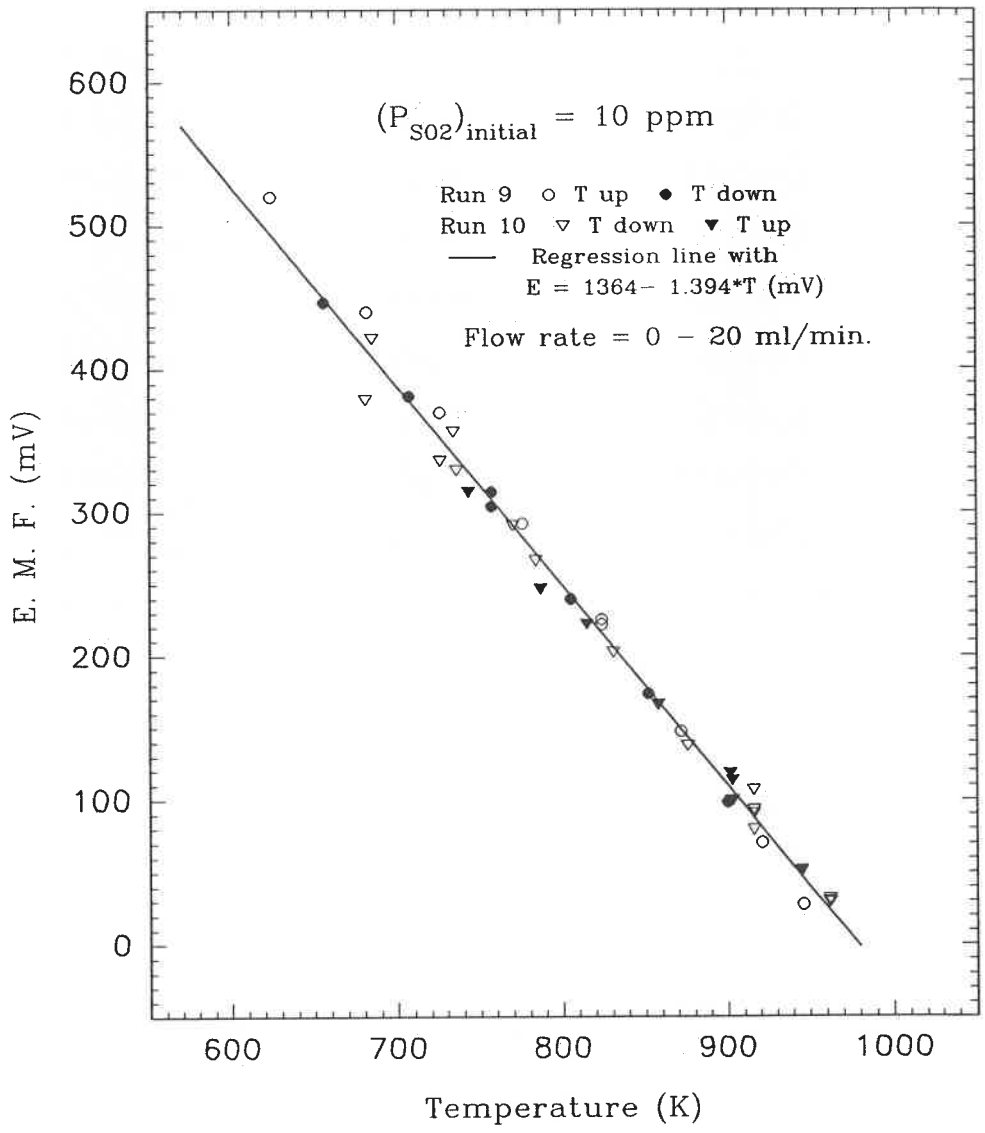

Figure 5.6 EMF Dependence on Temperature for Type 3 Electrode Preparation

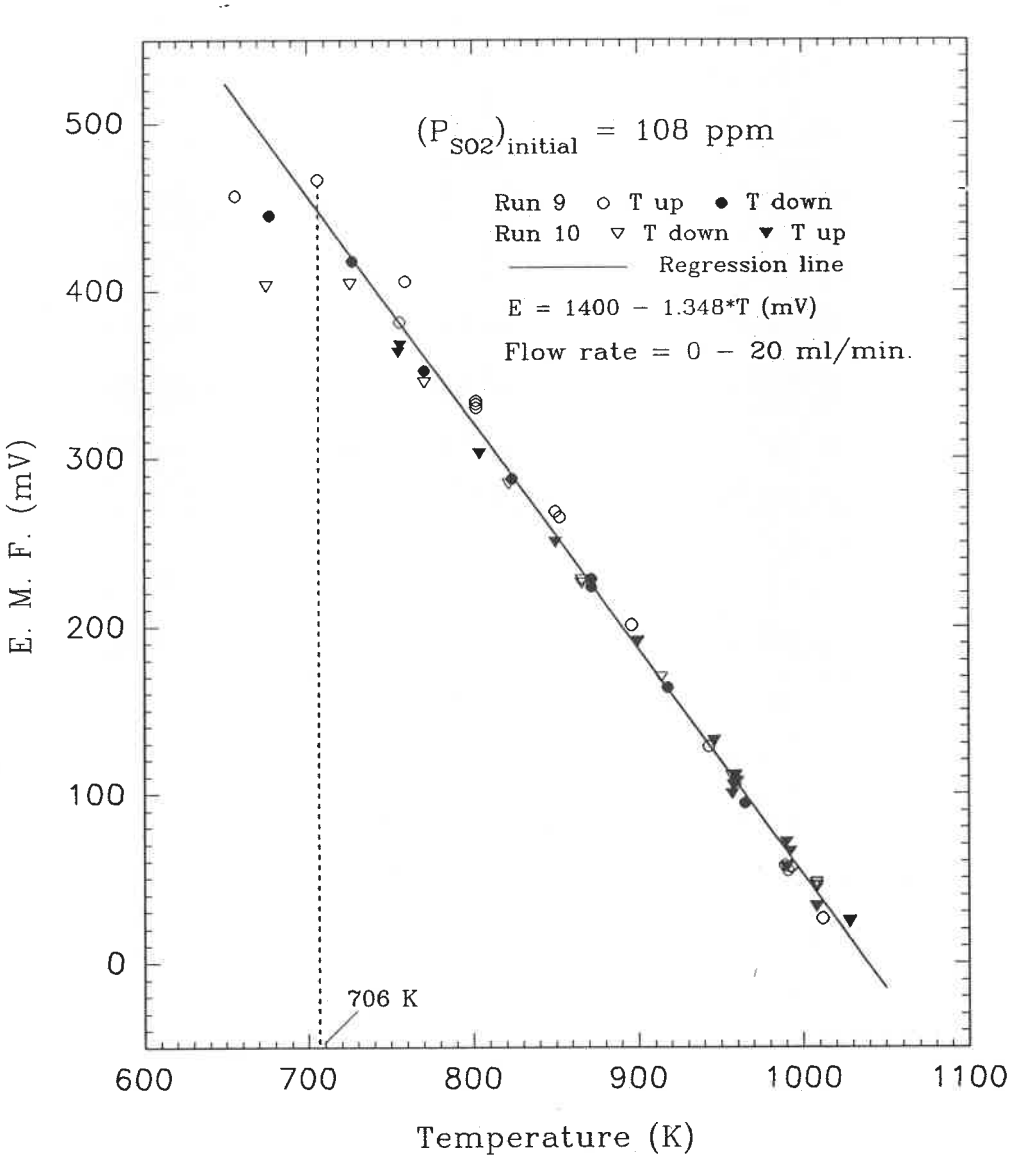

Figure 5.7 EMF Dependence on Temperature for Type 3 Electrode Preparation

The most reproducible and stable emf values were observed for type 3 electrode preparations. This is due to the reversibility of the type 3 electrode construction. As shown in Figures 5.6 through 5.9, a linear relation between emf and temperature predicted by equation (4.9) was observed for all the SO_2 concentration levels studied within a certain temperature range. The departure from the linear relation took place at low temperatures, depending on the concentration of SO_2. As indicated in Figures 5.7 through 5.9, the deviation occurred at approximately 706 K, 719 K and 794 K for SO_2 concentrations of 108 ppm, 980 ppm, and 8600 ppm respectively. Irrespective of the temperature history, the experimental emf points fall on a common line. In addition, the results are reproducible between different experimental runs. A linear regression analysis leads to the following expressions:

$$P_{SO_2} = 10 \text{ ppm} \quad E = 1364(\pm 15.8) - 1.394(\pm 0.019)\cdot T \quad (mV)$$

$$P_{SO_2} = 108 \text{ ppm} \quad E = 1400(\pm 12.2) - 1.348(\pm 0.014)\cdot T \quad (mV)$$

$$P_{SO_2} = 980 \text{ ppm} \quad E = 1517(\pm 14.3) - 1.366(\pm 0.021)\cdot T \quad (mV)$$

$$P_{SO_2} = 8600 \text{ ppm} \quad E = 1566(\pm 15.3) - 1.325(\pm 0.015)\cdot T \quad (mV)$$

EMF Dependence on SO_2 and O_2 Concentration

As discussed earlier, the emf was not sensitive to the

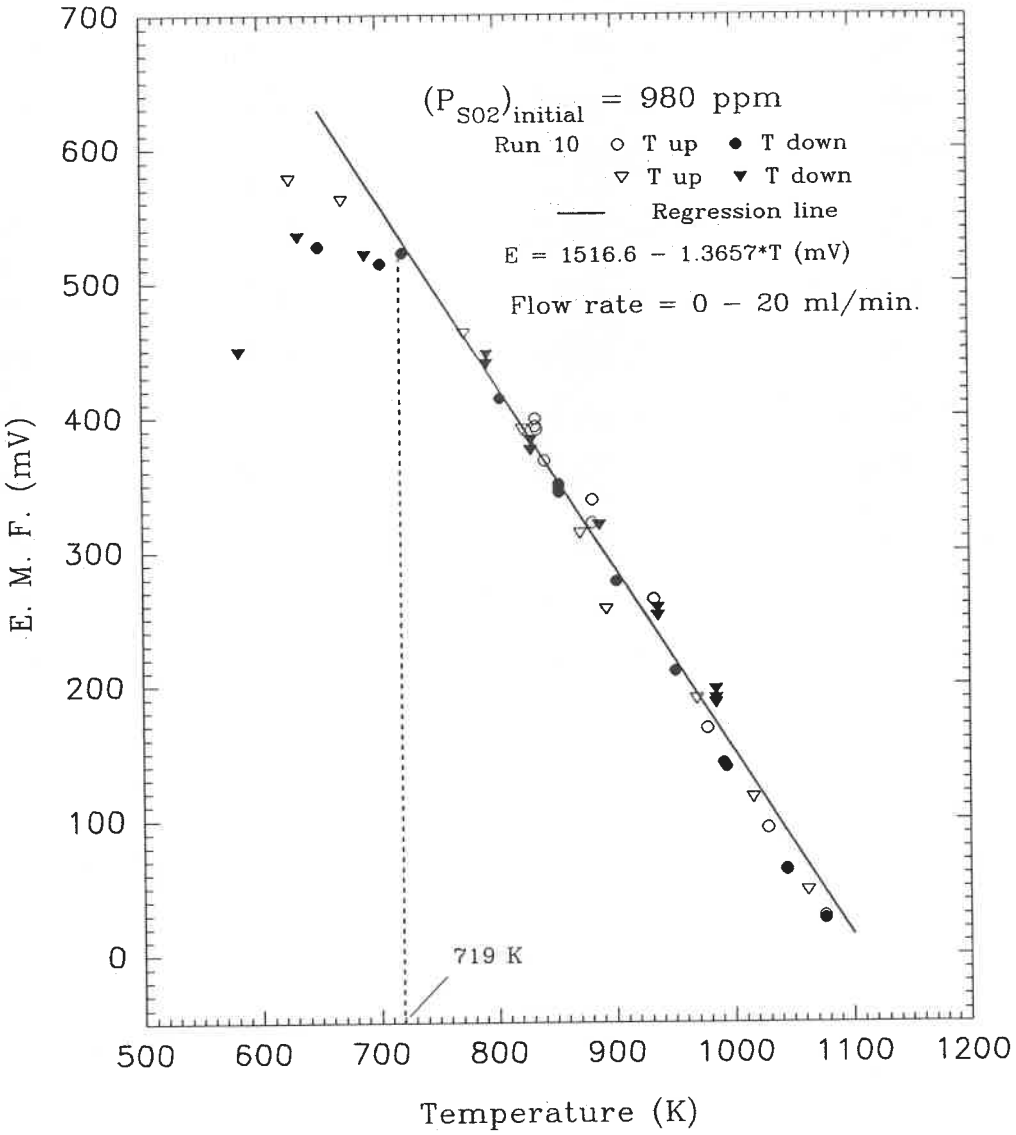

Figure 5.8 EMF Dependence on Temperature for Type 3 Electrode Preparation

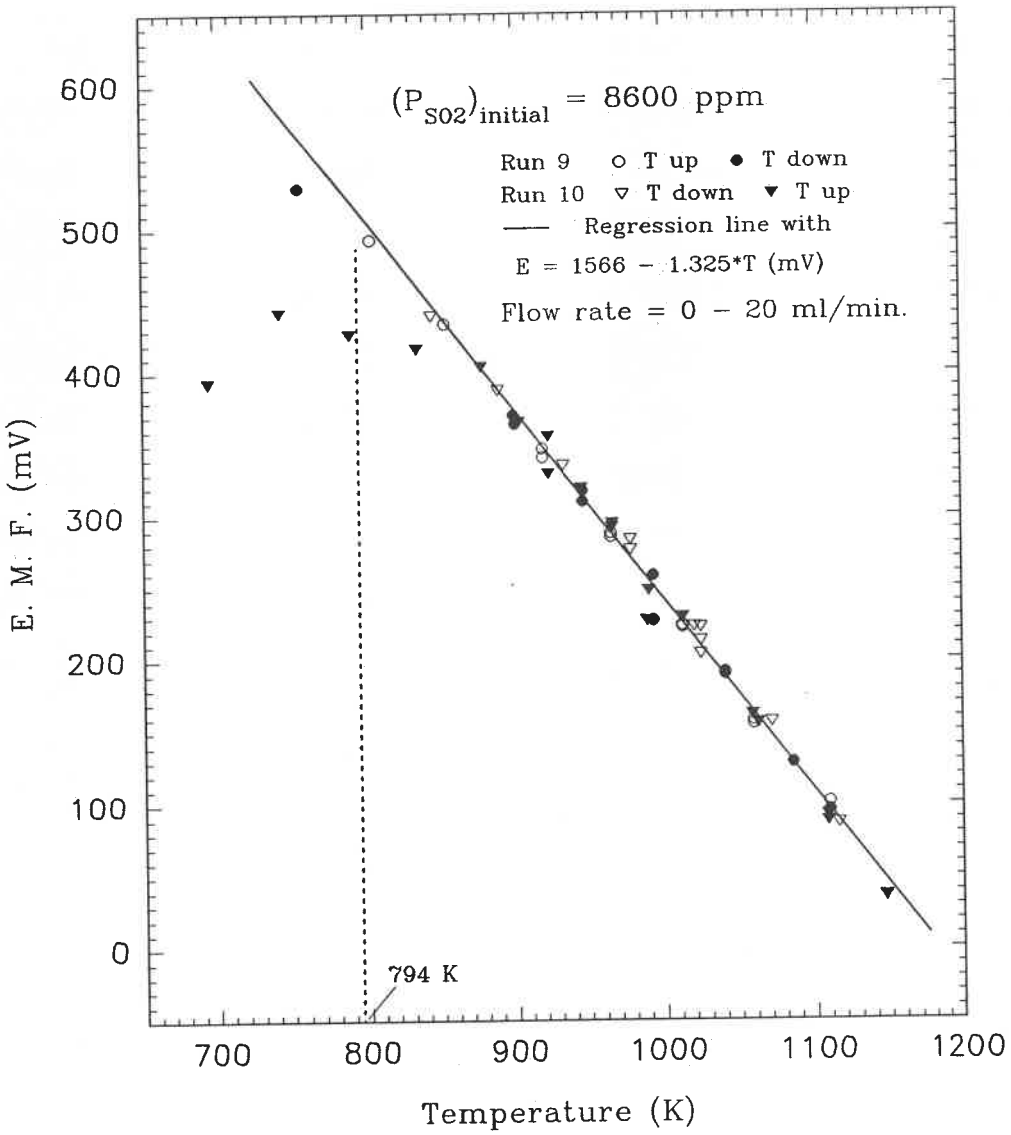

Figure 5.9 EMF Dependence on Temperature for Type 3 Electrode Preparation

concentration change of SO_2 in the gas phase, indicating that SO_2 was not an electro-active species. Furthermore, it was found that changing concentration of SO_2 from the highest level, 8600 ppm, to a lower one resulted in a higher emf in comparison with those directly measured at that level. This phenomenon was observed for all three types of electrode constructions. Figure 5.10 shows an example of the phenomenon for the type 1 electrode with the SO_2 concentration being changed from 8600 ppm to 10 ppm. Examples for type 3 electrode are shown in Figures 5.11 and 5.12. The higher emf value at the beginning of the SO_2 concentration change tended to decrease as the measurement was continued.

In Figure 5.13, following the measurements carried out with 8600 ppm SO_2, air was introduced and was kept flowing over the working electrode compartment for about 2 days. Then a lower level of SO_2 (10 ppm) was introduced. It is noted that there is good agreement between the two sets of experimental data.

In one experimental run, the dependence of emf on both P_{SO_2} and P_{O_2} was investigated at two different temperatures. Two P_{O_2} levels (air and pure O_2), were used while P_{SO_2} was changed from 30 ppm to 5000 ppm. It was found that the emf responded to the P_{O_2} change more quickly than to the P_{SO_2}

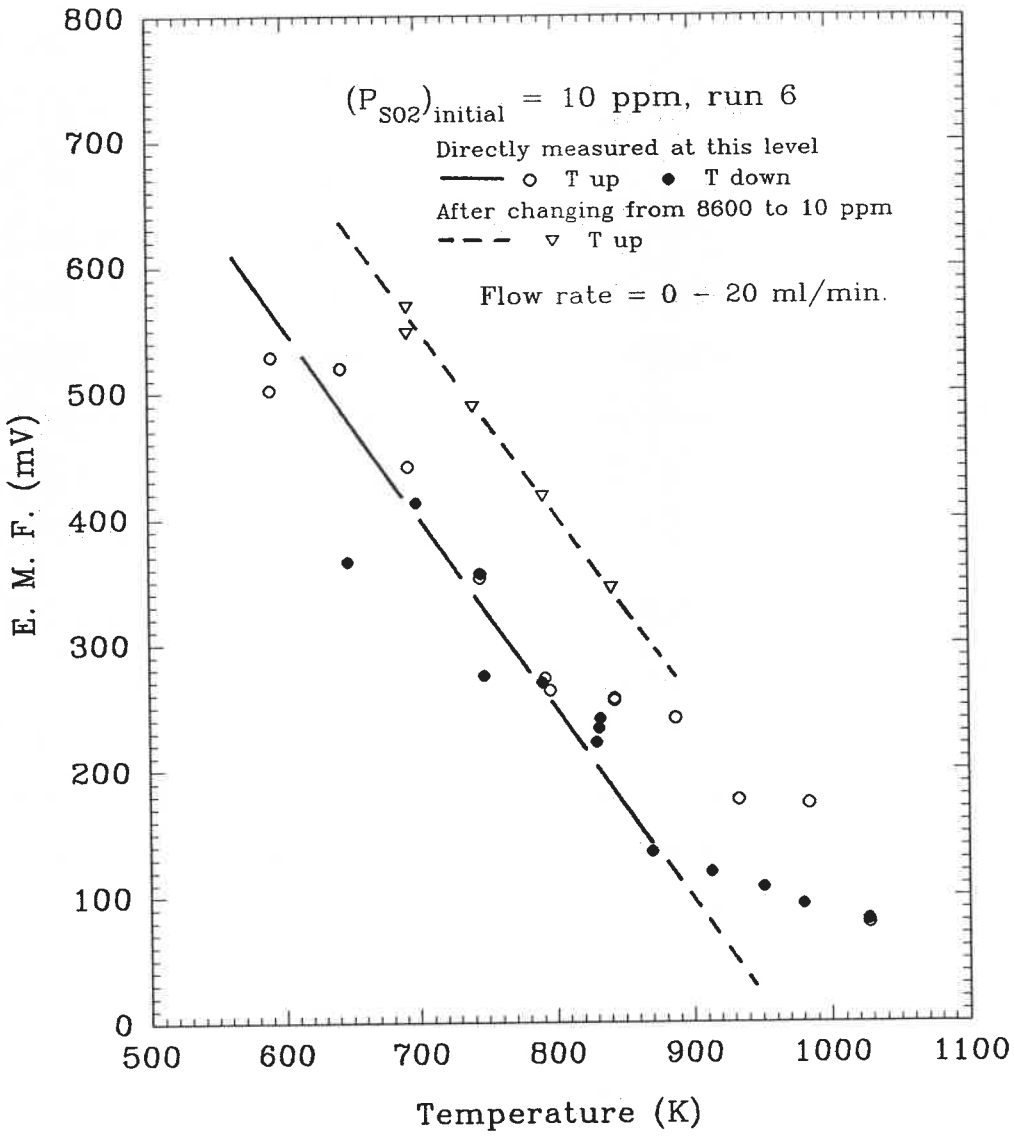

Figure 5.10 Comparison of emf values for Type 1 electrode

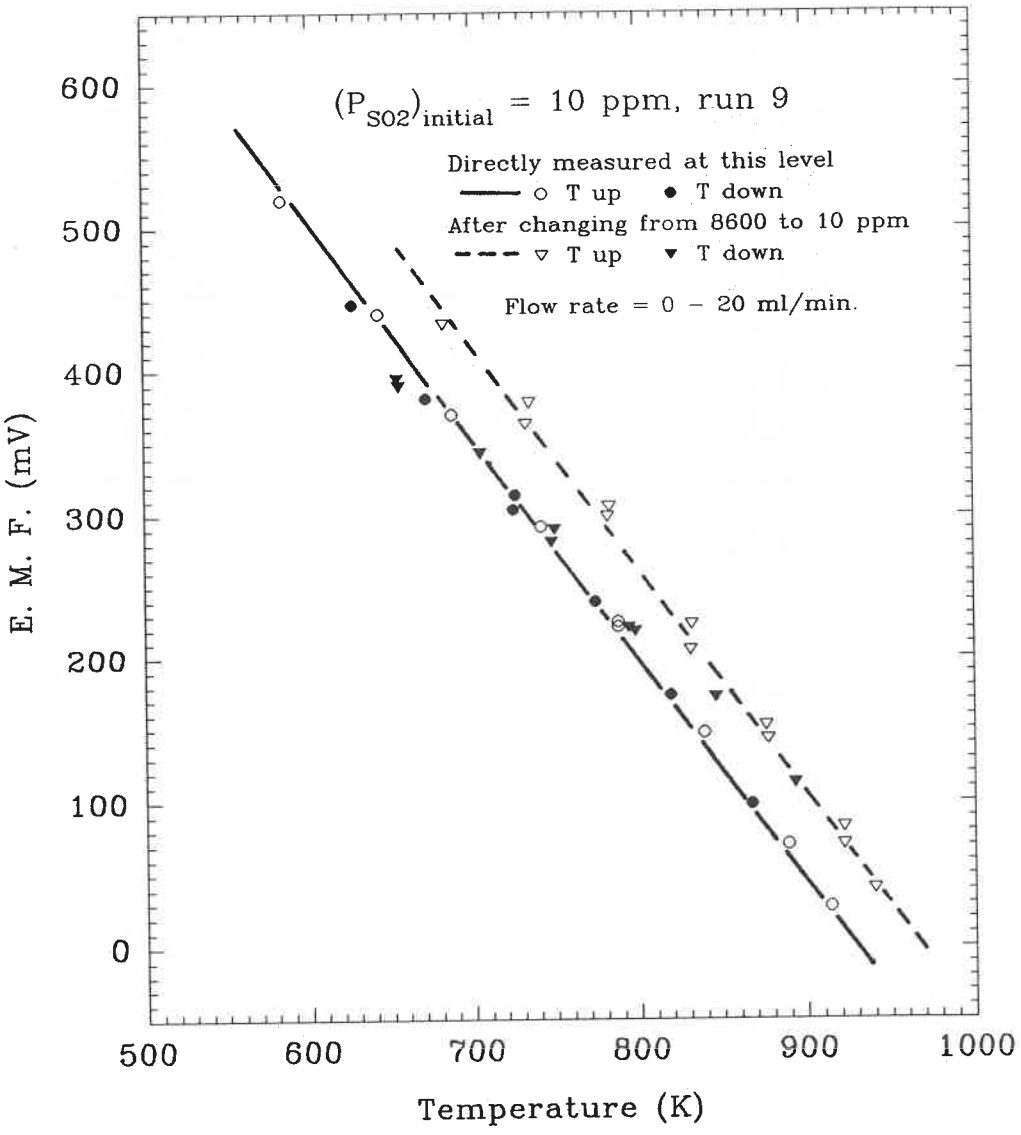

Figure 5.11 Comparison of emf values for Type 3 electrode preparation

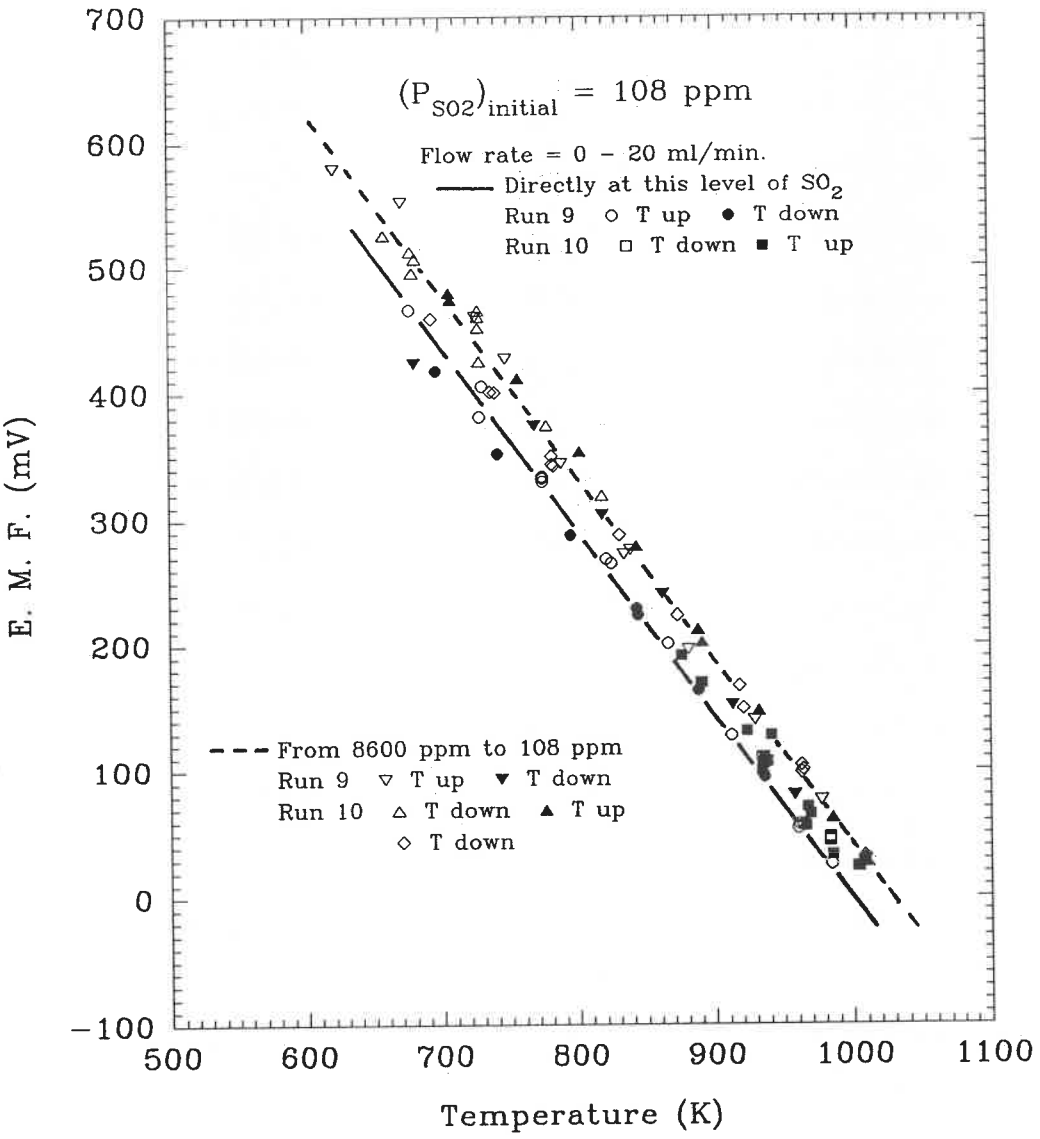

Figure 5.12 Comparison of emf values for Type 3 electrode preparation

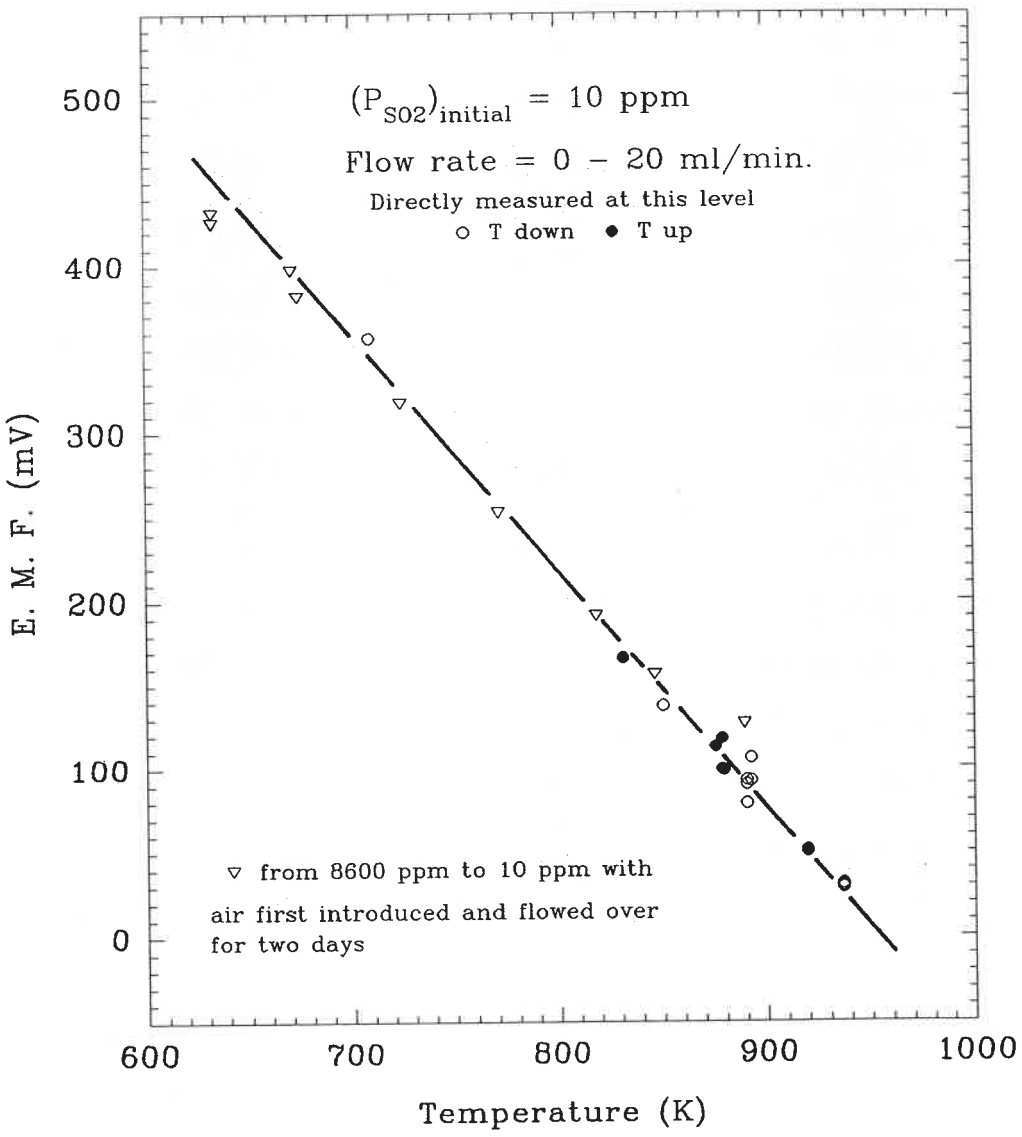

Figure 5.13 Comparison of emf values for Type 3 electrodee

change. The results are shown in Figure 5.14. As predicted by equation (4.9), a linear relation was observed for both P_{O_2} levels at 964 K, but only for the higher P_{O_2} level at 918 K. A deviation from the linear relation is noted as the concentration of SO_2 was increased for the case of low temperatures and low P_{O_2} level.

Long Term Stability

An evaluation was performed on the long term stability of emf at three temperatures with 108 ppm SO_2. At a given temperature, the steady emf value was unchanged within ±2.4 mV for up to 8 days. There was no indication that beyond that time the emf would change drastically. The results are shown in Figure 5.15. They can be expressed as:

848 K EMF = 272.4 ± 0.6 (mV)

891 K EMF = 221.9 ± 2.4 (mV)

942 K EMF = 166.4 ± 1.1 (mV)

Standard Gibbs Energy Change for the Cell Reaction

The standard Gibbs energy change for the proposed cell reaction (4.2) is related to the emf by equation (4.8) as long as the equilibria in the cell system are sustained during the

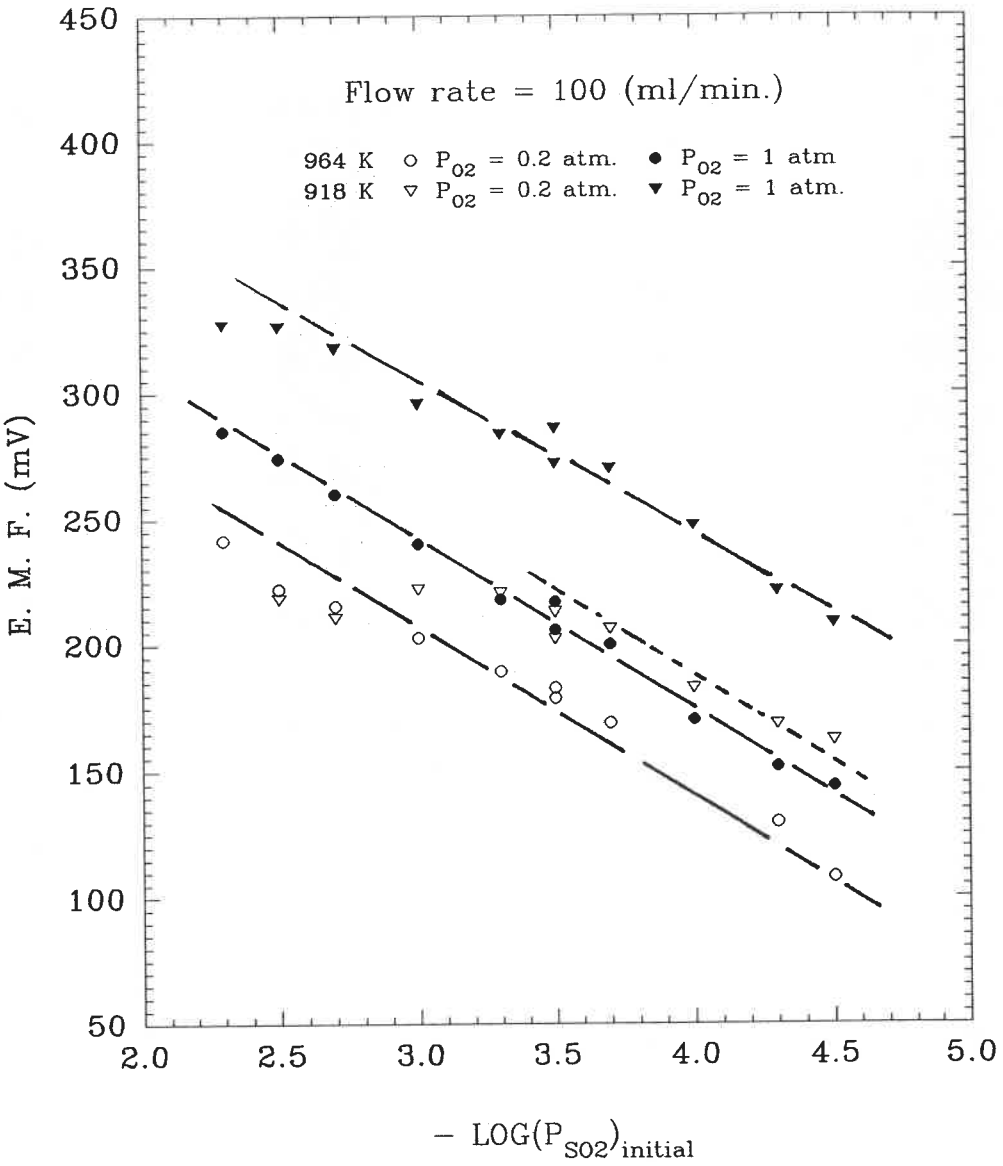

Figure 5.14 EMF Dependence on P_{SO2} and P_{02} at a fixed Flow Rate

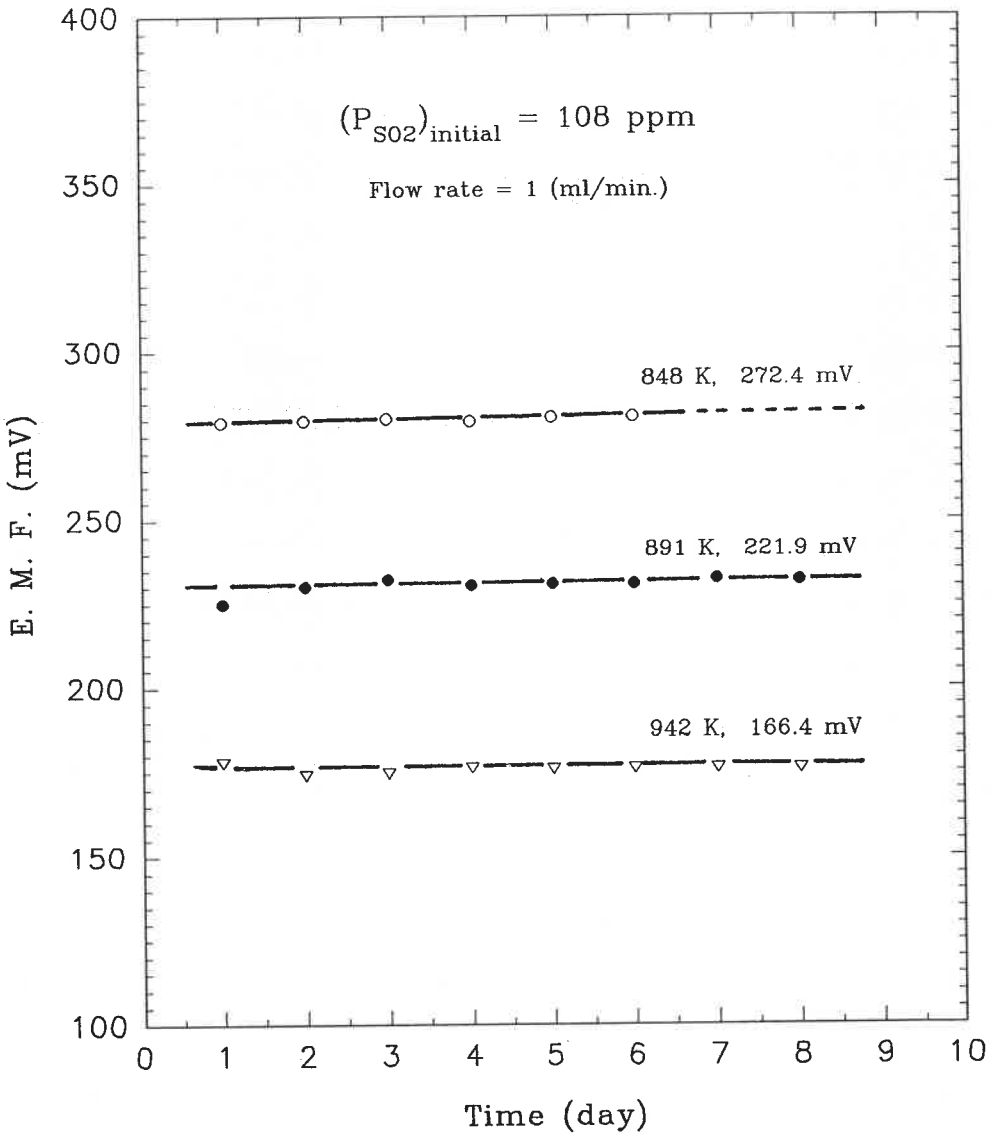

Figure 5.15 Long Term Stability of EMF at Three Different Temperatures

emf measurement. With $a_{Ag_2SO_4} = 1$, as in the type 3 electrode preparation of this study, equation (4.8) can be expressed as

$$\Delta G^{\circ} = -2FE + RT\ln\frac{(P_{SO_2})_i \cdot K \cdot (P_{O_2})_e}{1 + K \cdot (P_{O_2})_e^{1/2}} \qquad \ldots(5.1)$$

where ΔG°, $(P_{SO_2})_i$, $(P_{O_2})_e$, and K represent the standard Gibbs energy change for reaction (4.2), the initial partial pressure of SO_2, the equilibrium partial pressure of O_2 and the equilibrium constant for reaction (4.4) respectively.

The equilibrium constant K can be obtained by means of well-established thermodynamic data[132] for reaction (4.4). Experimentally $(P_{O_2})_i >> (P_{SO_2})_i$, so $(P_{O_2})_e$ in equation (5.1) can be replaced by $(P_{O_2})_i = 0.21$ atm.. As a result, ΔG° can be calculated from the experimental values of E, T, and $(P_{SO_2})_i$.

The emf vs. temperature plots in Figures 5.6 through 5.9 show a linear relation between emf and T, implying a linear function of T for the Gibbs energy change,

$$\Delta G^{\circ} = A + B \cdot T \qquad \ldots(5.2)$$

Each experimental point in these Figures leads to a value of ΔG° at that temperature (equation (5.1)). A plot of all the ΔG° values versus T is shown in Figure 5.16. Constants A and

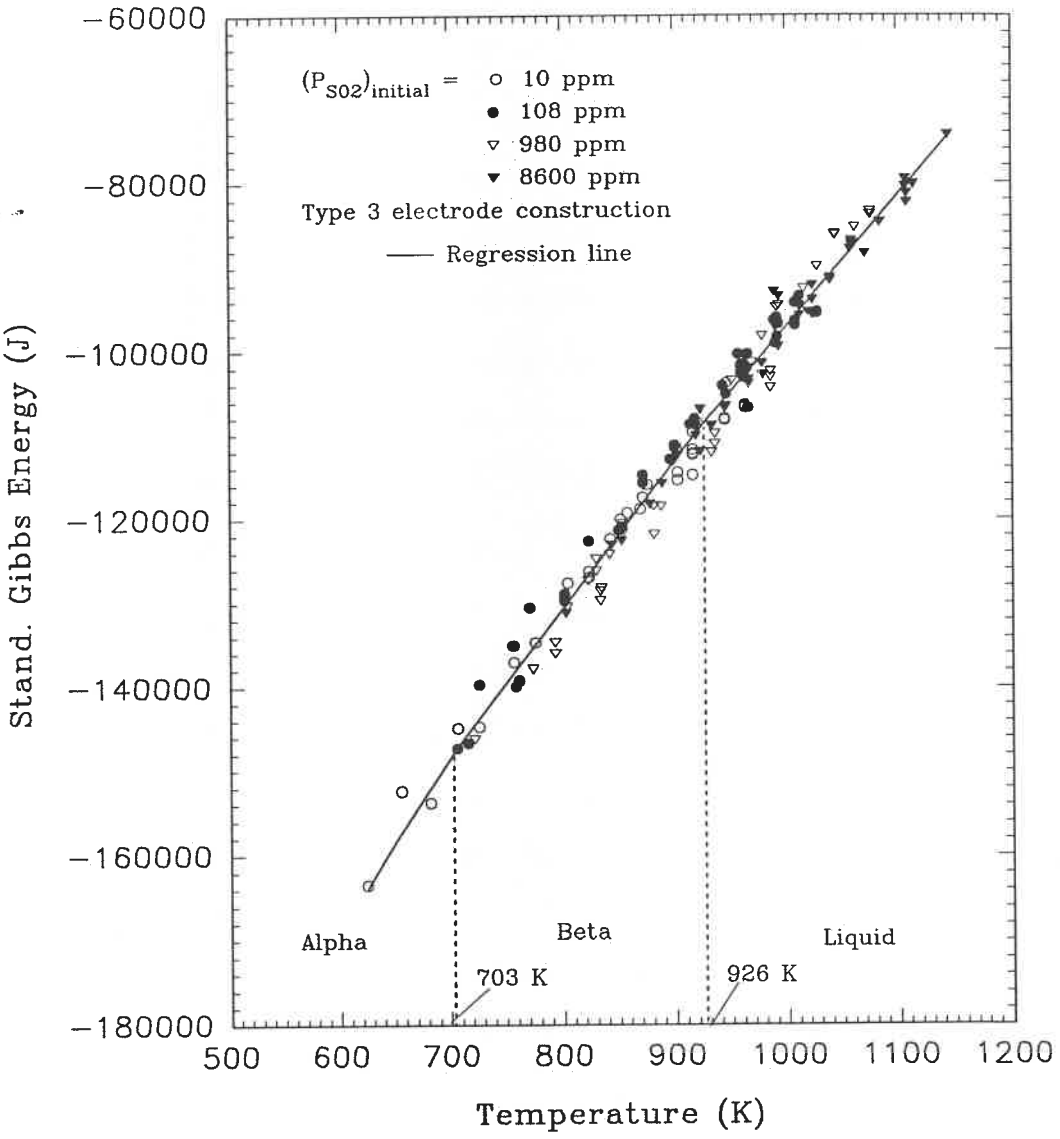

Figure 5.16 Standard Gibbs Energy Change as a Function of Temperature for Cell Reaction (4.2)

B in equation (5.2) can be obtained from a linear regression analysis (Table 5.1).

Table 5.1. Results of Linear Regression Analysis

$$\Delta G^\circ = A + B \cdot T \ (J)$$

$$2Ag(s) + SO_3(g) + 1/2\ O_2(g) = Ag_2SO_4(s,l)$$

Constant A	-271160
Standard Error of ΔG° Estimation	2236
Relative Coefficient	0.9842
Number of Observations	176
Degree of Freedom	174
T Coefficient B	175.54
Standard Error of Coefficient B	1.68

Solid silver sulphate undergoes an $\alpha \rightarrow \beta$ transformation at 703 K and melts at 926 K. The enthalpy changes at the phase transformation temperatures have been measured[145]. The Gibbs energy changes for the phase transformations are:

$$Ag_2SO_4(\alpha) = Ag_2SO_4(\beta) \qquad \ldots(5.3)$$

$$\Delta G^\circ = 19300 - 27.45 \cdot T \ (J) \qquad \ldots(5.4)$$

$$Ag_2SO_4(\beta) = Ag_2SO_4(l) \qquad \ldots(5.5)$$

$$\Delta G^\circ = 19100 - 20.63 \cdot T \ (J) \qquad \ldots(5.6)$$

An attempt to deduce the Gibbs energy changes for the values of transformation of Ag_2SO_4 (5.4 and 5.6) by dividing the emf data into three groups according to temperature and then carrying out a linear regression analysis for the three groups individually failed, particularly for the lower temperature range, because there are fewer experimental points at the two extreme temperatures and that leads to smaller relative coefficients.

The alternative way is to transform the Gibbs energy change in the lower and higher temperature ranges to a corresponding value of the ß-phase by adding an appropriate Gibbs energy change of transformation. Then, an expression of Gibbs energy for the ß-phase can be obtained through a linear regression analysis for all the experimental points. The result is given in Table 5.1 and shown in Figure 5.16 where the regression line for the ß-phase takes the form:

$$\Delta G^\circ(kJ) = -271.160(\pm 2.236) + 1.7554(\pm 1.68)10^{-3} \cdot T \quad \ldots(5.7)$$

For the purpose of comparison, ΔG° expressions from this study and from previous publications are listed in Table 5.2 and plotted in Figure 5.17.

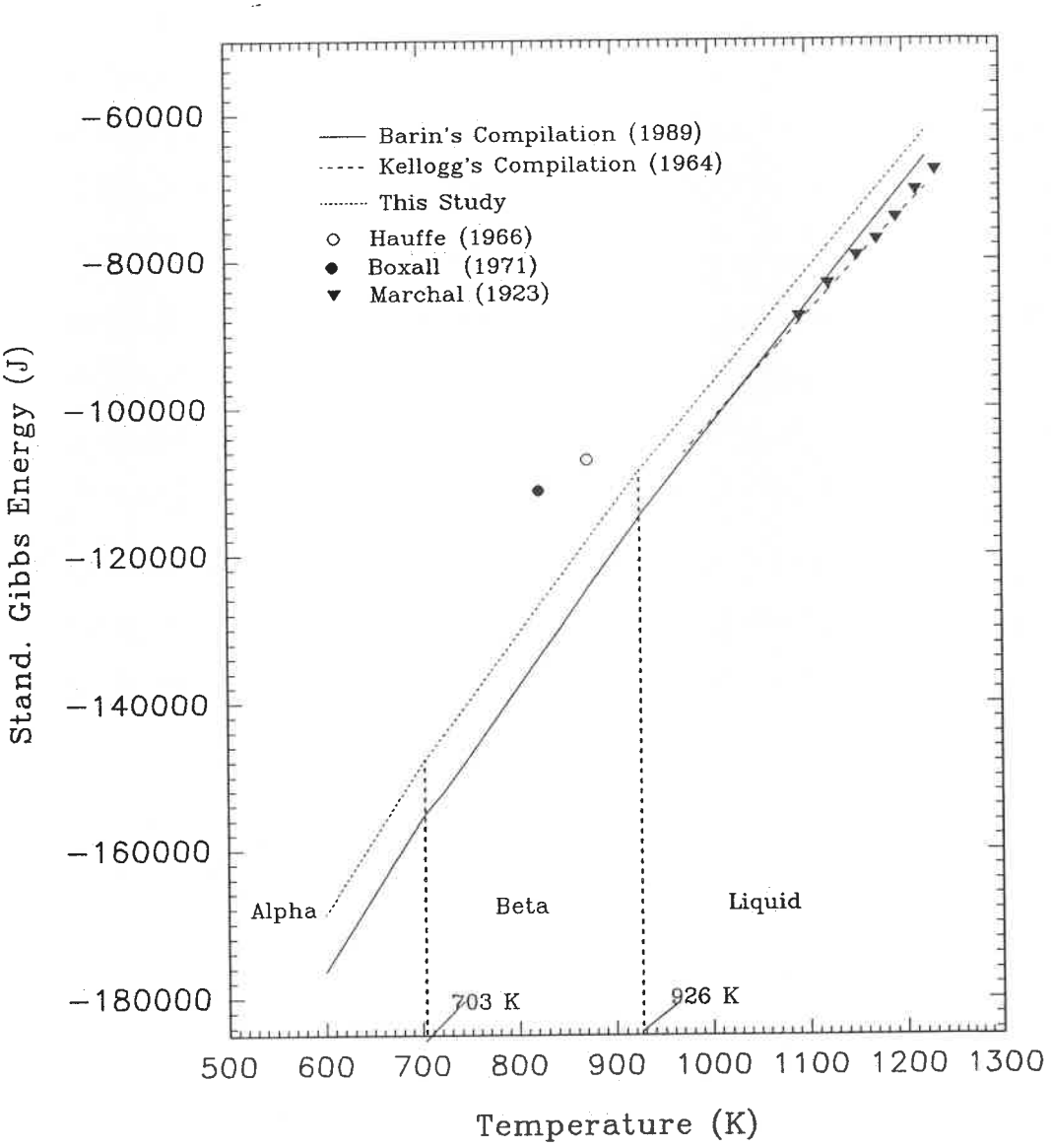

Figure 5.17 Standard Gibbs Energy Change for the

Reaction $2Ag(s)+SO_3(g)+1/2O_2(g)=Ag_2SO_4(s,l)$

Table 5.2. Standard Gibbs energy change for reaction (4.2)

Reaction: $2Ag(s) + SO_3(g) + 1/2O_2(g) = Ag_2SO_4(s,l)$

$\Delta G°$ expression (J)	T range (K)	$\Delta G°_{873}$ (kJ)	Ref.
-306 000-55.34TlnT+586.27T	930 - 1234	-121.286	128
-299 900 + 205.9·T	400 - 703		
-284 400 + 183.1·T	703 - 933	-124.553	133
-266 490 + 163.9·T	933 - 1200		
-290 460 + 202.99·T	624 - 703		
-271 160(±2236)+175.54(±1.68)T	703 -926	-117.913	(a)
-252 060 + 154.91·T	926 - 1146		
		-107.110	153

(a) this study

5.2 EMF Values Measured with $0.9CaO·0.72MgO·5.5Al_2O_3$

Quantitative conclusions can not be made at this stage with respect to experiments involving Ca^{2+}-conducting ceramic tubes since only a few successful experimental runs were carried out. Keeping the two separate electrode compartments gas-tight was the major experimental difficulty due to the cement failure after a temperature cycle. Any observations concerning the dependence of emf on the temperature, the flow rate of gas mixture over the working electrode, and the concentration of SO_2 are qualitative.

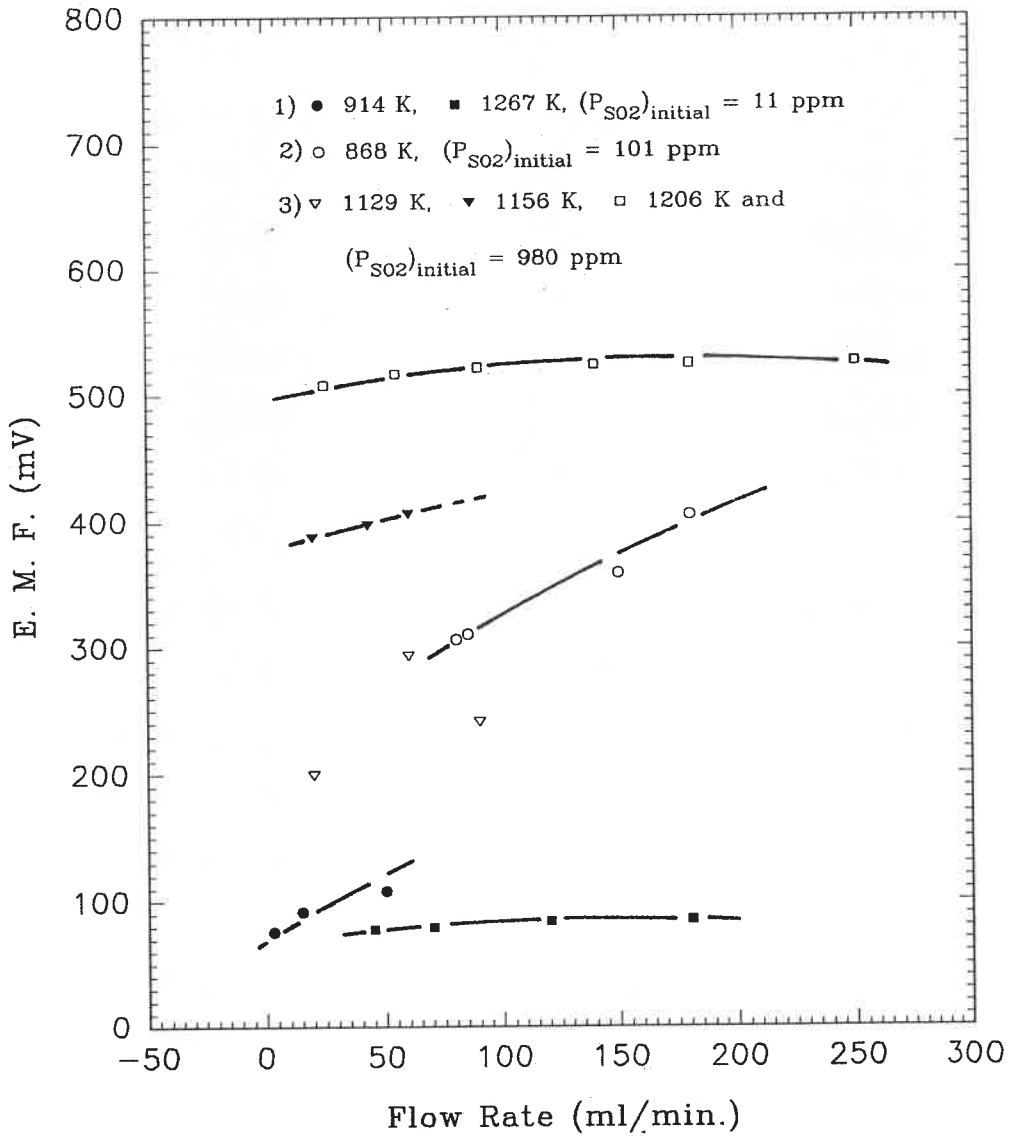

Figure 5.18 EMF Dependence on Flow Rate in a Cell with $0.9CaO*0.72MgO*5.5Al_2O_3$ as Solid Electrolyte

EMF Dependence on the Flow Rate of the Gas Mixture

In contrast to Ag^+-ß-alumina, a higher flow rate of the gas over the working electrode resulted in a higher emf response. As shown in Figure 5.18, at 1206 K and 1267 K there is little dependence of emf on the flow rate; this is understandable since the conversion ratio of SO_2 to SO_3 is less than 10 % over about 1200 K, so the concentration of SO_2 is less influenced by the flow rate. The dependence of emf on the flow rate became stronger at lower temperatures and the higher initial SO_2 concentrations.

EMF Dependence on Temperature

An expected linear relation between emf and temperature was not observed. Instead, a curvature in the plot of emf vs. temperature was obtained. The emf calculated from equation (4.17) did not correspond to the experimental values. In Figure 5.19, the measured emfs are compared with the theoretical values at 980 ppm SO_2 in air. It is seen that there is only one experimental point close to the theoretical line. In Figures 5.20 and 5.21, emf is plotted against temperature for two different concentrations of SO_2. Both figures show a similar response.

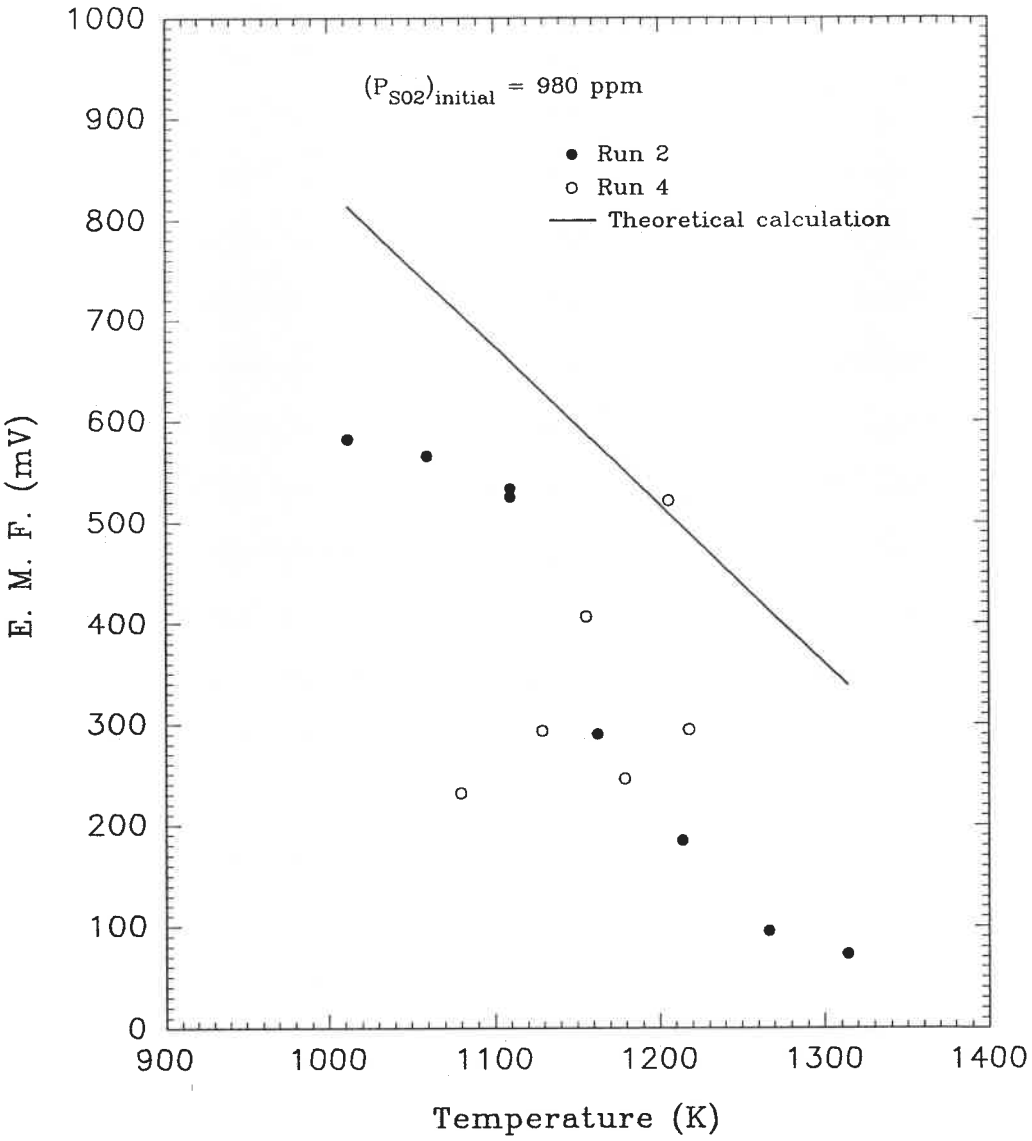

Figure 5.19 Comparison of EMF between Experimentally Measured and Theoretically Calculated Values

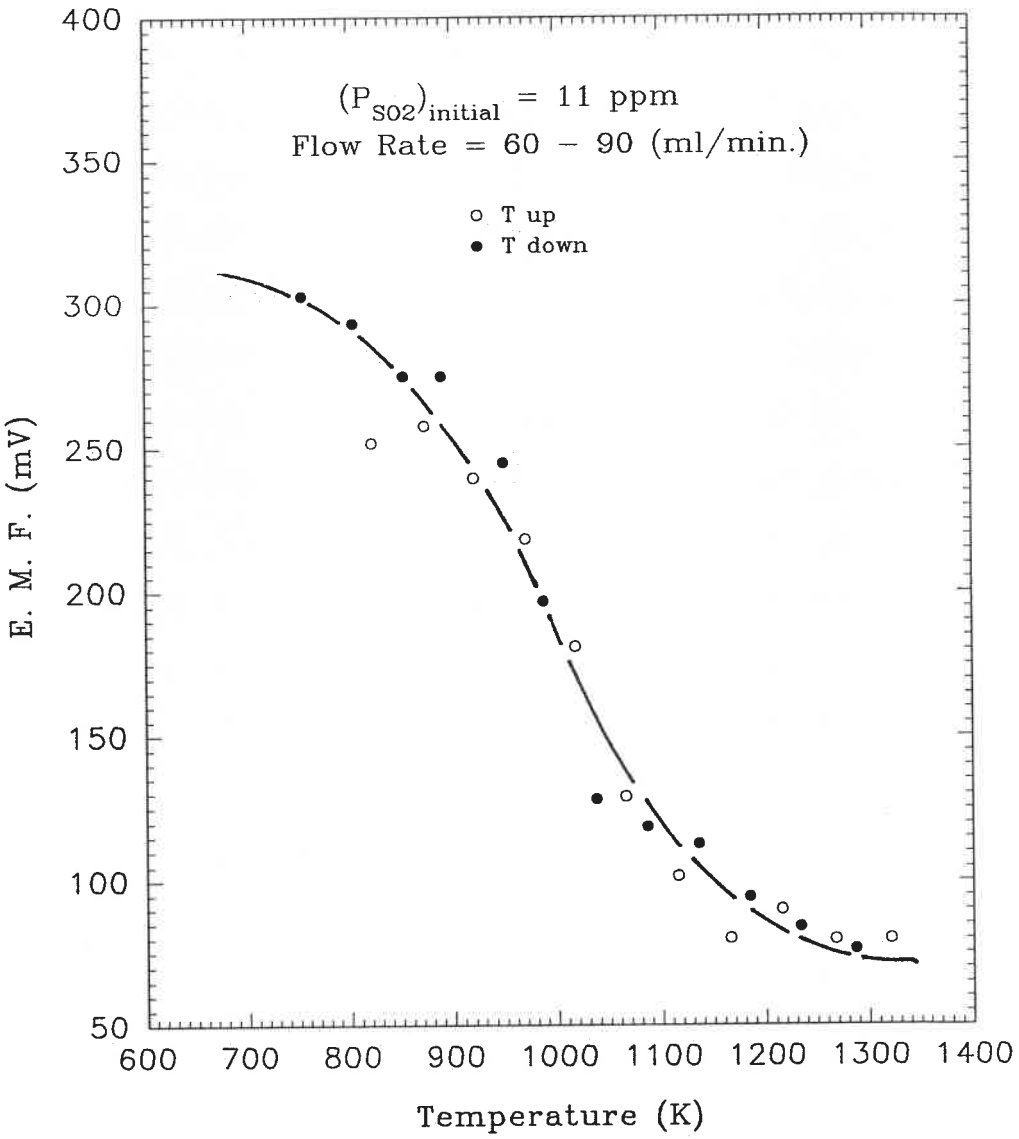

Figure 5.20 EMF Dependence on Temperature in a Cell with $0.9CaO*0.72MgO*5.5Al_2O_3$ as Solid Electrolyte

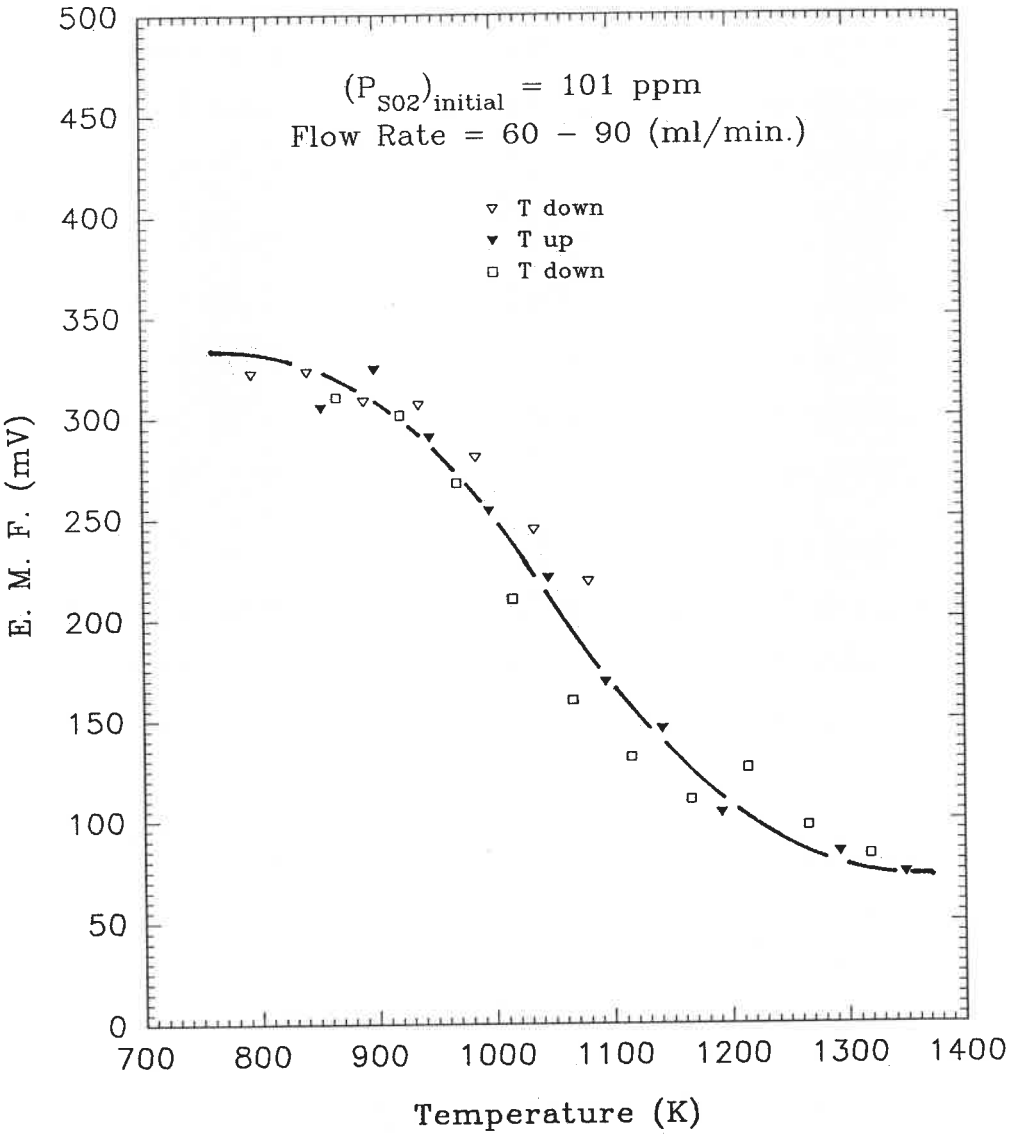

Figure 5.21 EMF Dependence on Temperature in a Cell with $0.9CaO*0.72MgO*5.5Al_2O_3$ as Solid Electrolyte

CHAPTER VI DISCUSSION

6.1 Electrode Reaction Mechanism

There are two noteworthy features of the dependence of the emf on the flow rate of gas mixture in the measurements with Ag^+-ß-alumina. First, the more concentrated the gas mixture in SO_2, the stronger the dependence; second, the lower the temperature, the stronger the dependence (see Figures 5.1, 5.2, and 1 - 10 in Appendix B).

In the investigation of Salzano[74], a molten sulfate mixture of Li_2SO_4, Na_2SO_4, and K_2SO_4 was used as the electrolyte. The oxidation of SO_2 is not favoured at high temperatures. Salzano concluded that when the concentration of SO_2 in the gas mixture was low, the rate of conversion to SO_3 could be first order with respect to the inlet concentration of SO_2. At a high flow rate, by assuming that the fraction of SO_2 converted was small and approximately independent of the inlet SO_2 concentration, Salzano proposed that both the SO_2 and SO_3 content could be monitored with his concentration cell. An emf dependence on the flow rate of the gas mixture, SO_2 + Air, was observed, implying a non-equilibrium gas mixture at high flow rates.

In the investigation of Vayenas[59], YSZ (yttria stabilized zirconia) tube was employed as an electrolyte to measure the activity of oxygen on various electrodes (Pt, Ag, and Au) in a set of SO_2 + air mixtures. In comparison with Salzano's results, Vayenas[59] observed that the rate of SO_2 oxidation was independent of the flow rate. A first order rate with respect to SO_2 partial pressure for P_{SO_2} below approximately 0.3 atm. was observed. Furthermore, Vayenas found that Pt was the more effective catalyst in the oxidation of SO_2 to SO_3. According to Vayenas, SO_3 was adsorbed on the platinum film surface to form a solid-like SO_3(Pt) layer which was not easily vaporized. This resulted in a poisoning effect to the catalyst, and consequently, the oxidation of SO_2 was hindered and the equilibrium partial pressure of SO_3 in the gas phase could not be established.

Both of the studies indicate that the partial pressure of SO_3 in the gas phase depends on the conversion ratio of SO_2 and is proportional to the initial partial pressure of SO_2. In addition, a higher conversion ratio of SO_2 is expected at lower temperatures (see Figure 4.4). This may explain the emf dependence on flow rate in this study and favor the proposal of cell reaction (4.2). From the Nernst equation for the cell reaction (4.2), it is apparent that there are three possible parameters which affect the emf of the cell, i.e. the activity

of solid sulfate and the partial pressures of SO_3 and O_2. According to Vayenas' results[59], the equilibrium between gaseous and adsorbed oxygen on the platinum surface in the presence of SO_2 has been established under the conditions (T range and P_{SO_2} range) in the present investigation. The activity of solid silver sulfate was independent of the flow rate of the gas mixture, at least in the cell with the type-3 working electrode construction. Clearly, the dependence of emf on the flow rate is related to the concentration of SO_3; therefore a lower emf at a relatively high flow rate must result from insufficient oxidation of SO_2 to SO_3, which is predicted from the Nernst equation.

In the present study, the observation of emf dependence on the flow rate of the gas mixture occurred in all the different experimental runs, irrespective of the types of electrode preparation, indicating an identical elementary reaction step which was essential in determining the electrode potential. The following qualitative discussion of the electrode reaction mechanism may be helpful to identify this step.

In general terms, the cathode reaction for cell (IX) can be divided into several elementary steps as follows:

(1) diffusion of the electro-active species to the three phase region, through the porous platinum layer for the gaseous species and through the solid electrolyte for silver ion respectively;
(2) adsorption/desorption of the gaseous species around the triple points;
(3) electron transfer;
(4) chemical reaction to form the silver sulfate;
(5) formation of the nucleus of the crystals.

Step (3) can not be the slowest step as long as there is a good electrical contact between the solid electrolyte and the electrode. In any case, the measurements were carried out under equilibrium conditions[141] with a negligible amount of current flowing through the solid electrolyte. If step (1) is the slowest one, the activities of the gaseous species on the surface of the electrode will depend on the factors which have strong effect on the diffusion process; consequently, emf dependence on these factors should be observed.

There is a plateau in the plot of emf against flow rate (Figure 5.2), indicating that beyond a certain flow rate, the diffusion process can be excluded from being the rate determining step. Unlike type-1, type-2 and type-3 electrode preparations are not platinized on the interior surface of the

solid electrolyte tube. Cells with these latter type electrode constructions would certainly have easier access for gaseous species to diffuse to and from the triple point area. These cells should have a quicker response of the emf to changes of temperature and/or concentration of gaseous species, if the step (1) was the decisive one. This was not observed in the present investigation.

Normally, the rate of step (4) at upper temperatures is relatively high, compared with the other steps in which additional energy is required to activate the particular process. This point was demonstrated by the observation that the measured emf did not immediately jump to a high value after the introduction of gas mixture of SO_2 and air into the cells with the type-1 and type-2 electrode preparation, where the activity of silver sulfate is zero at the beginning of experiment and a very high emf is expected according to equation (4.3).

Finally, step (5) was not the slowest step since irrespective of the activity of silver sulfate at the electrode (unity activity in the case of type-3 electrode preparation, or less than unity in the type-1 and type-2 electrode preparation), the response of emf to the change of temperature and the concentration of SO_2 was similar. In

conclusion, only step (2) was common in all three types of electrode preparations and therefore may be considered as the slowest step.

It was noted earlier that changing the concentration of SO_2 from the highest level in this study to a lower one resulted in a higher emf in comparison with those directly measured at the lower level. The higher value decreased gradually and finally merged with the regression line obtained from those experimental points measured directly at the lower level (Figure 5.11). In most cases, it took several cycles of temperature to attain this agreement.

The lagging phenomenon is an indication of a slow process which had a direct effect on the emf measurement. Usually, diffusion processes in solids are slow. The galvanic cell in this study is actually a silver concentration cell. Since silver is soluble in platinum, it is reasonable to expect a slow response of emf to the change of SO_2 concentration if the silver activity in the working electrode is fixed by the solid solution of silver in platinum. Following the experiment runs, the platinum mesh in the working electrode was analyzed by scanning electron microscopy. As shown in Figure 6.1, the analysis indicated no dissolution of silver in the platinum, ruling out any relation between the solid diffusion process

and the lag.

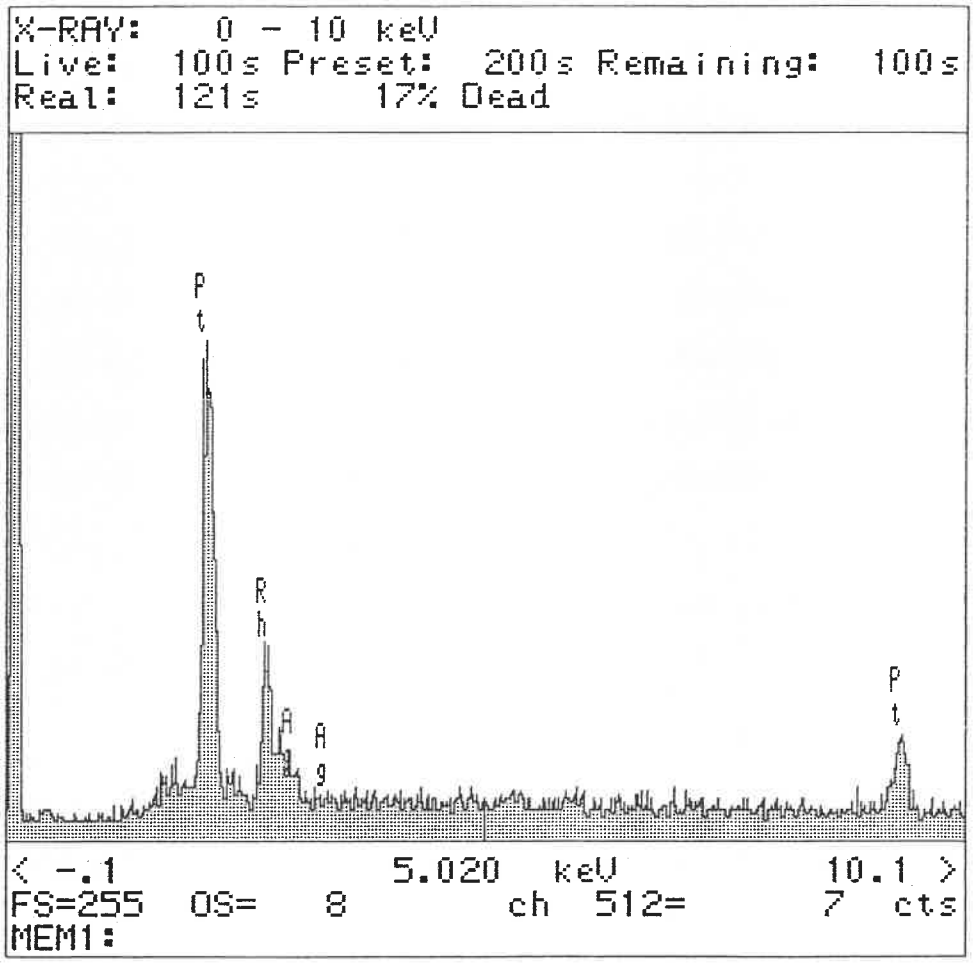

Figure 6.1 SEM analysis result for platinum mesh

The analysis above for the cathode reaction mechanism may be strongly corroborated by the lagging phenomenon. The hysteresis response of electrode to the change of concentration of electro-active species in the gas phase must

have resulted from the higher activity of that species around the triple point area because the partial pressure of SO_3 in the gas phase would be decreased immediately after changing the concentration of SO_2. When the measurement was carried out at the highest concentration of SO_2, more SO_3 molecules would be chemically adsorbed in the triple point area. Since the adsorption/desorption of SO_3 was the slowest step in the sequence of the elementary electrode reaction steps, it may have taken a longer time for the amount of SO_3 adsorbed to be reduced.

In a separate experiment, the measurements were taken at the highest SO_2 level. Then air was introduced into the working electrode compartment for about 2 days, followed by the introduction of the mixture of SO_2 and air, in which the SO_2 concentration was at a lower level. The emf measured showed agreement with those directly measured at that level (Figure 5.13). This can be explained in the following way: with air flowing over the working electrode, the process of desorption of SO_3 from the triple point area is accelerated by the presence of a maximum chemical potential gradient of SO_3.

From a thermodynamic point of view, the cathode reaction for cell (IX) is an irreversible one with respect to the concentration change of SO_2 from high to low. In general,

most processes of the chemisorption of gases on a solid are not reversible[146] because chemisorption involves electron-sharing or electron transfer between adsorbent and adsorbate leading to the formation of a surface chemical bond in a fashion related to bond formation in simple molecules; this, again, supports the electrode reaction mechanism proposed above.

It should be pointed out that the hysteresis phenomenon occurred only when changing SO_2 concentration from the highest level to a lower one, indicating that there is a limit of the SO_2 concentration above which the so-called chemisorption of SO_3 could take place. This is in agreement with Vayenas'[59] observation. He found that the stable chemisorbed SO_3 on the surface of platinum could exist only under certain conditions.

6.2 Sulfate Formation on the Surface of ß-alumina

According to the overall cell reaction (4.2) and the corresponding Nernst equation (4.3), the existing state of sulfate has an effect on the emf measurement. In other words, the activity of silver sulfate influences the magnitude of the emf. In order to explain their experimental results, which showed systematically higher emf values than those calculated theoretically, Itoh[86] et al suggested that the composition of

the reaction layer at the surface of the Ag^+-ß-alumina was in the range where a solution in the Ag_2SO_4-$Al_2(SO_4)_3$ binary system rather than the pure Ag_2SO_4 existed. An activity of Ag_2SO_4 ranging from 0.1 to 0.01 was deduced from their emf data.

In the present investigation, at a fixed low flow rate of the gas mixture, the emf measured for the cells with the type-1 electrode preparation was higher than that for the cells with the type-3 electrode preparation. In the latter case, the activity of Ag_2SO_4 was equal to unity. Therefore, the higher emf is related to the non-unity activity of Ag_2SO_4 in the former case. It is more likely that only a few atoms layer of Ag_2SO_4 could at most be formed in the cells with the type-1 electrode preparation because of the existence of the porous platinum layer, rather than the formation of a solution in the Ag_2SO_4-$Al_2(SO_4)_3$ binary system, leading to greatly reduced activity of Ag_2SO_4. In fact, under the conditions of electro-motive force measurement with a potentiometer, the massive migration of the conducting component ion from one side to the other side could not be expected unless the electronic conductivity was significant. Consequently, the formation of sulfate on the surface of ß-alumina would proceed very slowly and the activity of silver sulfate would depend on total duration of the experiment.

This argument is favored by the observation in measurements with the type-2 electrode preparation (Figure 5.4 and 5.5). As demonstrated in Figure 5.4, both the slope and the intercept in the emf vs. T plots gradually changed with time. The origin of the change is the variation of silver sulfate activity. From the Nernst equation (4.3), if the silver sulfate assumes a non-unity activity, there will be a contribution of Ag_2SO_4 to the emf value. If the activity of silver sulfate is a function of time, both the slope and the intercept in emf vs. T plot will change with time.

When the slope of emf vs. T plots for type-2 electrode construction agrees with the slope for the type-3 electrode construction (where the activity of silver sulfate is unity) the entropy change of the cell reaction is identical for both types of electrode construction. This indicates a final state of pure solid Ag_2SO_4 formed on the surface of Ag^+-ß-alumina in the cells with type-2 electrode. As shown in Figure 6.2, the slopes for the two types of electrode construction are almost identical. There is still a small difference between the two sets of data (about 30 - 40 mV). The higher emf for type-2 electrode results from a gradual process of formation of a few atoms layer of Ag_2SO_4 which has an apparent thermodynamic activity smaller than that in massive standard state[104].

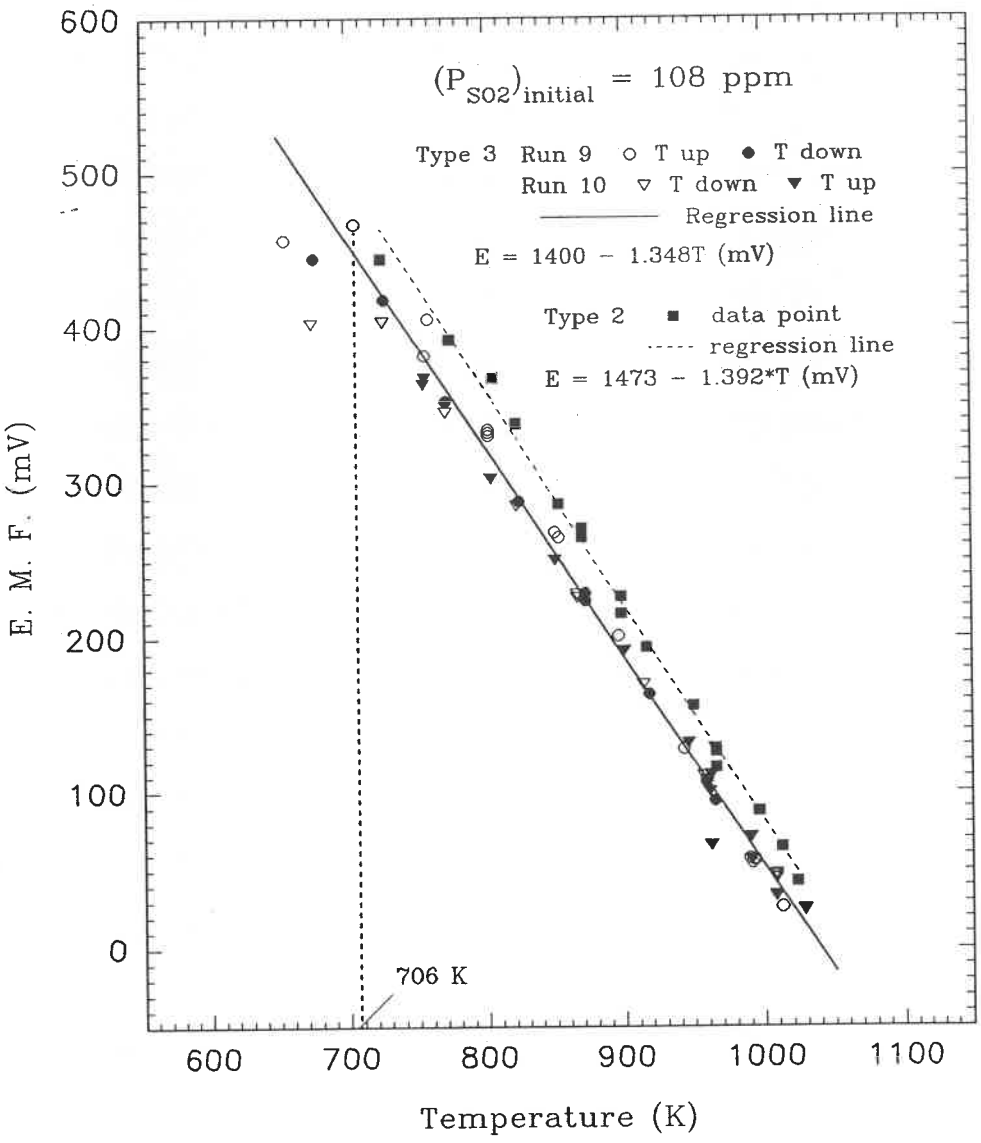

Figure 6.2 Comparison of EMF Dependence on Temperature for Type 2 and Type 3 Electrode Preparations

Furthermore, it has been found that at a relatively high concentrations of SO_2, the emf measured in the cells with the type-1 electrode preparation continued to increase as the flow rate approached zero, whereas in the type-3 electrode preparation, there was a maximum in the plot of emf vs. flow rate (compare Figure 2 with Figure 10 in Appendix B).

This phenomenon can also be explained by the reaction mechanism proposed above. Since only a few atoms layer of silver sulfate is possible to be formed on the surface of the solid electrolyte for the first type electrode preparation, the reaction will stop completely as complete coverage of the surface by the product is reached. Therefore, the activity of SO_3 around the triple point can be maintained even if there is no fresh gaseous SO_3 to be provided at zero flow rate. For the case of the type-3 electrode preparation, the cathode reaction could proceed continuously as long as the rate of transport of the reactants to the triple point area was fast enough. As the flow rate reached zero, the transport of gaseous SO_3 by diffusion might be too slow to keep up with the formation of the sulfate, leading to the marked activity decrease of SO_3 around the triple point which resulted in the decrease of emf.

6.3 Standard Gibbs Energy of Formation for Ag_2SO_4

Methods of obtaining ΔG° for a reaction

Tabulated values of the standard Gibbs energy change for a reaction as a function of temperature are usually obtained by means of integration[132,148] involving the basic thermochemical data, such as heat capacity, Cp, standard entropy and enthalpy at 25 °C, $\Delta S°_{298}$ and $\Delta H°_{298}$. Such data are found in compilations[133,147]. The uncertainty in calculating ΔG° is clearly dependent on the accuracy of the thermochemical data used in the integrated equation:

$$\Delta G^{\circ}_{T} = \Delta H^{\circ}_{298} - T\cdot\Delta S^{\circ}_{298} + \int_{298}^{T} \Delta C_p dT - T\cdot\int_{298}^{T} \frac{\Delta C_p}{T} dT \quad \ldots(6.1)$$

which is characteristic of the calorimetric method by which most of the basic thermochemical data are obtained.

An alternative way to obtain ΔG° is by the determination of the equilibrium constant particularly if gaseous species are involved in the reaction under study. For example, many of the decomposition reactions for sulfates have been investigated by measuring of the total decomposition pressure. The corresponding Gibbs energy changes have been evaluated and

compiled by Kellogg[128]. The drawbacks of total decomposition pressure measurements have been considered by Warner[149].

In general, the EMF measurement of a Galvanic cell can provide precise and accurate thermodynamic data for the overall cell reaction as long as the emf is obtained under reversible conditions. A few measurements are available[150,151] for several sulfate decomposition reactions, using alkali sulfate as the solid electrolyte. There is fair agreement among the ΔG° results from different investigators.

All the three kinds of methods presented above have been used previously to obtain the standard Gibbs energy change for reaction (4.2). Unlike most sulfates, Ag_2SO_4 decomposes to a metal and a gas mixture consisting of SO_3, SO_2 and O_2. The decomposition pressure was studied by Marchal[152], from which the standard Gibbs energy change was deduced by Kellogg[128]. Barin[133] also calculated and tabulated $\Delta G^\circ_{Ag_2SO_4}$ by integration from the basic thermochemical data evaluated by Kelley[162]. Hauffe[153] made an emf measurement at 873 K for the following cell:

$$Pt,Ag \;/\; Ag_2SO_4 \;/\; SO_3,\ O_2,\ Pt \qquad \ldots(XI)$$

and obtained a value of ΔG° for the reaction:

$$2Ag(s) + SO_3(g) + 1/2O_2(g) = Ag_2SO_4(l,s) \quad ...(6.2)$$

The standard Gibbs energy change for the above reaction was also derived in Chapter V from emf measured in present investigation. As shown in Figure 5.17, there is a disagreement among the various studies.

Total decomposition pressure measurement

In addition to thermal diffusion[149] which may result in a higher P_{SO_3} determination from the total pressure measurement, there are other factors, characteristic of this method, which can introduce errors into the calculation of the equilibrium constant.

The first factor lies in the assumption of equilibrium in the gas phase for reaction (4.4). A study of the kinetics of SO_2 oxidation employing various catalysts[59] has revealed that the equilibrium in the gas phase may only be established if precautions are taken to remove the limitation of the rate determining step in a series of elementary reactions. Thus it would be easy to understand the irreversible behavior with increasing temperatures for decomposition pressure measurements of $Al_2(SO_4)_3$[154] which were carried out in the absence of a catalyst for reaction (4.4). Fe_2O_3 has been used

as a catalyst in the kinetic investigation of SO_2 oxidation[155]. Higher decomposition pressures for $Al_2(SO_4)_3$-Fe_2O_3 mixtures than that for pure $Al_2(SO_4)_3$ in the same investigation can be explained by the catalytic effect of Fe_2O_3 on the equilibrium reaction (4.4). It was reported[154] that there was a curvature in the plot of $\log_{10}K$ vs. 1/T for aluminum sulfate decomposition, however the curvature could not be observed in subsequent measurement[163] for the same system with a platinum container which would tend to catalyze the reaction (4.4).

The second factor is characteristic of the means by which the equilibrium constant is calculated from the total decomposition pressure. The total pressure measurement does not directly provide the partial pressures which appear in the equilibrium constant expression. A numerical procedure is required under the assumption of equilibrium for reaction (4.4), to calculate the partial pressures. As pointed out earlier, for most sulfates, thermal diffusion tends to cause errors in the equilibrium constant determination. In the case of silver sulfate, the situation may be more complicated.

The following reaction has been proposed[128,152] for the decomposition of silver sulfate:

$$Ag_2SO_4(s,l) = 2Ag(s) + SO_2(g) + O_2(g) \qquad ...(6.3)$$

It is noted that silver and not silver oxide is stable. Taking reaction (4.4) into account, the equilibrium gas mixture also includes SO_3. It is possible that the decomposition mechanism may be represented by the reverse of reaction (6.2) where SO_3 decomposes further into SO_2 and O_2. If the decomposition of silver sulfate proceeds by equation (6.3), further reaction in the gas phase to form SO_3 will reduce the total number of moles of gaseous species over the sulfate. For decomposition pressure measurements in a closed system, the total pressure will decrease to a minimum value as the equilibrium is approached. On the other hand, back reactions (6.2) and (4.4) will tend to increase the total pressure of the system gradually to a maximum. In practice, these reactions may take place simultaneously, and it is difficult to determine whether the gradual increase of total pressure observed by Marchal[152] is due to the gradual decomposition of sulfate or due to the further decomposition of SO_3.

Pure silver has not been found to be a catalyst for SO_2 oxidation[59], and consequently, the establishment of equilibrium reaction (4.4) in Marchal's measurement is unlikely.

Integration method

The integration method is the most common method employed to obtain ΔG° for a chemical reaction. The errors in integration are created by uncertainties in the thermochemical data. Three kinds of basic thermochemical data are involved in the integration equation (6.1): heat capacities, standard enthalpies and entropies at 298 K. Kelley[162] made a critical evaluation for the thermochemical data of Ag_2SO_4 where an estimated expression for C_p was proposed. This value of C_p, together with other thermochemical data, is used in Barin's[133] calculation and tabulation of the standard Gibbs energy for silver sulfate. More recent measurements[145] of the heat content for Ag_2SO_4 by drop calorimetry indicate a different value for C_p (Figure 6.3).

The standard enthalpy of formation of Ag_2SO_4 at 298 K was also evaluated by Kelley[162] who recommended a value of -711.74 kJ/mole obtained from solubility measurements. More recently, Pan and Lin[164] deduced a value of -714.041 kJ/mole from their emf measurement results on the following cell:

Cd-Hg(2 phase)/$CdSO_4 \cdot 8/3H_2O$(satd.)/Ag_2SO_4(s)-Ag ...(XII)

The results are in fair agreement with the results of

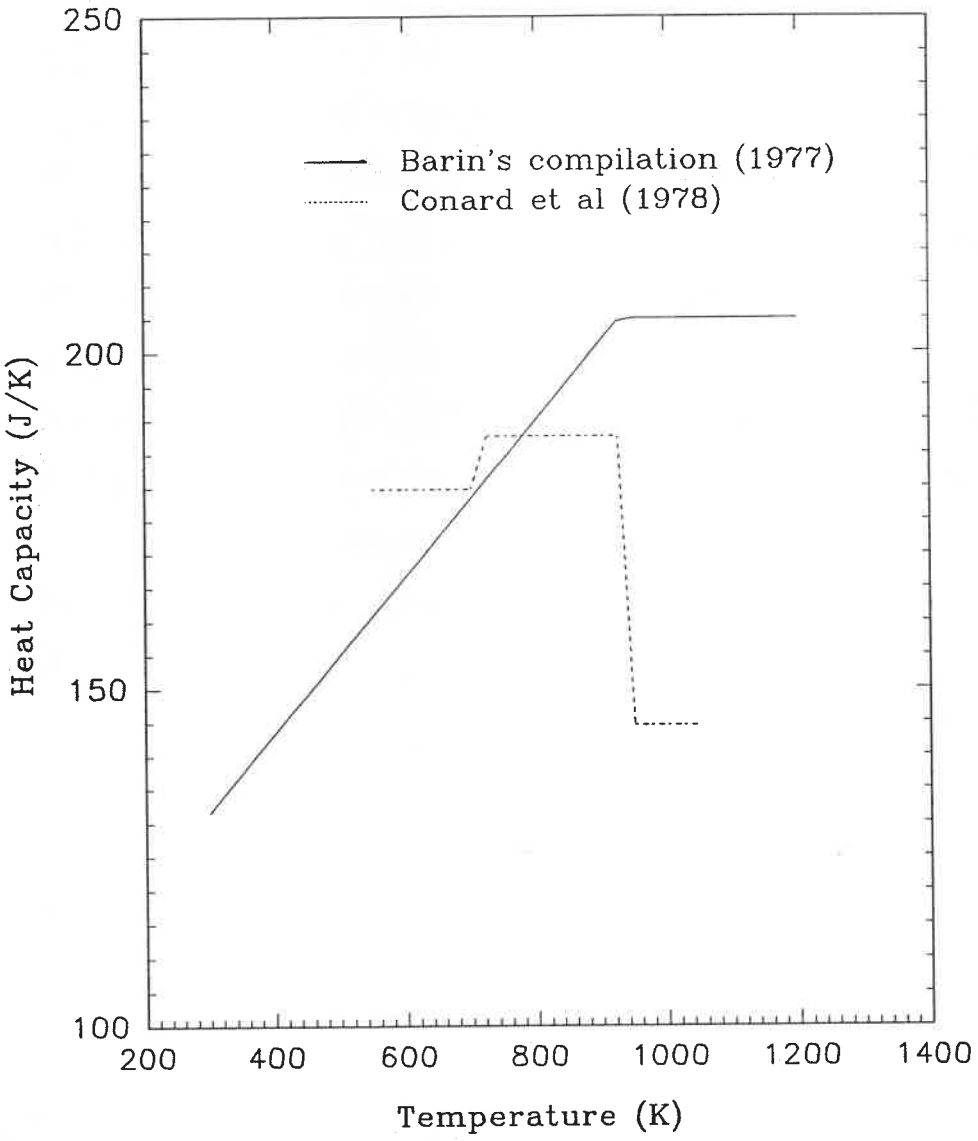

Figure 6.3 Comparison of heat capacity of Ag_2SO_4 as a function of temperature .

solubility measurements. The values are somewhat more negative than those obtained from reaction heat measurement[165] (-699.31 kJ/mole).

EMF measurement method

As discussed in Chapter IV in the present investigation, a porous platinum layer was plated around the internal wall of the gas mixture passage (Type-3 electrode). In addition, fine platinum wire and mesh were placed in the path of the gas mixture before it reached at the triple point vicinity where the electrode reactions take place. These precautions ensured the establishment of equilibrium in the gas phase.

In Hauffe's study[153], the emf for the cell reaction (6.2) was measured by employing Ag_2SO_4 as the solid electrolyte. The gas mixture of (SO_2+Air), which had flowed over the working electrode compartment, was analyzed, from which the equilibrium constant and the standard Gibbs energy change were calculated. As shown in Table 5.2, the reported value of ΔG° = -107.110 kJ at 873 K is in fair agreement with the value of ΔG°_{873} = -117.913 kJ obtained in present study.

Boxall[68] has reported a value of the standard Gibbs energy change for reaction (6.2) at 823 K from his emf

measurements using a mixture of molten sulfates as electrolyte. The result is shown in Figure 5.17 and is in reasonable agreement with the present study.

From Barin's tabulation[133], the standard Gibbs energy change for reaction (6.2) as a function of temperature has been calculated and is listed in Table 5.2. At 873 K, quite good agreement is found between Barin's result (-124.5 kJ) and the extrapolated value from Kellogg's result (-121.3 kJ). However there is approximately 7 kJ difference between the ΔG° from present study and that from Barin's compilation. This difference can be considered to be normal, taking into account the inherent error characteristic of the calorimetry method by which most of the basic thermochemical data were obtained. The standard Gibbs energy change for reaction (6.2) obtained in the present study is in agreement with that calculated from Barin's compilation, but it is proposed that the results in the present study are more reliable because of the smaller error (approximately 2.2 kJ in ΔH°) from the linear regression analysis of the experimental data.

In the present investigation, a linear function of temperature for ΔG° was observed, implying that the ΔC_p for reaction (6.2) is zero according to equation (6.1). In other words, the standard Gibbs energy change for reaction (6.2) can

be simply expressed as:

$$\Delta G^\circ = \Delta H^\circ_{298} - T \cdot \Delta S^\circ_{298} \qquad \ldots(6.4)$$

Consequently, the standard enthalpy of formation for Ag_2SO_4 at 298 K may be deduced. A value of -686.23 kJ/mole is obtained and, compared with those obtained by other method, is approximately 13 - 28 kJ/mole less negative. This is a result of the extrapolation of the regression equation from the higher temperatures to room temperature.

6.4 Electronic Conductivity in $0.9CaO*0.72MgO*5.5Al_2O_3$

As mentioned earlier (Chapter V), the measured emf for cell (X) is far below that predicted by equation (4.17). A possible reason may be due to electronic conductivity under the measurement conditions. Since neither the electrical conductivity nor the conduction mechanism of this ceramic material has been investigated at the present time, discussions can only be made on a hypothetical basis.

According to Heyne[157], a solid electrolyte material should be considered as a mixed conductor unless the chemical and thermodynamic conditions are well controlled. In solid electrolytes, it is the presence of defects and the equilibria

involving defects that lead to the characteristics of mixed conduction.

Assuming that the calcium ion, Ca^{2+}, is the only ion which may migrate in the ceramic material and that the equilibrium:

$$Ca + 2h^{\cdot} \rightleftharpoons Ca^{2+} \qquad ...(6.5)$$

is established at the interface between electrode and solid electrolyte. With the use of the symbolic system from reference [157], the equilibrium implies:

$$\mu^{*}_{Ca} + 2\mu_{h^{\cdot}} = \mu_{Ca^{2+}} \qquad ...(6.6)$$

or in terms of variations:

$$\Delta\mu^{*}_{Ca} + 2\Delta\mu_{h^{\cdot}} = \Delta\mu_{Ca^{2+}} \qquad ...(6.7)$$

The value of $\mu_{Ca^{2+}}$ is constant[157], and the variation in the chemical potential of the neutral component Ca and that of the electron hole are directly coupled:

$$\Delta\mu^{*}_{Ca} = -2\Delta\mu_{h^{\cdot}} \qquad ...(6.8)$$

Assuming that the electron holes exhibit ideal behaviour, the right side of equation (6.8) varies linearly with ln(p), whereas the left side shows the same dependence on P_{Ca} where p is the concentration of electron hole and P_{Ca} the partial pressure of metal calcium. Consequently, the concentration of electronic holes in the ceramic is inversely proportional to the square root of the partial pressure of calcium:

$$p \propto P_{Ca}^{-1/2} \qquad \ldots(6.9)$$

The lower the partial pressure of metallic calcium, the higher the concentration of electron holes induced by the defect reaction (6.5) in the ceramic. Taking equations (1.2) through (1.4) into account, a lower emf may be expected if the partial pressure of calcium is kept sufficiently low. In fact, in the equilibrium of air with solid CaO, the partial pressure of calcium can be calculated from the know thermodynamic data and it is as low as $3.5 \cdot 10^{-28}$ atm. at 1000 K.

It should be pointed out that it took some time for the electronic conductivity in the ceramic material to become significant. At the beginning the measurement, the theoretical emf was approached (see Figure 5.19), then the deviation of measured emf from the theoretical line occurred.

6.5 SO_x Sensor with Different Materials

According to the phase diagram calculations (Chapter III), Ag^+-ß-alumina may be superior to Na^+- and/or Ca^{2+}-ß-alumina for monitoring SO_2 concentration if the measurements are carried out in a relatively high concentration range of SO_2 which favors the formation of sulfates. This is because only for the Ag-Al-O-S system is there a temperature range where the silver sulfate can coexist with the ß phase (see Figures 3.9, 3.11, 3.13, 3.14, 3.20, and 3.21).

However, as a sensor for SO_x, all three ß alumina materials have their own particular applications.

Using Ag^+-ß-alumina to monitor SO_x by means of emf measurements, Itoh[86] have found a quicker response time to the concentration changes of SO_2 in comparison with Na^+-ß-alumina. In the present investigation, the analysis of electrode reaction mechanisms (Section 6.1) has shown an emf response to the concentration of SO_3. From a practical point of view, Ag^+-ß-alumina is the best candidate for monitoring SO_3 concentrations. A recommended procedure is to establish a calibration curve of emf versus logarithm of the concentration of SO_3 under extremely unfavorable conditions of SO_3 to SO_2 transformation, for example, at low temperatures, without a

catalyst and in high flow rate. Then, any emf value measured thereafter will correspond exclusively to a concentration of SO_3 on the calibration curve, irrespective of the measurement conditions.

The different emf dependencies on the gas flow rates for various materials imply a possible selectivity with these materials. As discussed in section 4.2, SO_2 rather than SO_3 is the predominant electro-active species when using the Ca^{2+}-conducting ceramic electrolyte. Therefore, SO_2 can be monitored by means of a Galvanic cell incorporating the Ca^{2+}-conducting electrolyte.

There may be relations between the decomposition reaction of sulfates and that of the gaseous sulfur oxides. For example, the decomposition reaction of silver sulfate is the reverse of equation (6.2) instead of (6.3), whereas that of calcium sulfate is represented by the reverse of (4.12) rather than the reverse of (4.13). In a Galvanic cell incorporating ß-alumina, the presence of the corresponding sulfate in one of its electrode compartments is essential to make the cell function reversibly. Consequently, the decomposition equilibrium of sulfate will have an effect on the emf response to the gaseous species. If this is true, it would be reasonable to expect that Na^+- and K^+-ß-aluminas could be used

to monitor SO_2 because the decompositions of these sulfates are similar to that of calcium sulfate. The observation of emf dependence on flow rate in a Galvanic cell using potassium sulfate as a solid electrolyte[58] supports this prediction where the emf value measured was higher as the flow rate of (SO_2 + Air) mixture was increased.

6.6 $Al_2(SO_4)_3$ Formation

As discussed earlier (section 5.1, Chapter V), at low temperatures with type-3 electrode constructions, the measured emf deviated from the regression line obtained from the experimental points at the higher temperatures. The temperature at which the deviation takes place depends upon the initial concentration of SO_2 (Figures 5.7 through 5.9). In addition, at temperatures far below the critical temperature the emf is no longer stable.

When the emf deviates from the regression line, it goes under the line and forms a convex curve in the emf vs. T plots. Since a high flow rate of gas mixture makes the measured emf vary in the same direction, it would be reasonable to relate the deviation to insufficient oxidation of SO_2 if the concentration of SO_3 at high flow rate of gas mixture was far below that at equilibrium.

Experimentally, attempts were made to reduce the flow rate as much as possible, but we were unable to avoid the deviation. For different gas flow rates, a maximum in emf vs. flow rate plots was usually observed, especially at the low temperature range (see Figure 10 in Appendix B), confining the measurement to a dynamic one.

On the assumption of equilibrium in the gas phase, the conversion ratio of SO_2 to SO_3 (defined by equation 4.16) is independent of the initial concentration of SO_2. Below about 800 K, the conversion ratio is not very much influenced by temperature (see Figure 4.4, in which the curve is rather flat below 800 K). In other words, the concentration of SO_3 does not depend appreciably upon temperature in the low temperature range. This means that insufficient oxidation of SO_2 is not the cause of the strong deviation and of the unsteady emf far below the critical temperature.

Emfs lower than predicted values may be caused by an unexpected reaction between the electrode and solid electrolyte[158-161]. If the reaction proceeds and finally leads to the failure of the solid electrolyte (for example by forming a dense layer of reaction product which is poor ionic conductor), unsteady emfs will be observed. In the present investigation under certain conditions, the attack on

ß-alumina by SO_x gas species may result in the formation of $Al_2(SO_4)_3$.

The possibility of aluminum sulfate formation is clearly indicated in the phase diagrams calculations of Chapter III. Figures 3.13 and 3.14 are typical temperature-composition phase diagrams for the Ag-Al-O-S system at a given value of P_{O_2} and various P_{SO_2} levels. According to these Figures, a Ag_2SO_4 + ß-alumina mixture will be replaced by a Ag_2SO_4 + $Al_2(SO_4)_3$ mixture below a certain temperature which depends upon the SO_2 partial pressure, P_{SO_2}. At relatively high values of P_{SO_2}, the temperature at which the aluminum sulfate is more stable than alumina is higher. The formation of aluminum sulfate has probably created the deviation of the emf from the regression line.

The possible reaction mechanism between ß-alumina material and sulphur oxides is schematically illustrated in Figure 6.4. At a certain concentration of SO_2 in air, if the emf measurement is carried out above the critical temperature, only traces of silver sulfate may be formed on the surface of ß-alumina (Figure 6.4 (a)). The existence of a micro-system for the equilibrium among ß-alumina, silver sulfate, and gas mixture ensures the reversibility of the electrode and maintains a stable emf. When the temperature drops below a

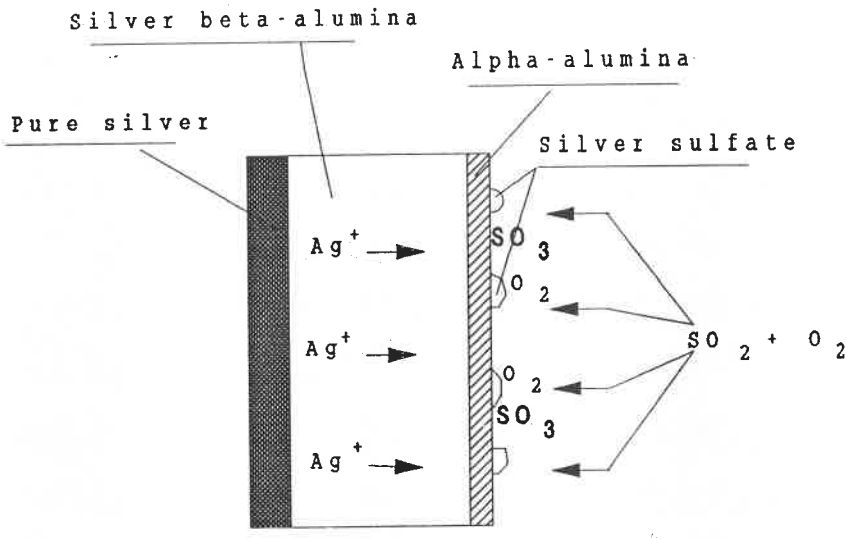

(a) Formation of silver sulfate

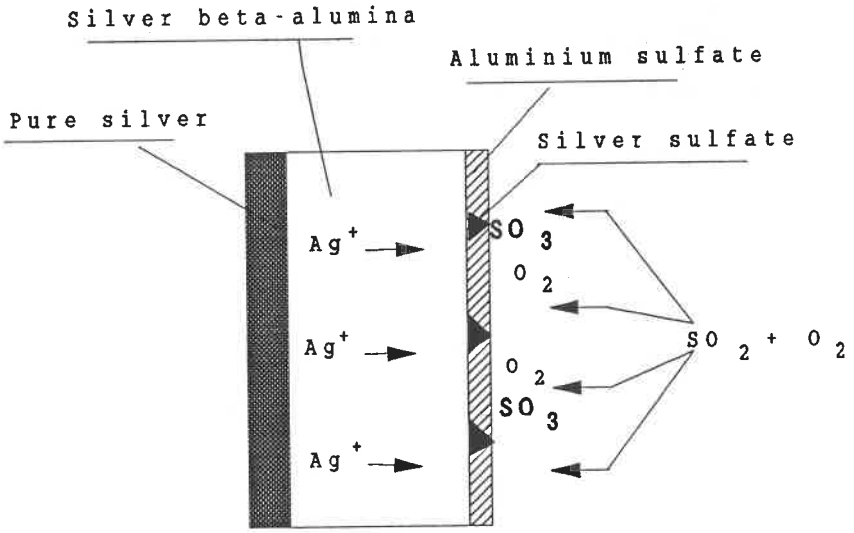

(b) Formation of sulfates mixture

Figure 6.4 A schematic illustration of sulfates formation on the surface of ß-alumina.

critical point, aluminum sulfate is thermodynamically more stable than alumina. As a result, the surface of ß-alumina will be completely covered by a layer of mixture of sulfates (Figure 6.4 (b)). Consequently, the electrode no longer behaves reversibly and this results in unstable emfs.

Similar to the Ag-Al-O-S system, aluminum sulfate may be formed in the Na-Al-O-S system at relatively low temperatures in the presence of SO_x. As shown in Figures 3.9 and 3.11, the critical temperature for the sulfate formation shifts from a higher one at a higher values of P_{SO_2} to a lower one at a lower P_{SO_2}. Experimentally, a convex curve in emf vs. temperature plot has been observed by Itoh[85] in the low temperature range of SO_2 monitoring with Na-ß"-alumina electrolyte. This may be due to the formation of aluminum sulfate by the reaction between SO_x and the solid electrolyte.

For the Ca-Al-O-S system, phase diagram calculations show comparable relations among the phases.

CHAPTER VII CONCLUSIONS AND RECOMMENDATIONS

The investigation of Ag^+-ß-alumina and Ca^{2+}-conducting aluminate solid electrolytes in thermodynamic measurements involving $SO_2(g)$ has led to the following conclusions and recommendations:

(1). The measured emf using a solid electrolyte in the presence of SO_2/SO_3 gas mixture is influenced by the flow rate of the gas mixture, and indicates a non-equilibrium state in the gas phase particularly at higher flow rates.

(2). In a galvanic cell with Ag^+-ß-alumina as the solid electrolyte, SO_3 is the electro-active species. The SO_3 concentration may be monitored precisely by emf measurements. The SO_2 concentration may be determined only under the conditions which favor the establishment of equilibrium in the gas phase.

(3). For monitoring SO_3 contents in air, if the concentration of SO_3 is below 1000 ppm, the procedure mentioned in section 6.5 is recommended. First, a standard (calibration) curve is established which relates emf to logarithm

concentration of SO_3 under conditions which do not favor the SO_3 to SO_2 transference. Subsequent emf measurements correspond to particular values of SO_3 on the standard curve.

(4). The adsorption/desorption of SO_3 on the platinum electrode is the slowest step among the elementary steps in the cathode reaction. The formation of a solid-like SO_3(Pt) in a chemisorbed state depends upon the concentration of SO_2 (or SO_3). The reliability of the emf measurement is influenced by the formation of SO_3(Pt).

(5). A reaction layer of a few atoms thickness is probably formed on the surface of the solid electrolyte during the experimental runs resulting in different physico-chemical properties of the product layer from that of the bulk product.

(6). The standard Gibbs energy change for the reaction:

$$2\ Ag(s) + SO_3(g) + 1/2\ O_2(g) = Ag_2SO_4(s,l)$$

has been determined from the emf measurements. $\Delta G°$ can be expressed as the following linear functions of temperature:

$\Delta G°(J) = -290\ 460 + 202.99T$ (624 - 703 K)

$\Delta G°(J) = -271\ 160(\pm 2236) + 175.54(\pm 1.68)T$ (703-926 K)

$\Delta G°(J) = -252\ 060 + 154.91T$ (926-1146 K)

(7). A thermodynamic analysis indicates that the use of ß (or ß")-alumina as a solid electrolyte in the presence of SO_2 in oxidizing atmospheres may be limited to relatively high temperatures (approximately above 800 K). The critical temperature below which the sulfate is more stable than α-alumina and electrolyte failure takes place is a function of the concentration of SO_2. The higher the concentration of SO_2, the higher the critical temperature.

(8). On a qualitative basis, calcium aluminate with the stoichiometric composition $0.9CaO0.72MgO5.5Al_2O_3$ may be used as solid electrolyte to monitor SO_2 contents at high temperatures. Further work is required on a reference electrode where the activity of Ca is relatively high.

The following additional studies are proposed:

(1). With Ag^+-ß-alumina, it is proposed that metal cathodes other than platinum should be

investigated. The metals should not allow the formation of chemisorbed SO_3 on the electrode surface.

(2). The use of other ß-aluminas such as Li^+- or K^+-ß-alumina should be studied, particularly with respect to the dependence of emf on the flow rate of the gas mixture.

REFERENCES

1. B.C.H. Steele and R.W. Shaw, "Thermodynamic Measurements with Solid Electrolytes" in Solid Electrolytes, ed. by P. Hagenmuller, Academic Press,(1978).

2. A.D. Pelton and W.T. Thompson, Progress in Solid State Chemistry, **10**, 119, (1975).

3. D.O. Raleigh, "Solid State Electrochemistry" in Progress in Solid State Chemistry, **Vol.3**, (1967).

4. D.O. Raleigh, "Electrode Processes in Solid Electrolyte Systems" in Electroanalytical Chemistry, ed. by Allen J. Bard, **Vol.6**, (1973).

5. C. Wagner, "The Electromotive Force of Galvanic Cells Involving Phases of Locally Variable Composition" in Advances in Electrochemistry and Electrochemical Engineering, **Vol.4**, ed. by P. Delahey, John Wiley, New York, (1966).

6. F.A. Kroger, The Chemistry of Imperfact Crystals, 2nd ed. **Vol.3**, North-Holland Publ., Amsterdam, (1974).

7. J.W. Patterson, "Ionic Conductivity and Electrochemistry of Crystalline Ceramics" in Electrical Conductivity in Ceramics and Glass, Part B, 453, ed. by N.M. Tallan, Dekker, New York, (1974).

8. H. Rickert, "Solid-state Electrochemistry" in Treatise on Solid State Chemistry, **Vol.4**, ed. by N.B. Hannay, Plenum Press, New York, (1976).

9. L. Heyne, "Ionic Conductivity in Oxides" in Mass Transport in Oxides, ed by J.B. Wachtman and A.D. Franklin, U.S. National Bureau of Standards, Washington D.C., (1968).

10. N.S. Choudhury and W. Patterson, J. Electrochem. Soc., **118**, 1398, (1971).

11. R.N. Blumenthal and M.A. Seitz, "Experimental Techniques" in Electrical Conductivity in Ceramics and Glass, Part A, ed. by Norman M. Tallan, (1974).

12. T.A. Ramanarayanan and W.L. Worrell, Can. Met. Q., **13**, 325, (1974).

13. T.H. Etsell and S.N. Flengas, Chemical Reviews, **70**, 339, (1970).

14. P. McGeehin and A. Hooper, J. Mat. Sci., **12**, 1, (1977).

15. W.L. Worrell, "Oxide Solid Electrolyte" in Solid Electrolyte, e.d. by S. Geller, Springer-Verlag, Berlin Heidelberg, (1974).

16. R.A. Rapp and D.A. Shores, "Solid Electrolyte Galvanic Cells" in Physiochemical Measurements in Metals Research, **Vol.6**, Part 2, ed. by R.A. Rapp, John Wiley and Sons, New York, (1970).

17. K. Goto and W. Pluschkell, "Oxygen Concentration Cells" in Physics of Electrolytes, **Vol.2**, 539, ed. by J. Hladik, Academic Press, New York, (1972).

18. C.B. Alcock, in Electromotive Force Measurement in High Temperature Systems, ed. by C.B. Alcock, 109, Elsevier, Amsterdam, (1968).

19. B.C.H. Steele, in Electromotive Force Measurement in High Temperature Systems, ed. by C.B. Alcock, 3, Elsevier, Amsterdam, (1968).

20. J.N. Pratt, Metall. Trans. A, **21A**, 1223, (1990).

21. H. Dietz, W. Haecker and H. Jahnke, "Electrochemical Sensors for the Analysis of Gases" in Advances in Electrochemistry and Electrochemical Engineering, **Vol.10**, Wiley Interscience, New York, (1977).

22. L.A. Simpson and R.E. Carter, J. Am. Ceram. Soc., **49**, 139, (1966).

23. W.H. Rhodes and R.E. Carter, J. Am. Ceram. Soc., **49**, 244, (1966).

24. W.D. Kingery, J. Pappis, M.E. Doty and D.C. Hill, J. Am. Ceram. Soc., **42**, (1959).

25. T.Y. Tien and E.C. Subbarao, J. Chem. Phys., **39**, 1041, (1963).

26. H. Schmalzried, Z. Phys. Chem. (NF), **38**, 87, (1963).

27. A.W. Smith, F.W. Meszaros and C.D. Amata, J. Am. Ceram. Soc., **49**, 240, (1966).

28. J.W. Patterson, B.C. Botren and R.A. Rapp, J. Electrochem. Soc., **114**, 752, (1967).

29. Ju.D. Tretyakov and A. Muan, J. Electrochem. Soc., **116**, 331, (1969).

30. R.J. Fruehan, L.J. Martonik, and E.T. Turkdogan, TMS-AIME, **245**, 1501, (1969).

31. J.B. Hardaway III, J.W. Patterson, D.R. Wilder, and J.D. Schieltz, J. Am. Ceram. Soc., **54**, 94, (1971).

32. F.J. Salzano, H.S. Isaacs and B. Minushkin, J. Electrochem. Soc., **118**, 412, (1971).

33. S.R. Levine and M. Kolodney, J. Electrochem. Soc., **116**, 1420, (1969).

34. R. Baker and J.M. West, J. Iron & Steel Inst., **204**, 212, (1966).

35. J.W. Patterson, J. Electrochem. Soc., **118**, 1033, (1971).

36. J. Patterson, in Physics of Electronic Ceramics Part A, ed. by L.L. Herch and D.B. Dove, Marcel Dekker Inc., New York, (1971).

37. D.A. Shores and R.A. Rapp, J. Electrochem. Soc., **118**, 1107, (1971).

38. N.S. Choudhury and J.W. Patterson, J. Electrochem. Soc., **117**, 1384, (1970).

39. R.W. Vest and N.M. Tallan, J. Appl. Phys., **36**, 543, (1965).

40. R.W. Vest, N.M. Tallan and W.C. Tripp, J. Am. Ceram. Soc., **47**, 635, (1964).

41. R.W. Vest and N.M. Tallan, J. Am. Ceram. Soc., **48**, 472, (1965).

42. J.J. Mills, J. Phys. Chem. Solids, **31**, 2577, (1970).

43. B.C.H. Steele and C.B. Alcock, Trans. Metall. Soc. AIME, **233**, 1359, (1965).

44. T.H. Etsell and N. Flengas, J. Electrochem. Soc., **119**, 1, (1972).

45. D.A.J. Swinkels, J. Electrochem. Soc., **117**, 1267, (1970).

46. M.H. Hebb, J. Chem. Phys., **20**, 185, (1952).

47. C. Wagner, Proc. Int. Comm. Electrochem. Thermo. Kinetics (CITCE), 7th, 361, (1957).

48. A.V. Joshi and J.B. Wagner, Jr., J. Phys. Chem. Solids, **33**, 205, (1972).

49. J. Fouletier, P. Fabry and M. Kleitz, J. Electrochem. Soc., **123**, 204, (1976).

50. P. Fabry, M. Kleitz and C. Deportes, J. Solid State Chem., **5**, 1, (1972).

51. L. Heyne and D. den Engelsen, J. Electrochem. Soc., **124**, 727, (1977).

52. R.J. Brook, W.L. Pelzmann and F.A. Kroger, J. Electrochem. Soc. **118**, 185, (1971).

53. H.S. Isaacs and L.J. OLmer, J. Electrochem. Soc., **129**, 436, (1982).

54. D.M. Haaland, J. Electrochem. Soc., **127**, 796, (1980).

55. J.I. Federer, J. Electrochem. Soc., **131**, 755, (1984).

56. Y.L. Sandler, J. Electrochem. Soc., **118**, 1378, (1971).

57. D.M. Haaland, Anal. Chem., **49**, 1813, (1977).

58. M. Gauthier and A. Chamberland, J. Electrochem. Soc., **124**, 1579, 1584, (1977).

59. C.G. Vayenas and H.M. Saltsburg, J. Catalysis, **57**, 296, (1979).

60. J. Kirchnerova, C.W. Bale and J.M. Skeaff, Proceedings of 2th International Meeting on Chemical Sensors, ed. by J.-L. Aucouturier et al, Bordeaux, France, 311, (1986).

61. C. Wagner, Electrochimica Acta, **15**, 987, (1970).

62. H. Salaun and M. Fouletier, Proceedings of 2th International Meeting on Chemical Sensors, ed. by J.-L. Aucouturier et al, Bordeaux, France, 277, (1986).

63. G. Vitter and H. Salaun, Proceedings of 2th International Meeting on Chemical Sensors, ed. by J.-L. Aucouturier et al, Bordeaux, France, 331, (1986).

64. C. Wagner, Advances in Catalysis, **21**, 323, (1970).

65. R. Cote, C.W. Bale and M. Gauthier, J. Electrochem. Soc., **131**, 63, (1984).

66. G.G. Barna and R.J. Jasinski, Anal. Chem., **46**, 1834, (1974).

67. R. Jasinski, G. Barna, and I. Trachtenberg, J. Electrochem. Soc., **121**, 1575, (1974).

68. L.G. Boxall and K.E. Johnson, J. Electrochem. Soc., **118**, 885, (1971).

69. G. Hotzel and W. Weppner, Solid State Ionics, **18 & 19**, 1223, (1986).

70. G. Hotzel and W. Weppner, Proceedings of 2th International Meeting on Chemical Sensors, ed. by J.-L. Aucouturier et al, Bordeaux, France, 285, (1986).

71. G. Velasco, J.Ph. Schnell, and M. Croset, Sensors and Actuators, **2**, 371, (1982).

72. W. Weppner, Sensors and Actuators, **12**, 107, (1987).

73. J. Kirchnerova and C.W. Bale, Sensors and Actuators, B, **2**, 7, (1990).

74. F.J. Salzano and L. Newman, J. Electrochem. Soc., **119**, 1273, (1972).

75. M. Gauthier, R. Bellemare, and A. Belanger, J. Electrochem. Soc., **128**, 371, (1981).

76. A. Belanger, M. Gauthier, and D. Fauteux, J. Electrochem. Soc., **131**, 579, (1984).

77. K.T. Jacob and D. Bhogeswara Rao, J. Electrochem. Soc., **126**, 1842, (1979).

78. Q.G. Liu and W.L. Worrell, in Chemical Metallurgy - A tribute to Carl Wagner, e.d. by N.A. Gokcen, The Metallurgical Soc., Warrington, PA, pp.43-49, (1981).

79. W.L. Worrell and Q.G. Liu, Sensors and Actuators, **2**, 385, (1982).

80. W.L. Worrell and Q.G. Liu, in Proceedings of the International Meeting on Chemical Sensors, 332, Fukuoka, Japan (1983).

81. N. Imanaka, G. Adachi, and J. Shiokawa, Anal. Chem. Symp. Ser., **17**, 348, (1983).

82. N. Imanaka, Y. Yamaguchi, G. Adachi, and J. Shiokawa, J. Electrochem. Soc., **132**, 2519, (1985).

83. N. Imanaka, Y. Yamaguchi, G. Adachi, and J. Shiokawa, J. Electrochem. Soc., **133**, 1026, (1986).

84. N. Imanaka, Y. Yamaguchi, G. Adachi, and J. Shiokawa, J. Electrochem. Soc., **134**, 725, (1987).

85. M. Itoh, E. Sugimoto and Z. Kozuka, Trans. Japan Inst. Metals, **25**, 504, (1984).

86. M. Itoh and Z. Kozuka, J. Electrochem. Soc., **133**, 1512, (1986).

87. M. Itoh and Z. Kozuka, Trans. Japan Inst. Metals, **26**, 17, (1985).

88. M. Itoh, K. Kimura and Z. Kozuka, Trans. Japan Inst. Metals, **26**, 353, (1985).

89. Y. Saito, T. Maruyama, Y. Matsumoto, and Y. Yano, Anal. Chem. Symp. Ser., **17**, 326, (1983).

90. J.T. Kummer, Progress in Solid State Chemistry, **Vol. 7**, 141, (1972).

91. J.H. Kennedy, "The ß-Alumina" in Solid Electrolytes, ed. by S. Geller, Springer-Verlag, Berlin Heidelberg, (1977).

92. R. Collongues, J. Thery, and J.P. Bailot, "ß-Alumina" in Solid Electrolyte, ed. by P. Hagenmuller and W. Van Gool, Academic Press, Inc., New York, (1978).

93. Y.F.Y. Yao and J.T. Kummer, J. Inorg. Nucl. Chem., **29**, 2453, (1967).

94. G.C. Farrington and B. Dunn, Solid State Ionics, **7**, 267, (1982).

95. M.S. Whittingham and R.A. Huggins, J. Chem. Phys., **54**, 414, (1971).

96. R. Galli, P. Longhi, T. Mussini, and F.A. Tropeano, Electrochim. Acta, **18**, 1013, (1973).

97. M.S. Whittingham and R.A. Huggins, J. Electrochem. Soc., **118**, 1, (1971).

98. D.O. Raleigh, J. Phys. Chem. Solid, **26**, 329, (1965).

99. Y.J. Van der Meulen and F.A. Kroger, J. Electrochem. Soc., **117**, 69, (1970).

100. J. Ni, Y.T. Tsai and D.H. Whitmore, Solid State Ionics, **5**, 199, (1981).

101. Y. Hong, D. Hong, Y. Peng, L. Li, and S. Wei, Solid State Ionics, **25**, 301, (1987).

102. R.V. Kumar and D.A.R. Kay, Metall. Trans., **16B**, 107, 287, 295, (1985).

103. E.A. Guggenheim, Thermodynamics, 5th edition, North-Holland Publ.,Amsterdam, (1967).

104. J.J. Lingane, Electroanalytical Chemistry, Chapt. X, Interscience Publishers, Inc., New York, (1958).

105. P.J. Jorgensen, J. Chem. Phys., **37**, 874, (1962).

106. P.J. Jorgenson, J. Chem. Phys., **49**, 1594, (1968).

107. H. Yanagida, R.J. Brook and F.A. Kroger, J. Electrochem. Soc., **117**, 593, (1970).

108. T.H. Etsell and S.N. Flengas, J. Electrochem. Soc., **118**, 1890, (1971).

109. T.H. Etsell and S.N. Flengas, Met. Trans., **2**, 2829, (1971).

110. C.J. Wen and D.M. Mason, J. Appl. Electrochem., **8**, 81, (1978).

111. S. Pancharatnam, R.A. Huggins, and D.M. Mason, J. Electrochem. Soc., **122**, 869, (1975).

112. P.H. Rieger, Electrochemistry, Ch. 5, Prentice-Hall, Inc., Englewood Cliffs, (1987).

113. V.S. Stubican and S.P. Ray, J. Am. Ceram. Soc., **60**, 534, (1977).

114. F. Sibieude and M. Foex, J. Nucl. Mater., **56**, 229, (1975).

115. A.D. Pelton, "Phase Diagrams" in Physical Metallurgy, ed. by R.W. Cahn and P. Haasen, Elsevier Science Publisher BV, (1983).

116. H.N. Baumann, Jr., Ceramic Bulletin, **35**, 358, (1956).

117. L. De Pablo-Galan and W.R. Foster, J. Am. Ceram. Soc., **42**, 491, (1959).

118. M. Rolin and P.H. Thanh, Rev. Hautes Temp. et Réfract., **2**, 175, (1965).

119. M. Bettman and C.R. Peters, J. Phys. Chem., **73**, 1774, (1969).

120. R.C. De Vries and W.L. Roth, J. Am. Ceram. Soc., **52**, 364, (1969).

121. I. Eliezer and R.A. Howald, High Temperature Science, **10**, 1, (1978).

122. J.D. Hodge, J. Am. Ceram. Soc., **66**, 166, (1983).

123. J.D. Hodge, J. Am. Ceram. Soc., **67**, 183, (1984).

124. D.J. Fray, Metall. Trans. B, **8B**, 153, (1977).

125. F.A. Elrefaie and W.W. Smeltzer, J. Electrochem. Soc., **128**, 1443, (1981).

126. A. Dubreuil, M. Malenfant, and A.D. Pelton, J. Electrochem. Soc., **128**, 2006, (1981).

127. R.J. Brisley and D.J. Fray, Metall. Trans. B, **14B**, 435, (1983).

128. H.H. Kellogg, Trans. Metall. Soc. AIME, **230**, 1622, (1964).

129. E.T. Turkdogan, Physical-chemistry of High Temperature Technology, Academic Press Inc., New York, (1980).

130. P.I. Fedorov and Chang Ch'ih-Yun, Russian Journal of Inorganic Chemistry, **11**, 362, (1966).

131. L.A. Kochubei, E.V. Margulis, F.I. Vershinina, and L.V. Vorob'eva, Russ. J. Inorg. Chem., **26**, 1069, (1981).

132. O. Kubaschewski and C.B. Alcock, Metallurgical Thermochemistry, 5th edition, Pergamon Press Ltd., (1979).

133. I. Barin, Thermochemical Data of Pure Substance, Part I, VCH, Weinheim, (1989).

134. I.V. Kutsenok, A.R. Kaul and Yu.D. Tret'yakov, Izvestiya Akademii Nauk SSSR, Neorganicheskie Materialy, **17**, 64, (1981).

135. S.G. Popov, V.A. Levitskii, Yu.Ya. Skolis, and V.V. Karlin, Izvestiya Akademii Nauk SSSR, Neorganicheskie Materialy, **15**, 1237, (1979).

136. M. Allibert, C. Chatillon, K.T. Jacob, and R. Lourtau, J. Am. Ceram. Soc., **64**, 307, (1981).

137. R.V. Kumar and D.A.R. Kay, Metall. Trans., **16B**, 107, (1985).

138. G. Eriksson, Private communication.

139. S.G. Popov, V.A. Levitskii, Y.Y. Skolis, and V.V. Karlin, Neorg. Mater., **15**, 1273, (1979).

140. W.T. Thompson and S.N. Flengas, J. Electrochem. Soc., **118**, 419, (1971).

141. J. Vedel, "Electrode Reactions at Electrode-Solid Electrolyte Interfaces, Use of Electroanalytical Techniques" in Electrode Processes in Solid State Ionics, e.d. by M. Kleitz and J. Dupuy, Reidel, Dordreeht, (1976).,

142. B. Claudel, "Adsorption and Catalysis on Ionic Solid" in Electrode Processes in Solid State Ionics, e.d. by M. Kleitz and J. Dupuy, Reidel, Dordreeht, (1976).

143. T.L. Francis, F.E. Phelps, and G. Maczura, Amer. Ceram. Soc. Bull., **50**, 615, (1971).

144. J. Kirchnerova, A. Petric, C.W. Bale, and A.D. Pelton, to be appeared in Mater. Res. Bull., 1991.

145. B.R. Conard, T.B. McAneney, and R. Sridhar, J. Chem. Thermodynamics, **10**, 889, (1978).

146. T.N. Rhodin and D.L. Adams, "Adsorption of Gases on Solids" in Treatise on Solid State Chemistry, **Vol.6A**, ed. by N.B. Hannay Plenum Press, New York, (1976).

147. D.R. Stull and H. Prophet, JANAF Thermochemical Tables, NBS, Washington, DC, (1971).

148. L.S. Darken and R.W. Gurry, Physical Chemistry of Metals, McGraw-Hill, New York, (1953).

149. J.S. Warner, Trans. Metall. Soc. AIME, **221**, 591, (1961).

150. C.W. Bale and G. Poncet, Can. Metall. Q., **25**, 277, (1986).

151. K.T. Jacob and G.N.K. Iyengar, Metall. Trans., **17B**, 323, (1986).

152. G. Marchal, J. Chim. Phys., **22**, 559, (1925).

153. K. Hauffe and D. Hoeffgen, Z. Phys. Chem. (NF), **49**, 94, (1966).

154. N.A. Warner and T.R. Ingraham, Can. J. Chem., **38**, 2196, (1960).

155. K.H. Kim, and J.S. Choi, J. Phys. Chem., **85**, 2447, (1981).

156. G. Marchal and M.H. Le Chatelier, Comptes Rendus, **176**, 299, (1923).

157. L. Heyne, "Electrochemistry of Mixed Ionic-Electronic Conductors" in Solid Electrolytes, e.d. by S. Geller, Springer-Verlag, Berlin Heidelberg, (1977).

158. C. Wagner and A. Werner, J. Electrochem. Soc., **110**, 326, (1963).

159. H. Schmalzried, in Thermodynamics Vol. I, Proceedings of International Conferences on the Thermodynamics of Nuclear Materials, International Atomic Energy Agency, Vienna, 97, (1966).

160. W.L. Worrell, ibid, 131.

161. T.A. Ramanarayanan, "Limiting Factors in Measurements Using Solid Electrolytes" in Solid Electrolytes and their Applications, e.d. by E.C. Subbarao, Plenum Press, New York, (1978).

162. K.K. Kelley, The Thermodynamic Properties of Sulpher and its Inorganic Compounds, US Bur. Mines, Bull. No. **406**, 105, (1937).

163. T.R. Ingraham, Trans. Metall. Soc. AIME, **242**, 1299, (1968).

164. K. Pan and J. Lin, J. Chinese Chem. Soc., (Taiwan) **6**, 1, (1959).

165. The reference [81] in (162).

166. M. Rivier and A.D. Pelton, Am. Ceram. Soc. Bull., **57**, 183, (1978).

167. FACT (Facility for the Analysis of Chemical Thermodynamics) Users' Instruction Manual, by W.T. Thompson, C.W. Bale, and A.D. Pelton, 3rd edition (1988)

168. C.W. Bale, Can. Met. Q., **29**, 263, (1990).

APPENDIX A

Predominance diagrams and Potential-Composition diagrams calculated by means of FACT.

1. Predominance diagrams;

   The Na-Al-O-S system, Figures: 1 - 4.

   The Ag-Al-O-S system, Figures: 5 - 10.

   The Ca-Al-O-S system, Figures: 11 - 16.

2. Potential-Composition diagrams;

   The Na-Al-O-S system,

   $Log(P_{SO_2})$ = -2, Figures: 17 - 23.

   $Log(P_{SO_2})$ = -6, Figures: 23 - 29.

   The Ag-Al-O-S system,

   $Log(P_{SO_2})$ = -2, Figures: 30 - 35.

   $Log(P_{SO_2})$ = -5, Figures: 35 - 40.

   The Ca-Al-O-S system,

   $Log(P_{SO_2})$ = -2, Figures: 41 - 50.

   $Log(P_{SO_2})$ = -5, Figures: 51 - 59.

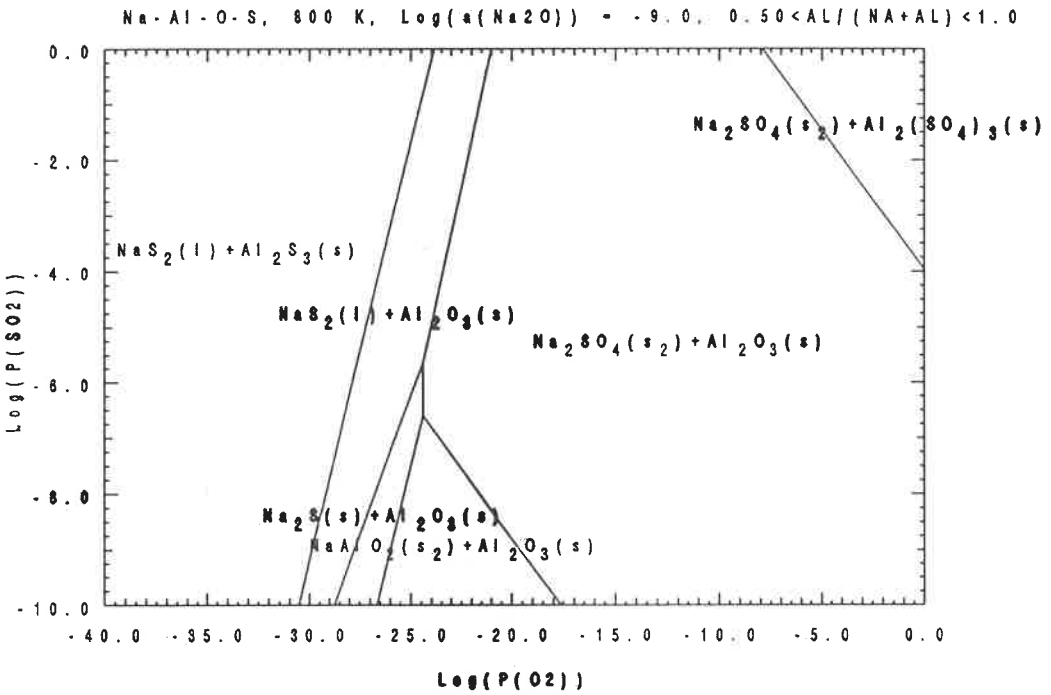

Figure 1. Predominance diagram for the Na-Al-O-S system

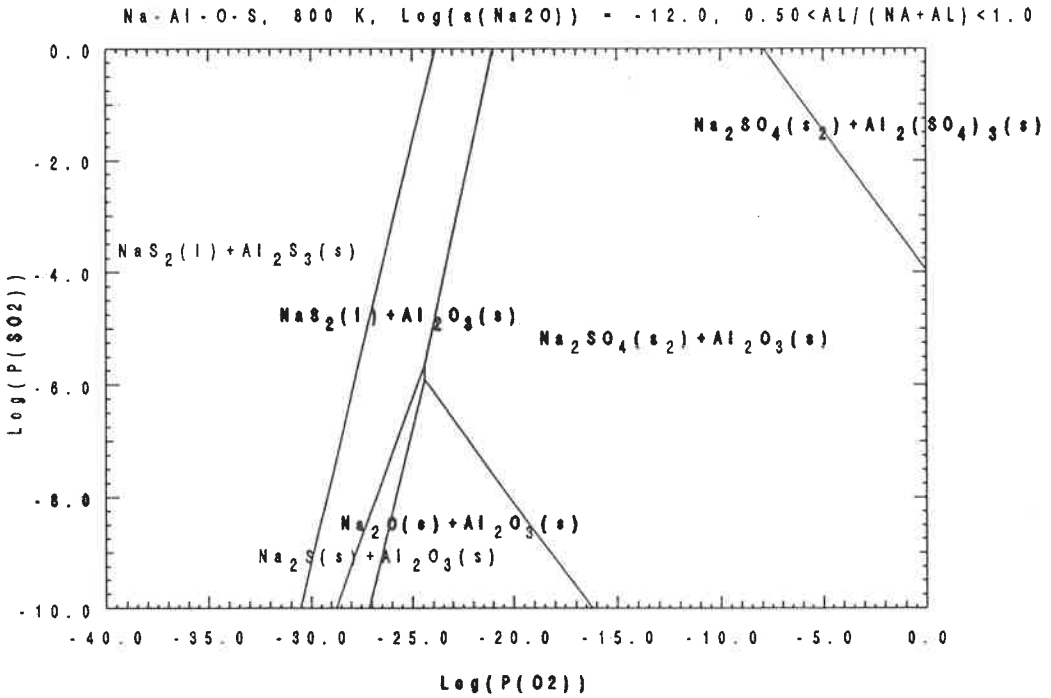

Figure 2. Predominance diagram for the Na-Al-O-S system

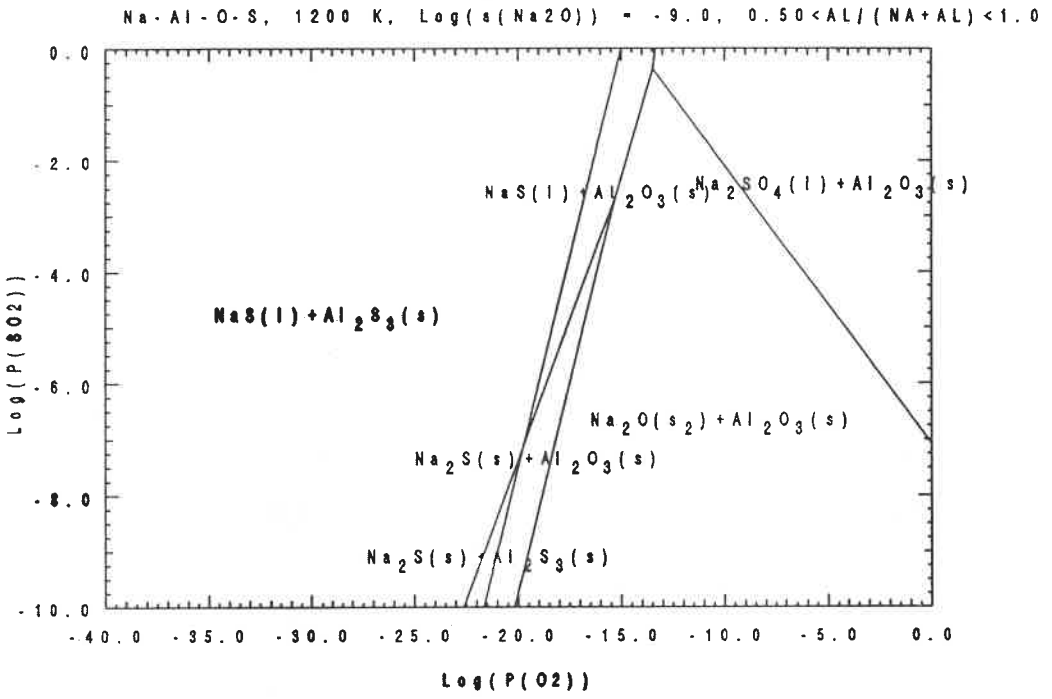

Figure 3. Predominance diagram for the Na-Al-O-S system

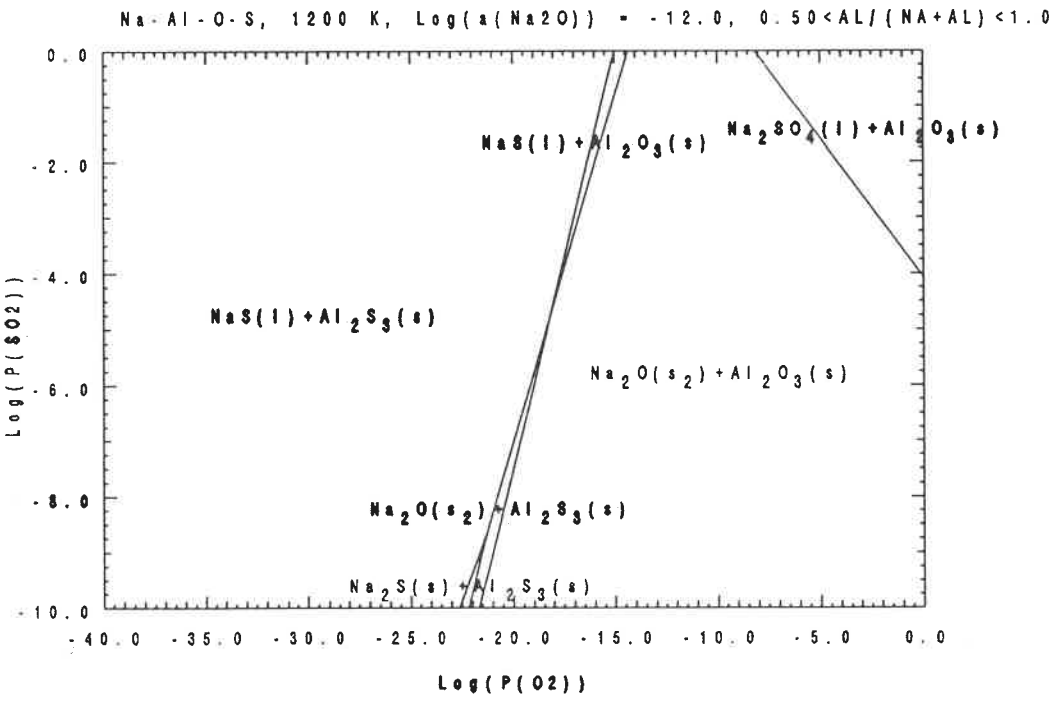

Figure 4. Predominance diagram for the Na-Al-O-S system

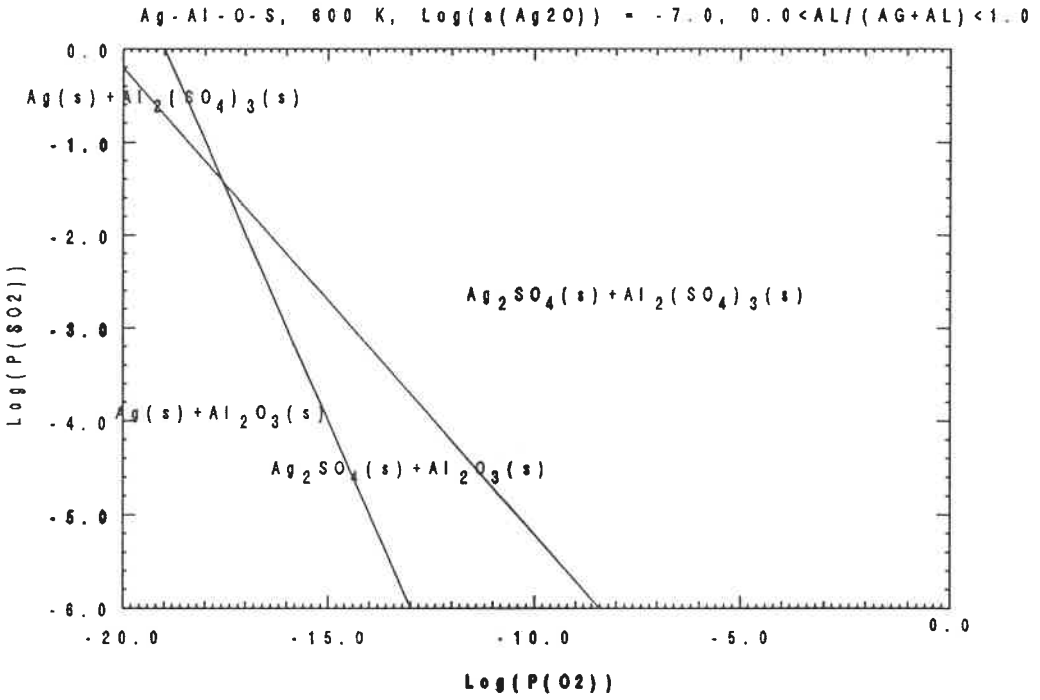

Figure 5. Predominance diagram for the Ag-Al-O-S system

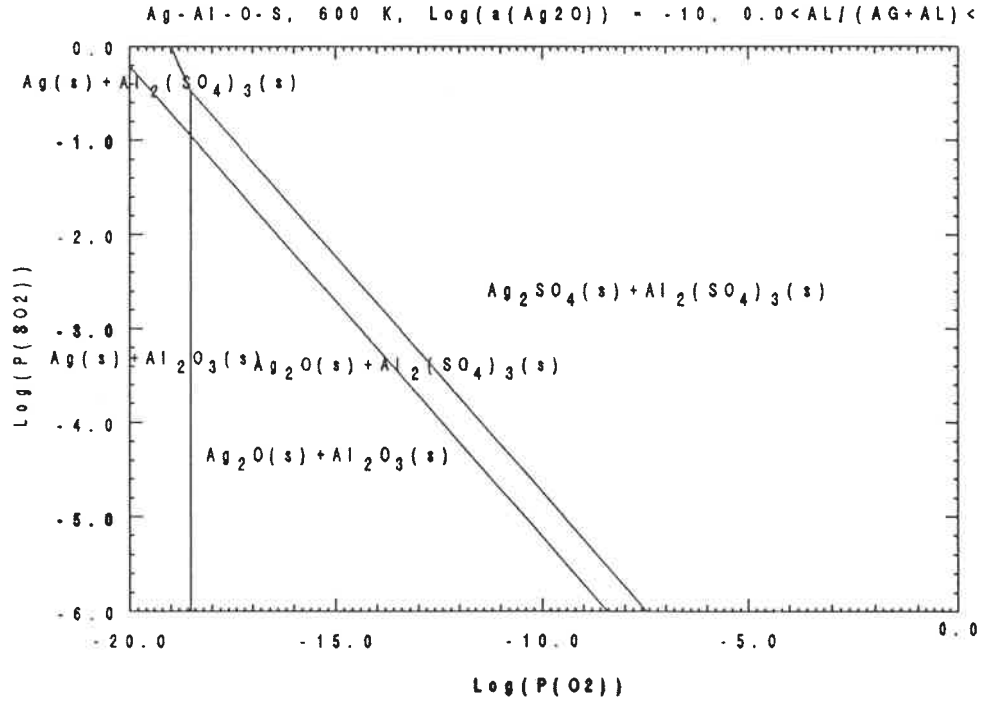

Figure 6. Predominance diagram for the Ag-Al-O-S system

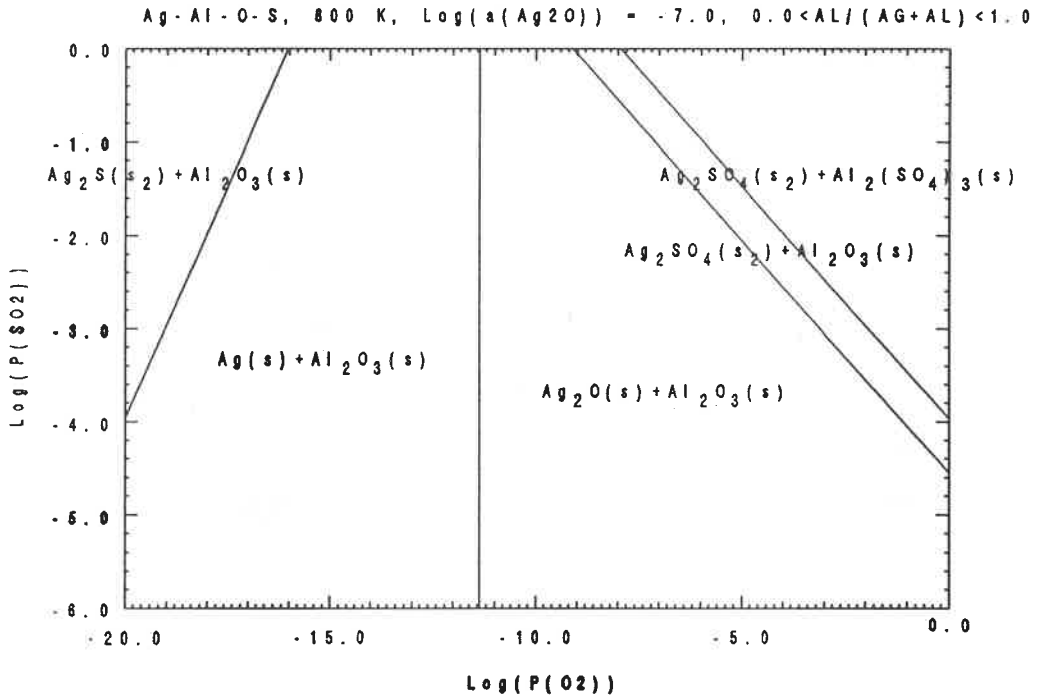

Figure 7. Predominance diagram for the Ag-Al-O-S system

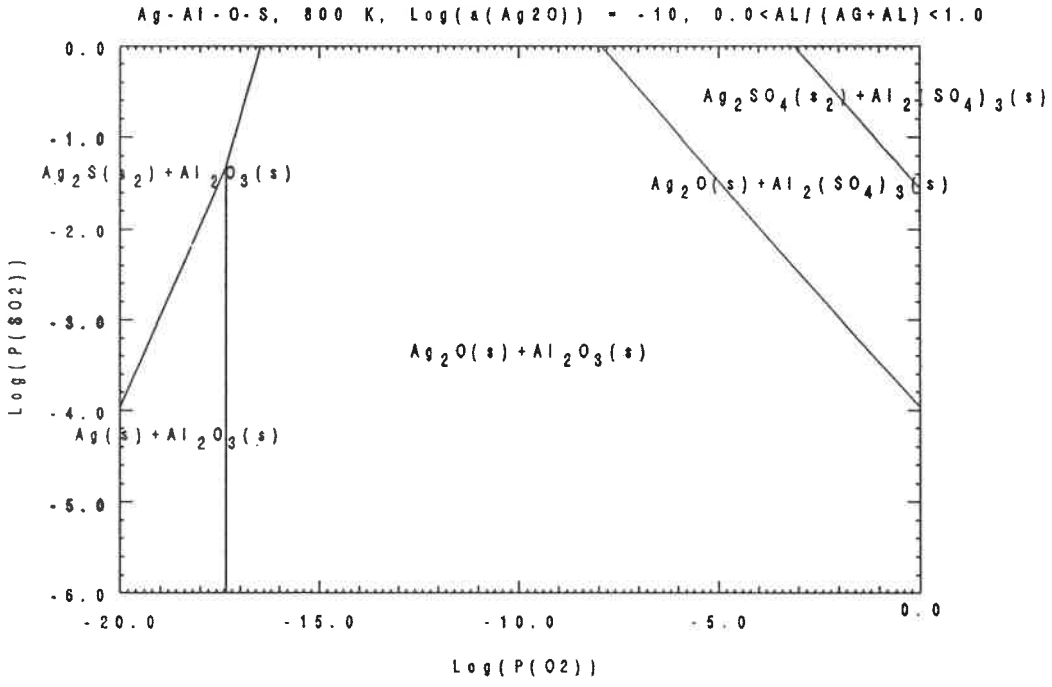

Figure 8. Predominance diagram for the Ag-Al-O-S system

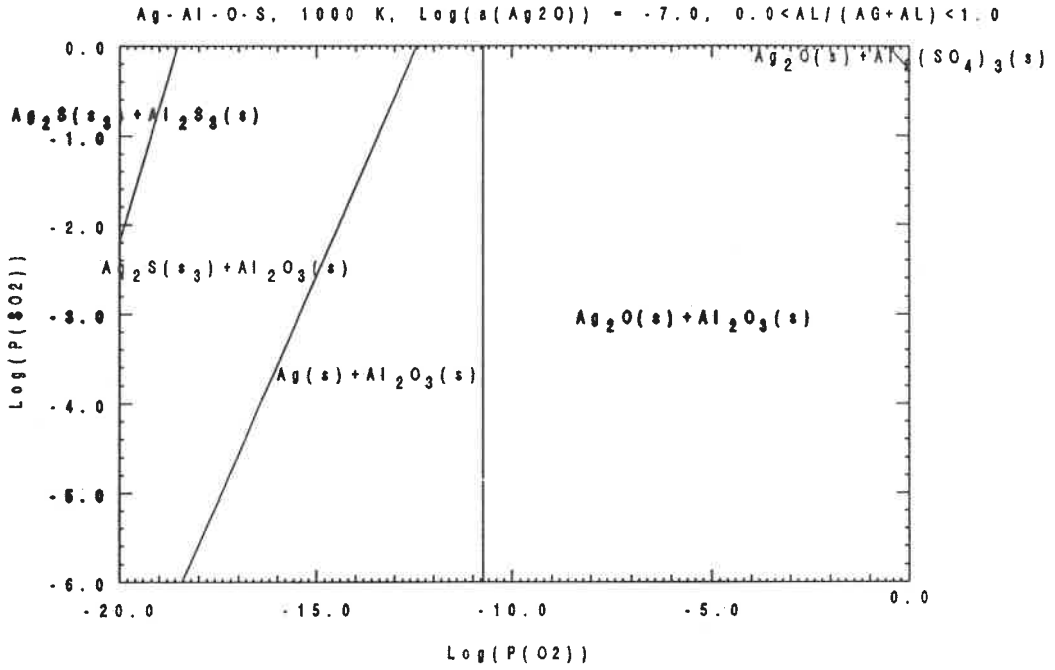

Figure 9. Predominance diagram for the Ag-Al-O-S system

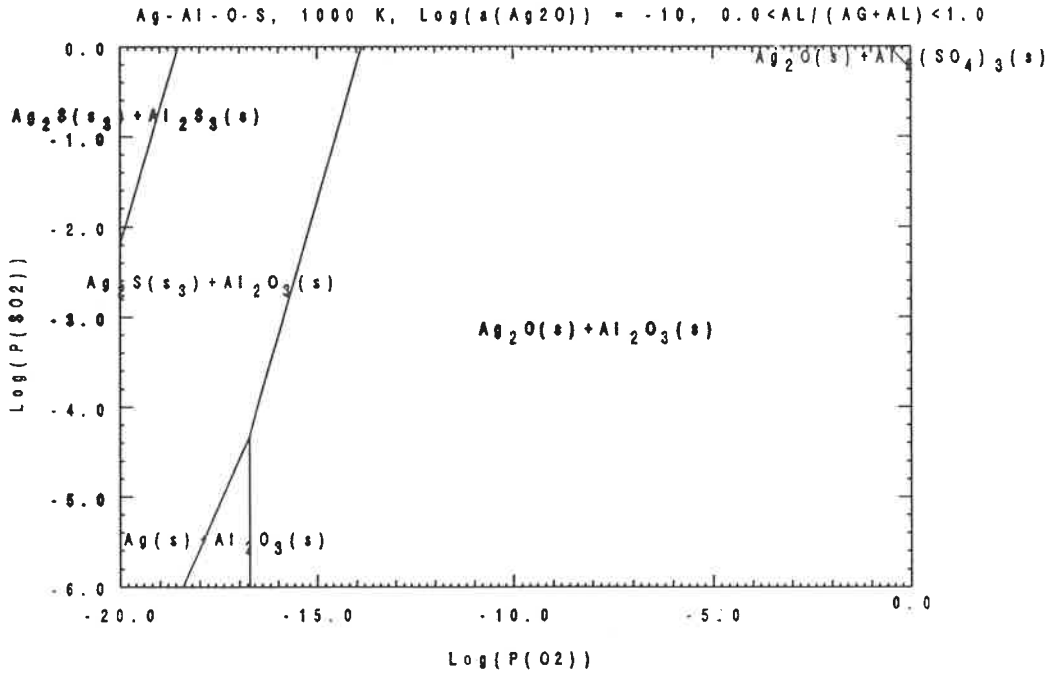

Figure 10. Predominance diagram for the Ag-Al-O-S system

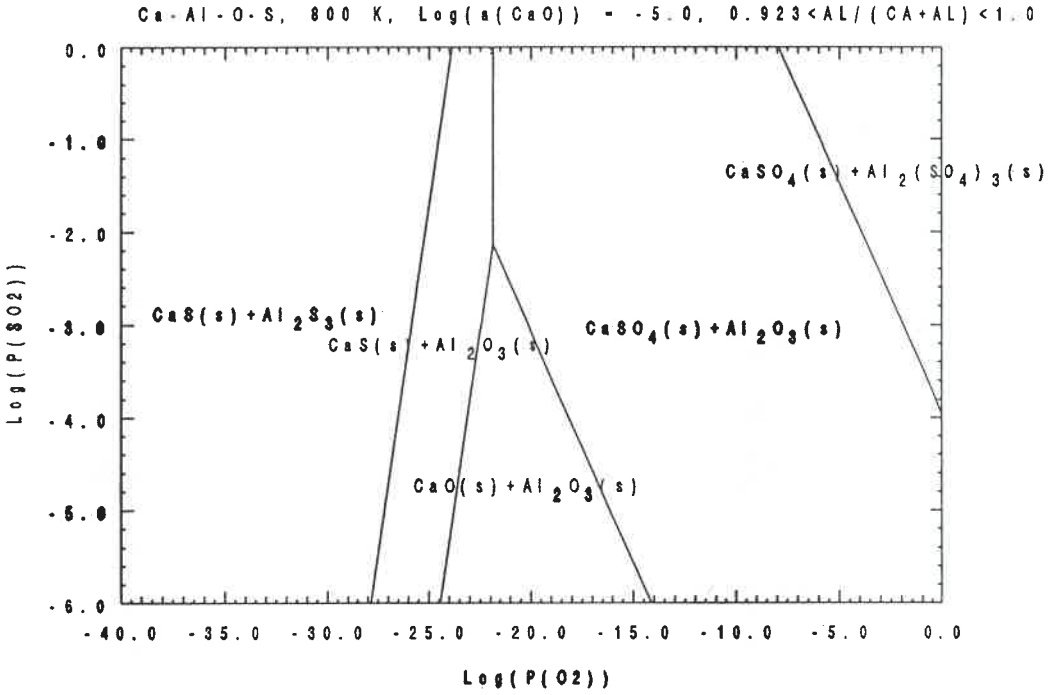

Figure 11. Predominance diagram for the Ca-Al-O-S system

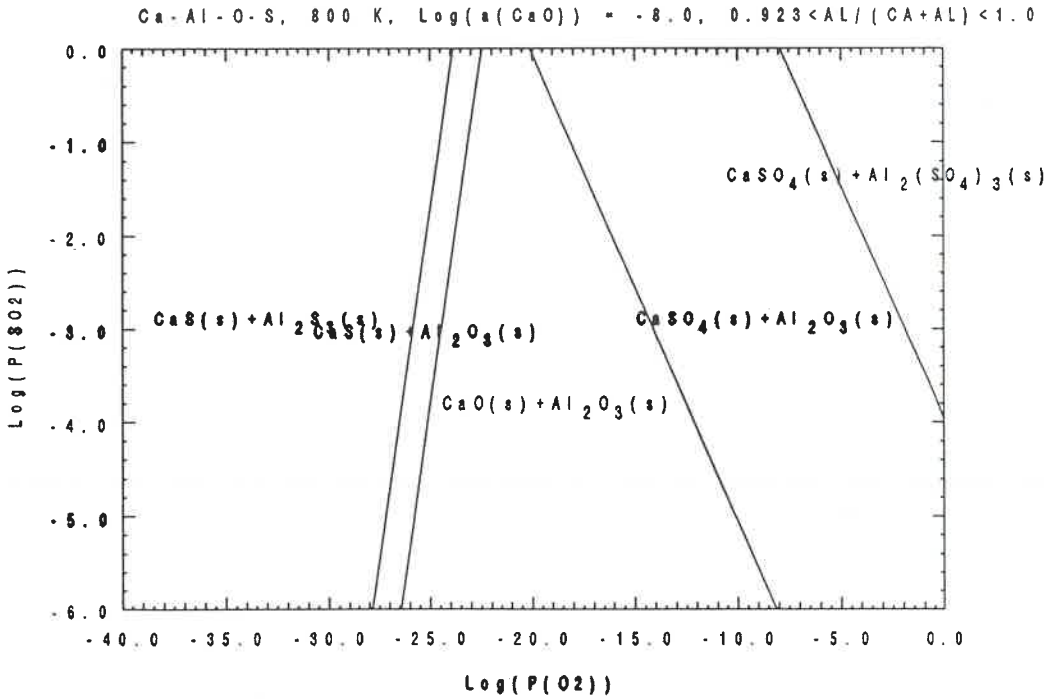

Figure 12. Predominance diagram for the Ca-Al-O-S system

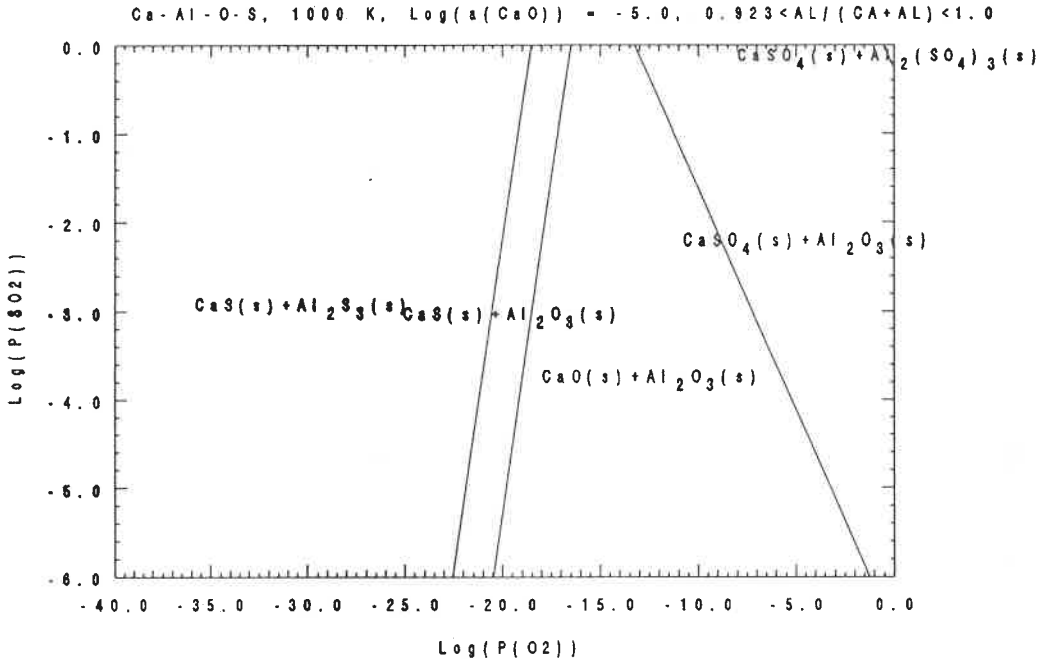

Figure 13. Predominance diagram for the Ca-Al-O-S system

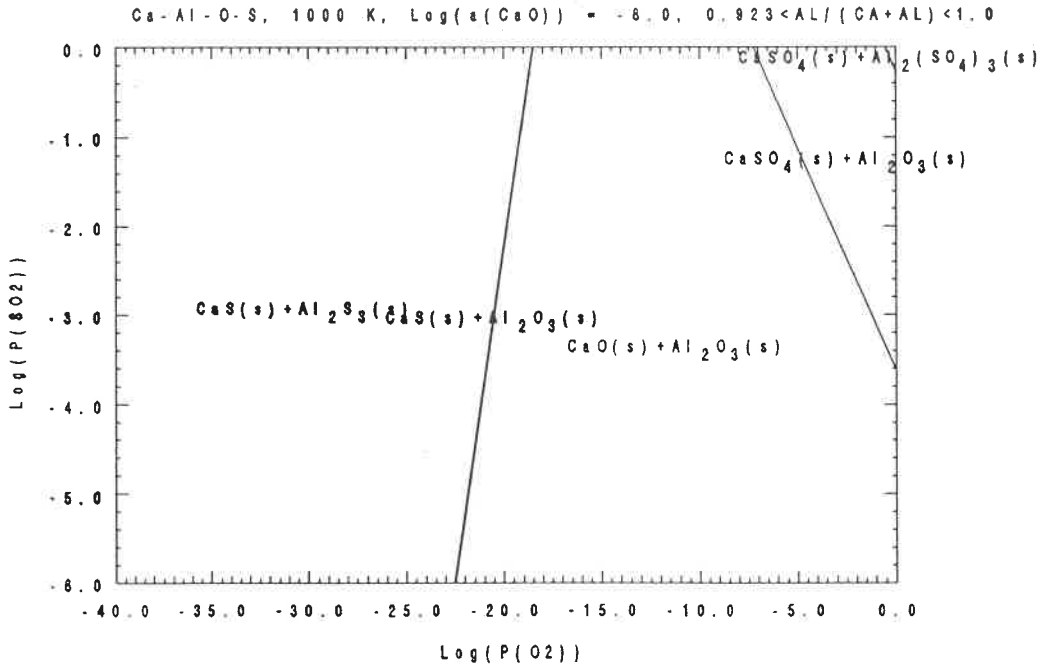

Figure 14. Predominance diagram for the Ca-Al-O-S system

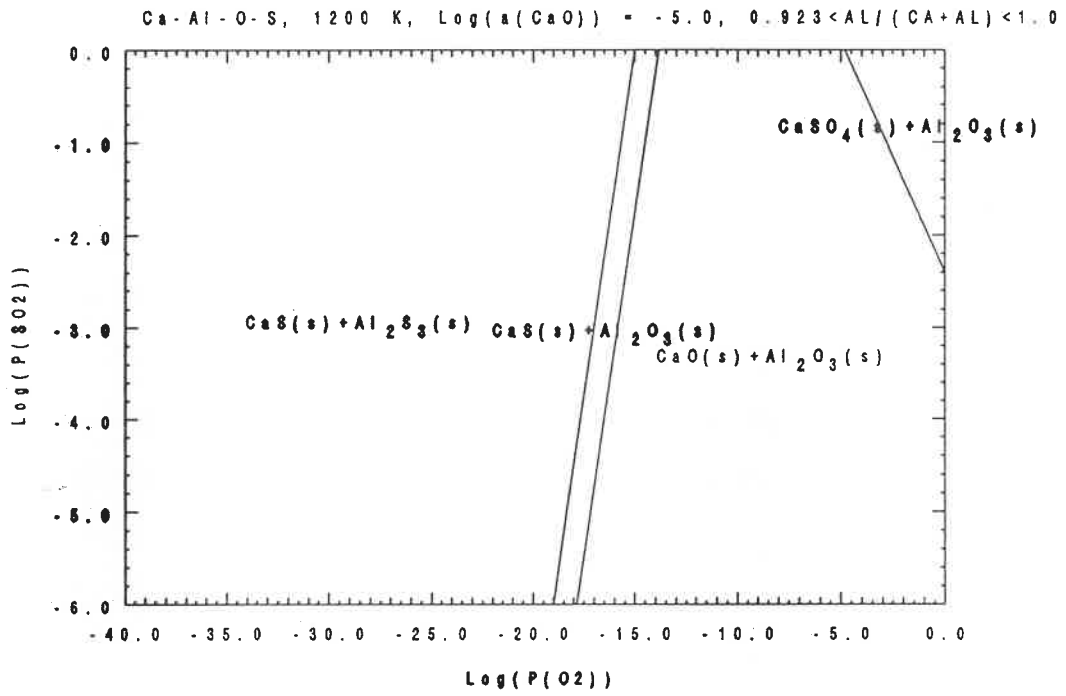

Figure 15. Predominance diagram for the Ca-Al-O-S system

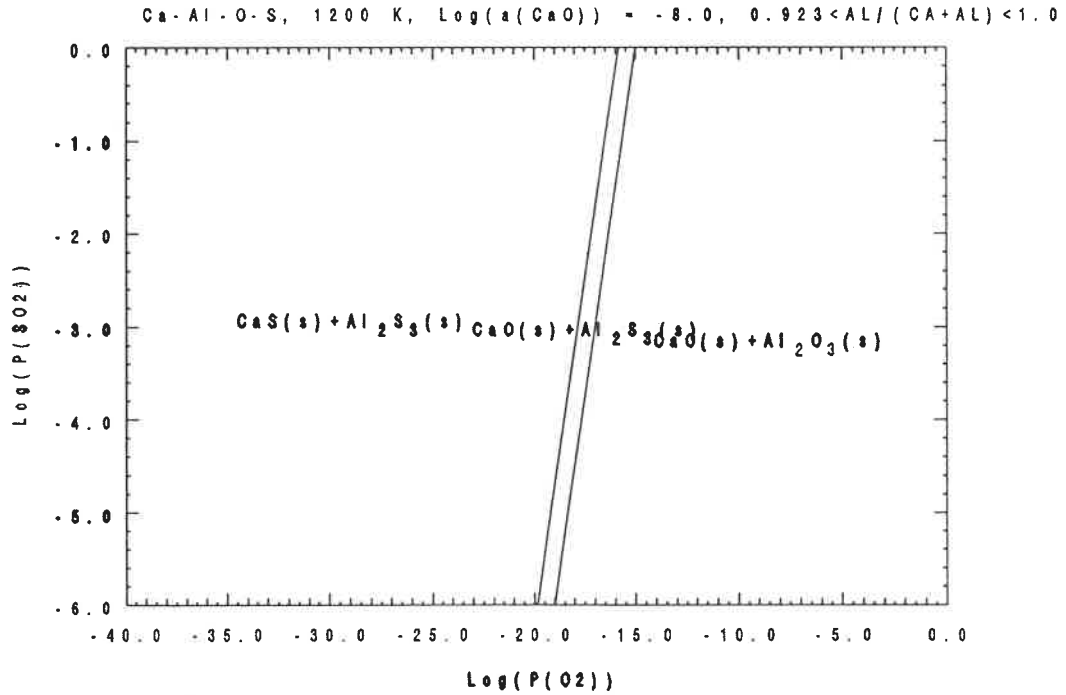

Figure 16. Predominance diagram for the Ca-Al-O-S system

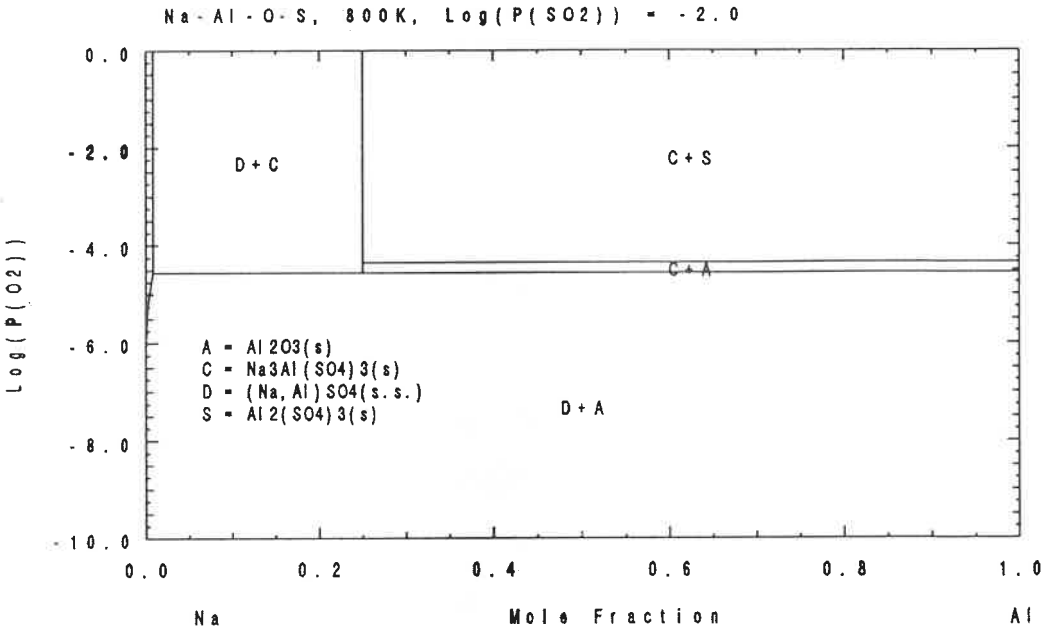

Figure 17. POTCOMP diagram for the Na-Al-O-S system

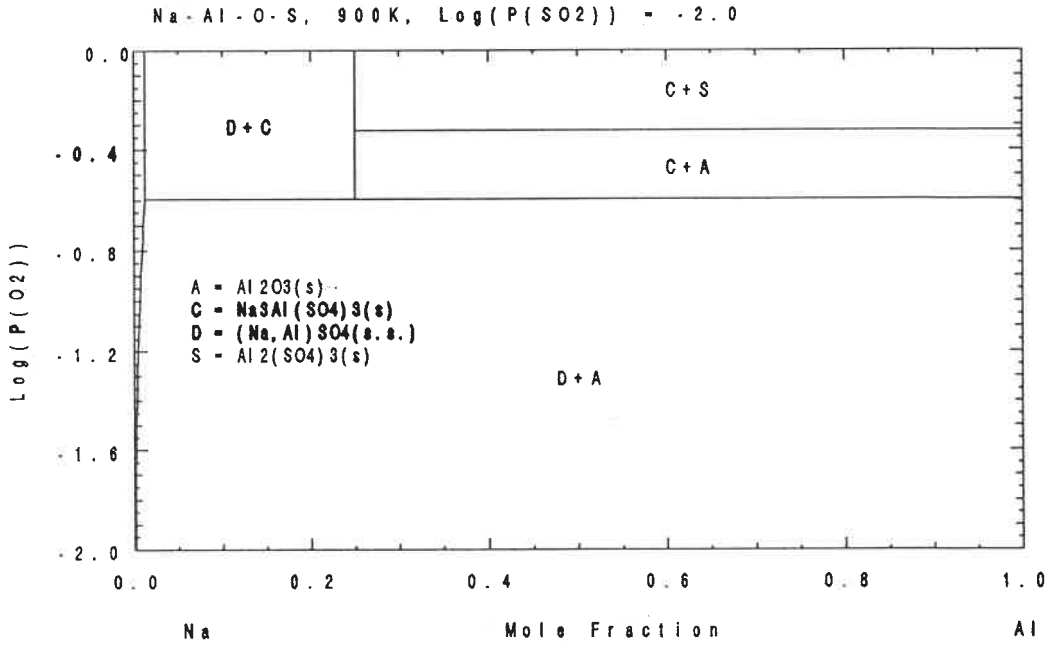

Figure 18. POTCOMP diagram for the Na-Al-O-S system

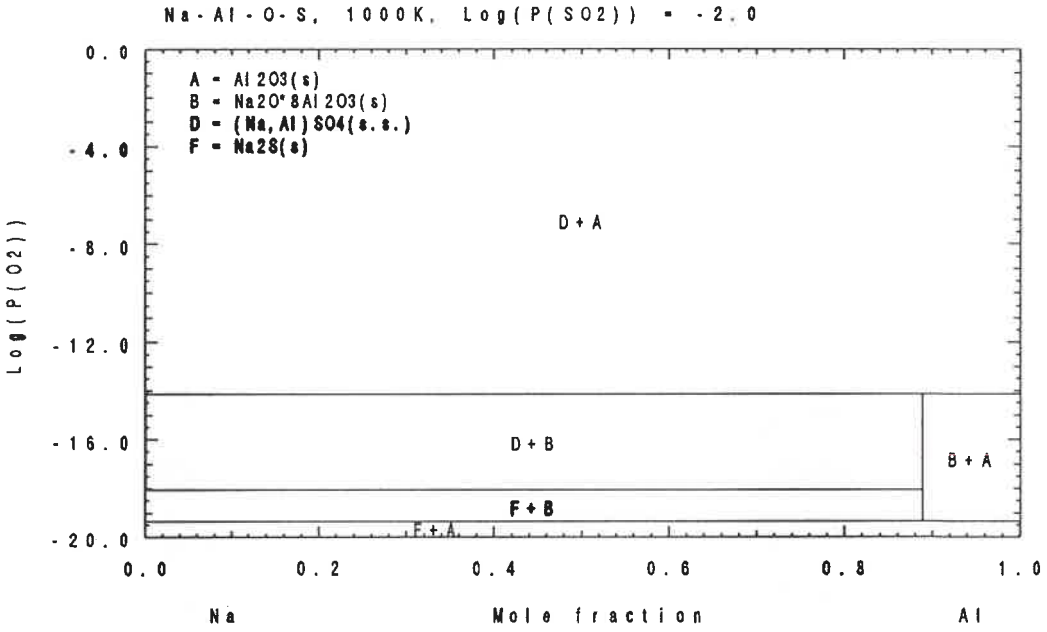

Figure 19. POTCOMP diagram for the Na-Al-O-S system

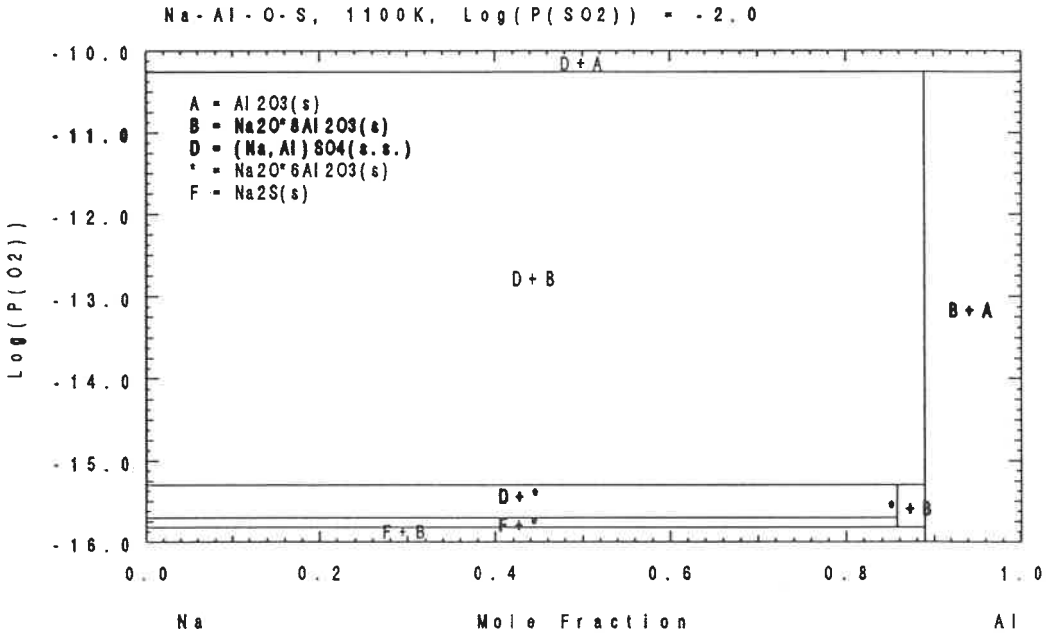

Figure 20. POTCOMP diagram for the Na-Al-O-S system

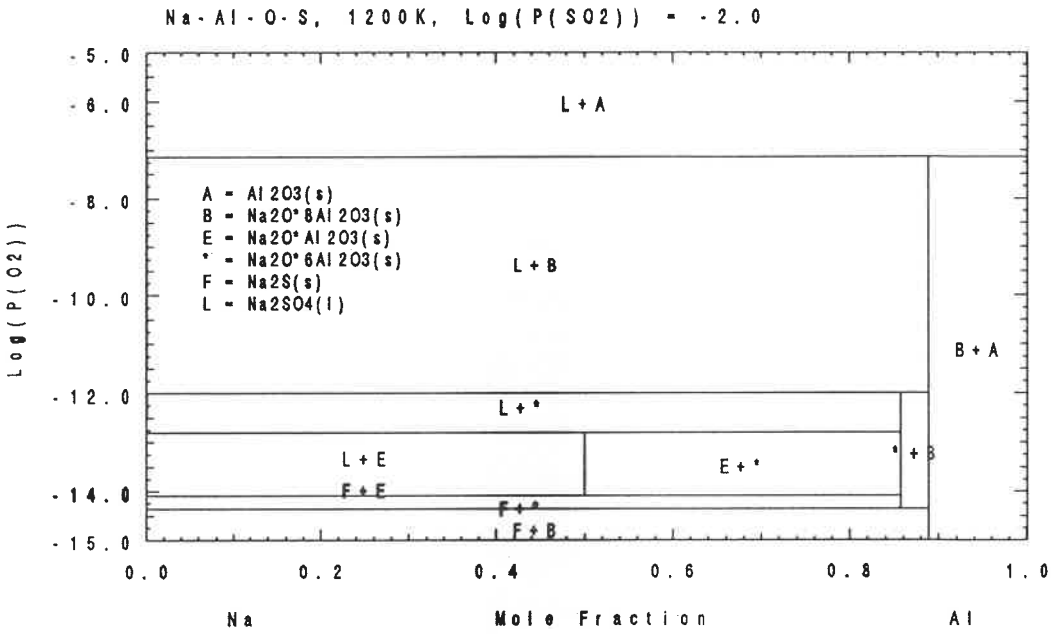

Figure 21. POTCOMP diagram for the Na-Al-O-S system

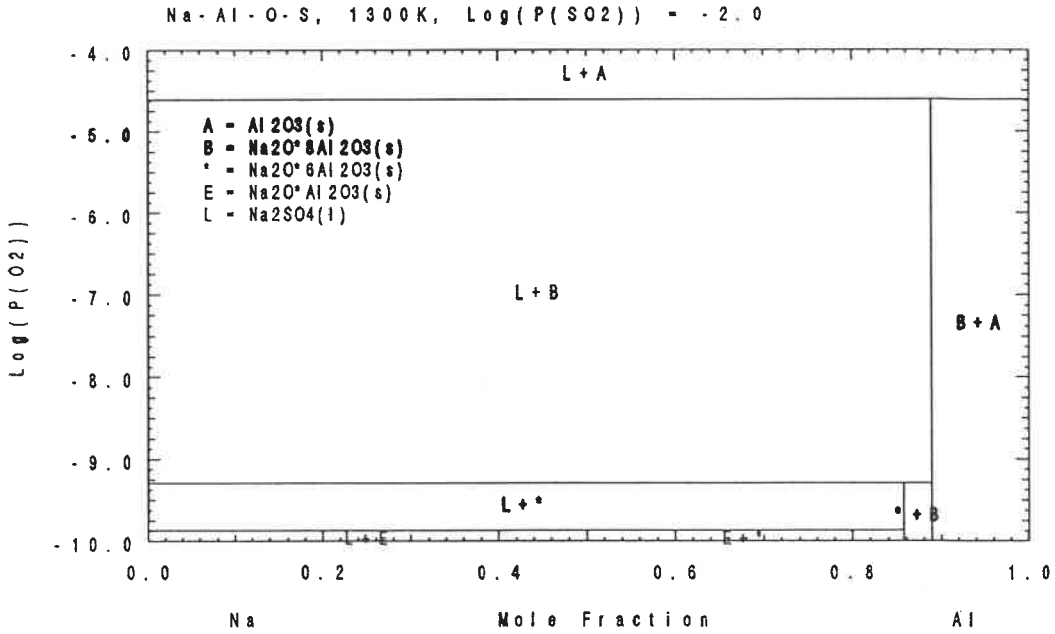

Figure 22. POTCOMP diagram for the Na-Al-O-S system

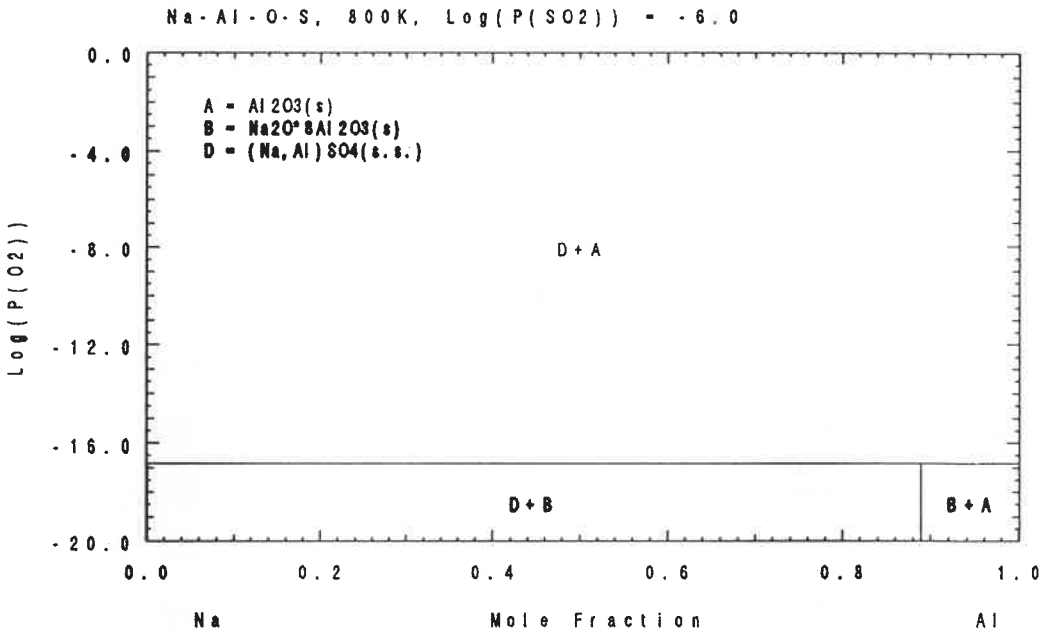

Figure 23. POTCOMP diagram for the Na-Al-O-S system

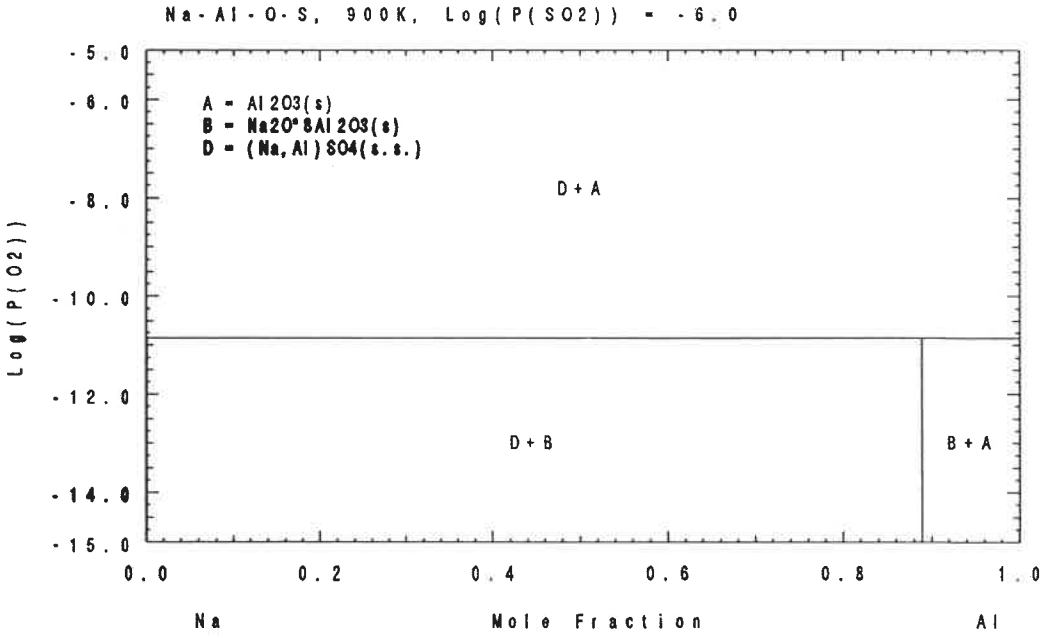

Figure 24. POTCOMP diagram for the Na-Al-O-S system

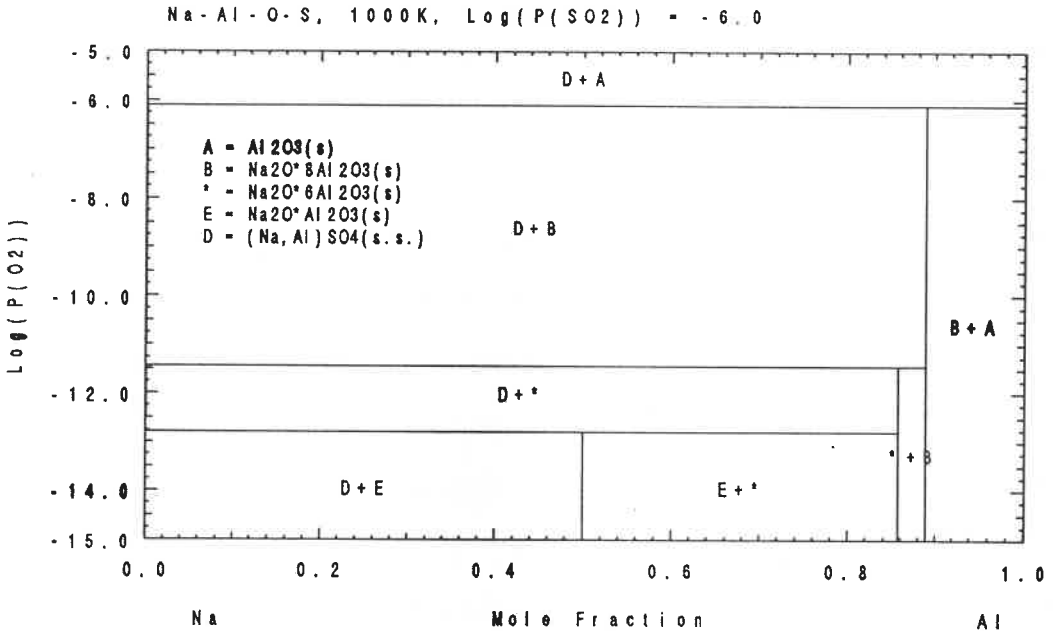

Figure 25. POTCOMP diagram for the Na-Al-O-S system

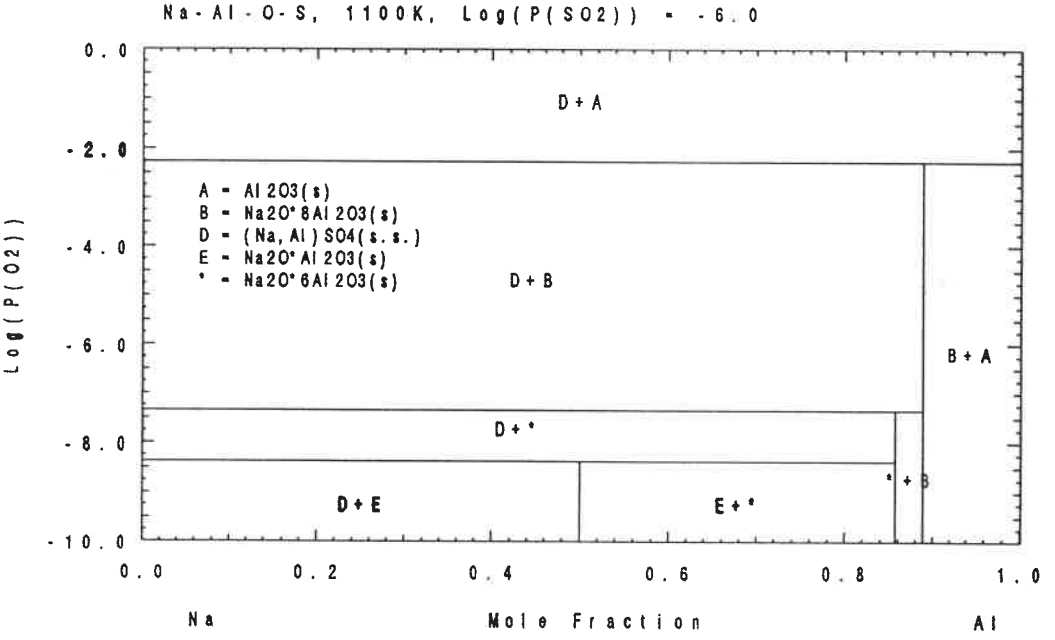

Figure 26. POTCOMP diagram for the Na-Al-O-S system

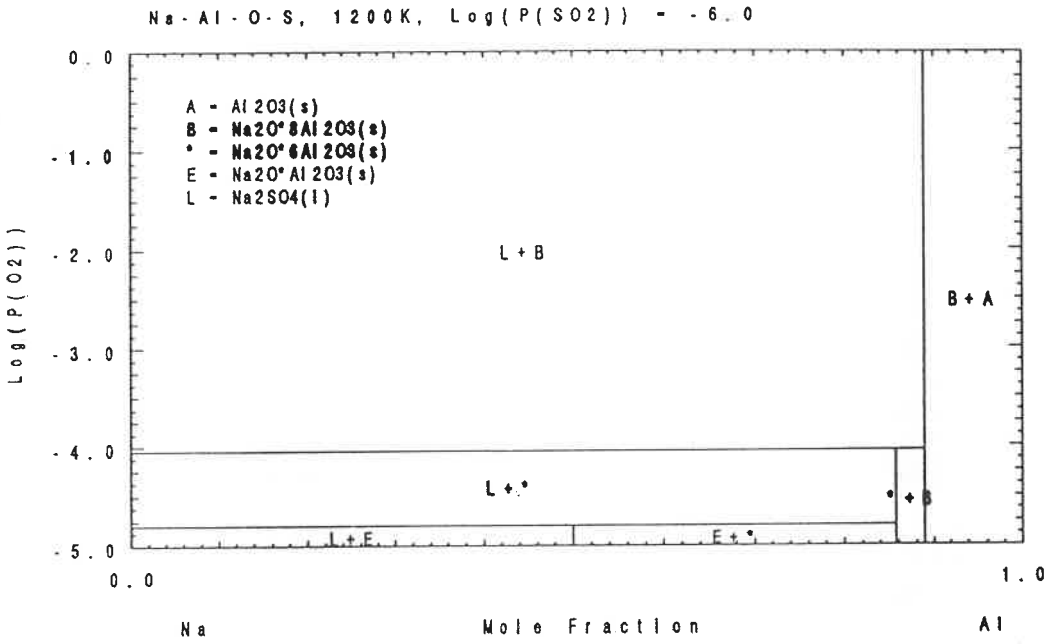

Figure 27. POTCOMP diagram for the Na-Al-O-S system

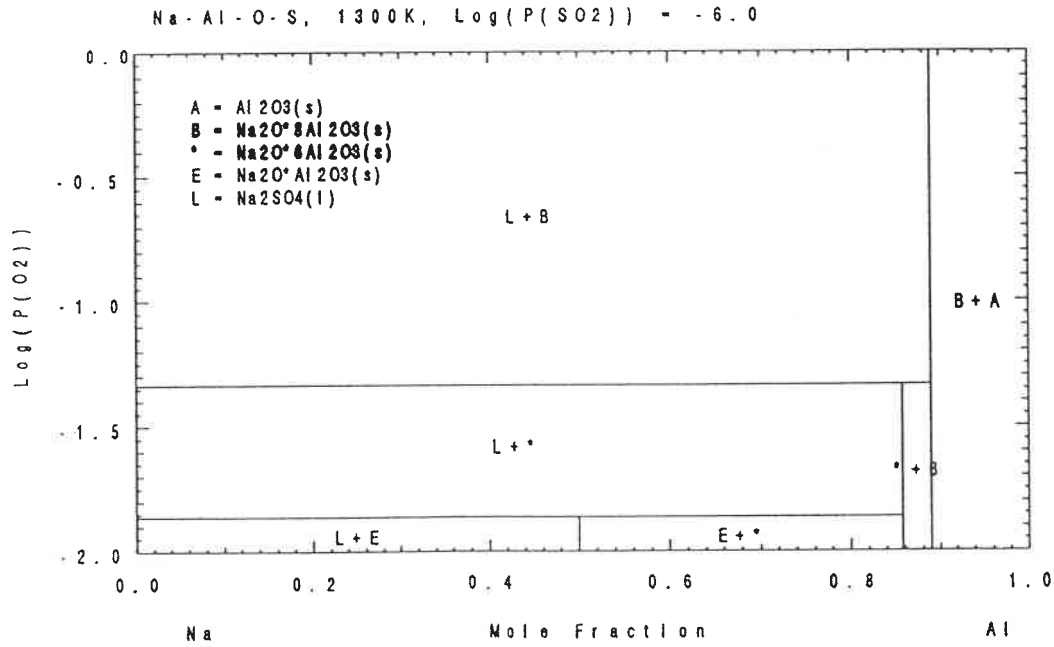

Figure 28. POTCOMP diagram for the Na-Al-O-S system

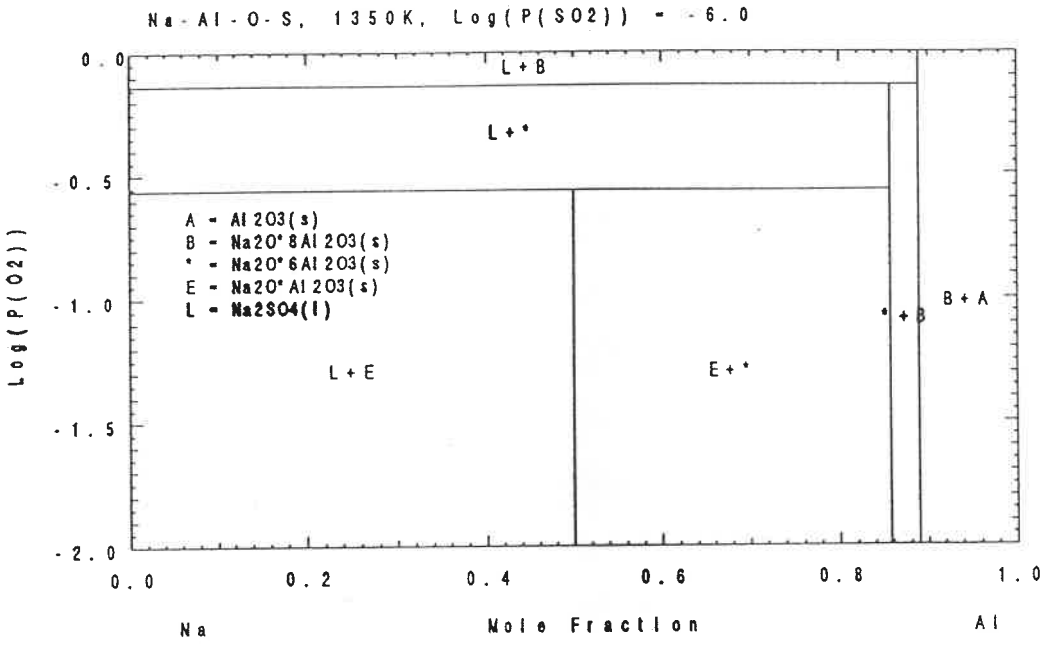

Figure 29. POTCOMP diagram for the Na-Al-O-S system

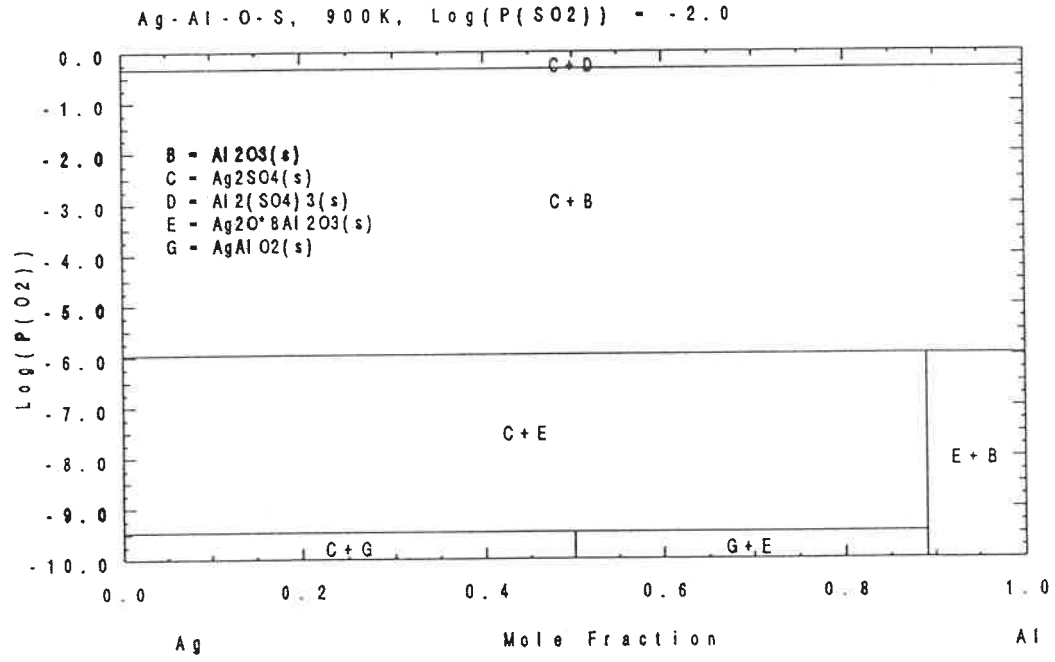

Figure 30. POTCOMP diagram for the Ag-Al-O-S system

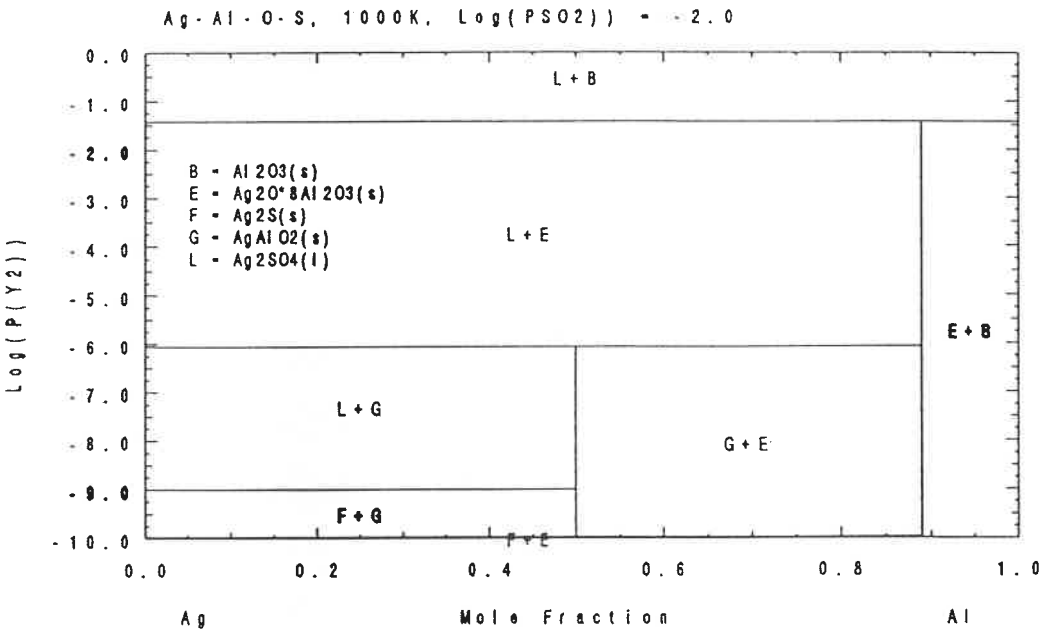

Figure 31. POTCOMP diagram for the Ag-Al-O-S system

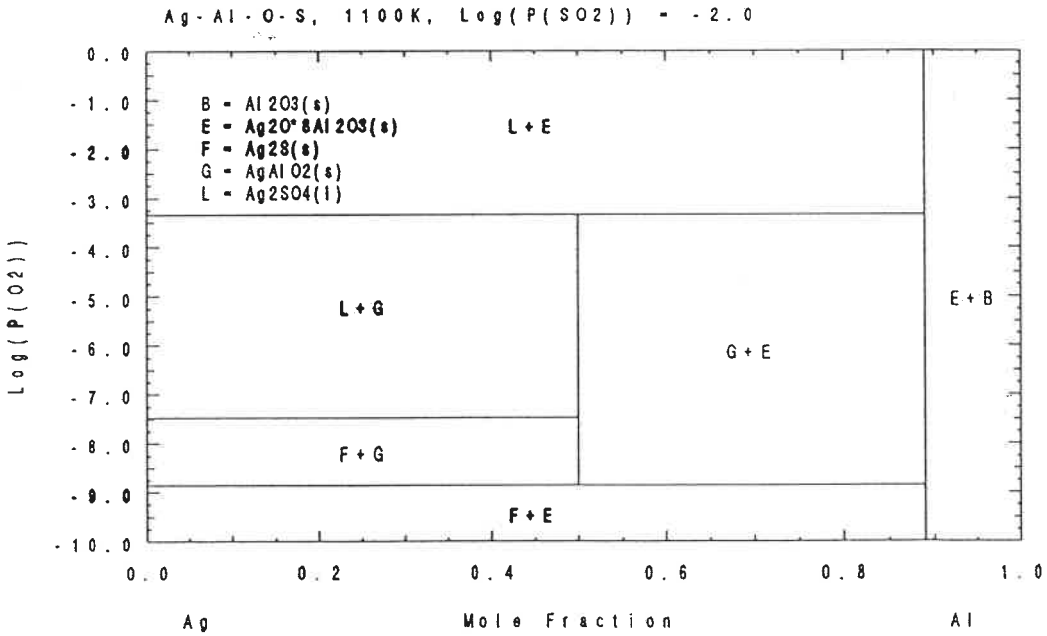

Figure 32. POTCOMP diagram for the Ag-Al-O-S system

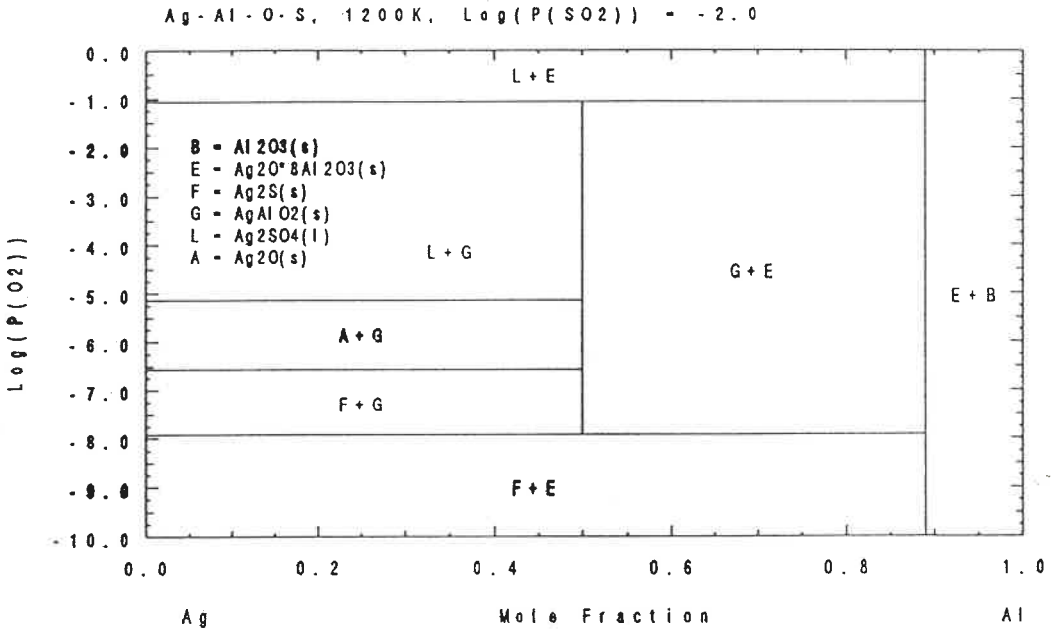

Figure 33. POTCOMP diagram for the Ag-Al-O-S system

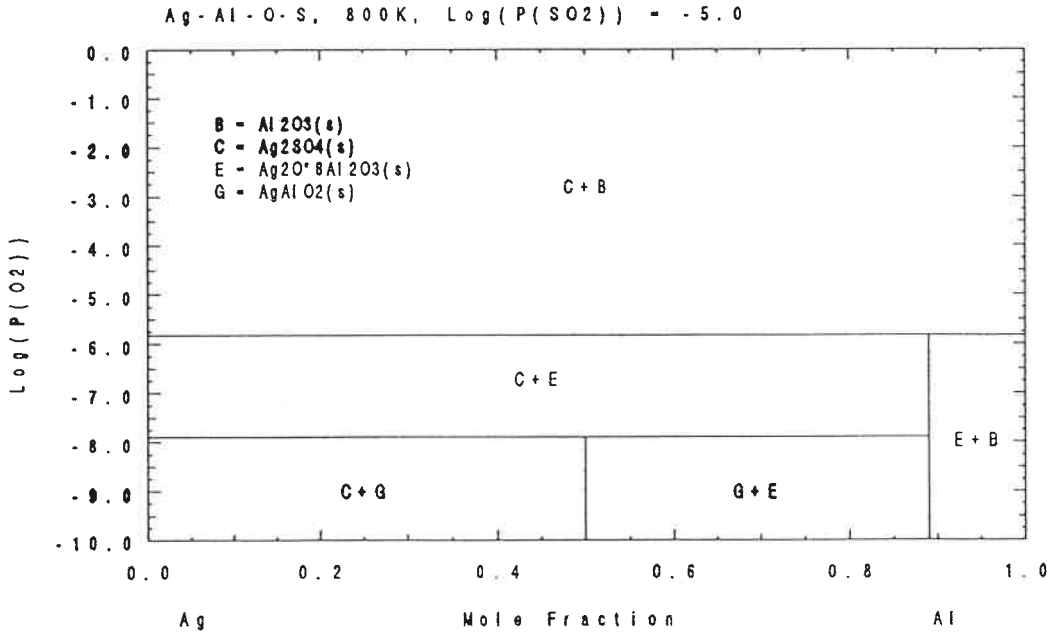

Figure 34. POTCOMP diagram for the Ag-Al-O-S system

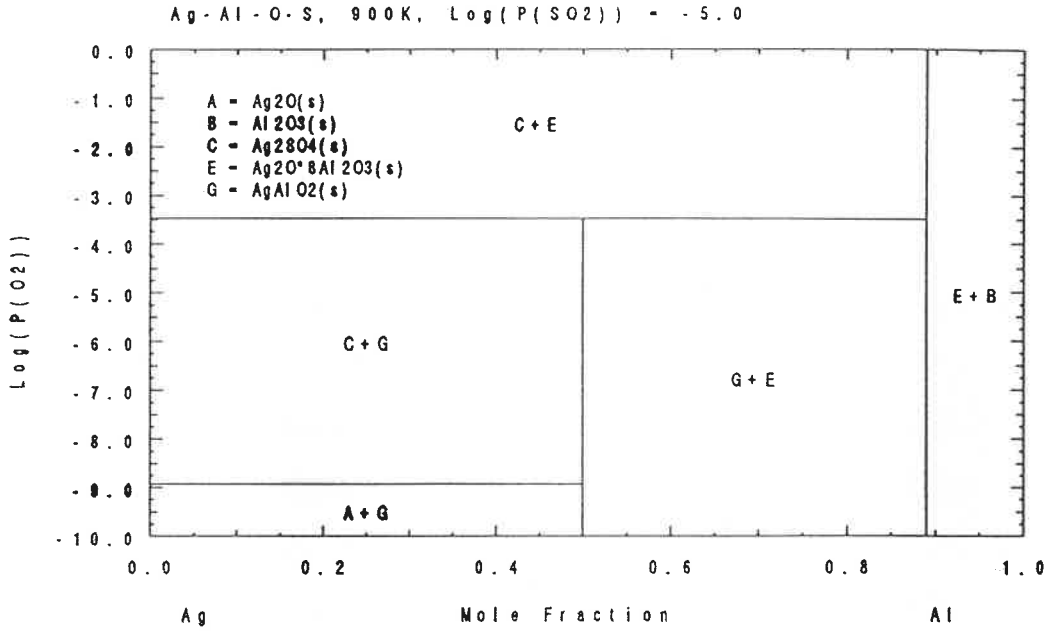

Figure 35. POTCOMP diagram for the Ag-Al-O-S system

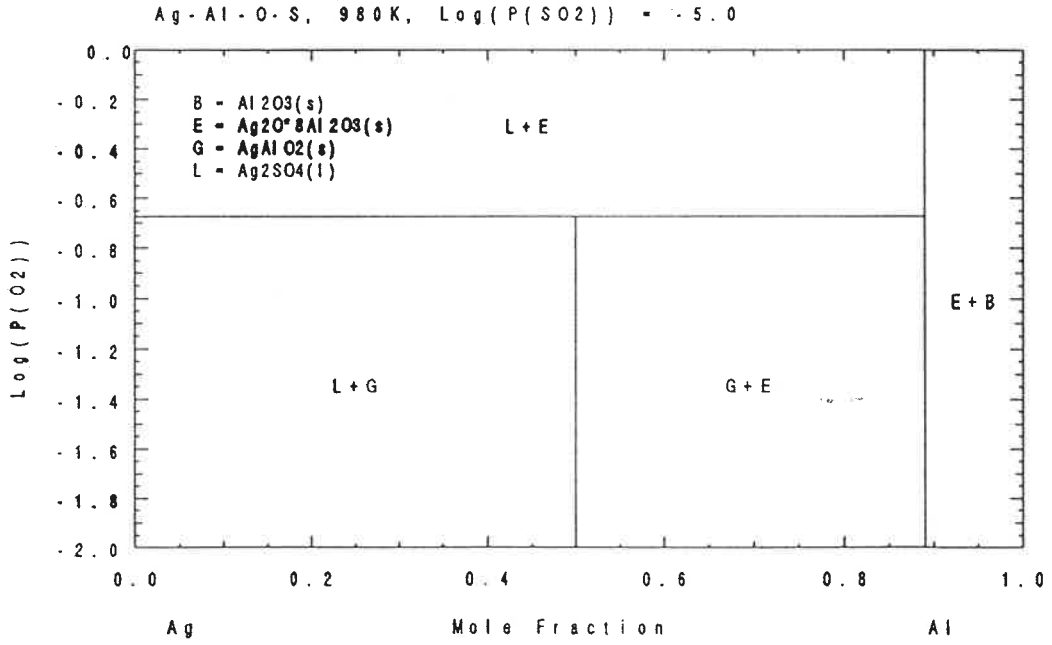

Figure 36. POTCOMP diagram for the Ag-Al-O-S system

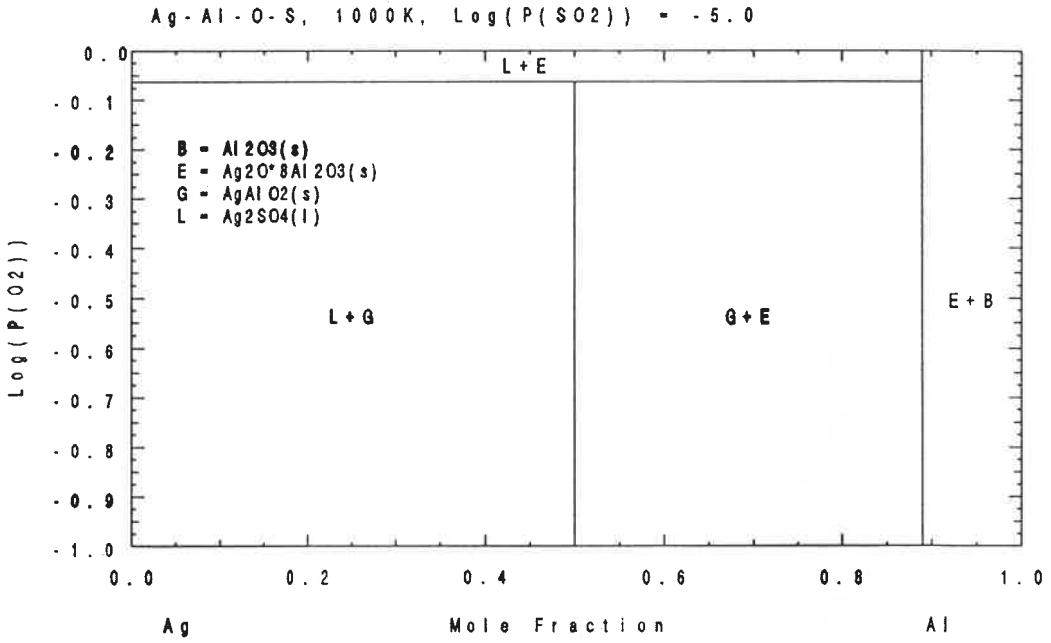

Figure 37. POTCOMP diagram for the Ag-Al-O-S system

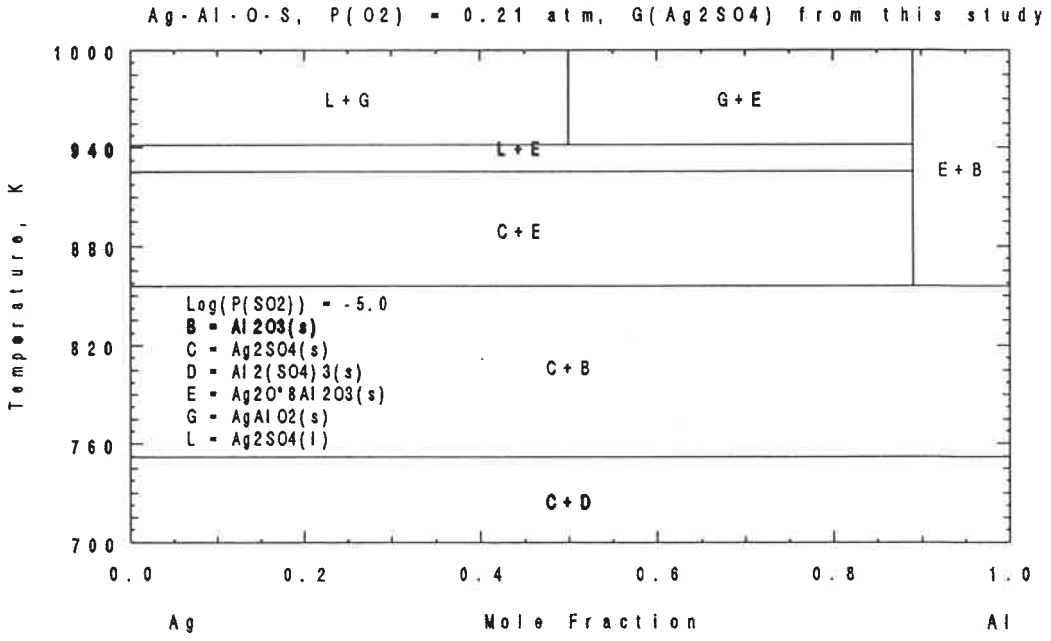

Figure 38. POTCOMP diagram for the Ag-Al-O-S system

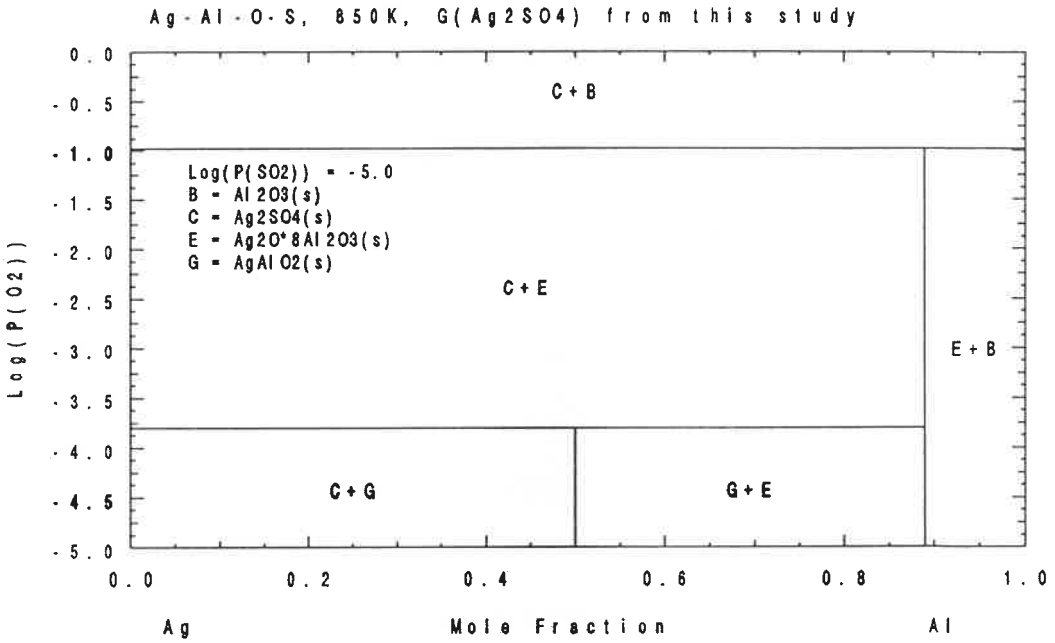

Figure 39. POTCOMP diagram for the Ag-Al-O-S system

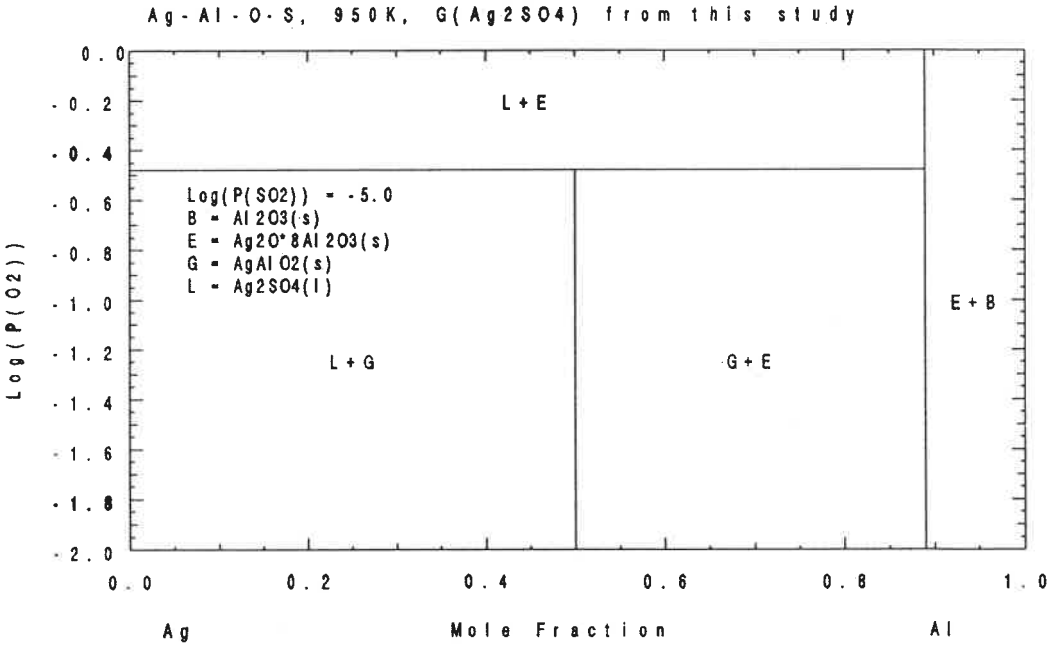

Figure 40. POTCOMP diagram for the Ag-Al-O-S system

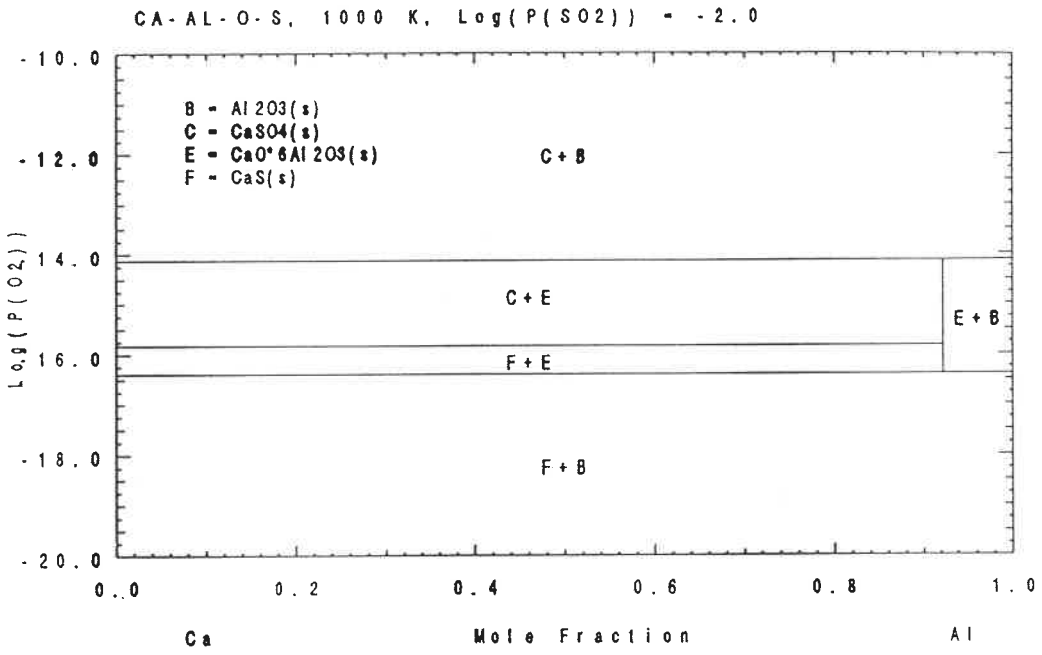

Figure 41. POTCOMP diagram for the Ca-Al-O-S system

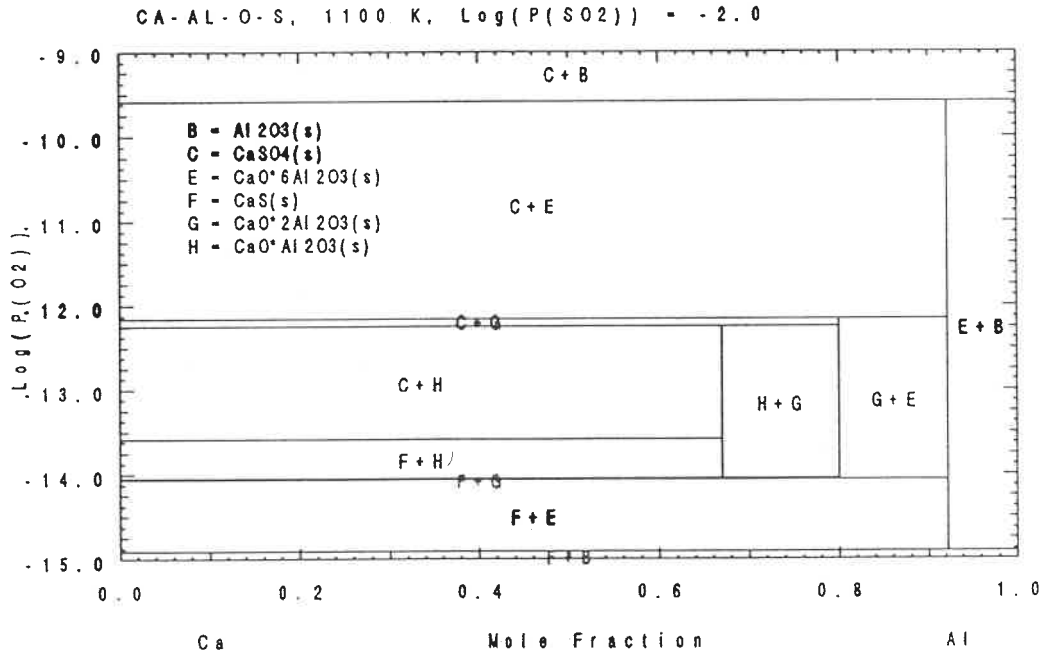

Figure 42. POTCOMP diagram for the Ca-Al-O-S system

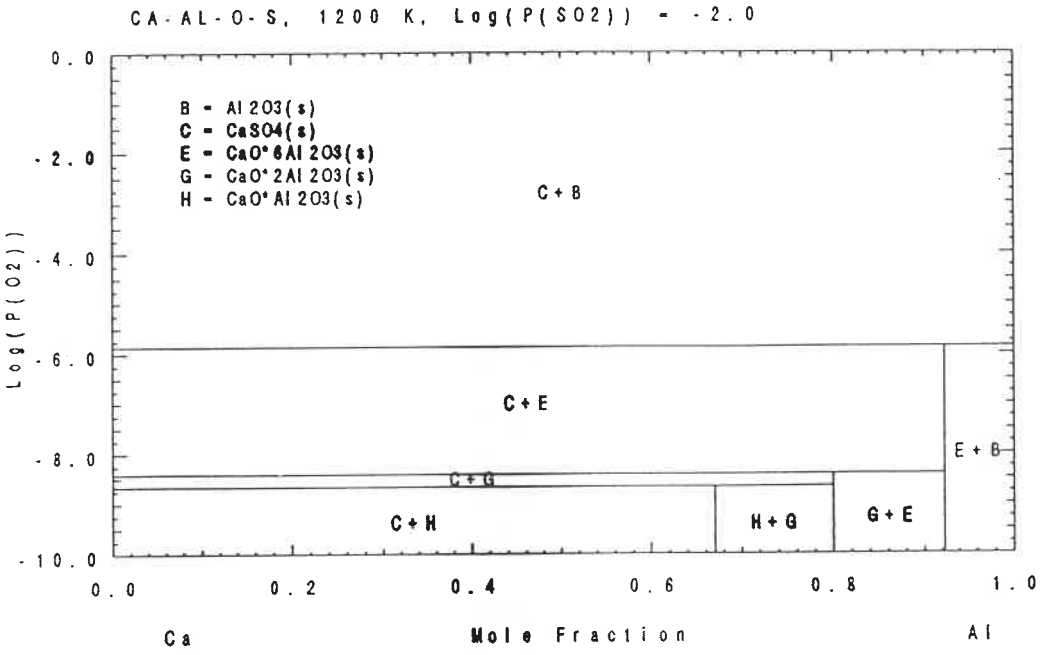

Figure 43. POTCOMP diagram for the Ca-Al-O-S system

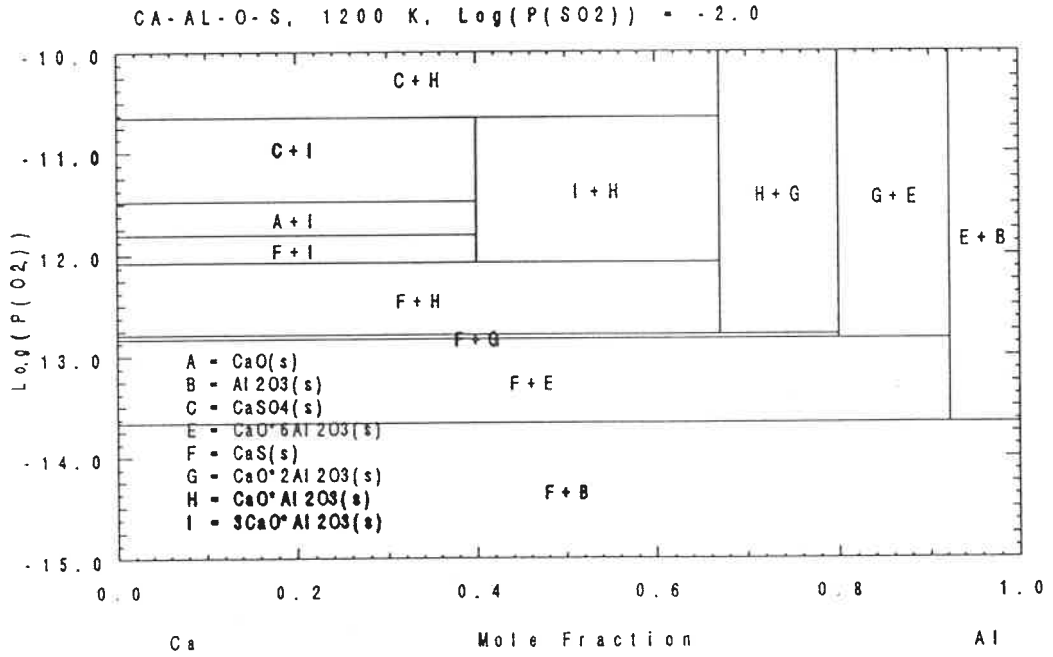

Figure 44. POTCOMP diagram for the Ca-Al-O-S system

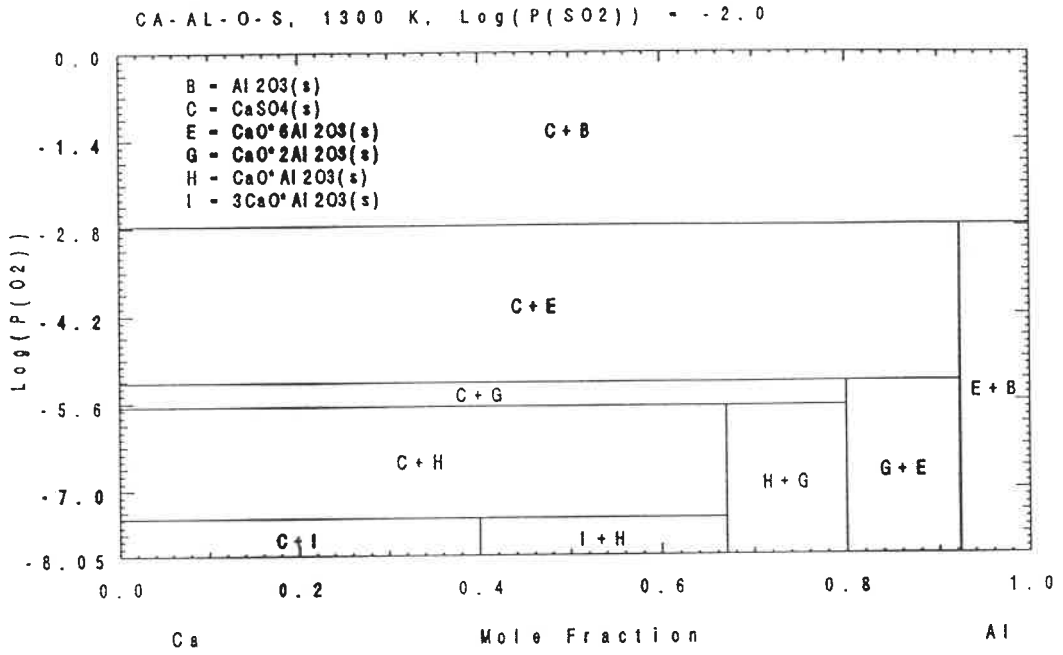

Figure 45. POTCOMP diagram for the Ca-Al-O-S system

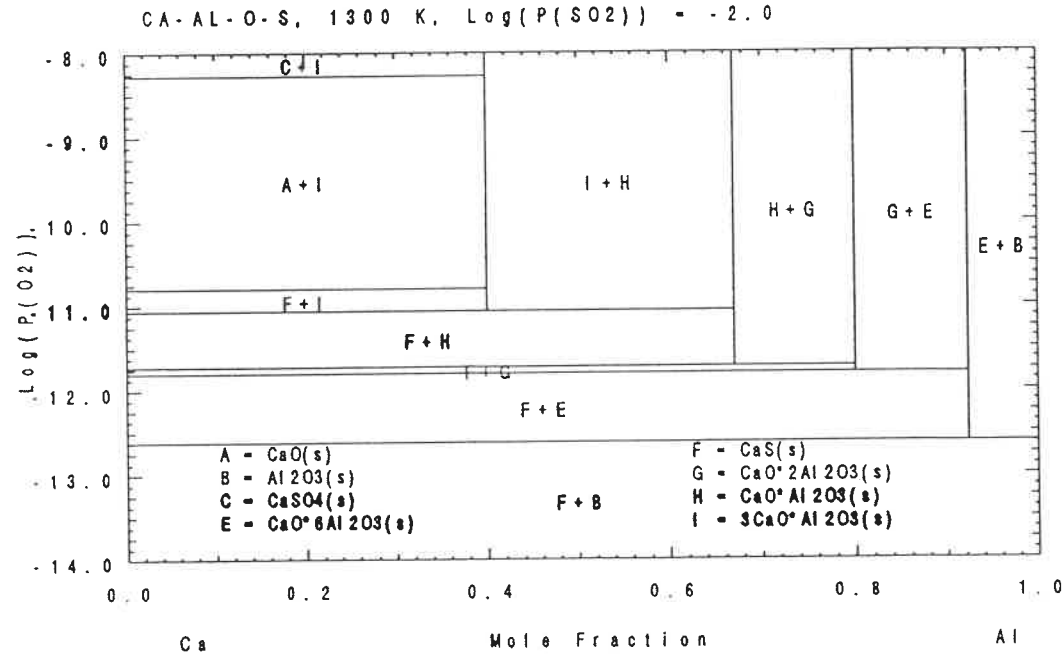

Figure 46. POTCOMP diagram for the Ca-Al-O-S system

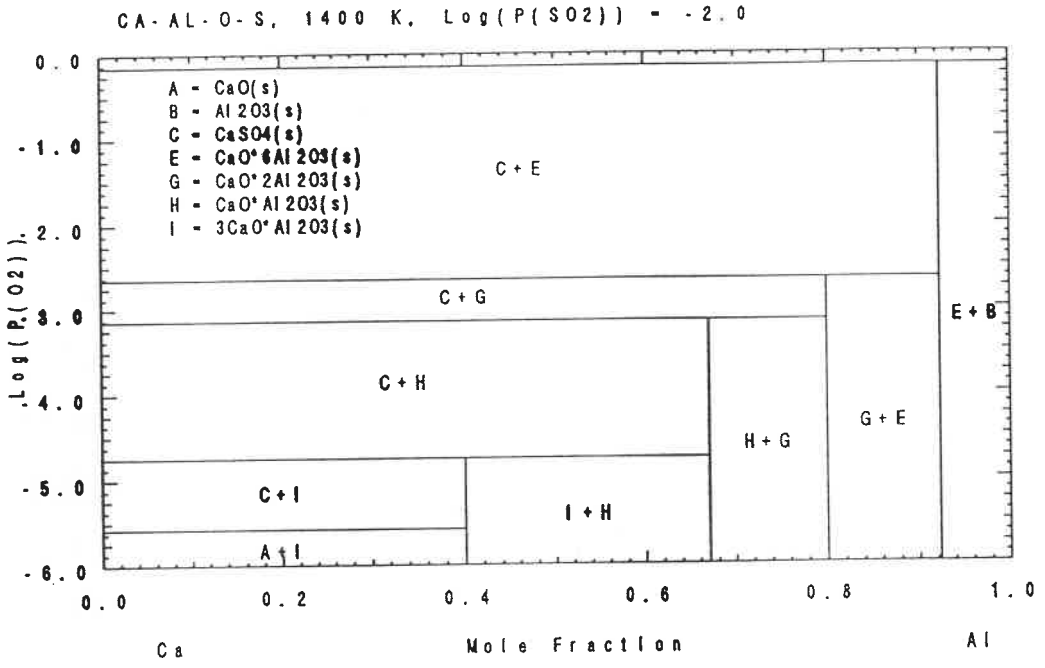

Figure 47. POTCOMP diagram for the Ca-Al-O-S system

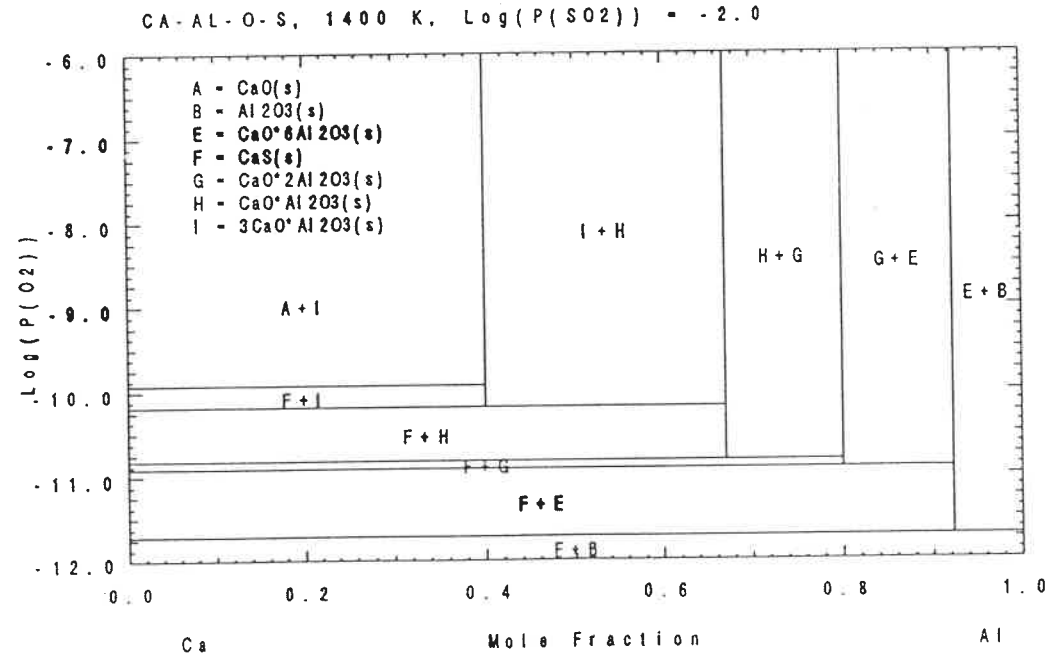

Figure 48. POTCOMP diagram for the Ca-Al-O-S system

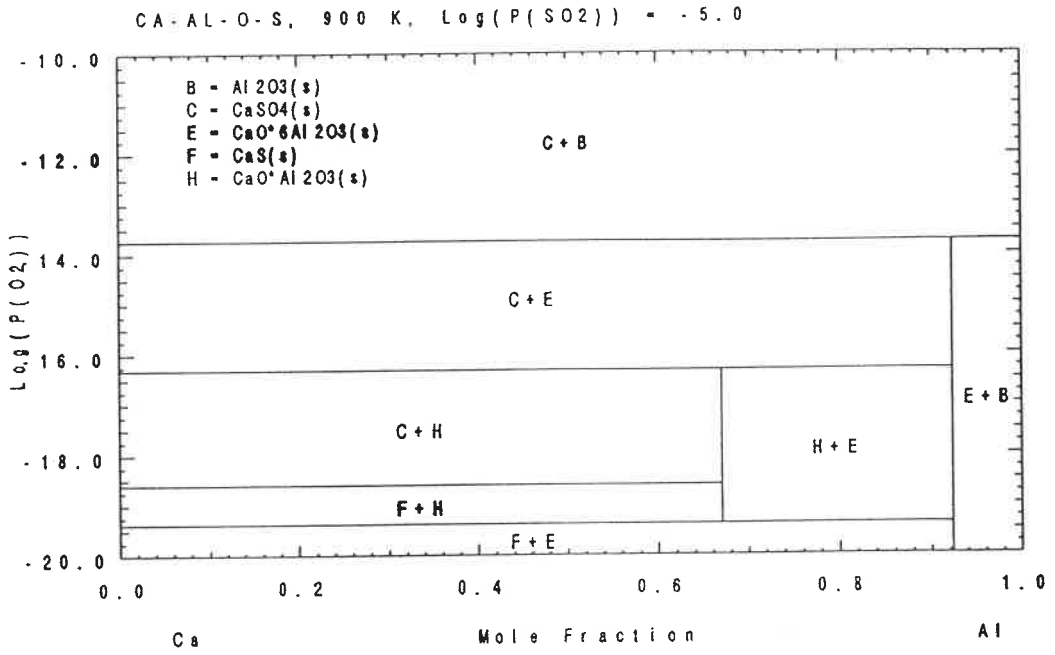

Figure 49. POTCOMP diagram for the Ca-Al-O-S system

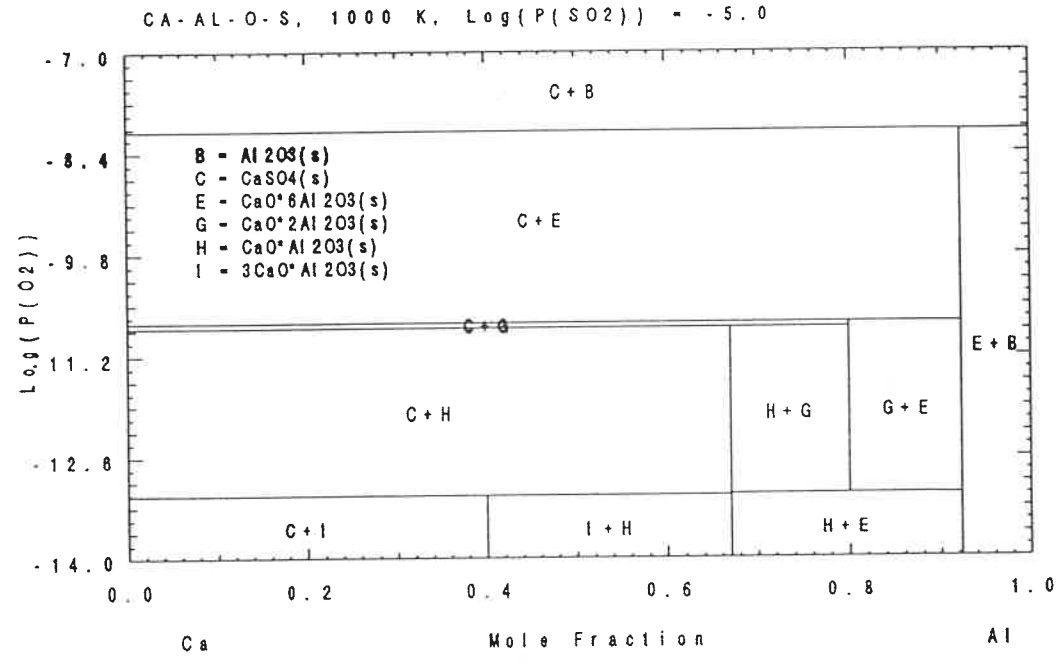

Figure 50. POTCOMP diagram for the Ca-Al-O-S system

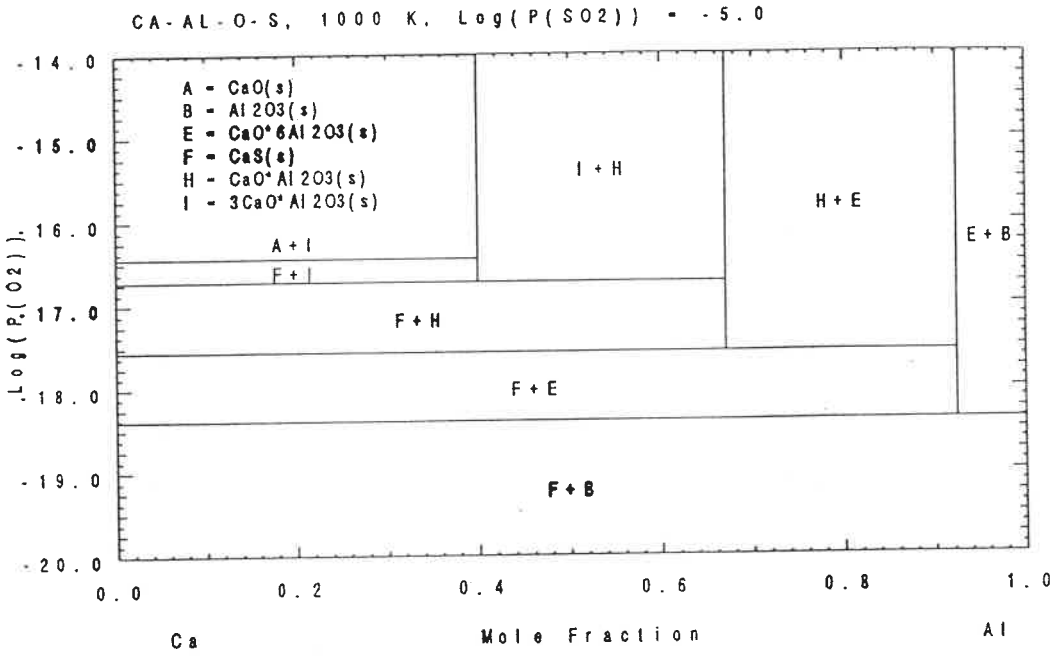

Figure 51. POTCOMP diagram for the Ca-Al-O-S system

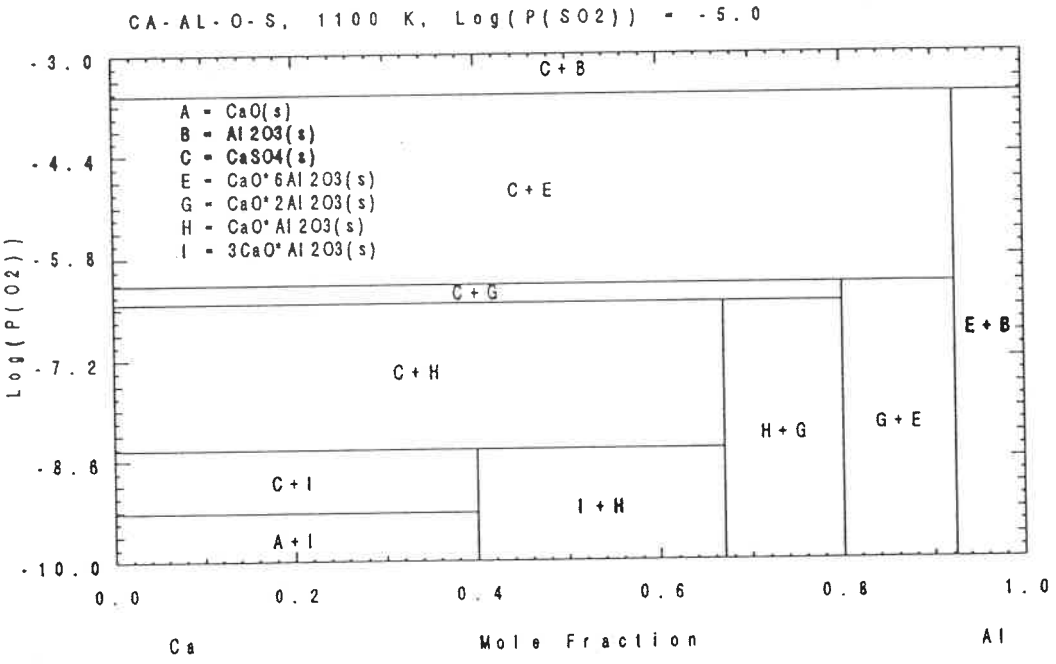

Figure 52. POTCOMP diagram for the Ca-Al-O-S system

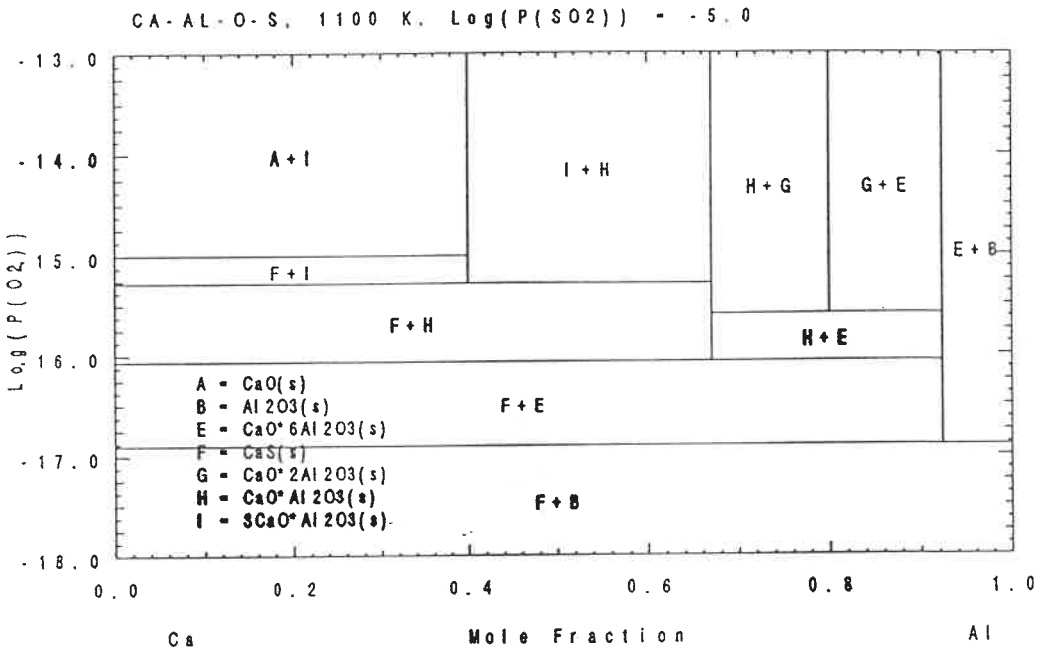

Figure 53. POTCOMP diagram for the Ca-Al-O-S system

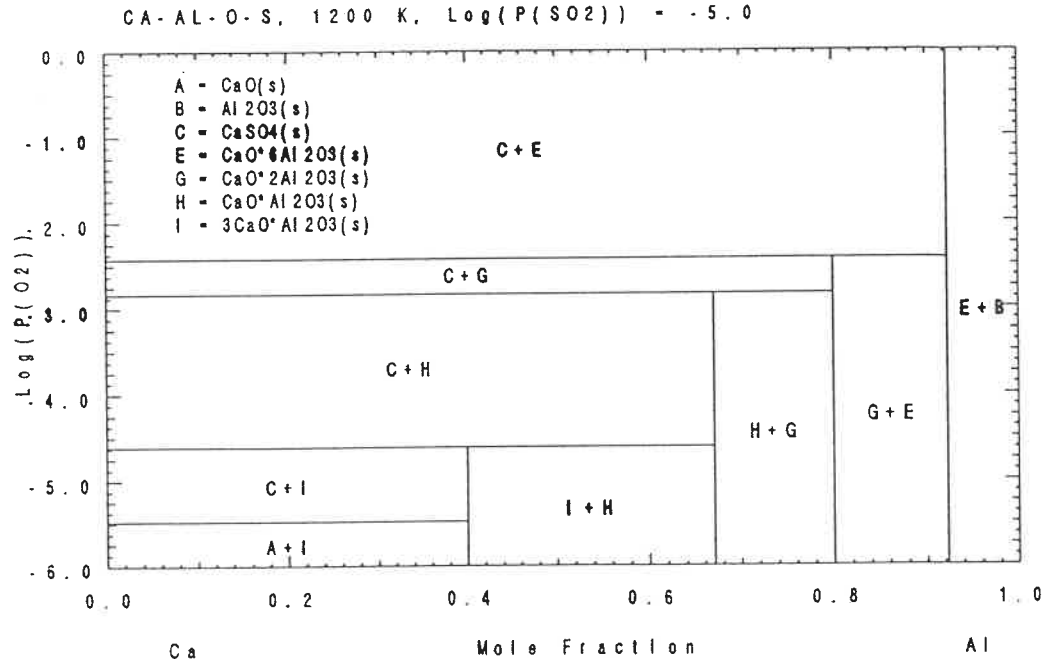

Figure 54. POTCOMP diagram for the Ca-Al-O-S system

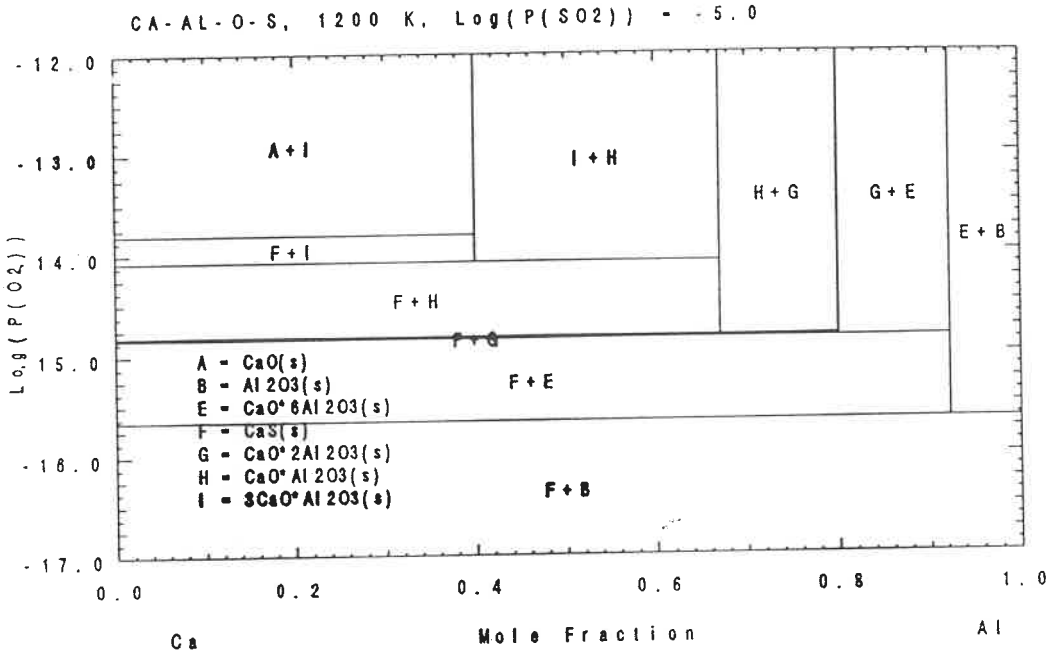

Figure 55. POTCOMP diagram for the Ca-Al-O-S system

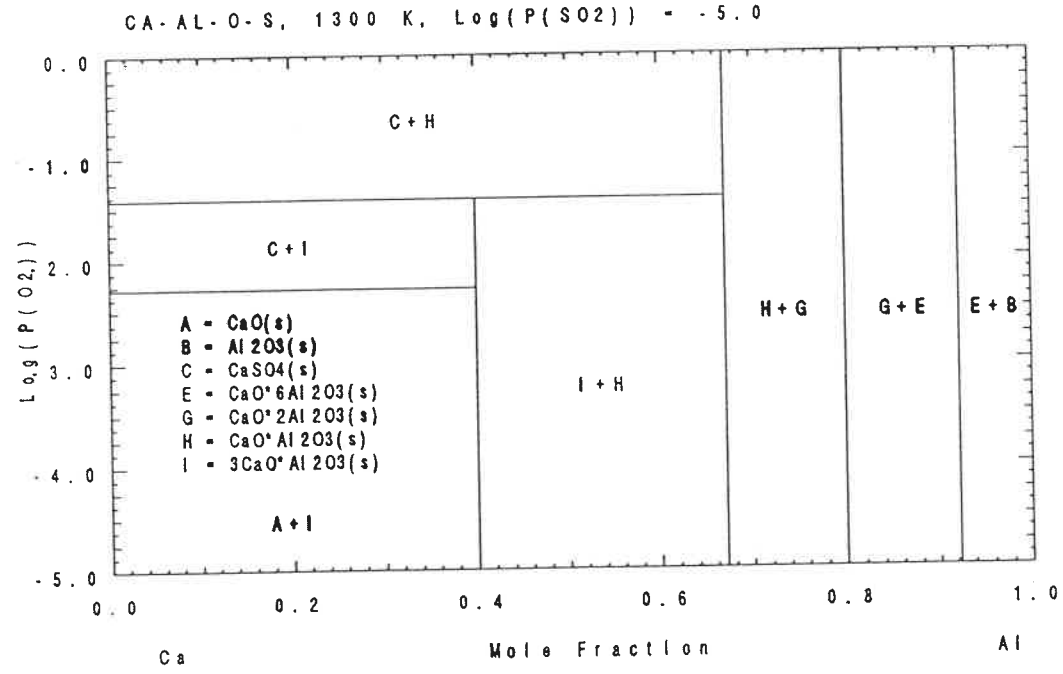

Figure 56. POTCOMP diagram for the Ca-Al-O-S system

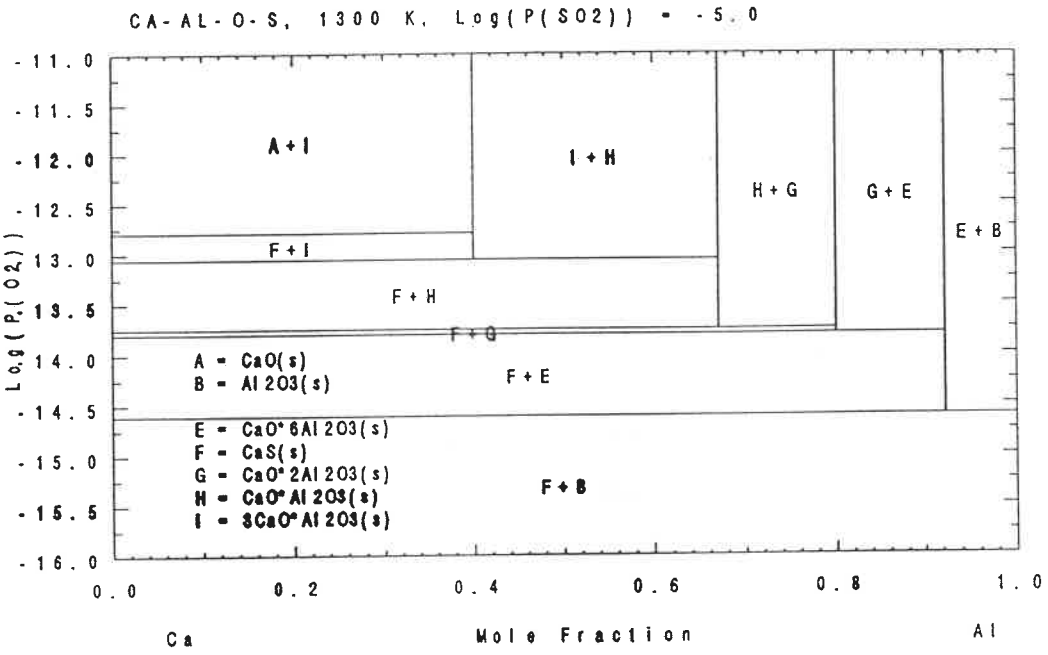

Figure 57. POTCOMP diagram for the Ca-Al-O-S system

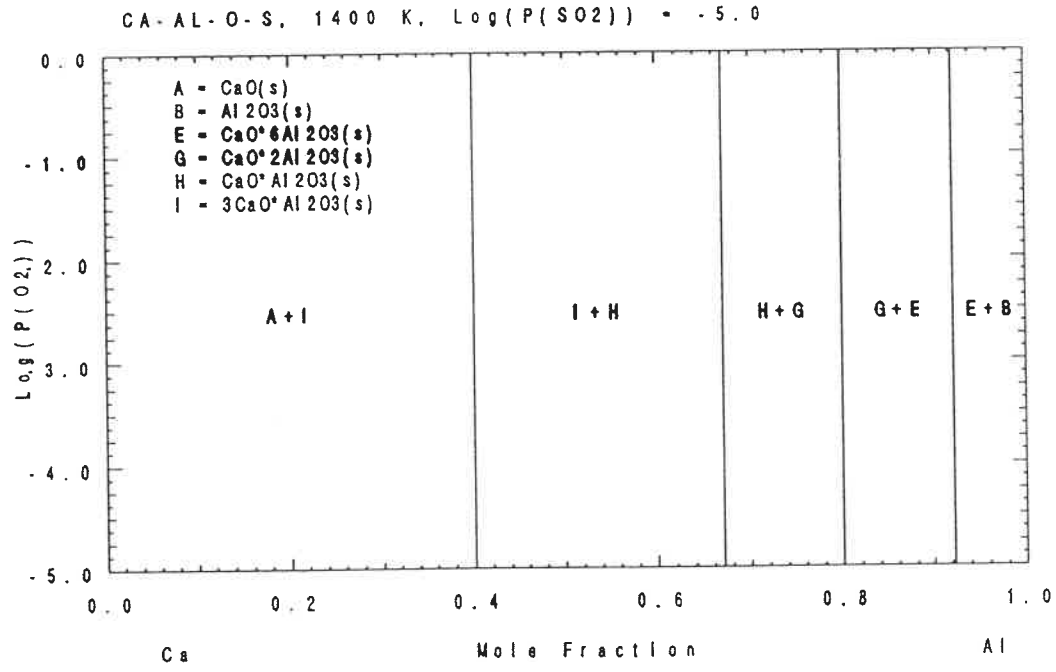

Figure 58. POTCOMP diagram for the Ca-Al-O-S system

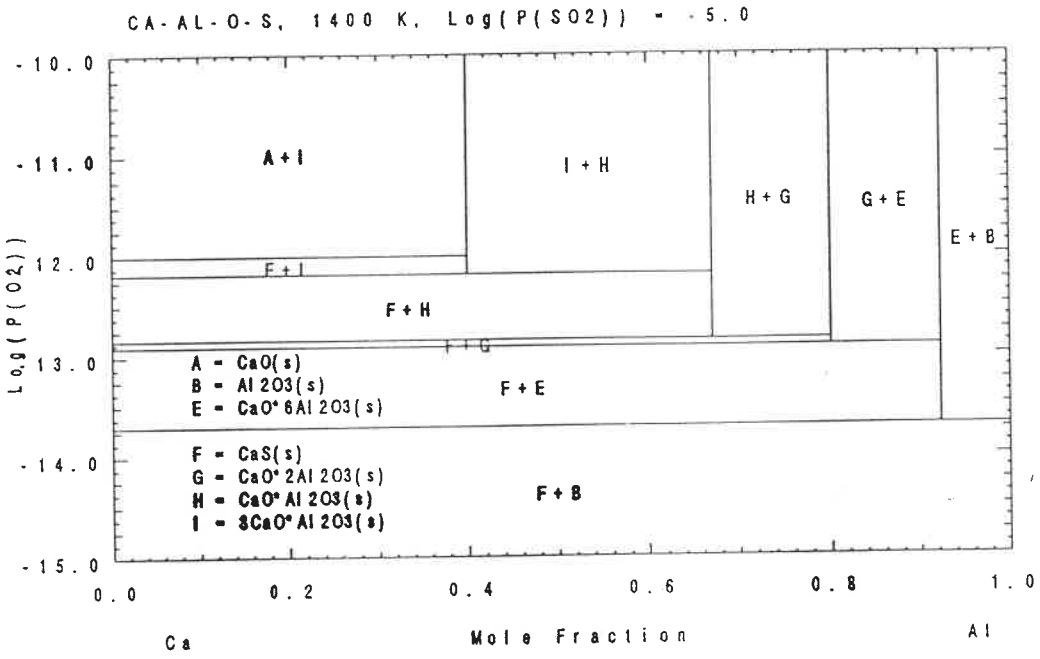

Figure 59. POTCOMP diagram for the Ca-Al-O-S system

APPENDIX B

Figures of experimental results

1. EMF dependence on flow rate,

   Figures: 1 - 10

2. EMF dependence on temperature,

   Figures: 11 - 12

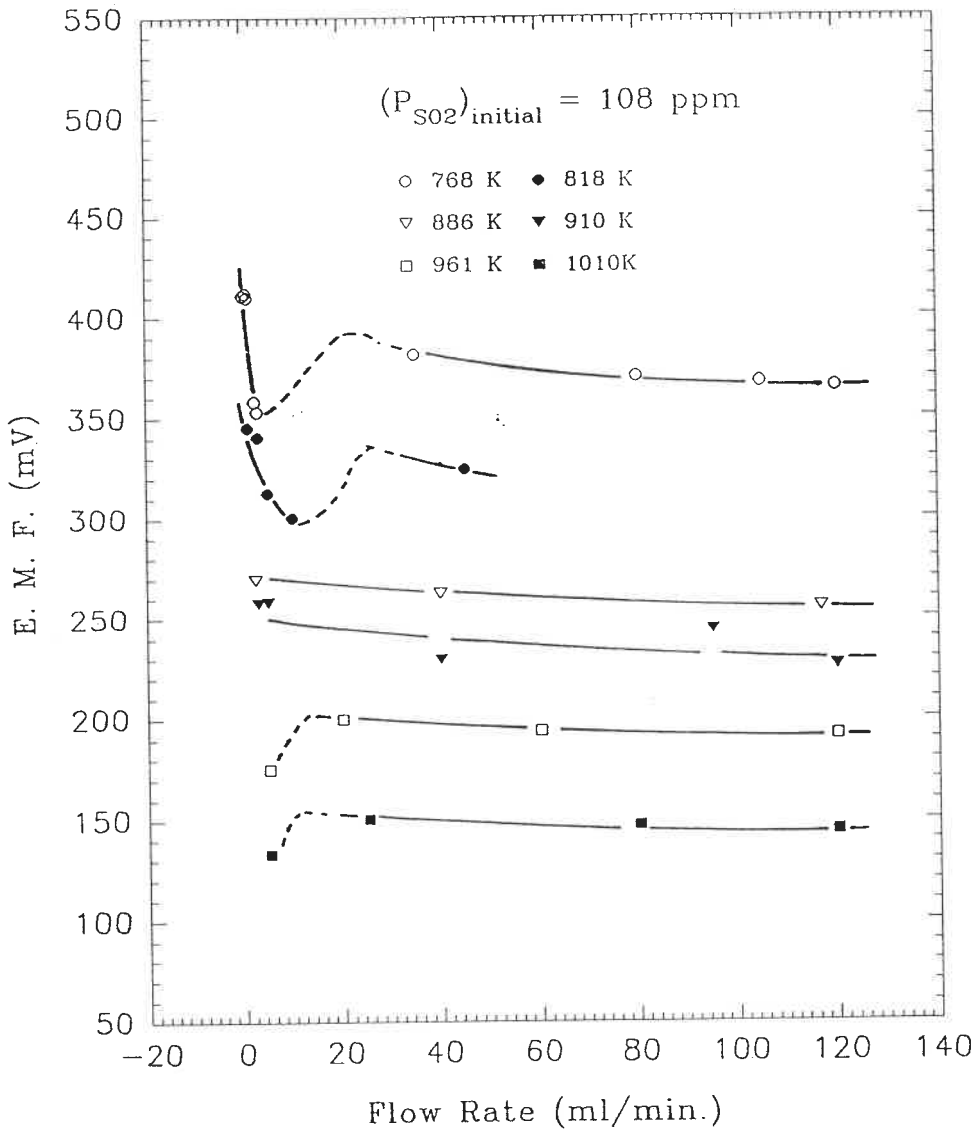

Figure 1 EMF Dependence on Flow Rate for Type 1 Electrode Preparation

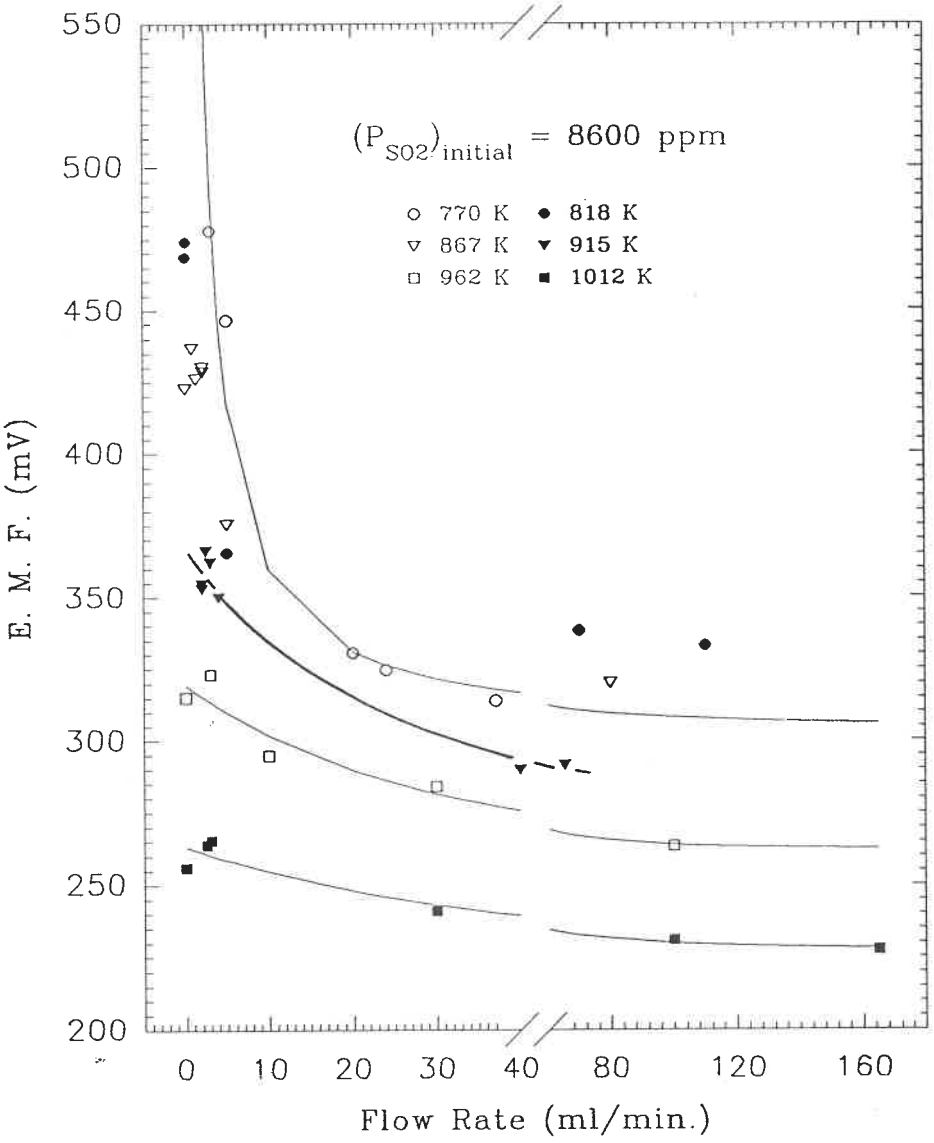

Figure 2 EMF Dependence on Flow Rate for Type 1 Electrode Preparation

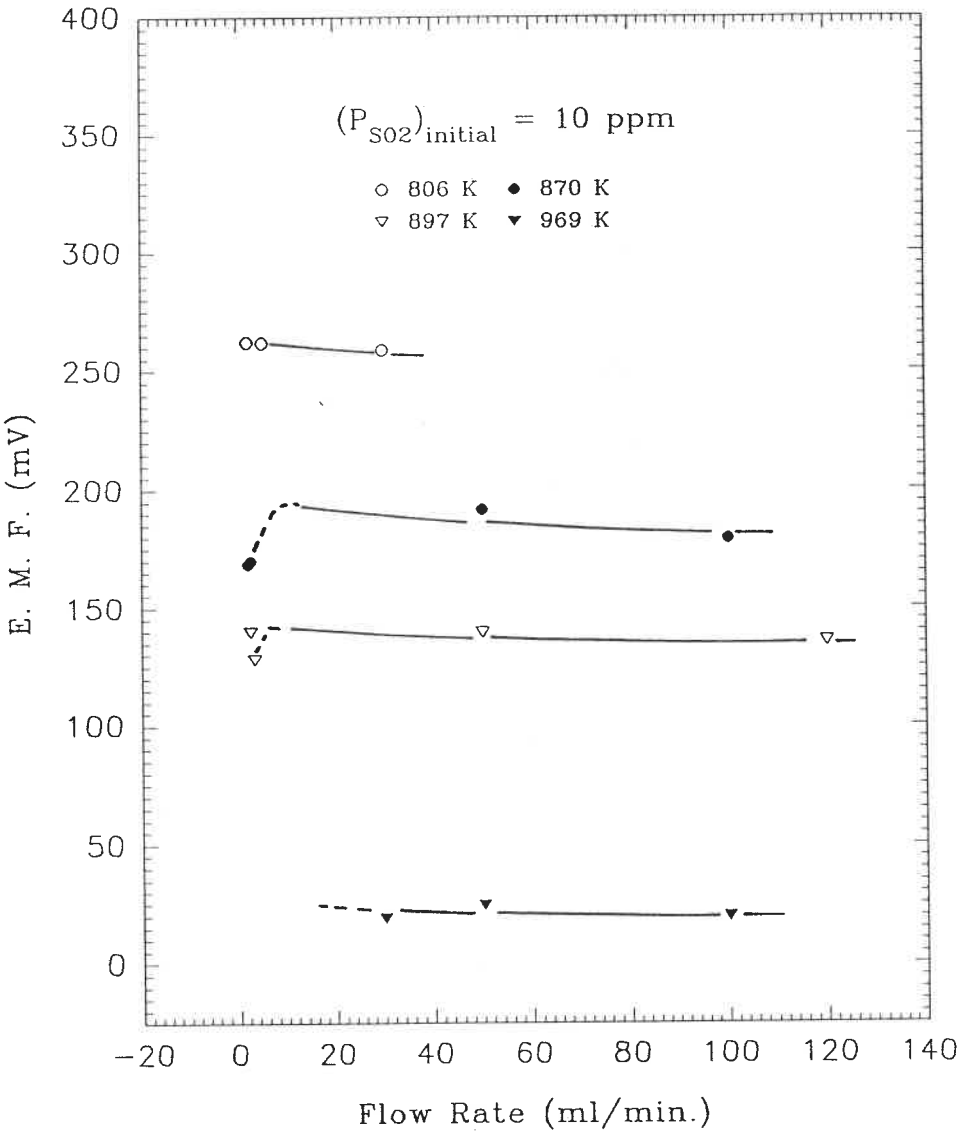

Figure 3 EMF Dependence on Flow Rate for Type 2 Electrode Preparation

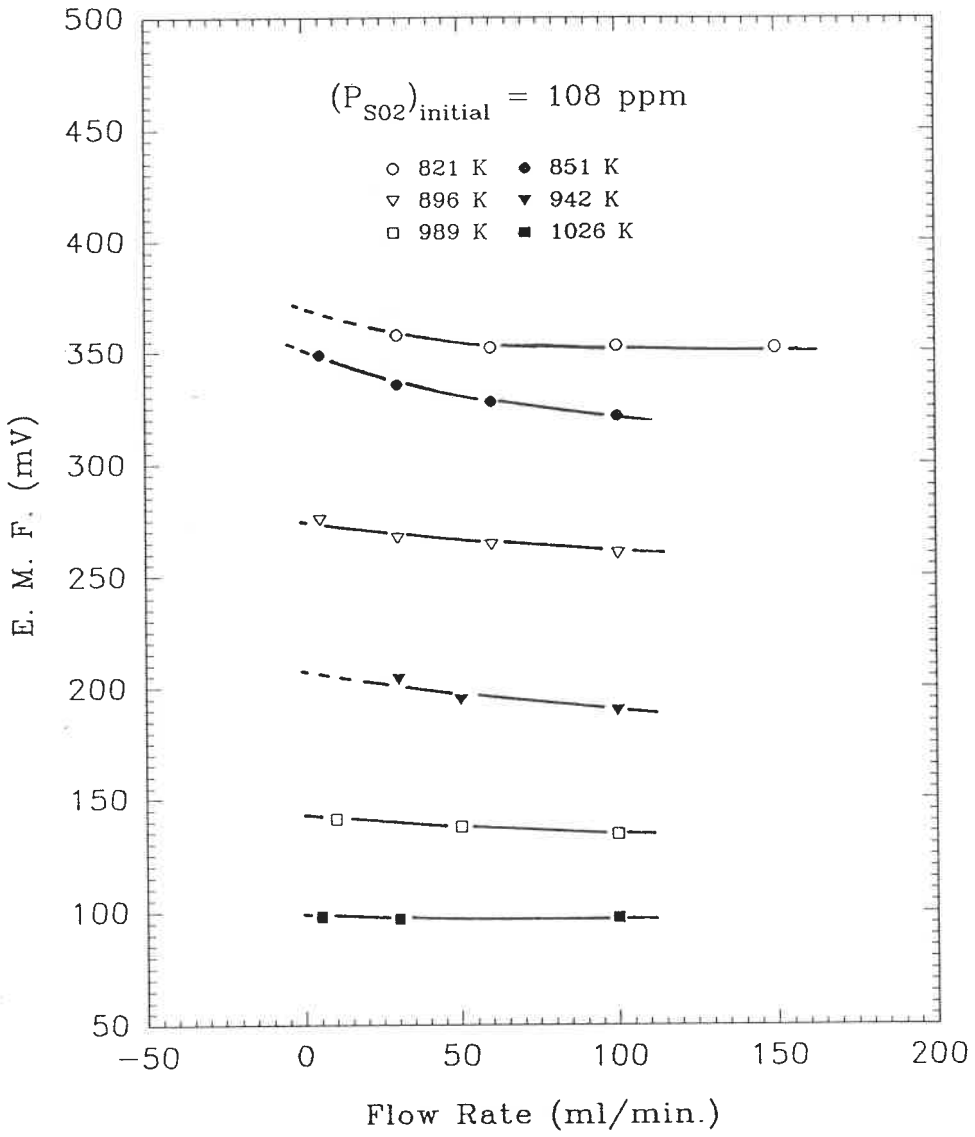

Figure 4 EMF Dependence on Flow Rate for Type 2 Electrode Preparation

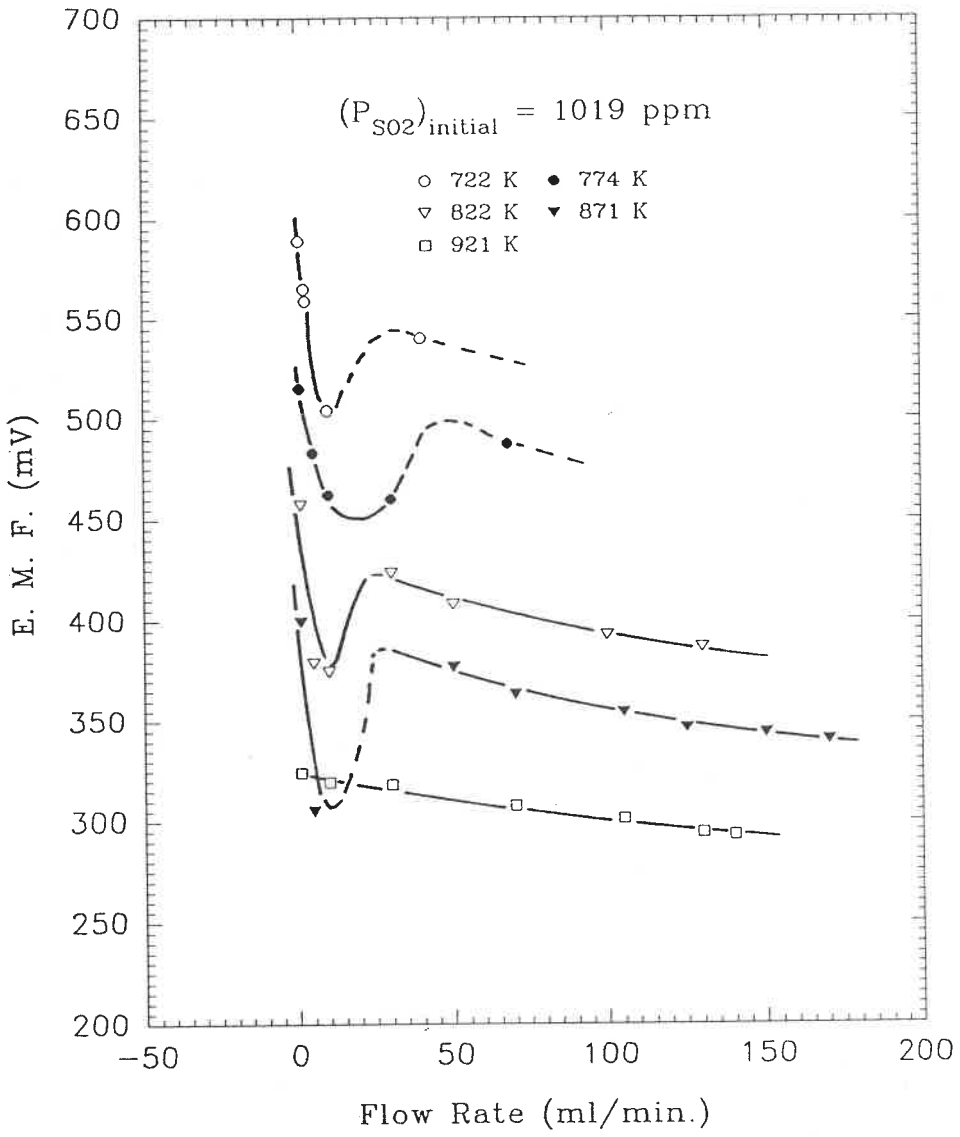

Figure 5 EMF Dependence on Flow Rate for Type 2 Electrode Preparation

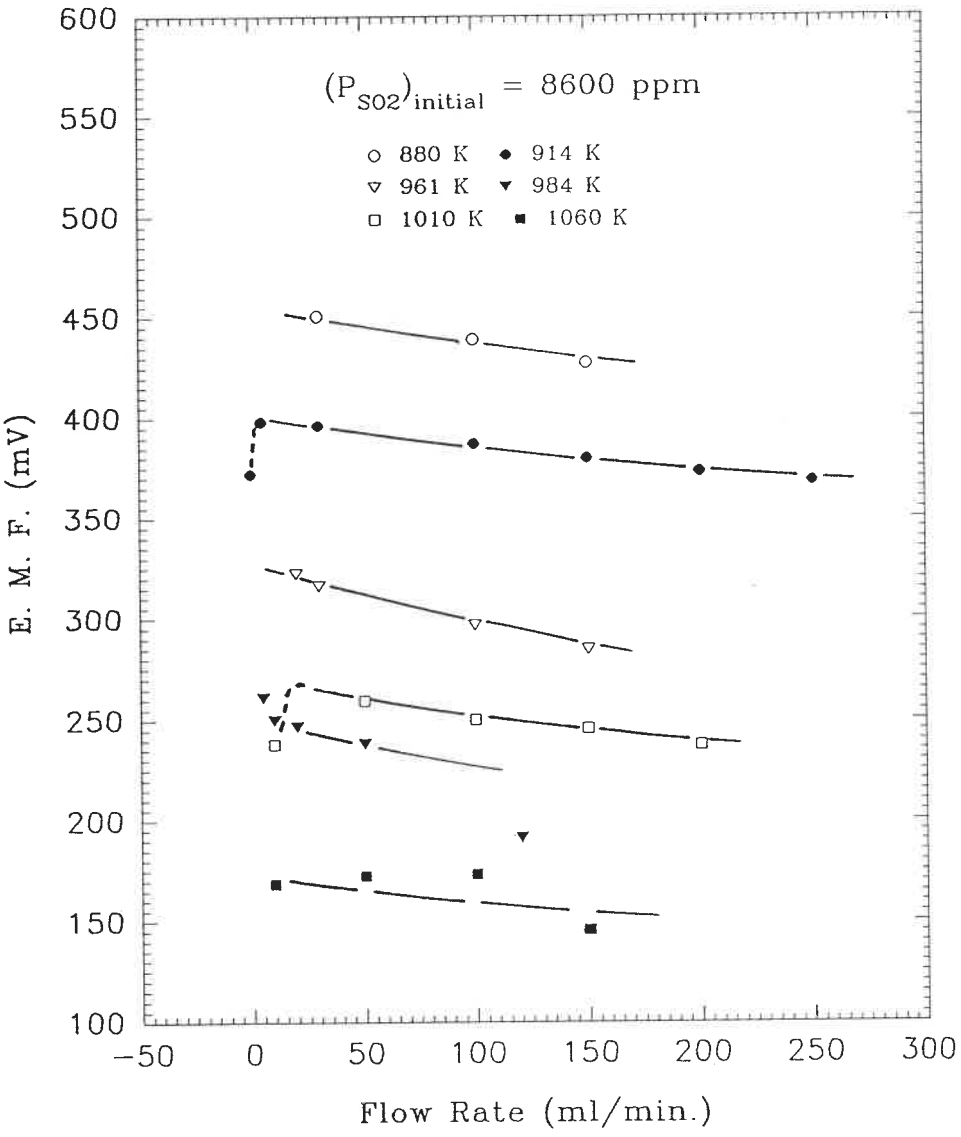

Figure 6 EMF Dependence on Flow Rate for Type 2 Electrode Preparation.

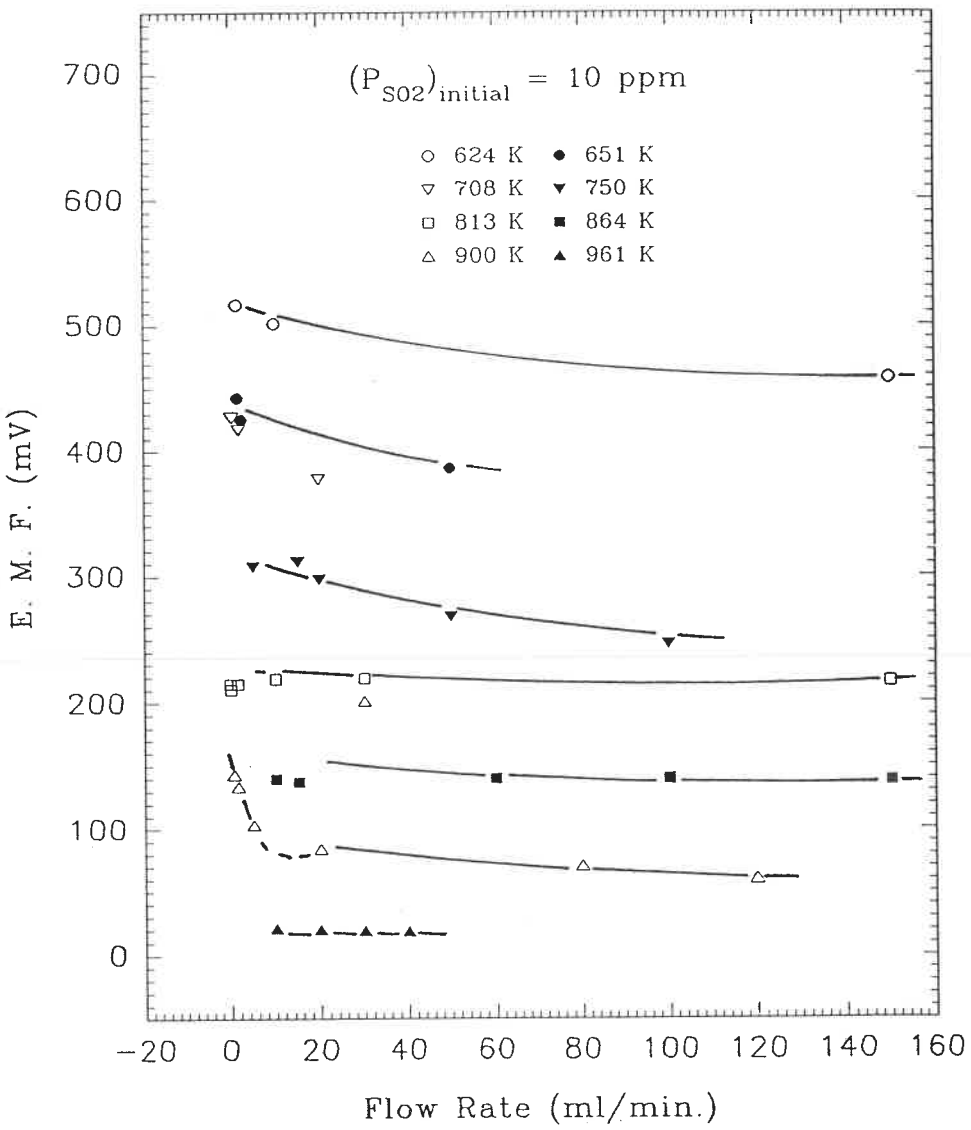

Figure 7 EMF Dependence on Flow Rate for Type 3 Electrode Preparation

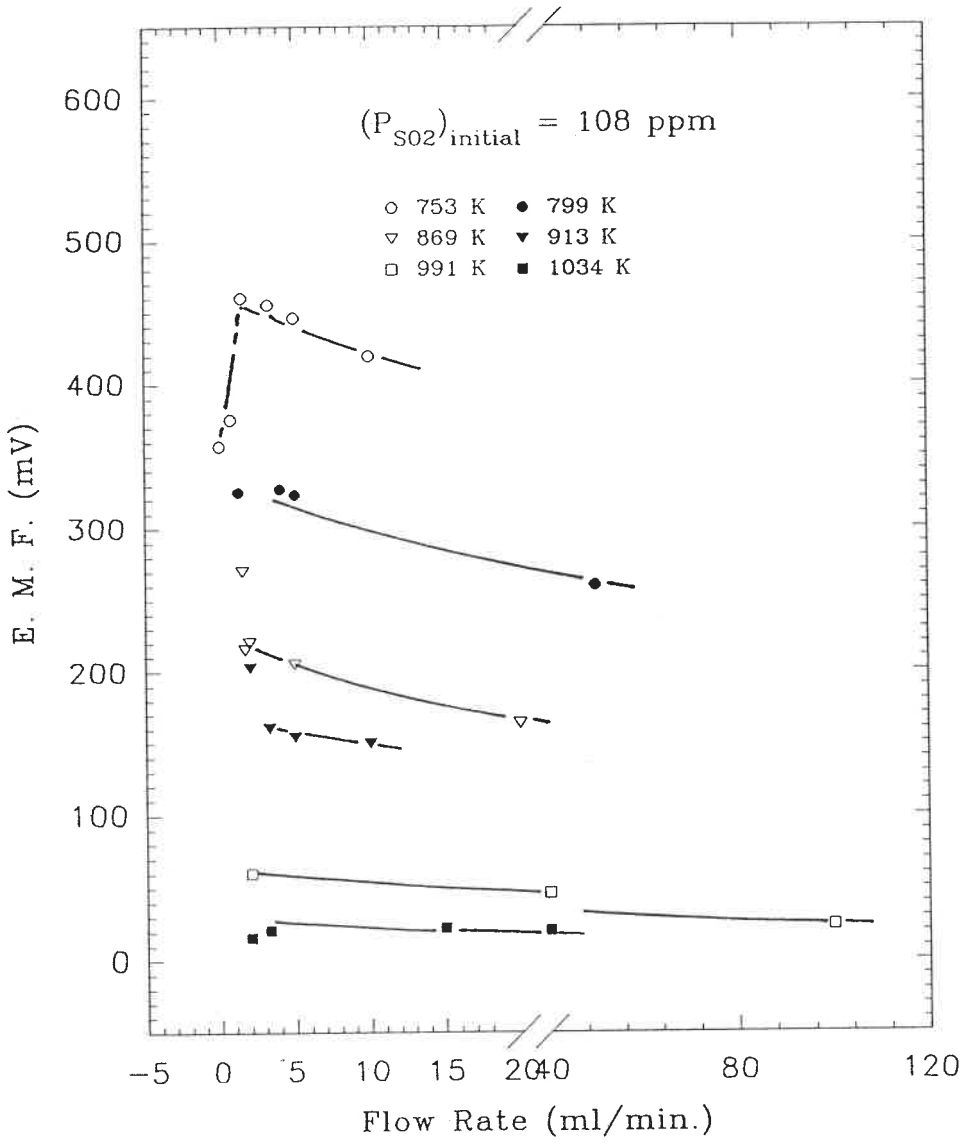

Figure 8 EMF Dependence on Flow Rate for Type 3 Electrode Preparation

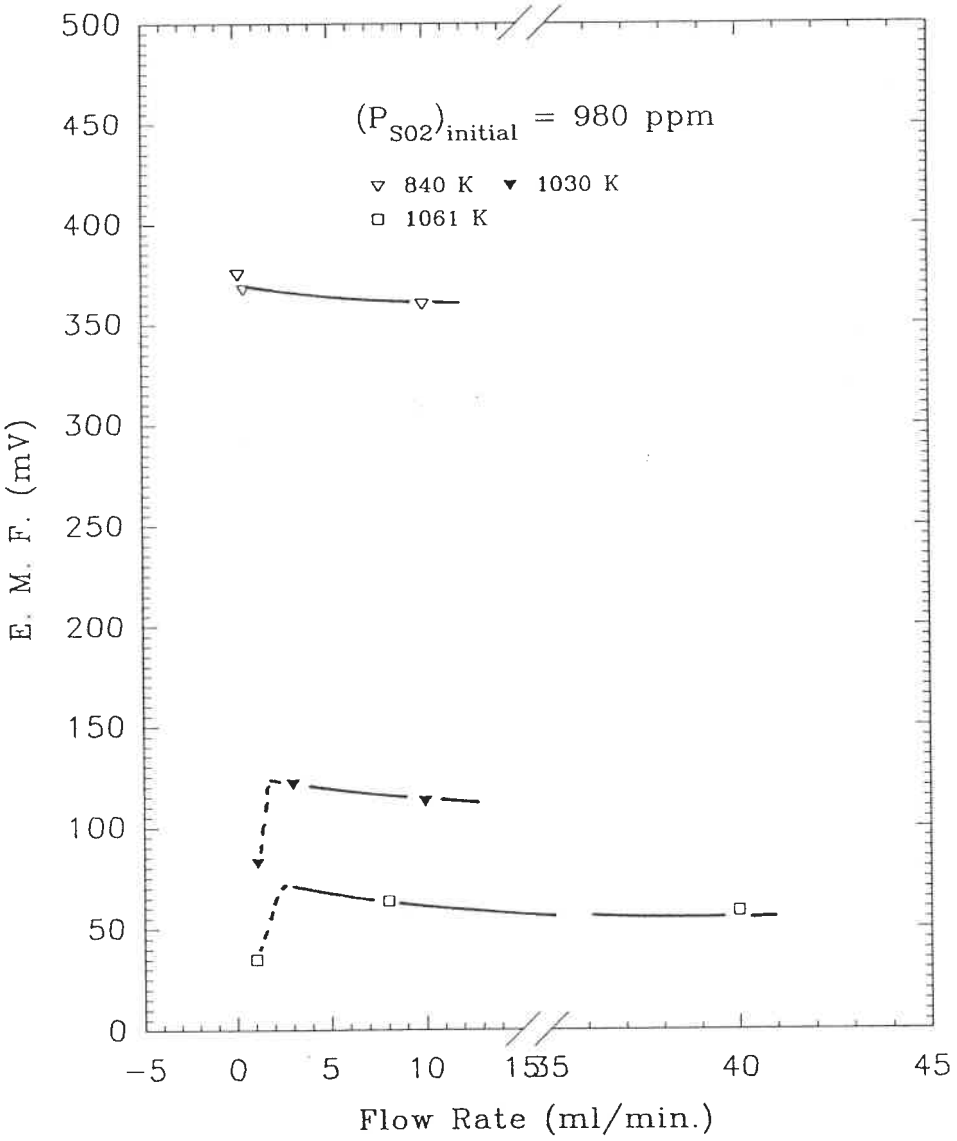

Figure 9 EMF Dependence on Flow Rate for Type 3 Electrode Preparation

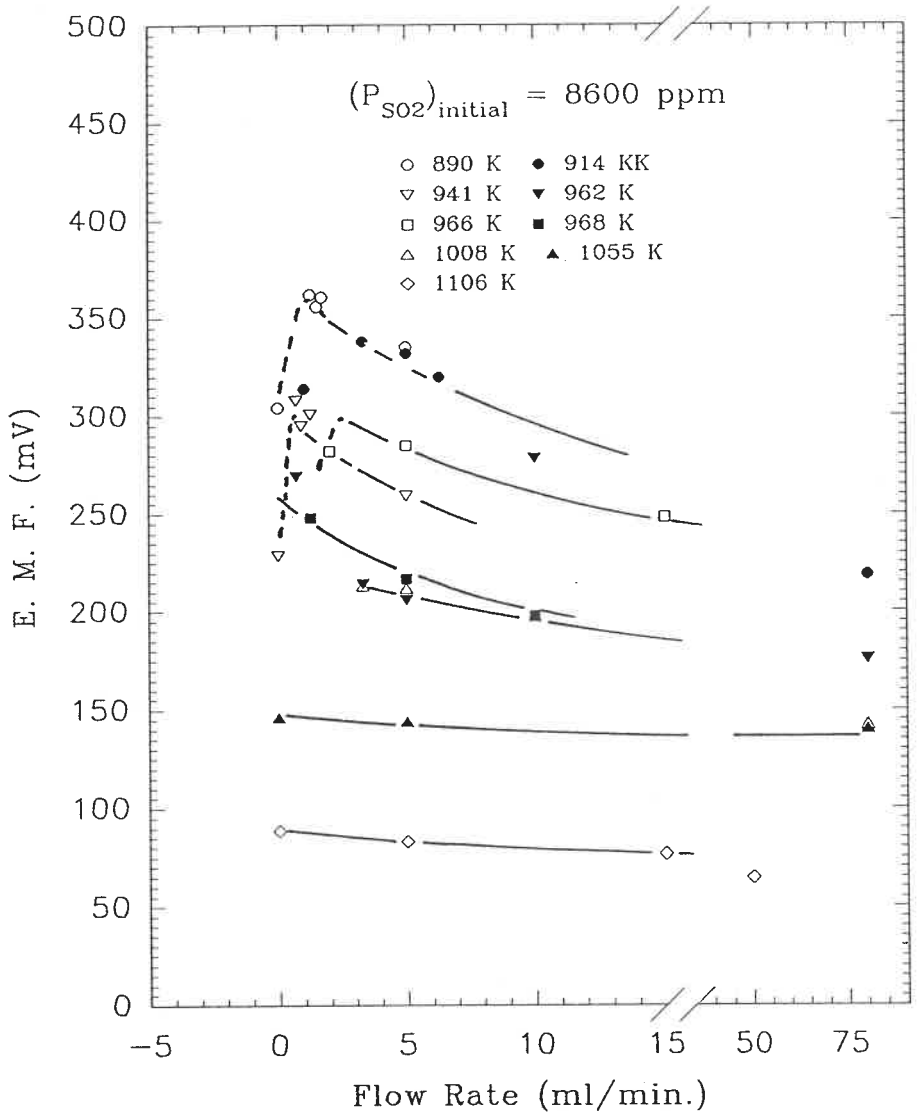

Figure 10 EMF Dependence on Flow Rate for Type 3 Electrode Preparation

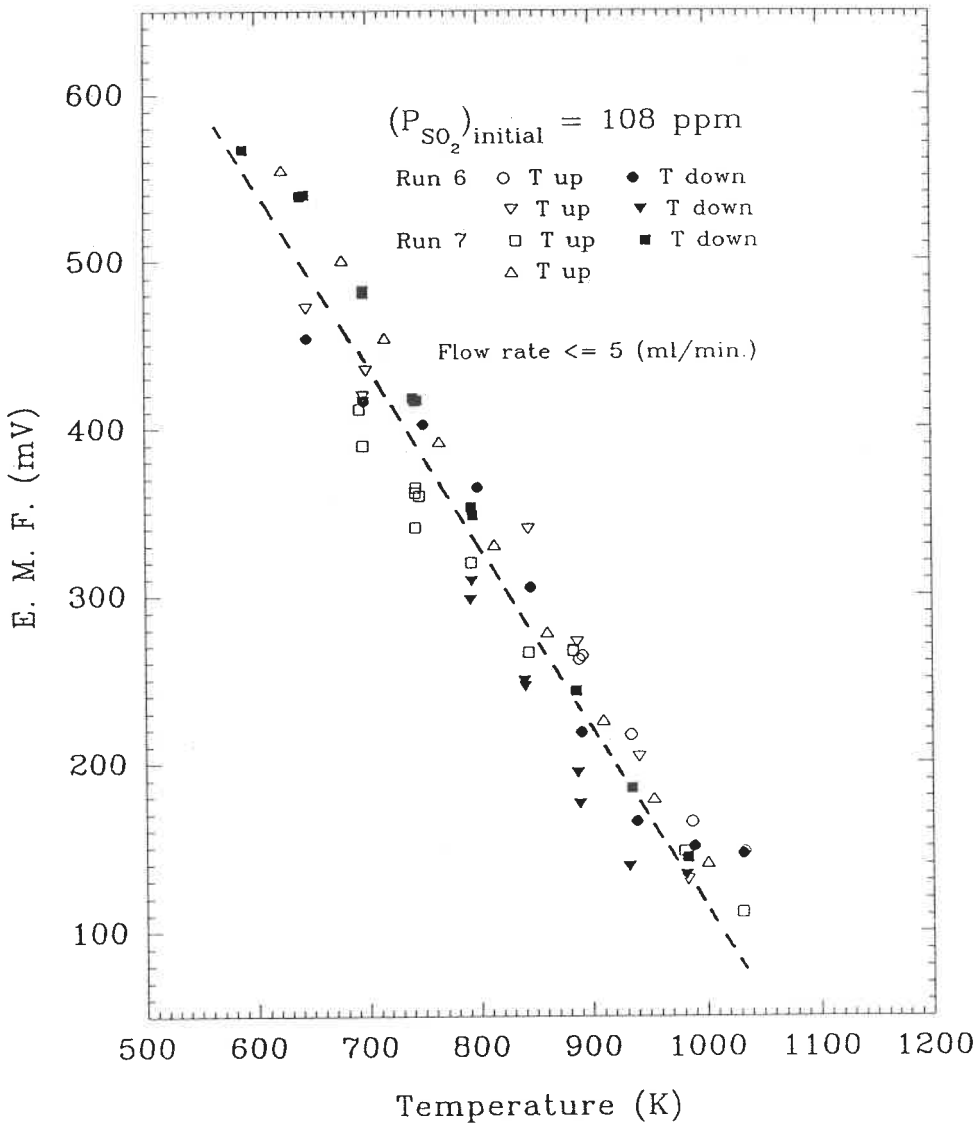

Figure 11 EMF Dependence on Temperature for Type 1 Electrode Preparation

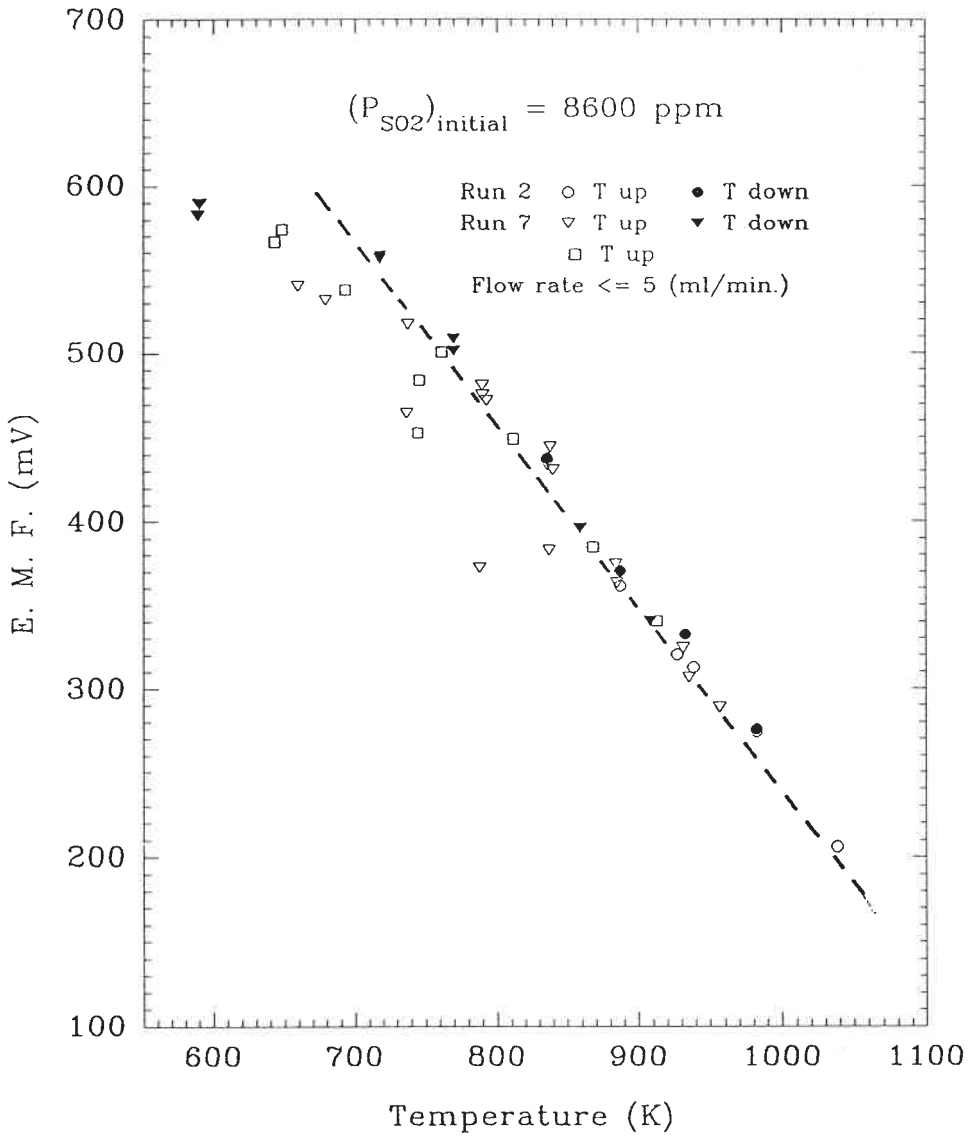

Figure 12 EMF Dependence on Temperature for Type 1 Electrode Preparation

APPENDIX C

Experimental data

(1) EMF values measured with Ag^+-ß-alumina as a solid electrolyte, Cell No. 2, 3, 4, 5, 6, 7, 8, 9, and 10.

(i) Cell No. 2, 3, 5, 6, 7 Type 1 electrode construction, Page 246 - Page 250.

(ii) Cell No. 4 and 8, Type 2 electrode construction, Page 251 - Page 254.

(iii) Cell No. 9, 10, Type 3 electrode construction, Page 255 - page 259.

(2) EMF values measured with $0.9CaO \cdot 0.72MgO \cdot 5.5Al_2O_3$ as a solid electrolyte, Cell No. 11, 12, Page 260 - Page 261.

Type 1 electrode, Cell No. 2

Temp. (K)	EMF (mV)	F.R. (ml/min)
(SO2)inintial = 10 ppm		
911	143.6	90
866	191.2	19.3
920	160.1	19.3
966	149.3	75
1016	153.5	75
672	442.4	1
673	429.1	1
772	328.3	1
855	153.6	70
871	221.2	1
868	191	18
842	181.8	15
871	173.9	70
919	144.2	68
926	152	112
970	168.2	1
771	321	1
817	258.6	1
920	147.6	69
822	261.3	1
863	146.8	69
918	144.6	53
727	220	112
724	378.4	1
863	179.4	15
871	197.9	7
722	388	1
920	171.5	1
816	220.9	14
(SO2)initial = 11 ppm		
1021	151.3	114
780	217.3	114
1070	157.3	114
728	302.7	114
731	249.6	114
680	386.6	114
925	138.3	114
626	451.1	114
831	169	114
679	381.7	114
833	137.8	114
626	392.7	114
877	142.5	114
1125	163.5	114

Temp. (K)	EMF (mV)	F.R. (ml/min)
(SO2)initial = 100 ppm		
721	369.5	105
1018	164	105
821	202.4	105
915	152.3	105
921	163	105
966	158.7	105
771	287	105
821	203.5	105
871	169.6	105
871	163.1	105
(SO2)initial = 400 ppm		
961	144.4	105
773	334.5	105
913	140.9	105
819	265.2	105
870	176.3	105
723	403.2	105
(SO2)initial = 1018 ppm		
917	287	1
821	343.3	2
821	327	25
870	231.9	150
870	236	105
965	226.5	10
870	262.5	45
965	225	19.8
821	297.9	195
1013	209	2
821	302.2	140
823	413	1
821	307.5	105
722	543.5	1
821	319.5	150
623	717	1
821	321	105
723	542	1
870	354	1
820	417	1
970	217.4	1
870	351	1
772	374.1	195
918	248	2
772	379.5	150
918	176.6	150

Type 1 electrode, Cell No. 2 (continied)

(SO2)inintial = 1018 ppm		
772	389.2	105
918	188.2	55
772	372.5	75
621	546.3	30
723	422.6	190
1015	177	140
723	427.5	150
773	473.5	1
723	434.2	105
673	604	1
723	440.4	70
821	408	1
673	472.4	195
918	234.8	5
673	473.4	150
870	229.6	195
673	477.6	105
1060	163	2
673	479.8	80
772	479.2	1
617	527	150
918	182.5	105
617	527.3	105
674	602	1
1015	196	19.8
918	270	1
621	543.3	80
(SO2)initial = 3000 ppm		
954	154.5	105
1008	153.8	105
671	510.4	105
1065	163.5	105

(SO2)initial = 3000 ppm		
675	515.5	105
1005	154	105
773	410.1	105
963	156	105
868	255.7	105
916	174.6	105
964	150	105
870	238.6	105
721	479	105
896	205.2	105
919	185.4	105
822	336.2	105
617	507.4	105
925	174.5	105
(SO2)initial = 8600 ppm		
964	276.2	2
1010	264	2.5
954	169	38
1065	194.5	2.5
954	311	2
1010	265.5	3
965	303.2	2
960	323	3
1010	256	0
915	362	3
954	175.8	27
915	350	4
1015	246	2
914	352.8	2
1012	230.8	2
864	430	2
866	428.5	2

Type 1 electrode, Cell No. 3

(SO2)initial = 11 ppm		
601	465.4	119
628	484.2	119
678	367.4	119
730	326.6	119
780	275.2	119
779	276.9	119
826	239.3	119
826	240.2	119
828	317	119
879	338.3	119
877	246.7	119

(SO2)initial = 11 ppm		
877	212.7	119
920	197.9	119
925	283.1	119
923	167.2	119
967	128	119
972	213.5	119
971	145	119
1021	120.6	119
1016	101.8	119
1020	105.7	119
1066	88.7	119

Type 1 electrode, Cell No. 3 (continied)

Temp. (K)	EMF (mV)	F.R. (ml/min)	Temp. (K)	EMF (mV)	F.R. (ml/min)
(SO2)initial = 119.7 ppm			(SO2)initial = 1018 ppm		
680	484.6	119	620	477.9	25
728	400.1	119	667	492.7	25
731	470.4	119	667	464.6	55
778	374.1	119	667	440.4	105
780	432.7	119	730	376	100
827	353.4	119	730	401.6	50
875	304.8	119	730	376.6	130
875	321.6	119	730	442.3	25
923	248	119	730	382.4	105
970	188.6	119	777	341.8	50
(SO2)initial = 242.7 ppm			777	317.8	95
680	450.6	105	777	313.2	150
731	449.3	105	777	307.3	195
780	430.7	105	777	318	105
829	387	105	824	393.6	142
873	324.8	105	824	390.9	195
875	333.1	105	829	396.2	80
876	343.1	105	829	391.8	105
923	266.4	105	878	354.2	55
923	262.7	105	878	350.3	105
922	284.4	105	878	348.5	150
967	207.5	105	878	347.6	180
970	194.8	105	914	299.7	195
(SO2)initial = 407.4 ppm			914	299.9	150
680	430.4	100	914	300.6	90
731	433.4	100	924	306.3	60
781	413	100	970	245.3	105
828	385.5	100	970	244.8	150
873	339.1	100	970	244.8	186
923	273.3	100	1017	196.2	105
967	226.3	100	1067	146.9	105

Type 1 electrode, Cell No. 6

(SO2)initial = 10 ppm			(SO2)initial = 10 ppm		
619	499.2	5	1055	69.6	10
619	525.2	0	1055	63	150
670	515	0.3	1008	83.2	50
722	435.4	50	979	97	50
772	311.4	50	940	110	50
772	345.8	5	896	127.1	50
822	255.5	50	858	232.6	0
821	243.8	100	858	224.9	50
821	265.3	15	858	214	40
870	246.4	50	819	262	50

Type 1 electrode, Cell No. 6 (continied)

Temp. (K)	EMF (mV)	F.R. (ml/min)
(SO2)initial = 10 ppm		
870	241	100
870	237	150
870	248	10
918	231.6	50
961	166.2	50
1012	162.2	50
1055	67	50
773	268.4	50
773	349.1	5
773	349.7	50
773	349.4	100
724	407	50
722	396.2	100
673	361.1	40
(SO2)initial = 108 ppm		
915	174.5	95
915	255	5
914	233.5	70
914	252.6	0.3
960	206.8	0.3
960	187	55
960	186.2	70
1010	154	0.5
1010	135	105
1060	135.4	0.5
1060	134.2	0.5
1010	139.6	0.5
963	155.5	0.5
963	151.3	110
915	209.3	0.15
915	197	105
870	296.6	0.4
869	261	110
821	356.9	1
819	329.2	45
772	395.8	0.5
773	366.8	55
721	411	1
721	380.8	55
672	449.1	4
672	467.4	0.4
723	429	0.15
722	414	1
722	410.5	1

Temp. (K)	EMF (mV)	F.R. (ml/min)
(SO2)initial = 108 ppm		
867	294.5	50
867	284.6	90
867	278	160
867	331.2	1.4
867	271.4	110
916	224.5	110
916	226.8	75
916	240.6	15
916	243.8	10
916	263.1	0
964	189.6	50
964	183	50
964	177	105
964	193.5	2.5
963	174.5	65
1010	113.5	65
1008	114.8	30
1009	119.6	5
1009	122.8	0.2
1057	93.3	55
1057	92.5	65
1057	93.3	10
1008	107.9	10
1008	105.9	40
1008	104.6	70
1008	103.7	100
962	124.8	30
962	122.7	75
962	121.6	100
962	128.7	5
915	166.4	5
915	156.9	50
915	185.3	2.5
869	237.4	0.8
869	197.6	40
869	240.9	0.4
819	290.3	0.4
819	256.2	10
819	301.6	0.3

Type 1 electrode, Cell No. 6 (continied)

Temp. (K)	EMF (mV)	F.R. (ml/min)
(SO2)initial = 1018 ppm		
673	496.4	1.25
673	504	2
726	456.4	50
722	488.4	1
772	491	1
819	421	65
819	420.5	140
868	356.3	135
868	361.5	100
868	400	10
915	314.3	120
915	299.7	150
915	289.7	210
915	292.8	165
915	320.1	75
960	237	180
960	239	120
960	243.7	85
960	249.2	55
1010	196	105

Temp. (K)	EMF (mV)	F.R. (ml/min)
(SO2)initial = 8600 ppm		
1010	232.3	105
1010	230	105
1010	254.2	70
1059	213	70
1006	252.7	70
1057	220	70
1008	260.8	70
957	312.2	70
957	384	0.5
908	450.3	0.5
915	366.7	70
863	476	2
866	424.6	70
820	539.9	0.25
820	482.6	70
766	550.1	0.3
769	511.3	70
721	590.3	0.25
720	542.5	70
671	617.7	0.5

Cell No. 5

(SO2)initial = 10 ppm		
964	218.5	34
917	289.7	35
918	292.8	0.3
918	277	110
868	340.6	115
821	424.8	25
821	416.5	70
822	409.3	107
821	401	145
777	478.7	5
776	466.5	45
776	454.1	110
726	469.5	118
771	475.5	118
821	416.4	115
863	356.6	125
909	296.4	105
914	301.2	45
960	221.3	120
1002	153.2	118
1055	123.3	30

Cell No. 7

(SO2)initial = 10 ppm		
1026	93	115
1076	87.4	115
1026	89.8	115
976	93.1	115
979	96.5	5
933	156.7	85
930	157.5	115
882	210.4	55
886	218.3	1.5
886	215	115
835	266	35
834	265.2	100
834	264.3	115
783	317.7	5
784	313.3	95
786	311.8	115
735	344.1	10
735	355.9	5
734	357.1	65
734	356	115
685	395.9	50

Type 2 electrode, Cell No. 4

Temp. (K)	EMF (mV)	F.R. (ml/min)
(SO2)initial = 10 ppm		
918	146	23
918	165	2
871	232.8	2
871	222.3	15
824	394	61
875	405.9	2
875	445.3	1
875	426.3	2
918	395.6	2.5
968	355	2.5
965	294.4	30
965	296	14
1018	285.4	14
1018	292.1	47
1018	305	47
915	427.1	45
884	447.5	48
866	458	47
814	470.8	75
814	472.1	55
821	471.5	15
821	500	10
821	469.4	90
771	512	85
771	511.2	50
771	516	75
721	450	110
774	352.5	105
823	305	105
872	268.4	105
914	223.3	105
(SO2)initial = 1018 ppm		
771	487.2	68
723	540	40
672	558.5	10
727	504	10
775	462.1	10
821	374.7	10
821	379	5
871	305	5
922	246.5	10
916	282.1	5
966	265.1	5

Temp. (K)	EMF (mV)	F.R. (ml/min)
(SO2)initial = 1018 ppm		
1014	236.3	5
1060	163.9	5
1111	208	5
1063	146.1	5
1012	163.1	5
966	215.4	5
920	289	5
918	319.5	10
918	318	30
918	307.5	70
918	301	105
918	294.3	130
918	292.9	140
918	324	1
918	304	1
868	373.5	1
868	376.9	50
868	363	70
868	354	105
868	346.3	125
868	343.5	150
868	340	170
868	399.6	1
822	457	1.25
821	408	50
821	392.5	100
821	386.5	130
821	423.5	30
774	460	30
774	483.5	5
774	515	1
722	589	1
722	559	3
722	565	2.5
668	637	2
(SO2)initial = 8600 ppm		
871	283.5	14
871	358.5	1
871	309.2	7
825	397.8	7
825	475	0.5
825	435.5	1
825	485	0
824	501	0.5

Type 2 electrode, Cell No. 8

Temp. (K)	EMF (mV)	F.R. (ml/min)
(SO2) initial = 10 ppm		
1012	68	50
1012	68	100
1012	67.5	30
1042	57.5	50
1042	62.7	50
991	61.7	50
945	88.3	50
898	139.5	50
898	135.5	120
852	199.5	50
804	258.9	30
804	262	5
756	328.3	20
778	300	50
766	311.1	50
823	268	50
872	191.6	50
872	179	100
919	141.6	100
963	88.1	100
966	24.4	50
966	19.5	100
966	19.2	30
918	88.5	20
918	94	2
918	109.1	1.5
872	168.5	2
872	170.1	2.5
825	218.1	2.5
825	228.6	2
777	284.7	2.5
728	334.9	2.5
677	314.5	150
680	323.5	5
680	324.5	2.5
709	329.3	2.5
757	314.9	2
806	262.1	2
824	230.1	2.5
853	192.8	2.5
900	140	2.5
900	128.5	3.3
900	105.2	100

Temp. (K)	EMF (mV)	F.R. (ml/min)
(SO2) initial = 108 ppm		
1017	180.2	100
1050	160.1	100
997	203	100
762	312.2	50
762	284.3	100
762	367.4	2.5
762	381.2	0.3
811	330	1
858	284.9	50
906	267.6	50
906	251.7	100
906	247.8	150
953	264.3	30
953	251.6	100
953	246.1	150
1000	182.5	150
1000	182.8	100
1000	184	50
1000	186.2	5
1049	124	150
1015	151	50
973	212.4	50
925	287.3	30
878	337.6	30
877	328	150
830	377.4	30
830	368.7	150
774	386.7	30
775	406.6	3
721	451.2	2.5
730	459	3
678	510.4	2
678	468	150
625	554	1.2
1057	74.5	10
1057	75.8	100
1057	75.8	3
1026	96.9	30
1026	98	5
1026	97.2	100
990	141	10
990	137.5	50
990	134	100
944	203.8	30
944	189.6	100

Type 2 electrode, Cell No. 8 (continued)

Temp. (K)	EMF (mV)	F.R. (ml/min)
(SO2) initial = 108 ppm		
944	195	50
896	275.5	5
896	267.3	30
896	264	60
896	260	100
850	348.9	5
850	335.6	30
850	328	60
850	321.4	100
799	370	30
799	386	2.5
751	448	2.5
754	446.5	5
754	430.4	30
754	431.8	30
693	533.6	5
693	517.7	30
653	606	50
653	607.3	150
675	620	50
675	615	150
675	570	150
726	495.5	60
726	490.6	100
776	418.3	30
776	418.2	30
821	357.7	30
821	352	60
821	351.8	150
821	353	100
873	287.5	100
871	286.5	150
871	293	30
914	261.3	30
914	257.5	100
960	204.2	30
960	201	60
960	200.1	100
1012	126.5	50
1012	125.7	100
1012	43.2	150
1012	53.8	50
966	109.1	50
966	81.3	150
966	116.4	10
916	184.7	5
870	249.6	5
870	256.5	2.5
870	262.4	1.25
822	299	10
822	330.8	0.5
774	386	0
774	366	5
725	398.4	10
725	439.1	0
674	381.7	0
805	343.7	3.3
805	360.2	0
805	335.2	5
853	278.3	5
898	218	5
898	206.8	5
950	146.4	4
996	77	2.5
995	51.9	100
995	70.1	30
1023	31.7	30
966	94.6	30
966	105.8	4
(SO2) initial = 8600 ppm		
963	316.5	30
963	296.7	100
963	322.3	20
963	284.5	150
1013	259.5	50
1013	250	100
1013	245.6	150
1013	237.3	200
1054	184	150
1115	119.8	150
1090	153	150
1031	224	150
980	272.1	150
931	321.5	150
885	390.8	50
850	378	50
850	445.2	10
798	524	2.5

Type 2 electrode, Cell No. 8 (continued)

Temp. (K)	EMF (mV)	F.R. (ml/min)	-Log(SO2)	EMF (mV)	F.R. (ml/min)	P(O2) (atm.
(SO2) initial = 8600 ppm			Temperature = 964 K			
758	580.5	0	2.3	231.7	100	0.21
758	501	30	3	193	100	
705	645.6	0	3.3	179.6	100	
656	698	0	2.7	205.5	100	
604	584	10	2.5	212.4	100	
680	668	0.3	3.5	168.8	100	
678	669.6	0	3.5	172.9	100	
731	621	0	3.7	159.1	100	
785	559.4	2	4.3	119.9	100	
777	584	0	4.5	98.2	100	
777	568	5	4.5	134.2	100	1
825	499	30	4.3	142	100	
825	471	100	4	160.5	100	
874	438.7	100	3.7	190	100	
874	427.5	150	3.5	207	100	
874	450.7	30	3.5	196	100	
917	396.2	30	3.3	208	100	
917	386.8	100	3	230.2	100	
917	379.4	150	2.7	250.2	100	
917	373	200	2.5	266.2	100	
917	368.3	250	2.3	275.5	100	
917	398.2	5	Temperature = 918 K			
917	372	0	2.3	317.7	100	1
918	360	2	2.5	317	100	
917	348.5	5	2.7	308.6	100	
965	295	5	3	286.4	100	
1013	234.2	50	3.3	274.4	100	
1063	172	50	3.5	276.6	100	
1063	173	100	3.7	260.8	100	
1114	106.8	100	4	238	100	
920	316.3	100	4.3	212	100	
920	331.4	30	4.5	199.1	100	
920	348.2	6	4.5	152.8	100	0.21
871	420.6	2.5	4.3	159.1	100	
821	494.7	3	4	173.5	100	
774	545	1.5	4	174.4	100	
825	486.3	5	4	181.4	100	
850	461	5	3.7	197	100	
900	394.6	5	3.5	207	100	
943	331	5	3.3	211.3	100	
992	261	5	3	213	100	
992	238.2	50	2.7	201.7	100	
992	191	120	2.7	196.8	100	
992	246.7	20	2.5	184	100	

Type 3 electrode, Cell No. 9

Temp. (K)	EMF (mV)	F.R. (ml/min)
(SO2)initial = 10 ppm		
623	502.2	10
623	457.7	150
624	516.7	1.7
680	450.6	1.7
682	435.5	2.5
726	364.8	1.7
781	302.1	1.7
776	285.7	1.7
824	217.2	1.7
824	214.8	1.7
824	216.1	150
824	218.5	30
824	218.4	10
872	137.4	15
872	139.7	100
872	137.7	150
872	140.1	60
872	139.8	10
921	61.3	15
946	18.3	15
900	89.6	20
852	165.9	20
805	232.7	20
757	297.9	20
757	268.2	50
757	245.7	100
757	308	5
707	376.3	2.5
657	425.4	2.5
657	386.6	50
656	424.2	1.7
656	442.4	1.7
(SO2)initial = 108 ppm		
656	453	5
706	461.4	1
759	399.7	1
756	375.8	0.8
806	307.6	0.9
804	260.4	50
802	327.5	4
802	325.6	1.25
802	323.4	5
853	257.1	5
850	260.8	5

Temp. (K)	EMF (mV)	F.R. (ml/min)
(SO2)initial = 108 ppm		
902	185.8	5
896	192.6	5
943	118.5	5
991	43.9	5
989	47.1	5
993	36.1	100
993	45.8	5
993	46.6	0.5
1012	15.3	5
965	84.5	5
918	154.6	5
872	205.6	5
872	163.7	20
872	220.4	2
872	215.4	1.7
824	280.5	1.7
771	346.1	1.7
726	398.1	1.7
727	412.7	1.25
677	440.7	0.9
678	413.4	1.4
918	314	1
919	331.9	5
919	319.7	6.3
919	218.5	80
919	338	3.3
965	269	0.7
965	278	10
965	275.3	30
965	175.6	80
965	124.6	0
965	92.7	30
965	112.6	10
965	114.2	3.3
(SO2)initial = 8600 ppm		
966	205.6	5
966	214	3.3
1012	235	10
1012	142.4	80
1012	162.5	30
1012	197.4	10
1012	213	3.3
1012	211.8	5
1059	144.1	5

Type 3 electrode, Cell No. 9 (continued)

Temp. (K)	EMF (mV)	F.R. (ml/min)
(SO2)initial = 8600 ppm		
1059	148.5	30
1059	140.2	80
1059	146.5	0
1109	88.6	0
1109	76.5	15
1109	64.5	50
1109	83	5
1085	116.3	5
1040	157.3	15
1040	178.7	2.5
1040	180.2	2.5
993	198	10
993	216.5	5
993	248	1.25
946	259	5
946	308	0.7
946	228.5	0
946	295	0.9
946	300.8	1.25
899	362	1.25
899	304.2	0
900	355.8	1.5
900	335.2	5
900	360.5	1.7
851	397.2	2
853	426.9	1
803	486	1
756	522.6	0.5
(SO2)initial = 108 ppm		
758	455	2
707	524.5	0.3
707	525	0
707	547.5	0.3
657	575.4	0.2
782	421	2
824	337	1.5
872	229.1	3
872	244.9	1
872	267.7	0.3
871	264	0.8
917	187	0.6
964	105.4	0.5
964	130.1	0
1012	65	0

Temp. (K)	EMF (mV)	F.R. (ml/min)
(SO2)initial = 108 ppm		
1012	32.8	1.3
1012	40	0.5
993	69.8	0.2
947	125	2.5
947	142.6	0.2
900	143.3	0.5
899	232.1	0.15
900	179.1	0.33
854	296.4	0.2
805	368	0
710	419	5
(SO2)initial = 10 ppm		
710	378	20
710	417.5	2
710	427.3	0.4
761	356.9	3.3
761	371.7	0.5
808	298.8	3.3
808	291.6	2.5
856	197	2
856	215.4	0.5
902	134.1	1.7
902	143.4	0.7
949	60.5	2
949	72.4	0.5
967	29.7	5
921	88.4	5
921	103.4	0.8
874	163.9	1
826	211	0.5
826	213.8	3.3
778	274.5	3.3
778	283.4	0.8
730	337.4	0.7
681	385	0.7
680	390.2	0.2
627	402.9	0.2
627	407.8	0.33
681	381.1	3.3

Type 3 electrode, Cell No. 10

Temp. (K)	EMF (mV)	F.R. (ml/min)
(SO2) initial = 108 ppm		
965	118	0.5
1008	22	50
1008	22.5	50
957	90	30
959	95.1	20
959	100.4	5
959	97	5
959	97.2	6.6
914	150.4	10
914	160.7	3.3
914	160.7	3.3
866	217.7	3.3
866	219.5	2
822	277.4	0.4
771	339	0.4
726	398.7	0.4
675	398.5	0
755	357.4	0
756	361.5	0
804	296	1
850	242.1	0.3
850	238	1
850	212.2	5
850	239	0.7
900	182.6	0.7
946	121.7	1.1
992	54.9	1
990	45.9	40
990	24	100
990	60.4	2
1028	12.7	2
1028	13	2
1028	13.4	0
1008	34.4	20
1008	35.8	5
1008	33.4	0
1008	36.3	10
961	100.4	10
962	93	20
962	96.9	10
962	101	5

Temp. (K)	EMF (mV)	F.R. (ml/min)
(SO2) initial = 10 ppm		
962	19.2	40
962	19.6	30
962	20.4	20
962	21.5	10
916	97	10
916	83.5	3.3
916	70	40
916	81.2	1
916	84.1	5
876	129.4	5
831	195	0.2
830	193.2	1
784	259.6	0.15
783	255.8	1
783	258.7	0.15
736	323.4	0.15
685	416.8	0.15
770	284.4	0.15
726	330.7	0.4
680	374.3	0.4
743	308.8	0.33
787	240.1	0.2
787	225.5	2.5
787	233.6	1.25
815	204.7	1
815	210.1	0.2
815	214.7	0.15
858	158.3	0.6
858	158.1	1
903	109	1
903	104.2	5
903	84.9	20
903	70.4	80
903	60.5	120
902	90.2	15
902	90.5	15
945	41.7	15
945	40.8	10

Type 3 electrode, Cell No. 10 (continued)

Temp. (K)	EMF (mV)	F.R. (ml/min)
(SO2)initial = 8600 ppm		
945	309.5	0.5
945	274.2	10
990	237.2	10
989	213	15
989	216	15
903	356.7	0.15
(SO2)initial = 10 ppm		
903	201	30
914	117.6	15
914	93.7	20
914	66.3	150
914	91	20
870	148.1	15
843	183.6	15
797	245.6	15
752	311.8	15
705	376.6	15
657	421.5	15
657	427.2	0.9
696	392.5	0.9
(SO2)initial = 8600 ppm		
695	388	0.5
743	435.7	1.25
789	420	1.25
834	409	1.25
878	395.8	1
923	346	1.7
923	320	5
966	284.7	5
966	248	15
966	282	2
1012	218.3	2
1062	144	2
1058	150	2
1108	79.3	2
1108	74.9	2
1146	21.8	2
1115	73.3	5
1071	144.5	5
1020	211.6	5
1024	201.6	1.7
1024	192.6	10
1024	211	3.3
978	266	3.3

Temp. (K)	EMF (mV)	F.R. (ml/min)
(SO2)initial = 8600 ppm		
978	273	1.7
933	326	1.7
889	379.3	1.7
844	432	1.7
(SO2)initial = 108 ppm		
844	311.4	10
800	367.4	10
752	419.6	10
752	446	5
752	455	3.3
752	460	1.5
706	510.8	1.1
706	490.6	2
706	507.8	1.7
687	521.4	1.7
735	468.8	1.7
735	474.5	1.5
782	405.6	1.7
827	346.6	1.7
871	270.5	1.5
917	193	1.5
915	203	2
960	138.5	2
1006	51.7	2
1032	16.2	2
1032	22.4	15
1032	20.6	40
1032	21	3.3
986	87.5	3.3
986	89.9	7
986	93.2	1.7
943	139.7	1.35
943	157.5	2.5
898	214.8	1.7
853	280	1.7
806	335.9	1.5
806	337	1.25
806	343.3	0.6
762	394.5	0.5
762	395.3	0.3
716	454	0.8

Type 3 electrode, Cell No. 10 (continued)

Temp. (K)	EMF (mV)	F.R. (ml/min)	Temp. (K)	EMF (mV)	F.R. (ml/min)
(SO2)initial = 980 ppm			(SO2)initial = 980 ppm		
842	359.8	10	670	557.6	0
835	383	8	722	517.2	1
834	385.5	1.25	774	455.9	0.1
834	391.2	0.3	823	383.3	0.2
882	312.8	0.5	872	305	1
882	330.4	0.9	920	247.6	1
933	255.4	1.1	969	179.3	1
933	255.2	1.1	1016	104.2	1
978	157.6	1.1	1062	35	1
1028	82.3	1.1	1062	58.4	40
1028	82.6	1.1	1062	63.6	8
1076	16.8	1.1	1083	35.6	8
1076	15	1.2	1082	46.7	10
1044	51.5	1.1	1032	112.7	10
1044	52.1	1.1	1032	121.1	3
991	131.7	1.1	985	175.4	3
993	129.2	1.1	985	179	2
951	200.9	1.1	985	185.6	1
902	268.8	1.1	936	242.1	1
854	336	1	936	248.3	0.5
854	340	0	888	310.6	0.5
854	342.1	0.4	830	367.5	0.5
804	406.9	0.6	830	374.8	0.2
754	454	0.6	793	432.8	0.5
754	457.4	0.6	793	439.5	0.2
755	467	0.4	740	492.7	0.2
703	509.5	0.3	740	491.4	0.2
650	523.6	0.15	690	516.1	0
575	362.8	2	633	530.8	0
626	574	0	583	446	0

Cell No. 11, 0.9CaO0.72MgO5.5Al2O3 as electrolyte

Temp (K)	EMF (mV)	F.R. (ml/min)
(SO2)initial = 980 ppm		
1012	582.3	20
1060	565.2	20
1110	533.2	20
1110	525	20
1162	290	20
1162	212	20
1162	160.3	20
1162	165.1	20
1162	178.9	80
1162	201.4	150
1162	201.9	6
1214	184.6	10
1267	95	10

Temp (K)	EMF (mV)	F.R. (ml/min)
(SO2)initial = 980 ppm		
1264	88.3	10
1264	88.1	1
1314	66.7	1
1314	69.6	1
1314	72.9	1
1314	70.5	1
1314	70.8	1
1367	66	1
1367	69.1	1
1367	62	10
1342	63.4	10
1342	64.8	10

Cell No. 12

(SO2)initial = 11 ppm		
914	92.1	15
914	76.5	3
914	108.5	50
965	100.4	15
1008	111.5	15
1060	116	15
1108	123.9	15
1160	110.6	15
1160	108.7	1

(SO2)initial = 980 ppm		
1156	406	60
1156	397.5	43
1156	388.1	20
1206	508.1	25
1206	516.7	55
1206	521.3	90
1206	523.6	140
1206	524.3	180
1206	525.4	250
1218	294.1	30
1179	245.7	15
1129	293.1	60
1129	199.3	20
1129	240.8	90
1080	231.5	75

Cell No. 12, 0.9CaO0.72MgO5.5Al2O3 as electrolyte

Temp (K)	EMF (mV)	F.R. (ml/min)
(SO2)initial = 101 ppm		
1080	218.5	65
1034	244	60
985	280	60
937	306	60
937	351	45
937	368	85
890	308	60
842	322.4	60
794	321.6	60
854	305	60
899	323.9	90
946	290	85
996	253.5	80
1046	220.5	80
1094	168.8	80
1141	145.3	70
1191	103.5	70
1191	127.2	180
1241	177.2	70
1292	83.9	65
1292	101.2	180
1348	73.4	60
1318	83	60
1265	97	60
1214	126	90
1165	110.3	90
1115	131.5	90
1066	159.8	90
1016	210	85
969	267.3	85
921	301.3	85
867	310.3	85
868	405.5	180
868	359.5	150
868	306.2	80
824	262.8	70
822	348.1	180

Temp (K)	EMF (mV)	F.R. (ml/min)
(SO2)initial = 11 ppm		
822	251.8	75
822	307.5	150
873	257.7	90
920	239.7	85
970	218.4	80
970	181.3	85
1065	129	80
1115	101.5	80
1165	79.9	75
1215	89.9	65
1215	99.4	150
1215	78.5	15
1267	78.1	45
1266	84.5	120
1320	79.8	85
1319	70.3	50
1286	76.3	80
1233	83.9	80
1184	94.3	80
1135	112.6	80
1086	118.6	80
1037	128	80
987	196.9	80
949	245	75
890	275	80
853	275	90
804	293.3	80
754	302.8	90